



Fluidization Behavior of Granular Activated Carbon

For drinking water treatment applications

Author

Pablo Daniel Roberto Dacomba Torres

Fluidization behavior of GAC

Thesis

Submitted in partial fulfillment of the requirements of the

Master of Science

degree in

Water Management

by

Pablo Daniel Roberto Dacomba Torres

at

TU Delft | Faculty of Civil Engineering and Geosciences

Student number: 4743555

Thesis Committee:	Prof. dr. ir. Jan Peter van der Hoek MBA	Waternet/TU Delft	j.p.vanderhoek@tudelft.nl
	Prof. dr. ir. Johan Padding	TU Delft	j.t.padding@tudelft.nl
	Ir. Onno Kramer	Waternet/TU Delft	onno.kramer@waternet.nl
	Ing. Eric Baars	Waternet	eric.baars@waternet.nl
	Ir. Peter de Moel	Waternet	peter.de.moel@waternet.nl

SUMMARY

For drinking water treatment applications, it is possible to predict the external porosity of an expanded bed of granular activated carbon in fluidized conditions. A new model has been developed with a 2% relative prediction error.

In order to supply sufficient and safe drinking water, water utilities use a treatment train consisting of several unit processes. One of these treatment unit processes is granular activated carbon (GAC) filtration, a crucial unit process widely used for its filtration and adsorption capabilities as a barrier for undesired macro and micro-pollutants. The point of interest for this research is one of the critical steps in the filtration part of the unit process, the backwashing procedure.

Backwashing is a cleaning procedure, which consists on stopping the normal operation of the filter and reversing the normal downward water flow. This upward flow leads to the expansion of the filter's media and washes away any undesired particles caught in between and on the surface of the media. Inadequate backwashing can lead to unwanted operational outcomes, for instance, solids accumulation and mud balls or media washout, resulting in costly operational expenses. In addition, currently there is a tendency for water utilities to explore new sustainable GAC filter media, which have different expansion tendencies. These operational requirements create the need for the development of prediction models to estimate the expansion degree of the filter bed during backwash procedures. Additionally, a deep understanding of the phenomena that governs this unit process is required to increase its resiliency.

The main goal of this research was to predict the expansion degree of GAC in the water phase. In order to achieve this goal, two innovative approaches combining advanced laboratory techniques and prediction models was the course of action. The first approach was the development of an input model known as the AquaGAC model, to describe the different characteristics of porous media and perform checks using calculated and measured hydraulic parameters. With the combination of the AquaGAC input model and an existing fluidization model (FBI) that computed the expressions of five classical models, the prediction of porosity of the performed experiments was achieved. The second approach consisted on using a data driven model, which consisted on the combination of the outputs the FBI and AquaGAC models with several morphological parameters to derive empirical expressions that accurately estimated the external porosity.

Obtained results suggest that using the 10th percentile of the particle diameter in classical models, delivers porosity prediction errors of 10% in comparison to the 50th percentile used in practice with errors up to 25%. Based on symbolic regression, data driven models produced expressions with accurate correlations with porosity errors ranging from 2-5%.

The results of this research are encouraging as the AquaGAC input model can serve as a basis for other fluidization models that use porous media with different shapes. Recommendations are made to improve the experimental set-up, the accuracy in estimating the particle envelope and wet densities, and the quantitative evaluation of the orientation. Future research of the expansion behavior of mixtures is also recommended.

ACKNOWLEDGEMENTS

Firstly, I would like to thank Jan Peter van der Hoek for his encouragement and unconditional support throughout this project.

Onno and Eric, it's been a pleasure to work by your side, I cannot thank you enough for dedicating a great investment of time and effort for this project. This amazing learning experience would not have been possible without you. A big thank you to Peter de Moel for his amazing insights and very critical feedback for the present report.

I would also like to express my sincere gratitude to Johan Padding, who always found the time to share his deep knowledge and passion for the subject. Every session was an exciting quest to find the missing piece of the puzzle.

A special thank you to my Waternet colleagues, Michel, Peter and both Marks who greatly supported me during my experiments and made me feel at home those winter days in the pilot plant. I promise that next time I will be very careful with the temperature settings of the expansion column.

I would also like to take the opportunity to thank Geert Jan van Heck, whose stories, advice and guidance on the early train made a positive impact in my way on seeing the world.

Special thanks to my TU Delft colleagues, Armand Middeldorp and Ron Penners for their constant help and kind support in the lab. I would also like to thank Nutonian, for kindly sharing their Eureka software used in this research.

A big thank you to Ben Cools and Dirk Bloemen of the Water Groep for their kind help and analysis performed.

This work would never have been possible without the support of my awesome friends, the Kids on the block, A63 roomies, Mexidelftianos, and the other amazing Water managers that I've met across this journey. This was a very special part of my life and was very happy to share it with you.

Special thank you for the library crew for the support on the last leg of this project.

I am incredibly grateful to CONACYT (Consejo Nacional de Ciencia y Tecnologia), who kindly sponsored my studies in the Netherlands.

Este reporte se lo dedico a mi amada familia. Blanquita, Martin, Arturo, Jess, sin su constante amor y apoyo a lo largo de este proyecto nunca hubiera podido recorrer este camino. Estos dos años han sido una gran experiencia llena de aprendizajes y aunque los extrañé en cada momento, quiero que sepan que siempre fueron la energía en mi corazón que me motivó a seguir adelante.

“Life moves pretty fast. If you don't stop and look around once in a while, you could miss it”.

This research is part of the project “Hydraulic modelling of liquid-solid fluidization in drinking water treatment processes” (PhD project Onno Kramer) carried out by Waternet, Delft University of Technology and HU University of Applied Sciences Utrecht. Financial support came from Waternet’s Drinking Water Production Department.

Table of contents

SUMMARY.....	i
ACKNOWLEDGEMENTS.....	ii
1. Introduction.....	1
1.1 Thesis background.....	1
1.2 Problem description.....	1
1.3 Knowledge gap.....	2
1.4 Research question.....	3
1.5 Hypothesis.....	3
1.6 Project objectives.....	3
1.7 Project relevance.....	4
1.8 Project approach.....	5
1.9 Thesis outline.....	5
2. Principles of fluidization and modeling aspects.....	8
2.1. Particle characterization.....	8
2.1.1 Particle size distribution and morphological parameters.....	8
2.1.2 Particle density definitions.....	8
2.2 Principles of fluidization.....	10
2.2.1 Pressure drop in a fluidized bed.....	10
2.2.2 Bed expansion.....	11
2.2.3 Degree of expansion.....	11
2.2.4 Fluidization flow regimes.....	11
2.3 Modeling aspects.....	13
2.3.1 White box modelling.....	13
2.3.2 Black box modelling.....	19
3. Materials and Methods.....	20
3.1 Particle characterization.....	20
3.1.1 Particle size distribution and morphology.....	20
3.1.2 Particle densities.....	23
3.2 Fluidization experiments.....	28
3.3 Particle orientation.....	30

3.4 Modelling approach	30
3.4.1 AquaGAC model	32
3.4.1.1 System definition	32
3.4.1.2 Model assumptions and limitations	32
3.4.1.3 Model Inputs	32
3.4.2 Data driven model.....	34
4. Results and Discussion	35
4.1 Particle size distribution	35
4.2 Particle densities and morphology	37
4.3 Particle orientation	45
4.3.1 Single particle orientation.....	45
4.3.2 Multiple-particle orientation.....	50
4.4 Fluidization experiments and models.....	52
4.4.1 Expansion Experiments.....	52
4.4.2 Classical model outputs.....	53
4.5 Data driven modelling.....	58
5. Conclusions	61
5.1 Particle size.....	61
5.2 Particle densities determination.....	61
5.3 Models and expansion experiments	62
5.4 Particle orientation	62
5.5 Particle sizing methods.....	62
6. Recommendations	63
6.1 Densities determination.....	63
6.2 Particle size and orientation experiments	63
6.3 Experimental set-up.....	64
6.4 Modelling aspects	64
6.5 Future research	64
References.....	66

Appendix.....	69
Appendix A1 - Main characteristics of activated carbon samples	69
Appendix A2 - Instruments specifications & morphological parameters	71
Appendix A3 – Particle size results.....	83
Appendix A4 – Comparison between different particle measurement methods	119
Appendix A5 - Density measurements.....	128
Appendix A6 – Morphological parameters of the particles.....	141
Appendix A7 – Wetting hours of expansion experiments	151
Appendix A8 – Orientation experiments observations	153
Appendix A9 – AquaGAC model	159
System definition	159
Volume definition	160
Nomenclature.....	160
Calculations	162
Appendix A10 –Expansion experiments data and results	168
Pressure difference.....	168
Carman-Kozeny porosity prediction	176
Porosity prediction error	190
Appendix A11 –Symbolic regression outputs	195
Symbolic Regression nomenclature	220

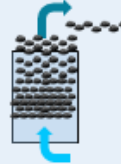
The project in a nutshell



PROBLEM AND RESEARCH QUESTION

PROBLEM

- Media washout
- Adaptability of infrastructure



RQ: IS IT POSSIBLE TO PREDICT “ ϵ ” FOR POROUS MEDIA (GAC)?

YES! It is possible, prediction errors from 2%-12%.

ϵ =porosity

APPROACH

HOW WAS THIS RESEARCH QUESTION TACKLED?

- | | |
|--|---|
| <p>1 <u>Experimental Data</u>
(Hydraulic & morphological)</p> | <p>2 <u>Hydraulic modelling (FBI)</u>
(Classical model comparison)</p> |
| <p>3 <u>AquaGAC input model</u>
(Adaptations for GAC)</p> | <p>4 <u>Data driven models (DDM)</u>
(Empirical correlations)</p> |

1+3+2 \longrightarrow ϵ_{CM}

1+2+4 \longrightarrow ϵ_{DDM}

ϵ_{CM} =Classical model porosity; ϵ_{DDM} = data driven model porosity

METHODOLOGY

HOW TO DO IT?

Using a combination of:

Particle size & morph	Hydraulic parameters	FBI+ AquaGAC model	Data driven model
<ul style="list-style-type: none"> - Microscope - ImageJ - Camsizer - Sieve 	<ul style="list-style-type: none"> - Expansion column experiments 	<ul style="list-style-type: none"> - Classical modelling comparison for GAC 	<ul style="list-style-type: none"> - Empirical expressions (FBI+morph)

1. Introduction

1.1 Thesis background

Waternet is the public water cycle utility in charge of supplying a safe and clean drinking water to the city of Amsterdam and other surrounding municipalities. Waternet has three core values, *service-oriented*, *working effective* and *sustainable*. Special attention has been put to sustainability as the organization has an ambition to reduce their carbon emissions and be climate neutral by 2020. Interests in the use of sustainable materials for drinking water treatment and the adaptability for processes future conditions has led to promote research in understanding the processes that governs several drinking water treatment steps.

Increasing levels of organic micro-pollutants (OMP) in surface water used as a source for drinking water production has led to water supply companies in the Netherlands to integrate activated carbon technologies in the drinking water treatment plants. Since 2013, the Water Framework Directive identified three substances and two pharmaceuticals for the inclusion in the first OMP watch list to identify and select appropriate measures to mitigate the risks posed by these emerging pollutants (Barbosa, Moreira, Ribeiro, & Silva, 2015).

As activated carbon unit processes became increasingly important for water supply companies in their treatment schemes, the design and operation of these units became a relevant factor in the production of drinking water due to the emergence of OMPs and other unwanted contaminants. To reduce the head-loss in GAC filtration units, they need to be backwashed to flush out unwanted particles trapped between GAC media. This is typically achieved by reversing the normal downward flow and fluidizing the media at a certain velocity, causing the media to expand and attached particles to flush out of the reactor. This report will focus on the prediction of how GAC particles expand in a fluidized condition.

1.2 Problem description

Operational constraints of the activated carbon filters like the degree of expansion and grain stratification are influenced by the water temperature, flow, particle size, particle size distribution and shape. In particular, the degree of expansion in the GAC bed is not predicted accurately. This can lead to two main operational problems, media washout and solids accumulation. If backwash velocities are too high, media washout is likely to happen. This results in high economic losses for water companies or drinking water treatment plant operators. If backwash velocities are too low, solids accumulation or formation of mud balls is likely to happen. This not only affects the filter performance, it also leads to increased backwashing operations which results again in increased operational expenses.

In addition, when adapting existing infrastructure to serve different process conditions (for instance to adapt a sand filter to a GAC filter), the adequacy of filter media must be re-evaluated.

Another problem with fluidization of GAC is that the particle size distribution might have negative effects on water quality. GAC filters need to be stratified to prevent the movement of contaminant-saturated particles to lower parts of the bed, which increases the risk of being desorbed and compromise the effluent of this treatment process. Understanding the fluidization behavior of porous media like GAC can improve the decision process of managers and increase the resiliency of infrastructure.

1.3 Knowledge gap

Scientific papers dating from the 1930's (Carman, 1937) described the hydraulic behavior of non-spherical particles using shape factors that intend to describe the particle's morphology through sphericity, surface area to volume ratios or other types of correlations using spheres. These empirical correlations however, are mostly shape specific or only valid for specific hydraulic flow regimes (Mcnown & Malaika, 1950).

Several experimental investigations concerning activated carbon fluidization and particle size distribution have also been performed. Experimental data presented by (van Lier, 1984) revealed that the different models that he applied to describe the fluidization behavior of different types of activated carbon performed well only to specific carbon types and conditions. Similarly, findings of (Akkoyunlu, 2003) point out that the proposed model seems to fit well but also had limitations in the accuracy and application. (Dabrowski, Spaczyńska, & Mackie, 2008) proposed using a general model to predict the media expansion assuming that the fluidization velocity is inversely proportional to the water viscosity, finding a useful correlation with not exact but acceptable results. The results however increased in accuracy if they were corrected depending on the type of commercial carbon that was analyzed.

In general, there is no agreement in which model is the most adequate to describe the fluidized behavior of irregular shapes, especially for porous media GAC in liquid-solid fluidization processes. It is common practice to use shape factors to correct for particle diameters to improve numerical results, this can be seen in classical models, for example, in the Carman-Kozeny model, based on the work of (Kozeny, 1927) and (Carman, 1937) or (Ergun & Orning, 1949), where they use experimental shape factors to correct the particle diameter. The problem here is that shape factors in the fixed bed state are not suitable for the fluidized state due to the different particle orientation.

To our knowledge, a current model that describes accurately the fluidization behavior of activated carbon grains that differ in particle size distribution, shape, morphology and low particle to fluid density does not exist. The classical hydraulic models in the reviewed literature provide limited applicability for irregularly shaped media, which limits their

optimization. The present study looks towards further closing the current knowledge gap regarding the fluidization behavior of activated carbon grains for drinking water production applications.

1.4 Research question

The main research question discussed in this report will be: How can an accurate model to describe the hydraulic behavior of GAC that differ in particle size, morphology, distribution and density be developed?

The Sub research questions that will be discussed throughout the present report are:

- What is the influence of particle and fluid properties in the porosity of GAC?
- What is the influence of morphological parameters on porosity?
- What phenomenon affects the positioning/re-orientation of the particles?
- How are carbon grains stratified during backwash procedures?
- Why are classical models less accurate in terms of porosity and expansion degree for particles with irregular morphology?

1.5 Hypothesis

The hypothesis used as the basis of this work is: An accurate hydraulic prediction model can be developed to improve the prediction of porosity in the GAC treatment unit process for drinking water treatment.

1.6 Project objectives

This study aims to find a model that is able to predict the porosity of GAC applied in drinking water treatment processes. Existing classical hydraulic models found in the reviewed literature will be compared with experimentally determined expansion characteristics to determine their accuracy and application constraints.

Two goals are targeted to be achieved in this report. The first goal is of academic nature, where a good data set of experimental data and empirical models and correlations for different types of activated carbon will be obtained and compared to existing classical hydraulic models. Based on the findings, the ambition is to use the model for other types of GAC or porous media with similar characteristics, this is considered to be a stepping stone into the understanding of the fluidization behavior of activated carbon grains.

The second goal is focused more in the drinking water engineering full scale or industrial applications, where it looks to contribute in guaranteeing the delivery of the right quantity and quality of drinking water. An important contribution of this research to practical aspects are the lower costs (by preventing media washout), increased sustainability (using less energy to clean activated carbon filters, and sustainable materials) and impacting positively in the image of the water companies as an improved operation of their facilities increases their business performance.

1.7 Project relevance

Several aspects of practical importance were identified from understanding the hydraulic behavior of activated carbon grains under fluidized conditions. It is particularly relevant in the drinking water treatment sector, as the design, optimization and control of widely used GAC units are greatly influenced by the hydraulic behavior of the porous, irregularly shaped and polydisperse particles. Furthermore, this behavior is influenced by the particle morphology, orientation and particle size distribution.

The first aspect is the development of models that can predict bed expansion and porosity. These prediction models can lead to increased process control, process optimization and improved reactor design. Accurate prediction models have the potential to decrease operational and capital expenses, leading to the future design of more robust unit processes that can easily adapt to changing circumstances.

The second aspect is the increase in the unit process resiliency and sustainability. Ambitious sustainability goals of water companies and the adoption of the circular economy models are challenging the current infrastructure of water utilities. This promotes the start of a quest to search alternatives that can deliver the same service while creating a positive impact in the environment in alignment with the circularity objectives. One of these alternatives is to use new sustainable materials, for example substituting fossil based GAC with coconut shell or wood based GAC or other adsorbents with more advanced properties. However, whenever their implementation is required in a water treatment plant, extensive research must be performed to investigate their behavior and the design implications on the existing infrastructure. Having a deep understanding of the unit process, and a readily available model that can take into account shape, pore volume¹ and other material properties, it is possible to cope with these changes and increase the resiliency of the unit process, making it adaptable to meet the desired objectives.

The irregular morphology aspects of this report are relevant to other industrial applications that involve Gas-Solid (G-S) fluidized beds. Gasification, combustion of biomass, drying and pharmacy are examples of applications in the chemical and energy industries, as cited by (Ma, Xu, & Zhao, 2017), of the fluidization behavior of shapes with irregular morphology. Other applications are the coating, drying, granulation, food processing and gas phase polymerization as cited by (Mahajan, Nijssen, Kuipers, & Padding, 2018) or even fluidized bed combustion processes for municipal solid waste particle incineration disposal (Chen, Zhong, & Heindel, 2017). In short, the different insights obtained in this project will spin-off to different industries concerning the fluidization of particles with irregular morphology. The behavior of particles with irregular morphology are also relevant to several industries as fluidized beds involving rod-like particles are often used in chemical and energy industries (Ma et al., 2017).

¹ Refers to the volume of the internal porous structure of GAC particles, refer to section 3 of this document.

1.8 Project approach

In order to answer the main research question of this project, a brief overview of the approach used to tackle the research question will be described in this section.

The main research question of this project is to develop a model that accurately describes the fluidization behavior of GAC in the water phase. The starting point of this project was an existing fluidization model, referred to as the fluid bed inside or FBI² model. Since this model was developed for non-porous calcite pellets, adapting different characteristics of porous media was required to describe the fluidization behavior of GAC particles. This adaptation was done using an input model referred to as the AquaGAC model, which consists on several expressions (based on conservational laws) of the porous media system that perform checks on different parameters of porous media and provides the required inputs for the FBI model.

Both the FBI and AquaGAC model require several inputs to predict the expansion degree of porous media. These inputs were obtained from the characterization of the different samples and experimental data performed (and further described) in the present research.

Finally, to find out the influence of the morphs in the fluidization behavior, two approaches were combined. Using the morphological parameters in combination with the outputs of the combination of the AquaGAC and FBI models, several data driven models were obtained that also describe the fluidization behavior of GAC particles.

A summary of the workflow is presented in the following list:

- 1) Obtain data set 1 for model inputs: particle characterization (particle size, density, morphological parameters, among others).
- 2) Obtain data set 2 for model inputs: Expansion experiments (temperature, differential pressure, flow, bed height, insipient onset points).
- 3) Use data set 1 for the AquaGAC (input) model.
- 4) Use data set 2 for FBI model in combination with the AquaGAC model.
- 5) Use data set 1 and outputs of the AquaGAC+FBI models to develop a data driven model based on the particles' morphological parameters.

1.9 Thesis outline

This report is organized as follows: It starts with the identification of the knowledge gap and challenges for the water sector as it changes to the use of sustainable GAC materials. It then covers the project objectives and research questions to limit the scope of the present report. The next section describes some of the main principles regarding particle characterization and fluidization are explained to provide the reader with a basic a theoretical background.

² The FBI model uses an algorithm to calculate and compare 5 classical models.

Further on, the materials and methods used in the experiments will be explained in detail to illustrate the conditions and characteristics of the activities performed to obtain the data and results. This finally leads to the formulation of conclusions and discussion points, which were based on the data and observations performed in the experiments.

As additional help for the reader that is interested in the details of this investigation, an Appendix is made available at the end of the report. Eleven appendices are organized as follows:

Appendix A1 – The main characteristics of each carbon sample analyzed in this report are provided, including the commercial name, manufacturer, raw material and particle size (d_{10} , d_{50} , d_{90}).

Appendix A2 – The specifications of the utilized instruments in this investigation. For the case of the particle size distribution instruments, a table of the output morphological parameters is presented with the description and units. For the case of the microscope and ImageJ instruments, the results of a validation experiment of their measurements is presented. Additionally, for the specific case of the ImageJ analysis, the workflow followed to obtain the measured results are also presented.

Appendix A3 – The measurements of the particle size distribution using four particle sizing methods for the nine GAC samples is presented. For the case of sieving, the frequency and cumulative distributions are presented. For the case of the microscope, ImageJ and the Camsizer, the cumulative distributions of the minimum (width) and maximum (length) diameters are presented (figures include illustrations of the d_{10} , d_{50} , d_{60} , d_{90}).

Appendix A4 – The obtained diameters with every particle sizing method are presented and compared with the specifications (when available). Minimum and Maximum diameters are presented in separate graphs.

Appendix A5 – Here all the information regarding the measured densities is presented. For the case of the skeletal density, the ten output measurements from the instrument are summarized in a table. For the case of the wet density, the mass conservation inputs and calculation table for the three performed runs are presented. The support 3D images for the particle volume calculation using the microscope as well as the sample profile used to calculate the particle height is illustrated for all the analyzed samples.

Appendix A6 – The obtained morphological matrix of different parameters from the four particle sizing methods are presented. For the description of each parameter please refer to appendix A2.

Appendix A7 – A detailed table with the wetting hours of each expansion experiment is presented.

Appendix A8 – The detailed observations and measured angles of all analyzed flow velocities the orientation experiments are presented.

Appendix A9 – The system definition, nomenclature, and expressions used for the derivation of the AquaGAC model is presented in this section of the document. Refer to this section when an expression for the expansion experiments results is not understood.

Appendix A10 – The differential pressure measurements as well as the Carman-Kozeny porosity for all the thirty expansion experiments is presented. In addition, the porosity prediction error, output of the AquaGAC model for the d10 and d50 diameters is presented.

Appendix A11 – The output expressions and correlation coefficients of the symbolic regression simulations using the Eureqa³ commercially available software is presented.

³ www.nutonian.com/products/eureqa/

2. Principles of fluidization and modeling aspects

In order to predict the fluidization behavior of GAC, several important input parameters for the modelling exercise are required. The mentioned inputs consist of several particle characteristics (size, density, morphological properties), which are determined using different methods. This section firstly will summarize relevant methods to characterize a particle, then it will introduce the reader to the basic classical fluidization models and finally provide an overview of the models used for this research. The overall purpose of this section is to provide the underlying theory that enhance the understanding of the present report.

2.1. Particle characterization

2.1.1 Particle size distribution and morphological parameters

There are three different methods that are typically used to define the size and morphology of particles. The first one is sieving (refer to Figure 7), a frequently applied method in which one physically separates particles using a mesh. Particles smaller than the mesh size can pass through to another mesh and larger particles will stay in the mesh.

The second method is static image analysis, where one can take a referenced picture or scan of a sample and using specialized software (such as ImageJ-refer to Figure 5) that analyses pixels, it is possible to compute the size and different morph parameters of each particle in the picture. This method outputs different dimensions of irregularly shaped particles and many other morphological parameters.

The third and last method used is dynamic image analysis (Figure 6), where it is possible to analyze thousands of pictures of falling particles with high speed cameras coupled with a specialized software. The main advantage of this method is the speed and accuracy that it provides to analyze a more complete and representative sample of particles.

2.1.2 Particle density definitions

Particle density is a critical parameter influencing the fluidization behavior of particles. It strongly influences both the porosity and bed expansion expressions. There are however, several densities associated with a particle, the main ones are defined in the following list according to (CEFIC, 1986):

- a) Bulk (vibrated) density - Mass of a unit volume of the sample in air, including voids and pores between particles. Normally used for packing volume. Usually performed using a measuring cylinder according to ASTM D 2854. It is important to mention that the bed is not stratified when the density is measured.
- b) Skeletal (helium) density - Mass of a unit volume of the solid carbon skeleton (excluding the porosity and void bed, this only includes the open pores but not the closed pores of the carbon). Usually performed using gas displacement with a helium pycnometer.

- c) Particle (envelope) density - Mass of a unit volume of the carbon particle (including its open pores). Usually performed using a mercury intrusion pycnometer.
- d) Wet density - This refers to the wet mass per unit volume of a particle. Normally obtained using a pycnometer after the carbon has been wetted for at least 144 hours. This density is basically the skeletal density but the mass considers that the open pores are completely filled with water. Refer to the materials and methods part for a more detailed description of how this density was obtained.
- e) Absolute density - Refers to the mass of a unit volume of the carbon particle (including its open and closed pores). This volume is usually approximated with the help of other methods as the closed pores of the material are inaccessible and cannot be measured accurately.

Figure 1 illustrates how these different densities differ from each other based on the considered volume in which they are calculated. The bulk volume takes the know volume of a container and divided by the mass of a sample of particles the bulk density can be obtained. When analyzing only the particle, the envelope volume is the volume that includes the open and closed pores of one particle. Now if the volume of open pores of the particle are subtracted from the envelope volume, we obtain the skeletal volume and with it the skeletal density. Finally, if we subtract the volume of closed pores to the skeletal volume we obtain the absolute volume and with it the absolute density.

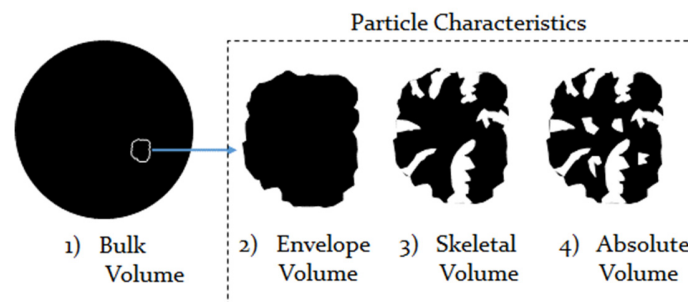


Figure 1 –Particle volume definitions, adapted from (Micrometrics, 2010)

Due to the porous nature of activated carbon particles, measuring the density is not a straightforward process. It is important to differentiate the volumes that make up a porous GAC particle as well as the different techniques used to measure these volumes. Different densities are required for fluidization equations to accurately calculate the porosity and pressure drop, as these expressions are very sensitive in terms of the density it is important to have accurate values. In the materials and methods section of the present document, the main aspects of techniques on how to measure each of these volumes will be covered.

As a side note, another important parameter for GAC is usually the surface area, as this is directly related to the adsorption capacity of the material. This however is out of the scope of this research.

2.2 Principles of fluidization

In the following section, basic principles of fluidization will be explained to enhance the understanding of further sections of the present research.

2.2.1 Pressure drop in a fluidized bed

A packed bed starts to fluidize when the difference in pressure (ΔP) is approximately equal to the weight of the bed. This happens when the analyzed fluid, in this case water, has reached the minimum fluidization velocity (v_{mf}), illustrated in Figure 2. This phenomenon occurs mainly because the drag force that the fluid is exerting on the solids bed is equal to the gravitational force holding the particles inside the reactor/column.

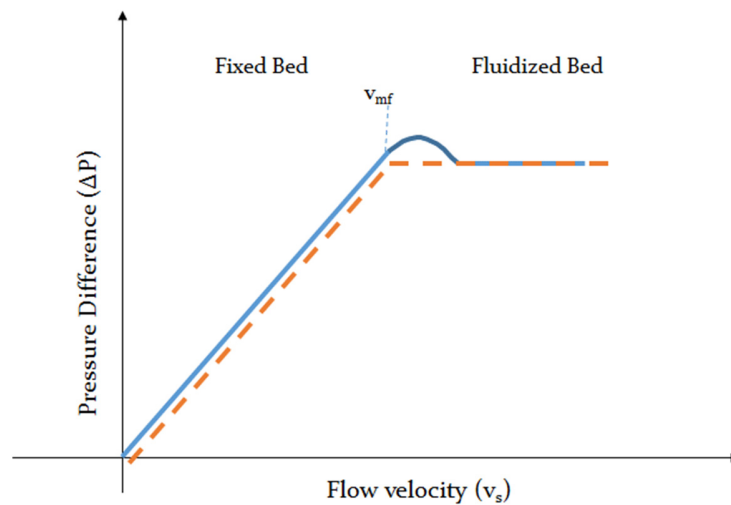


Figure 2 - Pressure drop in a fluidized bed

From this point on, the pressure different will remain constant and if the bed experiences other increases in the flow velocity it would only result in changes in the bed height and the bed porosity. The blue solid line illustrated in Figure 2 represents the normal theoretical fluidization curve, in some cases (especially when dealing with spherical particles) it is possible to find a small bump due to the initial packing of the bed. The particles need a slightly higher velocity to unpack and then stabilize again with the minimum fluidization velocity's constant pressure. The dashed line in represents the de-fluidization curve.

To describe the pressure drop in a fluidized bed, an expression (equation (1)) relating the liquid and particle densities, length of the bed, porosity and the gravitational force can be used (Richardson, 1954).

$$\frac{\Delta P}{L} = (1 - \epsilon_{ext})(\rho_{wet} - \rho_f)g \quad (1)$$

Where:

ΔP - Pressure drop head loss [kPa]

L - Fixed bed height [m]

ε_{ext} – External porosity or voidage of the system [m^3/m^3]
 ρ_{wet} – Wet (saturated) density of GAC [kg/m^3].
 ρ_f – Fluid density [kg/m^3]
 g – Local gravitational field of earth equivalent to the free-fall acceleration [m/s^2]

2.2.2 Bed expansion

Another basic principle of fluidization is the bed expansion, which is frequently used in GAC backwashing procedures. A relationship between the bed height in porosity is illustrated in equation (2), as cited by (Yang, 2003).

$$\frac{L}{L_{mf}} = \frac{(1 - \varepsilon_{mf})}{(1 - \varepsilon_{ext})} \quad (2)$$

Where:

L – Fixed bed height [m]
 L_{mf} – Fluid bed height (minimum fluidization) [m]
 ε_{ext} – External porosity or voidage of the system [m^3/m^3]
 ε_{mf} – External porosity or voidage of the system in minimum fluidization [m^3/m^3]

It is important to mention that there are different models that predict porosity for different flow regimes. These will be further described in the modelling aspects section of the document.

2.2.3 Degree of expansion

When the particles are in fluidization state, the pressure drop on the bed will be constant even though the bed height will keep increasing. The degree of expansion, which is an indication of how much the bed expands in comparison to the original fixed bed state, can be calculated using equation (3).

$$E = \frac{L_{mf}}{L} - 1 \quad (3)$$

Where:

E – Bed expansion [%]
 L – Fixed bed height [m]
 L_{mf} – Fluidized bed height [m]
 ε_{ext} – Fixed bed external porosity or voidage of the system [m^3/m^3]

2.2.4 Fluidization flow regimes

Another important aspect concerning fluidization are the laminar, transitional and turbulent flow regimes that apply. In order to determine the flow regimes for a particle in fluidized conditions, the particle Reynolds number is typically used (equation (4)). If equation (4) is corrected with the external porosity, a Reynolds number applicable for a fluidized bed can be applied as defined in equation (5). For the case of particle settling, the

single particle Reynolds number under terminal settling conditions is defined in equation (6).

$$Re_p = \frac{\rho_f d_p v_s}{\eta} \quad (4)$$

$$Re_\varepsilon = \frac{\rho_f d_p v_s}{\eta} \frac{1}{1 - \varepsilon_{ext}} \quad (5)$$

$$Re_t = \frac{\rho_f d_p v_t}{\eta} \quad (6)$$

Where:

Re_p – Particle Reynolds number [-]

Re_ε – Modified particle Reynolds number [-]

Re_t – Terminal settling Reynolds number [-]

ρ_f - Fluid density [kg/m³]

d_p – Particle diameter [m]

v_s - Linear superficial velocity or empty tube fluidisation velocity [m/s]

η - Dynamic fluid viscosity [kg/m/s]

v_t – Terminal particle settling velocity [m/s]

ε_{ext} – External porosity or voidage of the system [m³/m³]

In general, there is no agreement in which are the exact values of the modified particle Reynolds number to classify each of the flow regimes. For the purposes of this report a combination of findings of different authors will be utilized as a reference as presented in Table 1.

Table 1 – Modified particle Reynolds number flow regime limits

Flow Regime	Source	Re_ε limits
Laminar	(Kozeny, 1927)	$Re_\varepsilon < 2$
	(AWWA, 2011)	$Re_\varepsilon < 6$
Transitional	(Carman, 1937)	$2 < Re_\varepsilon < 600$
	(Ergun & Orning, 1949)	$2 < Re_\varepsilon < 2,000$
Turbulent	(Burke & Plummer, 1928)	$Re_\varepsilon > 2,000$

In many water treatment applications, higher velocities are required to achieve fluidization of particles and the flow may be in the transitional regime (AWWA, 2011). When backwashing a filter for example, the fixed bed first goes through a laminar flow regime, then goes up to, and maintains a transitional flow regime.

It is important to mention that for gas-liquid-solid (G-L-S) fluidization systems the fluidization flow regimes vary. Authors like (Kunii, Daizo; Levenspiel, 1991) illustrate the different types of fluidized beds when gas or a liquid are used for fluidization (refer to

Figure 3). Different flow regimes are very relevant for this study as they can affect the particle orientation or imply particle wash-out.

Furthermore, (Briens, Briens, Margaritis, & Hay, 1997) found three different types of fluidized beds (Fluidized bed, Agitated bed, Compacted bed) in their investigation using low density particles. (Chen et al., 2017) found six flow regimes for rods gas-solid experiments in a bed containing water silica sand and rod-like particles. In general, when comparing G-L-S to L-S fluidization, different flow regimes can be identified. Bubbling fluidization might only be present in GAC backwashing processes when air scouring is utilized.

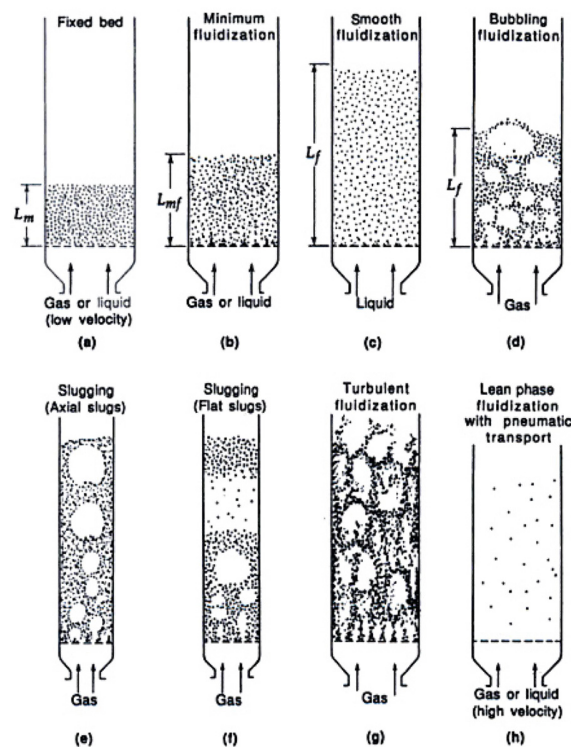


Figure 3 – Types of fluidized beds (Kunii, Daizo; Levenspiel, 1991)

2.3 Modeling aspects

In this section, an overview of existing white box (classical) and black box or data driven (based on symbolic regression) models that describe different aspects of the fluidization behavior of particles is provided.

2.3.1 White box modelling

A white box model is a model that is based on conservational laws, it is possible to construct it from prior knowledge and physical insights about the system (Ljung, 2001). For the point of interest of this study, several authors have proposed models for the fluidization of particles (normally assumed perfectly round spheres). A brief overview of the most relevant fluidization and drag models will be explained in the following sections.

2.3.1.1 Fluidization models

- Hagen-Poiseuille (1846)

The Hagen-Poiseuille expression (equation (7)) describes the laminar flow resistances in a cylindrical pipe (Sutera & Skalak, 1993). When applying this expression for fluidization purposes, it assumes that fluidization behaves in the same way as multiple capillaries. This expression was used as the basis for the different hydraulic models developed by scientists that followed, for example Kozeny.

$$\frac{\Delta P}{L} = \frac{8\nu Q}{\pi g r^4} \quad (7)$$

Where:

ΔP - Pressure drop head loss [kPa]

L - Length of capillary [m]

g - Local gravitational field of earth equivalent to the free-fall acceleration [m/s²]

Q - Volumetric flow rate of capillary [m³/s]

r - Hydraulic radius [m]

ν - Kinematic viscosity [m²/s]

- Kozeny (1927)

Kozeny defined a fluidization expression (equation (9)) by transferring the theory of capillary flow (developed by Hagen-Poiseuille) to a packed bed of particles. The main assumption that he made was that the relation of the void volume and the surface area of particles in a packed bed is the same as in the capillaries. The basis of this assumption was that the drag force exerted on the particles are more or less the same as the drag force on the inner side of the capillaries.

It is important to mention that the Kozeny expression is a semi-empirical equation as it was derived on mathematical expressions, but utilizes a constant to fit the data based on empirical experiments. The main limitation of the Kozeny expression is that it is only applicable for laminar flow (refer to Table 1) for Reynolds numbers details.

$$C_D = \frac{180}{Re_\varepsilon} \quad (8)$$

$$\frac{\Delta P}{L} = 180 \frac{v_s \eta (1 - \varepsilon_{ext})^2}{d_p^2 \varepsilon_{ext}^3} \quad (9)$$

Where:

ΔP - Pressure drop head loss [kPa]

L - Bed height [m]

d_p - Particle diameter [m]

v_s - Linear superficial velocity or empty tube fluidization velocity [m/s]

η - Dynamic fluid viscosity [kg/m/s]

ε_{ext} – External porosity or voidage of the system [m³/m³]

C_D – Drag coefficient [-]

Re_ε – Modified particle Reynolds number [-]

- Carman-Kozeny (1937)

The Carman-Kozeny expression (equation 11) is a special form of the Darcy's law, with the exception that the resistance coefficient value is expressed in other known parameters. This equation tries to solve the limitations of the original Kozeny equation and describes the fluidization at a laminar and transitional flow regimes. As in a packed bed you do not have straight capillaries, water flow is constantly changing in direction.

$$C_D = \frac{180}{Re_\varepsilon} + \frac{2.87}{Re_\varepsilon^{0.1}} \quad (10)$$

$$\frac{\Delta P}{\Delta L} = 180 \frac{v_{mf} \eta (1 - \varepsilon_{mf})^2}{d_p^2 \varepsilon_{mf}^3} + 2.87 \frac{\rho_f^{0.9} v_{mf}^{1.9} \eta^{0.1} (1 - \varepsilon_{mf})^{1.1}}{d_p^{1.1} \varepsilon_{mf}^3} \quad (11)$$

Where:

ΔP - Pressure drop head loss [kPa]

L - Bed height [m]

d_p - Particle diameter [m]

v_{mf} - Superficial fluid velocity [m/s]

η - Dynamic fluid viscosity [kg/m/s]

ε_{mf} - External porosity or voidage of the system [m³/m³]

C_D - Drag coefficient [-]

Re_ε - Modified particle Reynolds number [-]

- Ergun (1954)

The Ergun equation was developed to describe the pressure drop across a packed bed for laminar, transitional and turbulent flow conditions. He performed experiments using a broad data set that included particles with different shapes and sizes. As seen in equation 11, this expression has two terms, the first term describes the laminar flow and the second term turbulent flow. When laminar flow conditions occur, the first terms dominates and this expression reduces to similar expression as the Carman-Kozeny equation with some slight variations. When turbulent flow conditions are applicable, the second term of this expression dominates and both density and the squared flow velocity have relationship and play an important role in the expression. As in a packed bed you do not have straight capillaries, water flow is constantly changing in direction. Ergun considered this phenomenon by adding a tortuosity factor in his expression.

$$C_D = \frac{150}{Re_\varepsilon} + 1.75 \quad (12)$$

$$\frac{\Delta P}{\Delta L} = 150 \frac{v_{mf} \eta (1 - \varepsilon_{mf})^2}{d_p^2 \varepsilon_{mf}^3} + \frac{7 \rho_f v_{mf}^2 (1 - \varepsilon_{mf})}{4 d_p \varepsilon_{mf}^3} \quad (13)$$

Where:

ΔP - Pressure drop head loss [kPa]

L - Length of fixed bed [m]

d_p - Particle diameter [m]

v_{mf} - Minimum fluidization superficial fluid velocity [m/s]

η - Dynamic fluid viscosity [kg/m/s]

ρ_f - Fluid density [kg/m³]

ε_{mf} - External porosity or voidage of the system [m³/m³]

C_D - Drag coefficient [-]

Re_ε - Modified particle Reynolds number [-]

- Richardson-Zaki (1954)

Richardson and Zaki developed a fluidization model based on the behavior of settling particles. They investigated the effects that delayed particle settling due to the concentration of many particles. Extensive data from different sources was used to find a very simple expression (equation (14)), which is still cited in many chemical engineering handbooks today.

$$\varepsilon^n = \frac{v_s}{v_t} \quad (\varepsilon_{mf} < \varepsilon_{ext} < 1) \quad (14)$$

Where:

v_s - Linear superficial velocity or empty tube fluidization velocity [m/s]

v_t - Terminal particle settling velocity [m/s]

ε_{mf} - External porosity or voidage of the system in minimum fluidization [m³/m³]

ε_{ext} - External porosity or voidage of the system [m³/m³]

n - Richardson-Zaki index [-]

This expression depends on an empirical index (“n”) that is related to the Reynolds particle number for terminal velocity conditions (Re_t). Equation 7 illustrates how the Re_t is defined and for terminal velocity conditions. Table 2 provides the ranges of applicable “n” values for different flow regimes.

Table 2 - Applicable empirical index “n” for different flow regimes.

Flow Regime based on Reynolds number	Richardson-Saki n value
$Re_t < 0.2$	$n = 4.65$
$0.2 \leq Re_t < 1$	$n = 4.4 Re_p^{-0.03}$
$1 \leq Re_t < 500$	$n = 4.4 Re_p^{-0.1}$
$Re_t \geq 500$	$n = 2.39$

The main limitation of this expression is that it was developed for monodisperse spheres. Even though, the authors mention that the obtained relations can be used for non-spherical particles by using dimensionless coefficients as a criterion of the shape, they disregard the applicability for porous media and non-spherical particles that are in the transitional flow regime. Another important limitation is that settling velocities must still be determined experimentally.

- Improved Richardson-Zaki equation

The accuracy in predicting the minimum fluidization porosity of the Richardson-Zaki equation was improved with an expression developed by (Kramer et al., 2018) using a model based on hydraulics (refer to equations (15) and (17)). With a combination of the Carman-Kozeny and the Brown-Lawler (equation (17)) equations promising results were made for particles applied in the softening process for drinking water production.

$$n = \frac{\log\left(\frac{Re_{\varepsilon,mf}}{Re_t}(1 - \varepsilon_{mf})\right)}{\log \varepsilon_{mf}} \quad (15)$$

$$Re_{\varepsilon,mf} = \frac{\rho_f d_p v_{mf}}{\eta} \frac{1}{1 - \varepsilon_{mf}} \quad (16)$$

$$C_D = \frac{24}{Re_t} (1 + 0.15 Re_t^{0.681}) + \frac{0.407}{1 + \frac{8710}{Re_t}} \quad (Re_t < 200,000) \quad (17)$$

$$C_D = \frac{4}{3} \frac{g d_p (\rho_p - \rho_f)}{v_t^2 \rho_f} \quad (18)$$

Where:

n - Richardson-Zaki index [-]

$Re_{\varepsilon,mf}$ - Modified particle Reynolds number at minimum fluidization [-]

Re_t - Terminal settling Reynolds number [-]

ε_{mf} - External porosity or voidage of the system in minimum fluidization [m^3/m^3]

d_p - Particle diameter [m]

v_{mf} - Minimum fluidization superficial fluid velocity [m/s]

ρ_f - Fluid density [kg/m^3]

η - Dynamic fluid viscosity [$kg/m/s$]

C_D - Fluid dynamic drag coefficient [-]

- Van Dijk (1991)

The van Dijk model (Dijk, Van & Wilms, 1991) is another popular fluidization model that uses the same basis as the Kozeny model, but uses $n=0.8$ and $K_{CK}=3.61$ which is applicable to the transitional-turbulent flow instead of $n=1$ and $K_{CK}=5$ applicable only for the laminar flow. This model will serve as an additional point of comparison to estimate the external porosity and compare it with the experimental data.

$$C_D = \frac{36K_{CK}}{Re_\varepsilon^n} \quad (19)$$

$$\frac{\Delta P}{\Delta L} = 36K_{CK} \frac{\eta^n \rho_f^{1-n} v_s^{2-n}}{d_p^{n+1}} \frac{(1 - \varepsilon_{ext})^{n+1}}{\varepsilon_{ext}^3} \quad (20)$$

Where:

- K_{CK} - Carman-Kozeny coefficient [-]
- n - Carman-Kozeny index coefficient [-]
- ε_{ext} - External porosity or voidage of the system [m³/m³]
- d_p - Particle diameter [m]
- v_s - Linear superficial fluid velocity [m/s]
- ρ_f - Fluid density [kg/m³]
- C_D - Drag coefficient [-]
- Re_ε - Modified particle Reynolds number [-]
- η - Dynamic fluid viscosity [kg/m/s]

2.3.1.2 Drag models

The drag is another critical factor in the fluidization behavior. In the present study, the equation proposed by (Hölzer & Sommerfeld, 2008) was used to gain more insights regarding the orientation of the rod-like particles.

- Holzer-Sommerfeld

(Hölzer & Sommerfeld, 2008) developed a correlation that can predict the single particle drag coefficient for irregularly shaped particles. As seen in equation (21), the expression relates the sphericity, crosswise sphericity, lengthwise sphericity and the particle Reynolds number. As the sphericities depend only on the particle area, this expression can be easily applied if the particle size, particle orientation angle and particle Reynolds are known. The four terms that compose the Holzer-Sommerfeld equation describe the drag coefficient for a single particle for the entire range of particle Reynolds numbers in terms of the particle orientation. The first two terms have the best correlation for the stokes region and the last two terms for the newton region.

$$C_D = \frac{8}{Re_p} \frac{1}{\phi_{ll}} + \frac{16}{Re_p} \frac{1}{\sqrt{\phi}} + \frac{3}{\sqrt{Re_p}} \frac{1}{\phi^{\frac{3}{4}}} + 0.4210^{0.4(-\log\phi)^{0.2}} \frac{1}{\phi_+} \quad (21)$$

Where:

- C_D - Drag coefficient [-]
- ϕ_{ll} - Lengthwise sphericity [-]
- ϕ_+ - Crosswise sphericity [-]
- ϕ - Sphericity [-]
- Re_p - Particle Reynolds number [-]

2.3.2 Black box modelling

A black box model of a system is one when you do not need previous knowledge of the character or physics of the relationships involved (Ljung, 2001). As mentioned by (Ljung, 2001), black box models serve as a good guide whenever there is a considerable amount of “noisy” data from which a function or expression must be estimated. Only the symbolic regression model will be described in this subsection.

- Symbolic Regression models

Symbolic regression (SR) is the process of determining the symbolic function, which describes a data set-effectively developing an empirical model, which summarizes the data and is useful for predicting response behaviors as well as facilitating human insight and understanding (Awange & Paláncz, 2016). This particular model works based on a genetic algorithm, where only the fittest population of functions are selected to reproduce and construct subsequent generations of better functions following the evolutionary theory approach. These types of models have two main features, complexity and fitness (Awange & Paláncz, 2016). The user must find the balance between a very complex and accurate model or a very simple but inaccurate model. The objective of these types of models is to find functions and coefficients that minimize as much as possible the prediction errors. The main setback for this model is the strong demand for computational power (Awange & Paláncz, 2016) and a representative data set.

3 Materials and Methods

This section intends to describe in depth the experiments performed for the reader to familiarize with the experimental set-up, conditions and other important considerations that were used to acquire the data of the present project.

3.1 Particle characterization

For this investigation, nine GAC samples were analyzed due to their geometry, they can be classified into three different categories: spherical, non-spherical (granular) and rod-like. The overall particle characterization that will be discussed consists of particle size, morphology (geometrical properties) and density (skeletal, wet and bulk densities).

Table 3 summarizes the name of the sample, manufacturer and type organized by category. A comprehensive table with all the main characteristics of the samples is presented in section A1 of the appendix.

Table 3 – Overview of GAC particles.

Name	Manufacturer	Type	Picture
Saratech Spherical	Blücher	Synthetic polymer	
Filtrisorb 300 C	Calgon	Fossil	
Filtrisorb TL830	Calgon	Fossil	
Aquasorb K-GA	Jacobi	Coconut shells	
Aquasorb K-6300	Jacobi	Fossil	
Resorb HC	Jacobi	Fossil	
Norit GAC 830	Cabot	Fossil	
Norit ROW o.8 Supra	Cabot	Wood	
Norit RB 4C	Cabot	Wood	

3.1.1 Particle size distribution and morphology

In order to correctly determine the particle size and morphology of the different GAC samples, three methods were used: *microscope* static image analysis, *ImageJ*⁴ static image analysis and *Camsizer* dynamic image analysis.

- Microscope static image analysis

High-resolution images (up to 20,000 x 20,000 pixels) taken from a digital microscope (model VHX 5000, illustrated in Figure 4) were analyzed to determine the average particle morphology and particle size distribution. With the help of an embedded image processing system, this microscope can accurately measure particles in 2D and 3D. In order to make

⁴ Free image processing and analysis program.

sure that the samples are representative, at least 300 particles were used per image as recommended by (Mauget, Montillet, & Comiti, 2005) and (Yang, 2003). This will guarantee that the standard deviation of the average geometrical properties remains relatively stable. Three sets of measurements were performed for every GAC sample. The embedded software also provides several morphological characteristics based on pixel operation. A table with the microscope's specifications and a list of the measured morphological parameters are presented in Appendix A2. The main advantages of this method are the great accuracy in measuring particles with a good range of sizes and its wide range of output morphological parameters. This sophisticated instrument can even produce 3D images of samples and perform some measurements. The main disadvantage of this method is the high cost of the instrument.



Figure 4 – Microscope VHX-5000 (Keyence user's manual)

To validate the measurements, a test was made by measuring the known diameter of 1 euro cent coins. The results are considered satisfactory finding an error less than 1%. Refer to Appendix A2 for an illustration of the coin test and further detail of measured values. further details.

- ImageJ static image analysis

The obtained microscope measurements are corroborated with the ImageJ image processing freeware to establish a reference to guarantee the reliability of the particle size measurements. For this, an Epson V550 scanner (refer to Figure 5) was used to obtain high-resolution images (2,400 dpi) of all samples and then process them in ImageJ. The ImageJ image processing workflow, list and description of morphological parameters obtained and the scanner's specifications is presented in Appendix A2. Similarly to the microscope, the validity of measurements were put to the test in a coin experiment, finding errors around 3% (refer to Appendix A2 for the detailed measurements). This is attributed to the calculation method of the ImageJ as it approximates the maximum and minimum diameter using the axes of the best fitting ellipse. The main advantage of this method is the good

measuring accuracy and the wide range of morphological properties that can be obtained. In addition, this method is very economic and can be easily implemented for any analysis as the only requirement is a scanner and downloading the free software.



Figure 5 - Epson V550 scanner (Epson)

- Camsizer dynamic image analysis

The Camsizer is a commercial instrument that uses dynamic image analysis to determine the particle size distribution. This instrument consists of two high speed cameras that take pictures of falling particles at a steady rate (Figure 6). The built-in software then analyzes these pictures and it outputs a number based or volume based distribution of several parameters of interest. For this study, the parameters of interest were the maximum diameter, the minimum diameter and the area equivalent diameter (X_{Fe_max} , X_{c_min} , and X_{area}), refer to Table 29 in Appendix A2 for a description of each parameter. The main advantages of this instrument is the high volume of particles that it can analyze in a short time period. A brief table with some of the instruments specifications and a list with the definition of the output morphological parameters is presented in Appendix A2.

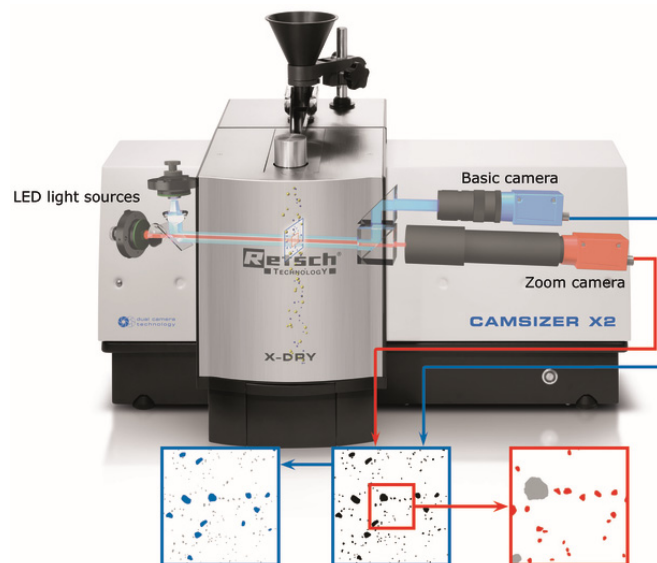


Figure 6 - Camsizer Instrument illustration (Retsch Technology).

- Sieving Analysis

The final validation for the particle size range of each sample was to perform a Sieve analysis using 8 different sieve fractions for every sample. The sieving was performed for a time of 5 [min], an amplitude of 0.8 [mm/g] and an interval of 6 [sec]. These settings were chosen in order to avoid as much as possible error for the rod-like particles, allowing enough time to disperse but not to realign and go to lower sieves.



Figure 7 – Sieve used for experiments.

3.1.2 Particle densities

In this subsection, the determination of the densities (bulk, skeletal, wetted, particle) of interest is further explained.

- Bulk Density

As illustrated in the particle characterization section, the bulk density is determined by placing the material in a container with a known volume and then measuring its mass. To determine this GAC particles were placed in a measuring cylinder until a volume of 1.3 [L] was reached, then the mass of the particles was determined with the use of a scale. This density is also referred as the bed density in this document as the volume and mass measured was the one that was placed in the expansion column. As an important side note, the sample size was determined based on the requirement to experiment on a bed height of at least 50 [cm] to avoid misleading measurements caused by smaller bed volumes.

- Skeletal (Helium) Density

The skeletal density was obtained using the AccuPyc 1330 pycnometer manufactured by Micrometrics, the instrument is shown in Figure 8. This instrument works using the gas (helium) displacement method to determine the volume of a given sample and with the known mass, the skeletal density can be obtained. Table 27 in the appendix illustrates the

specifications of this instrument. In order to guarantee the reliability of the results, ten runs (available Appendix A5) were made for all of the carbon samples with minimal deviations.



Figure 8 – AccuPyc pycnometer.

- Wet particle density

To determine the wet particle density, four methods were used: water displacement pycnometer, mass conservation method, image analysis and differential pressure. The first method consisted on calculating the volume of the carbon particles using water displacement using a pycnometer (Figure 9). The steps performed to determine the wet particle density were the following:

1. Put GAC particles in a sealed container filled with water for at least 48 hours.
2. Obtain the volume of the dry pycnometer. This is a well-defined value that is normally written down in the pycnometer itself.
3. Measure the mass of the pycnometer.
4. Put the GAC particles in a sieve in order to drain the excess water in the particles.
5. Measure the mass of the wet GAC particles.
6. Introduce the measured mass of GAC inside the pycnometer.
7. Fill the remainder of the pycnometers volume with demineralized water.
8. Measure the temperature of the water.
9. Measure the mass of the pycnometer filled with water (to corroborate density of water).



Figure 9 - Water displacement pycnometer

Figure 10 illustrates the experiment and calculation process followed to obtain the wet density of GAC particles. It is important to mention that three sets of this experiment were performed twice, one after particle wetting time of around 48 hours and then again after particle wetting time of more than 130 hours.

Inputs		Calculated values		Calculations
$V_{\text{pycnometer}}$	$m_{\text{pycnometer}}$	m_{water}	V_{water}	$m_{\text{water}} = m_{\text{pycnometer+water+GAC}} - m_{\text{GAC (wet)}} - m_{\text{pycnometer}}$
ρ_{water}	$m_{\text{GAC (wet)}}$	V_{GAC}		$V_{\text{water}} = m_{\text{water}} / \rho_{\text{water}}$
$m_{\text{pycnometer+water+GAC}}$		ρ_{GAC}		$V_{\text{GAC}} = V_{\text{pycnometer}} - V_{\text{water}}$
				$\rho_{\text{GAC}} = m_{\text{GAC}} / V_{\text{GAC}}$

Legend:
 $v \rightarrow$ Volume $m \rightarrow$ Mass $\rho \rightarrow$ Density

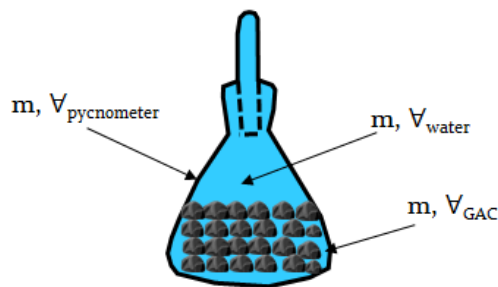


Figure 10 - Pycnometer experiment and wet density determination.

The second method was using the mass conservation principle. Figure 11 illustrates the experiment and calculation process followed to obtain the wet density of the GAC particles using this method. The different steps performed were the following:

1. Use a defined mass of material (6 [g] for this experiment).
2. Add a known volume and mass of water (150 [mL] for this experiment).
3. Let the samples wet for approximately 72 hours in a closed container.
4. After 72 hours, sieve the carbon and measure both the mass of the water left and the mass of wet carbon.
5. This will output a ratio between the wet and dry particles. By multiplying this ratio with the dry particle density, the wet density can be obtained by:

$$\rho_{\text{wet}} = \rho_{\text{dry}} * (m_{\text{wet}} / m_{\text{dry}})$$
6. Calculate the error by comparing the total mass (carbon and water) before wetting the total mass after water adsorption.

Inputs	Calculated values	Calculations
m_{flask} $m_{\text{GAC (dry)}}$	$m_{\text{water-before}}$	$m_{\text{water-before}} = m_{\text{water-before + flask}} - m_{\text{flask}}$
$m_{\text{water-before + flask}}$	$m_{\text{GAC(wet)}}$	$m_{\text{GAC(wet)}} = m_{\text{flask + GAC (wet)}} - m_{\text{flask}}$
$m_{\text{water-after + flask + GAC (wet)}}$	R (wet to dry ratio)	$R = m_{\text{GAC(wet)}} / m_{\text{GAC(dry)}}$
$\rho_{\text{GAC (dry)}}$	$\rho_{\text{GAC (wet)}}$	$\rho_{\text{GAC (wet)}} = R * \rho_{\text{GAC (dry)}}$

Legend:
 $v \rightarrow$ Volume $m \rightarrow$ Mass $\rho \rightarrow$ Density

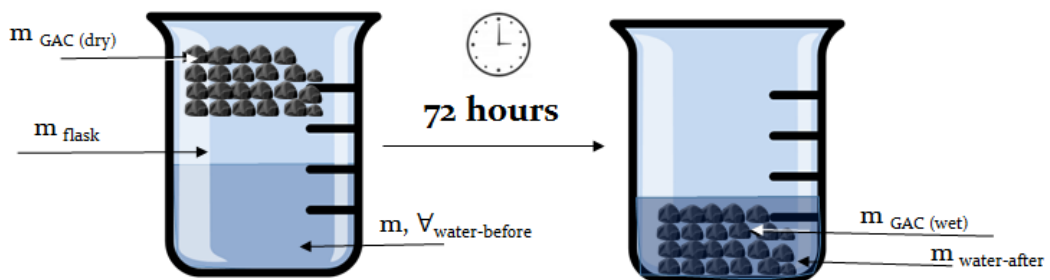


Figure 11 – Mass conservation experiment and wet density determination

The third method was using image analysis. This consisted on using the Keyence VHX-5000 microscope to determine the volume of a sample of particles using the embedded image processing software. Then the particles were wetted for at least 72 hours, then sieved to remove the excess water and finally a measured their wet mass. Figure 12 illustrates the workflow followed to obtain the wet density of the GAC particles using this method.

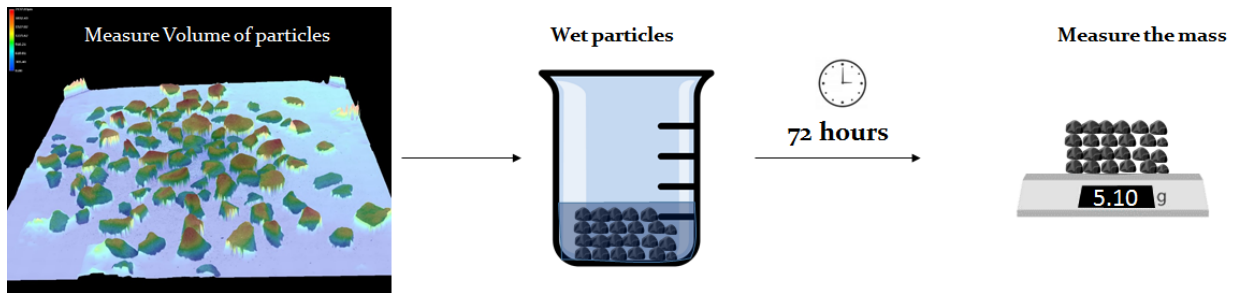


Figure 12 – Image analysis experiment.

Finally, the fourth method was calculating the wet density indirectly, parting from the differential pressure measurements. Applying equation (1) and solving for the wet density delivers the theoretical wet density value for all of the experiments.

- Particle (envelope) density

The particle envelope density is defined as the dry mass of particles in the sample over the envelope volume of these particles (volume includes both the solids and internal pores). This density was calculated using the embedded image analysis software in the VHX microscope. This workflow consisted on obtaining a 3D model of the particles using the image processing software, this model helps us determine the average height of several particles in the sample. After the average height of particles is determined, the area can also be easily calculated and obtain the volume of the particles in the sample. When this envelope volume is known, it suffices to know the mass of the analyzed particles to determine the particle density. Figure 13 illustrates the workflow of this process. Since Saratech samples were too small to determine with the microscope, these were determined using ImageJ in combination with the scanner, providing accurate results due to its fairly homogenous geometry.

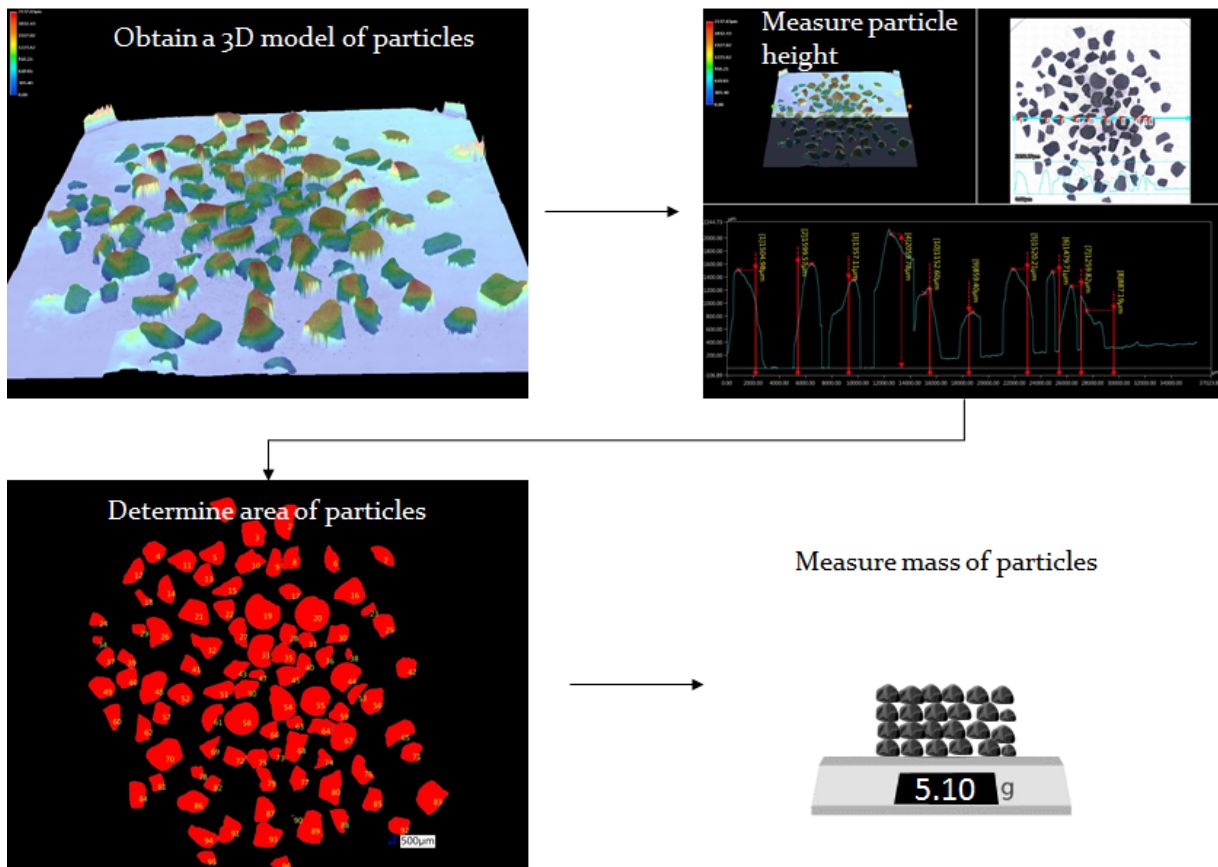


Figure 13 – Particle density determination.

3.2 Fluidization experiments

Fluidization experiments were conducted using the set-up illustrated in Figure 14. The experimental set-up consists on a PVC transparent expansion column of 4 [m] in length and 5.7 [cm] in diameter.

The set-up has two main circuits in which water flows, the expansion circuit and the temperature conditioning circuit. In the expansion circuit, a pump takes water from a buffer water reservoir of 1,000 [L] and feeds water to the expansion column with a certain flow rate. The flow rate that goes into the system can be controlled opening and closing of a valve in combination with an installed flow meter (output in [L/h]).

The temperature conditioning circuit is used to deliver a desired temperature to the expansion circuit to perform expansion experiments at different temperatures. The circuit consists of a pump that feeds water into an integrated heating or cooling unit. The cooling unit can condition the water to a temperature as low as 5 [°C] and the heating unit up to a temperature of 40 [°C]. The effluent of the conditioning unit feeds the flow-checking unit, which is directly connected to the buffer reservoir.

The supporting instruments of the experimental set-up are a flow-checking unit, differential pressure measurement unit, flow measuring unit, measuring tape, stopwatch and a thermometer.

The flow-checking unit is a water reservoir of 50 [L], it has an integrated transparent tube where the water level can be measured with a ruler. With the known water level, the volume can be measured, making it possible to calculate volume in a given time with the help of a stopwatch.

The differential pressure measurement unit consists of two hydrostatic hoses, one measuring the pressure on the bottom of the bed and one on the upper part of the bed. The difference of heights outputs the pressure difference in centimeters of water column.

In order to measure the bed height of the granular material, a metallic measuring tape was secured in the outer wall of the expansion column. An electronic hand thermometer was placed in the buffer reservoir to confirm the output temperature of the heating or cooling units.

Every carbon sample was wetted for at least 135 hours before performing expansion experiments. In Appendix A7, a table with the wetting hours of the experiments is presented.

In summary, the parameters measured with this experimental set-up for 30 experiments using nine different GAC samples were: flow rate [L/h], differential pressure [mwc], temperature [°C], bed height [cm], revised flow rate [L/h].

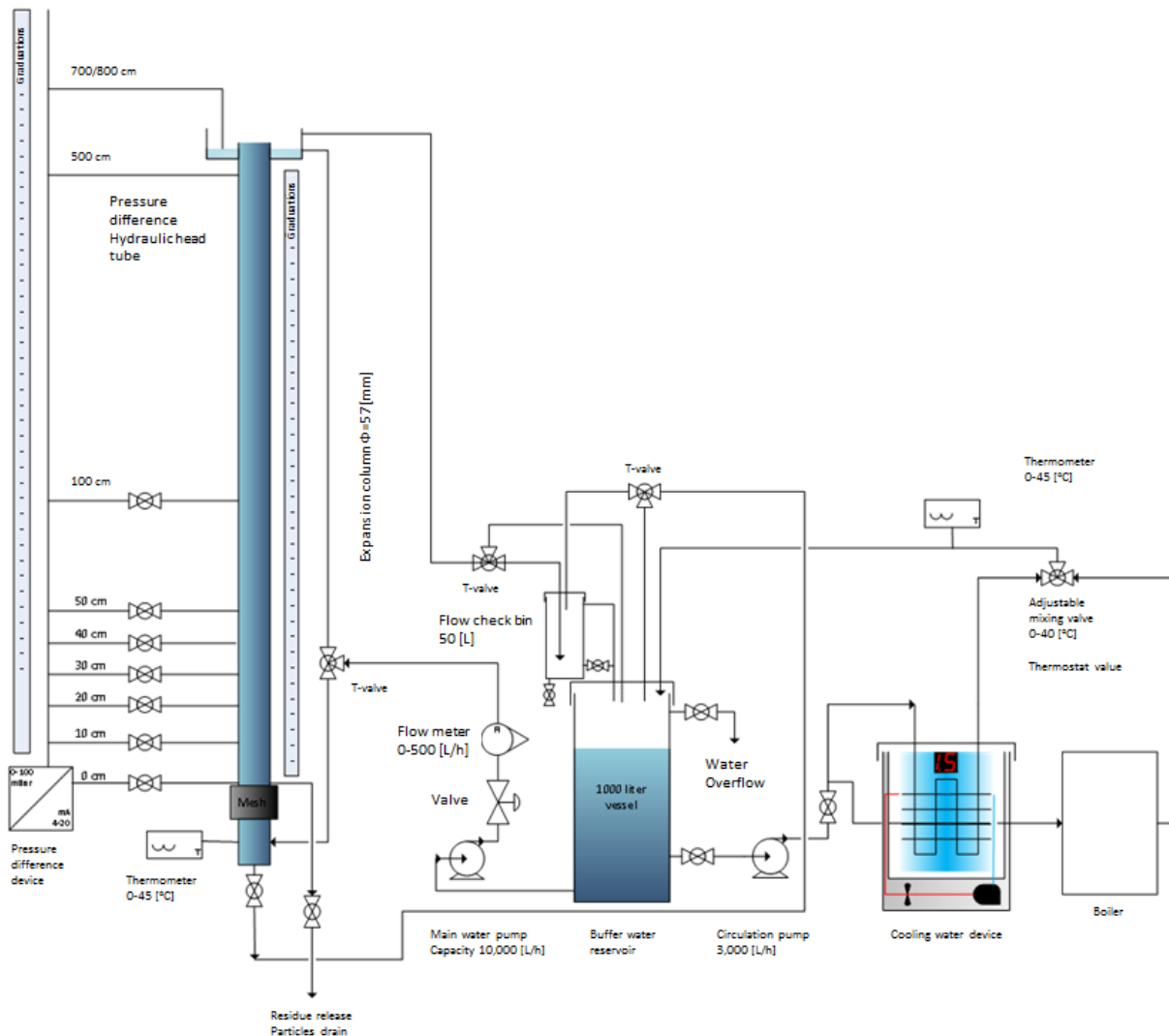


Figure 14 – Fluidization experiments set-up.

3.3 Particle orientation

As a part of the scope of this project was understanding particle orientation, influencing only the two rod-like samples (Norit ROW 0.8 Supra and Norit RB4C). The particle orientation is measured in a CAD software from images of videos taken in the same experimental setup as the fluidization experiments (Figure 14). Single particle orientation videos were taken in a smaller scale expansion column (length: 6 [cm], diameter: 1.3 [cm]) that was fed by the expansion circuit but with a small-bypass.

3.4 Modelling approach

In this section, the modelling approach will be clearly defined. As a good introduction, the reader can refer to Figure 15 for a graphical overview of the modelling approach. The main research question of this project is to develop a model that accurately describes the

fluidization behavior of GAC in the water phase. Two different approaches were used in this scheme that predicted the porosity (degree of expansion in a fluidized bed).

The first approach was using an existing fluidization model referred to as the FBI model. The FBI model is an algorithm that can simultaneously predict the porosity using 5 classical models: Kozeny, Carman-Kozeny, Ergun, van Dijk and Richardson-Saki. Since this model was originally designed for non-porous media, the definition of all the new variables in the system needed to be defined using another input model. This input model, referred to as the AquaGAC model, was derived to describe the main hydraulic characteristics of porous media. The required inputs to predict the porosity was the combination of the AquaGAC model and the expansion (hydraulic) measurements from the fluidization experiments performed.

Modelling approach

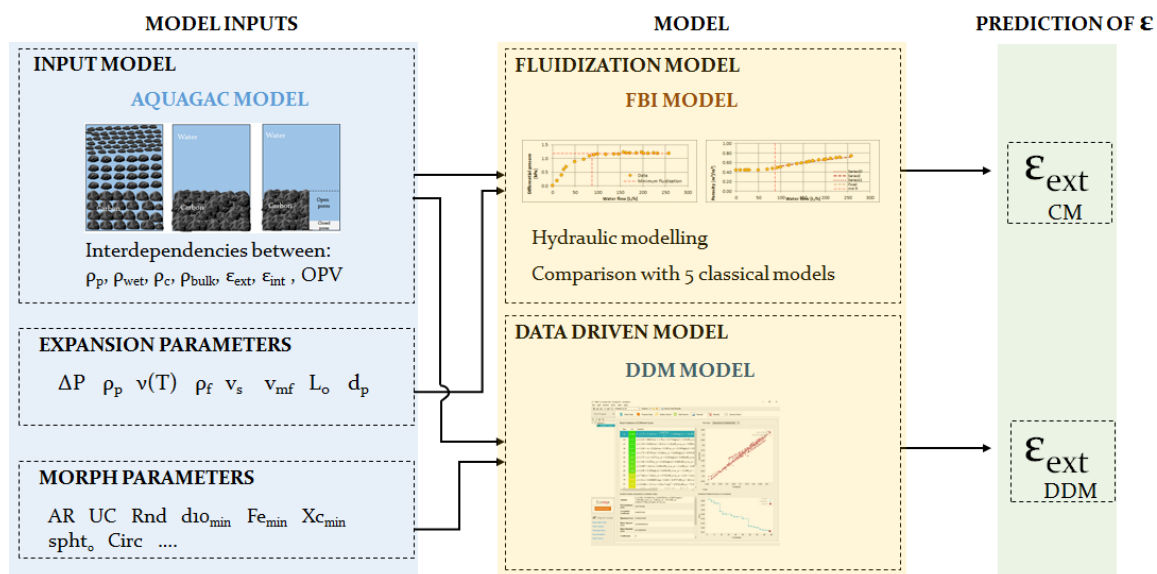


Figure 15 –Modelling approach overview.

The second approach to predict the porosity was with the use of several data driven models (DDMs), where the outputs of the AquaGAC model and the morphological parameters (output of the particle characterization) were combined to determine several empirical equations that have very good accuracy in the prediction of the external porosity. This model is based on symbolic regression and finds expressions with the best correlation of a given matrix of data.

A more detailed description of the AquaGAC and DATA driven models will be described in the following sections.

3.4.1 AquaGAC model

To get further insights in how GAC particles fluidize in water, an input model for porous media was derived to complement an existing fluidization model (FBI). This input model will be referred to as the AquaGAC model. The combination of the AquaGAC, FBI and experimental data, an estimation of the external porosity of the bed can be estimated and compared to the prediction of several classical models.

This section will first present the definition of the system and the derivation of all of the equations utilized to either obtain parameter or to perform checks on the measured data. Then model assumptions and model inputs will be shortly discussed.

3.4.1.1 System definition

In order to provide a better understanding of the parameters and calculations performed to obtain the fluidization model outputs, the GAC system was defined. A nomenclature of the variables used, some figures and the derivation of used expressions are presented in Appendix A9. Around 43 equations could be derived performing mass balances from this system approach. These equations are used to check the consistency of the data and identify possible deviations in the measurements of the particle properties.

3.4.1.2 Model assumptions and limitations

- The volume and mass of closed pores is almost negligible (considered as 0.5% of particle volume). This assumption was based on the percentage of mass of floaters⁵ within the total mass of the sample found in the expansion experiments.
- Differential pressure measurements are accurate and are the starting point of calculations.
- Changes in size of particles due to biofilm growth, particle-to-particle interaction or reactivation are ignored and not considered in this study.

3.4.1.3 Model Inputs

Particle diameter- The hydraulic diameter output of the Carman-Kozeny (C-K) expression (equation (11)). A comparison between the obtained diameters from the all the used methods and the C-K hydraulic diameter are presented in section 5.4.2 of this report.

Wet density – The implemented wet density of particles was calculated (using equation (1)) from the differential pressure measurements. Refer to Table 12 for an overview of the implemented densities.

Skeletal Density – The skeletal density, measured using a helium pycnometer, was used as an input to calculate the particle density and as additional check to ensure agreement with other measured parameters. This decision was taken due to the reliability of the measurements.

⁵ Particles that had a big volume of air trapped inside, which made them buoyant regardless of the wetting degree.

Particle density – The implemented particle density in the model was calculated using the skeletal density. Refer to Table 7 for an overview of the implemented particle densities.

Open pore volume (OPV) – OPV information for most of the GAC samples found in literature, they were normally the output of the mercury porosimetry or nitrogen adsorption techniques, the OPV was always reported in [cm³/g]. This parameter served also as a check to revise data consistency.

Internal porosity – The internal porosity was calculated to check data consistency of several parameters, refer to the internal porosity subsection of appendix A9 for the derived expressions.

Expansion experiments data – The basic required inputs are the characteristics of the column (length and diameter). The measured data from the expansion experiments was differential pressure, volumetric flow, bed height and temperature. From these measurements, the minimum fluidization volumetric flow and bed height as well as the fixed bed height were approximated. Other data collected was the dry mass of the sample, the volume of the sample and consequently the bulk density of each GAC. It is important to mention that there was a small offset in the pressure differences tubes when there was a static (no flow) bed. This deviation was corrected by adding the magnitude of this static bed offset to all of the pressure measurements under the assumption that the offset was the same throughout all of the pressure measurements.

3.4.1.4 Additional checks

A system that uses porous media is much more complex than for solid non-porous materials. This is mainly due to the changes in the particles properties when they are completely saturated. The internal porosity of porous media increases the number of variables that are interdependent to describe the fluidization phenomena in the system.

In order to deal with the system's complexity and assure the consistency of the data, several checks were performed. An overview of all the performed checks is presented in Figure 16. These checks consisted in calculating one parameter of the system based on the other interdependent parameters and check if this parameter delivered similar results than the measurements, specifications or literature.

Let us take the particle density as an example of the performed checks. The particle density was measured using the microscope (green box in illustration). This measurement was an input to calculate the internal porosity, skeletal density, mass of water in the internal pores and open pore volume. The particle density was found in literature (only for two samples) and compared with the obtained value. The measured value could be directly compared with the information in literature, but also could be used to calculate different parameters in the system with the derived expressions using the system approach presented in

Appendix A9. This calculated parameters where checked for reliability (realistic values) and again compared with the measurements.

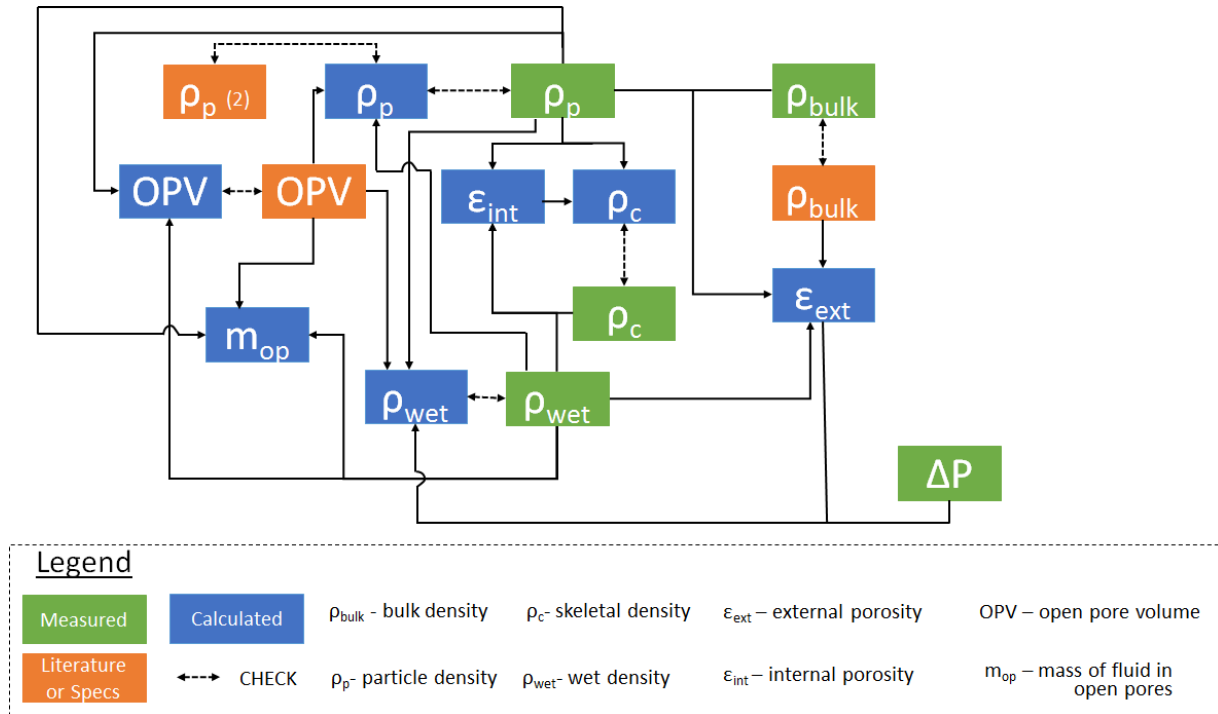


Figure 16 – Overview of performed checks for consistency.

3.4.2 Data driven model

As an additional input for the present report, a data driven model (DDM) model based on symbolic regression was used to obtain an empirical expression that represents the experimental data obtained. One hundred morphological parameters using four particle sizing methods were obtained for all nine GAC samples (refer to Appendix A6 for the complete data set). The following morphological parameters were considered relevant for simulations: Uniformity coefficient, roundness, Feret diameter, aspect ratio, circular equivalent diameter, maximum diameter (length), minimum diameter (width). As only morphological parameters are enough to describe the fluidization behavior, the following hydraulic parameters were also included in the simulations: superficial flow velocity, kinematic viscosity, wet particle density, particle envelope density and skeleton density.

Parting from the combination of morphological, hydraulic parameters and the external porosity outputs of the AquaGAC model, it was possible to obtain a set of empirical equations that were able to calculate the external porosity of the performed experiments quite accurately (refer to Appendix A11 for the equations and correlation coefficients obtained). These equations were obtained with the help of the commercial software *Eureqa*, which using symbolic regression, finds the best fitting correlations between the previously mentioned input parameters.

4 Results and Discussion

In this section the results and discussion of all performed experiments and measurements will be presented. Similarly to previous sections, results will be presented in the following order: particle size distribution, particle densities, particle orientation, expansion experiments and data driven model. As an important note, all calculated errors mentioned in this section refer to the absolute relative error (ARE), presented in equation (22).

$$ARE = \frac{1}{n} \sum_{i=1}^n \left(\frac{|y_{calc,i} - y_{exp,i}|}{y_{exp,i}} \right) \tag{22}$$

Where:

ARE - Absolute relative error

$y_{calc,i}$ - Calculated value

$y_{exp,i}$ - Experimental value

4.1 Particle size distribution

This subsection will illustrate the results obtained for the particle size distribution of all four particle sizing methods employed in this research. In Appendix A3, the cumulative distribution of the particle size measurements of the nine analyzed samples using the sieve, microscope, ImageJ, and Camsizer are presented.

For the case of static and dynamic image analysis methods, the particles maximum (length) and minimum (width) diameters are presented and for the sieve analysis, the cumulative and frequency distributions are presented.

As a brief example, the results of one rod, one rock and one sphere are presented in Figure 17 to Figure 19, respectively. In Appendix A4, a comparison of minimum and maximum particle size measurements produced by all four particle-sizing methods and manufacturers' specifications (when available) is presented.

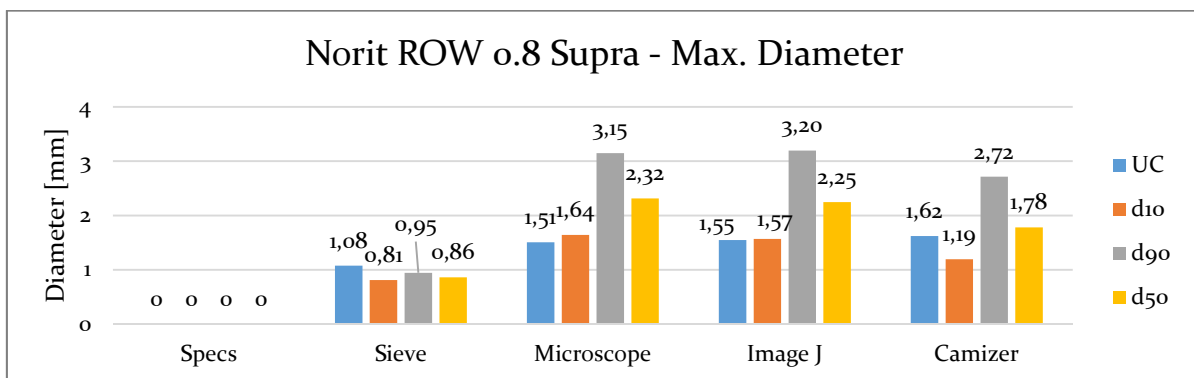


Figure 17- Particle sizing comparison maximum diameter Rod.

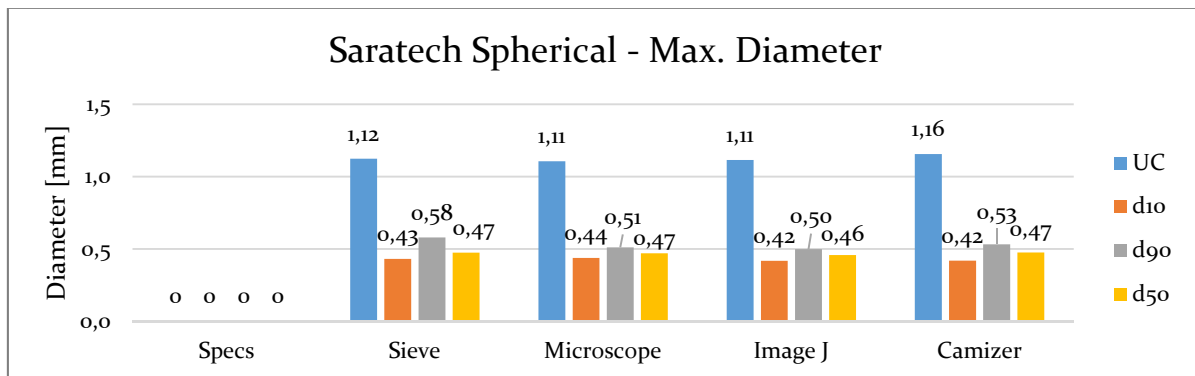


Figure 18 - Particle sizing comparison maximum diameter sphere.

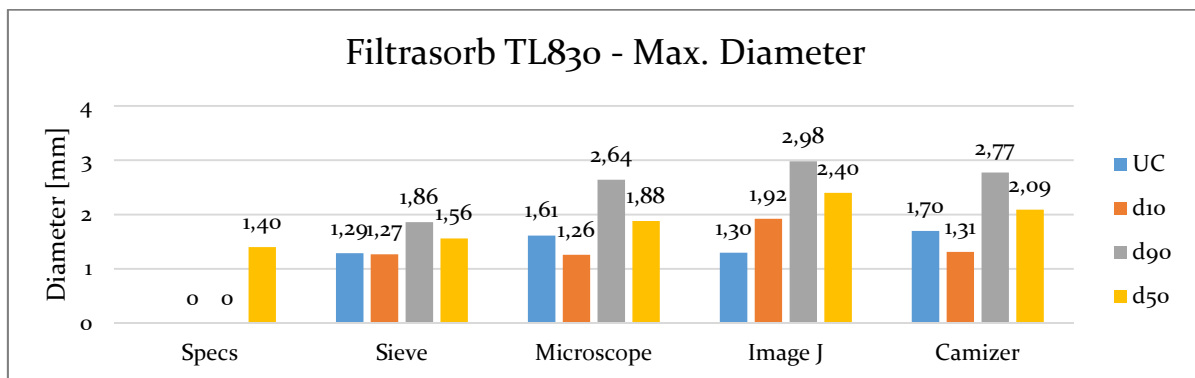


Figure 19 - Particle sizing comparison maximum diameter grain (rock).

Several differences can be observed when comparing the particle size measurements from the different methods applied. The Camsizer data is used as a baseline for all the measuring methods, as it was the method that was able to accurately process a representative sample of particles. When comparing the results of the Camsizer and ImageJ deviations averaging up to 32% can be observed, this is attributed to both a much smaller sample size and small deviations due to the estimation algorithm of the diameter (using the axes of the best fitting ellipse). Both the microscope and the ImageJ results have some agreement with each other (average 15% difference) since they are both static image analysis methods with similar algorithms to measure particle sizes.

The sieve analysis was found to be inadequate to characterize particles with high aspect ratios. In the experiments performed, for rod-like particles, the sieve analysis was only able to measure the minimum diameter (width) of the rods with the sieving configuration used. This can be illustrated in Figure 17, where the maximum diameter (length) of a rod particle is not well described by the sieve data. Another illustration of the inadequacy of the sieve is Figure 20, where it is possible to see the comparison between the error in the sieve measurements compared to the Camsizer and the aspect ratio of the rod-like particles.

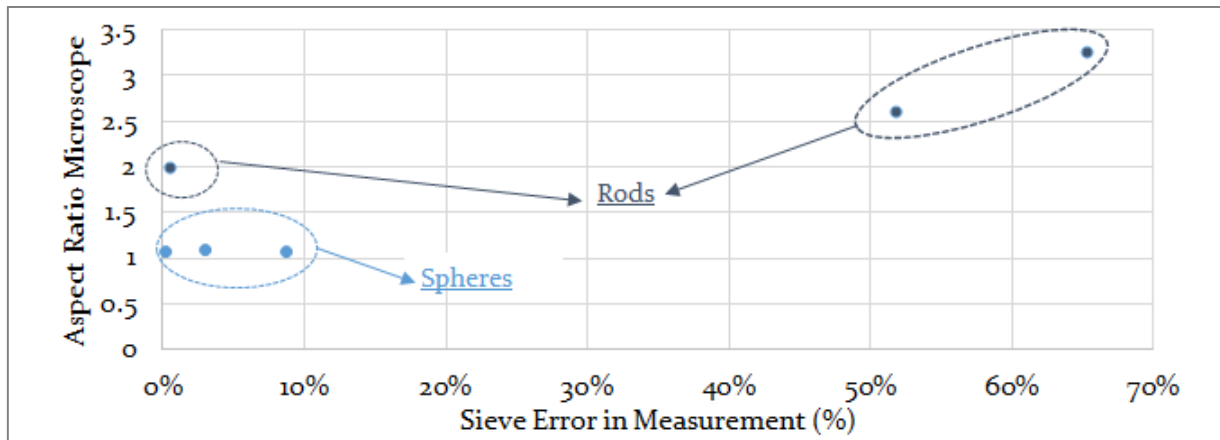


Figure 20 – Influence of aspect ratio on the sieve error measurements.

4.2 Particle densities and morphology

In this section, the results from the different density experiments are presented. Firstly, the bulk and skeleton density measurements are presented, then the particle envelope density and lastly the wet density measurements using four methods.

- Bulk density

As mentioned previously, the bulk density was determined using a constant volume of 1.3 [L]. The bulk density measurements for every sample are presented in Table 4.

Table 4 – Bulk density measurements overview.

Sample Name	Measured Bulk Density [kg/m ³]	Deviation in comparison to specifications
Filtrisorb 300 C	675	15%
Aquasorb K-GA 830	408	-10%
Saratech Spherical	454	-10%
Norit ROW 0.8 Supra	343	-14%
Norit RB 4C	435	-15%
Filtrisorb TL830	596	14%
Aquasorb K-6300	442	-1%
Resorb HC	437	-3%
Norit GAC 830 S	461	-4%

The deviations in the measurements are attributed to human measuring errors. A graduated cylinder was used to measure the volume of the dry particles. The 1.3 [L] volume was hard to reproduce consistently, leading to slight variations in mass and causing deviations in the bulk density calculations.

- Skeletal density

An overview of the average skeletal density and standard deviation (σ_{avg}) on measurements obtained for every GAC sample is presented in Table 5.

Table 5 – Skeletal density measurements overview.

Sample	σ_{avg} [kg/m ³]	Average Skeletal Density [kg/m ³]
Filtrisorb_300C	0.0016	1,637
Aquasorb KGA	0.0053	2,028
Saratech Spherical	0.0051	2,201
Norit ROW 0.8 Supra	0.0023	2,153
Norit_RB4C	0.0058	2,202
Filtrisorb_TL830	0.0008	1,647
Aquasorb K-6300	0.0027	1,734
Resorb HC	0.0022	1,928
Norit GAC 830 Supra	0.0039	2,090

This density was measured using a very accurate instrument, achieving small average standard deviation for the 10 different measurements per sample performed. The accuracy in the skeletal density measurements of this instrument was the main reason why it was chosen as a starting point in the calculations using the AquaGAC model.

- Particle (envelope) density

An overview of the particle envelope density (particle volume includes internal porosity and carbon solids) is presented in Table 6. The sample size refers to the amount of particles that were analyzed under the microscope, the percentage of analyzed particles represents the amount of particles, which height was analyzed and finally the approximated particle density is also presented. In Appendix A5, the output 3D model of the particles is presented as well as a sample profile where the different particle heights were taken.

Table 6 – Particle (envelope) density measurements overview.

Sample Name	Sample Size [#]	Sample Particles analyzed [%]	Approximated Particle Density [kg/m ³]
Filtrisorb 300 C	165	46%	787
Aquasorb K-GA 830	86	60%	489
Saratech Spherical	2047	100%	702
Norit ROW 0.8 Supra	74	64%	675
Norit RB 4C	15	100%	764

Sample Name	Sample Size [#]	Sample Particles analyzed [%]	Approximated Particle Density [kg/m ³]
Filtrisorb TL830	120	61%	647
Aquasorb K-6300	96	96%	493
Resorb HC	152	79%	498
Norit GAC 830 S	166	61%	492

As an additional check, the particle envelope density was calculated using the skeletal density (equation A9.42 in appendix A9), presented in Table 7.

Table 7 – Calculated particle (envelope) density measurements overview.

Sample Name	Calculated Particle Density [kg/m ³]
Filtrisorb 300 C	1,150
Aquasorb K-GA 830	1,053
Saratech Spherical	1,204
Norit ROW 0.8 Supra	675
Norit RB 4C	780
Filtrisorb TL830	1,040
Aquasorb K-6300	860
Resorb HC	970
Norit GAC 830 S	1,150

When we compare the particle envelope density of Table 6 with the one from Table 7, deviations up to 57% are found. This is attributed to several uncertainties in the measurement of the volume of small irregularly shaped particles. Even though the microscope provides a good initial approximation of this volume, there will be always an over or under estimation of the real particle volume due to the irregularity of the shape. This again, is caused by the small sample and weight of particles and because the estimation of the height is dependent on the lowest and highest possible level of focus of the lens of the microscope, which is not always easy to determine.

Since the skeleton density was assumed to have an accurate and reliable value, the particle density was determined from this value using a derived expression from mass balances. For the particular case of the Filtrisorb 300C and Norit ROW 0.8 Supra, the particle density employed was the measured (microscope) one, as it was found in agreement with values

found in (Livingston, 2005) and (Mauget et al., 2005). Several methods to improve the measurements of this density are listed in the recommendations section of this report.

- Wet particle density

The wet density is one of the most critical parameters in the fluidization of porous media. Due to the criticality of this parameter, a corroboration of the measurements was required and a total of three different measurement methods and one independent calculation method were used. An overview of the measured average wet particle density of all the four methods will be presented in this subsection.

- Mass conservation measurement method

Table 8 illustrates the wet particle density measurements performed with the mass conservation approach, all of the inputs and numbers in the table are provided in Appendix A5.

Table 8 – Mass conservation wet density.

Mass conservation wet density [kg/m ³]					
Wetting time [hrs]	74.00	66.75	73.23	σ [kg/m ³]	Average
Sample	Run 1	Run 2	Run 3		
Filtrisorb 300C	1,479	1,397	1,494	43	1,457
Aquasorb KGA	1,368	1,281	1,427	60	1,359
Saratech spheres	1,937	1,801	1,979	76	1,906
Norit ROW 0.8 Supra	2,253	2,100	2,159	63	2,171
Norit RB 4C	1,894	1,525	1,909	178	1,776
Filtrisorb TL830	1,280	1,161	1,306	63	1,249
Aquasorb K-6300	1,242	1,162	1,314	62	1,240
Resorb HC	1,394	1,258	1,328	56	1,327
Norit GAC 830 Supra	1,251	1,141	1,221	46	1,204

- Pycnometer measurement method

As a rule of thumb, the wet particle density measurements were performed after a wetting time of around 3 days. These measurements were performed again after approximately 4 months. In Table 9 and Table 10, the measured pycnometer density with low and high wetting hours are respectively presented.

Table 9 –Pycnometer density (low wetting time)

Pycnometer wet density [kg/m ³] (low wetting time)								
Wetting time [hrs]	72.58	76.00	81.00	Not available	Not available	Not available	σ	Average
Sample	Run 1	Run 2	Run 3	Run 4	Run 5	Run 6		
Filtrisorb 300C	1,189	1,211	1,178				14	1,193
Aquasorb KGA	1,068	1,119	1,132	1,113			24	1,108
Saratech spherical	1,159	1,137	1,188				21	1,161
Norit ROW o.8 Supra	1,098	1,091	1,273	1,181	1,177	1,165	61	1,164
Norit RB 4C	1,203	1,185	1,194				7	1,194
Filtrisorb TL830	1,206	1,210	1,189				9	1,202
Aquasorb K-6300	1,188	1,180	1,176				5	1,181
Resorb HC	1,176	1,053	1,166	1,185	1,216	1,207	54	1,167
Norit GAC 830 Supra	1,154	1,108	1,232	1,164	1,178	1,180	37	1,169

Table 10 –Pycnometer density (high wetting time)

Pycnometer wet density [kg/m ³] (high wetting time)					
Wetting time [hrs]	3,384	3,547	3,552	σ	Average
Sample	Run 7	Run 8	Run 9		
Filtrisorb 300C (F300)	1,239	1,239	1,244	3	1,241
Aquasorb KGA	1,157	1,161	1,174	8	1,164
Saratech spherical	1,206	1,191	1,196	6	1,198
Norit ROW o.8 Supra	1,143	1,162	1,164	9	1,156
Norit RB 4C	1,243	1,248	1,278	15	1,256
Filtrisorb TL830	1,212	1,240	1,260	20	1,238
Aquasorb K-6300	1,194	1,230	1,235	18	1,219
Resorb HC	1,189	1,200	1,204	7	1,198
Norit GAC 830 Supra	1,199	1,199	1,222	11	1,207

Figure 21 illustrates a comparison between the high and low wetting time pycnometer densities. For the specific case of the ROW o.8 Supra sample, the outlier of run 6 was not considered in the average wet density calculation.

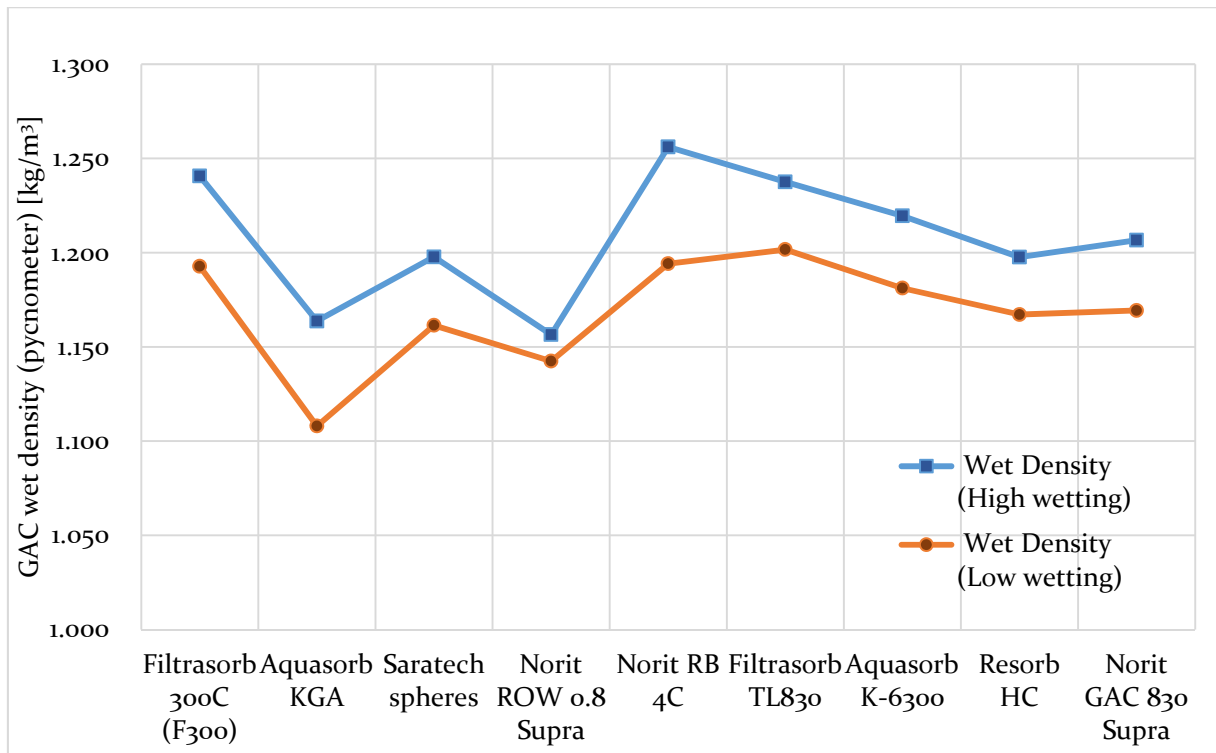


Figure 21 – High and low wetting pycnometer wet density.

Figure 21 illustrates that the degree of wetting plays an important role in the fluidization behavior of GAC particles. In the performed experiments, a comparison between particles with 72 and over 1,300 hours of wetting revealed a difference of up to 5%, indicating that the degree of wetting is not 100% after wetting the particles for only 72 hours.

- o Image analysis measurement method

The obtained wet particle density using the image analysis method is presented in Table 11. The 3D models generated by the microscope were used to calculate the volume of the particles used to calculate this density, the wet mass was measured similarly as the pycnometer procedure.

Table 11- Wet density using image analysis

Image Analysis wet density [kg/m ³]	
Wetting time (average) [hrs]	198.99
Sample	Run 1
Filtrisorb 300C	1,448
Aquasorb KGA	1,472
Norit ROW 0.8 Supra	1,782
Norit RB 4C	1,459
Filtrisorb TL830	1,443
Aquasorb K-6300	1,158
Resorb HC	1,262
Norit GAC 830 Supra	1,229

- Differential pressure (wet particle density) calculation method

With the help of equation (1), the wet particle density was calculated by fixing the differential pressure measurements, the output calculations are is presented in Table 12.

Table 12 – Wet density results based on the differential pressure measurements.

Pressure measurements wet density [kg/m ³]						
Average Wetting time [hrs]	522				σ [kg/m ³]	Average
Sample	Exp 1	Exp 2	Exp 3	Exp 4		
Filtrisorb 300C	1,494	1,487	1,464	1,440	21	1,471
Aquasorb KGA	1,467	1,449	1,475	1,418	22	1,452
Saratech spheres	1,510	1,548	1,538	1,532	14	1,532
Norit ROW 0.8 Supra	1,360	1,343	1,305		23	1,336
Norit RB 4C	1,426	1,409	1,387		16	1,407
Filtrisorb TL830	1,417	1,412	1,413		2	1,414
Aquasorb K-6300	1,407	1,406	1,364		20	1,392
Resorb HC	1,457	1,464	1,456		3	1,459
Norit GAC 830 Supra	1,476	1,457	1,490		14	1,474

A comparison between the four obtained wet particle densities is presented in Figure 22 and a comparison between the errors of all the methods with respect to the pressure based wet particle density is presented in Table 13.

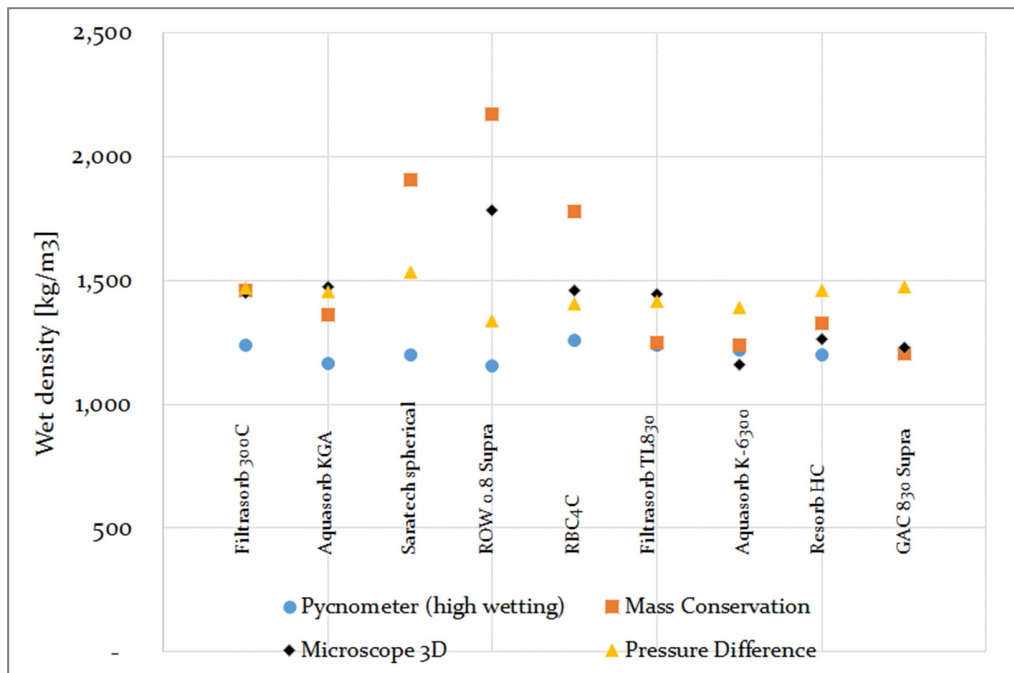


Figure 22 – Wet density comparison.

Due to the criticality of the wet particle density parameter in the fluidization behavior of GAC, extensive measurements were made using three different measuring methods and one calculation method. Even though in Figure 21 one can observe certain agreement with some of these measurements, when comparing the pycnometer to the calculated wet density using the pressure loss, deviations ranging from 11-22% were found. The measuring errors are attributed to mainly the low mass samples used causing possible instrument deviations and to the drainage or excess water in the GAC particles when measuring the wet mass, causing a misleading measurement. As using a lower mass requires a very high accuracy in the instruments, the method is very sensitive to deviations. This was one of the main reasons why the differential pressure wet particle density calculation was used as an input for the model, leading to less uncertainties.

Table 13 – Error between wet particle density measurements.

Sample	Pyc/pressure	Mass/pressure	Mic/pressure
Filtrisorb 300C	16%	5%	2%
Aquasorb KGA	20%	12%	1%
Saratech spheres	22%	18%	N/A
Norit ROW 0.8 Supra	13%	57%	33%
Norit RB 4C	11%	8%	4%
Filtrisorb TL830	12%	18%	2%
Aquasorb K-6300	12%	17%	17%
Resorb HC	18%	14%	14%
Norit GAC 830 Supra	18%	23%	17%
Average Error	16%	19%	11%

Pyc=Pycnometer measurements, *Mass*= mass conservation measurements, *Mic*= microscope/image analysis measurements and *pressure*= differential pressure wet particle density calculation output.

Overall, the average error using the pycnometer, mass conservation and image analysis (microscope) methods deliver an average error of 16, 19 and 11%, respectively. The highest overall error was found using the mass conservation method as it depended both on the measurement of the wet mass and on the dry particle envelope density. Since both of these measurements had deviations due to uncertainties, then error turned out to be higher.

For the case of the particle morphology, the description of the obtained parameters are presented in Appendix A2 and the detailed relevant parameters obtained per instrument are presented in Appendix A6.

4.3 Particle orientation

As mentioned previously, the particle orientation measured only in the X-Y plane by taking a sample of particles in a moment in time of the taken videos and then measuring the angle using CAD software. Only the Norit RB4C particles were analyzed as their favorable size allowed seeing their behavior easily.

4.3.1 Single particle orientation

Firstly, the single particle orientation was analyzed. Figure 23 shows the fluidization of the rod with a sudden increase in the flow from 0 to 150 [L/h] (flow velocity from 0 to 1,130 [m/h]). Initially the fluidization angle is approximately 42°. Particle starts stabilizing with an angle of 14-15° and finalizes on an angle of 2°. All angles are measured from the long axis of the rod with perpendicular line from the walls of the tube.

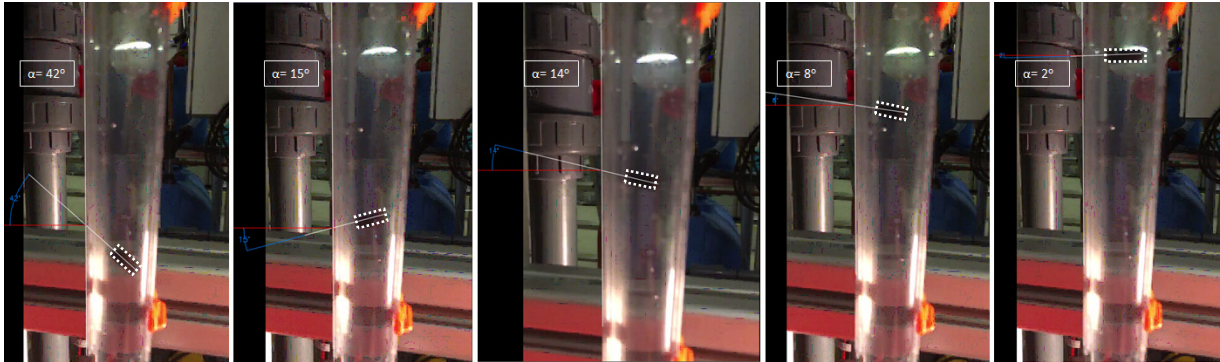


Figure 23 – Single rod orientation – RB₄C sample.

Other videos show that for velocities from 415 to 500 [m/h] the individual rod maintains a stable horizontal position. In some cases, two effects disturbed this horizontal equilibrium, one was a clockwise spin in the x-z axis of the rod (illustrated in Figure 24) and the second was a wobbly periodic oscillation of the particle (shown in Figure 25).

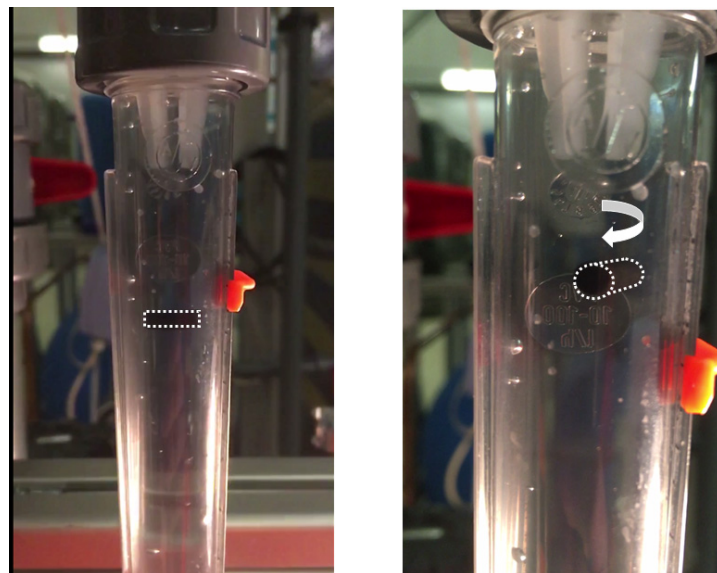


Figure 24 – Single rod equilibrium and spin.

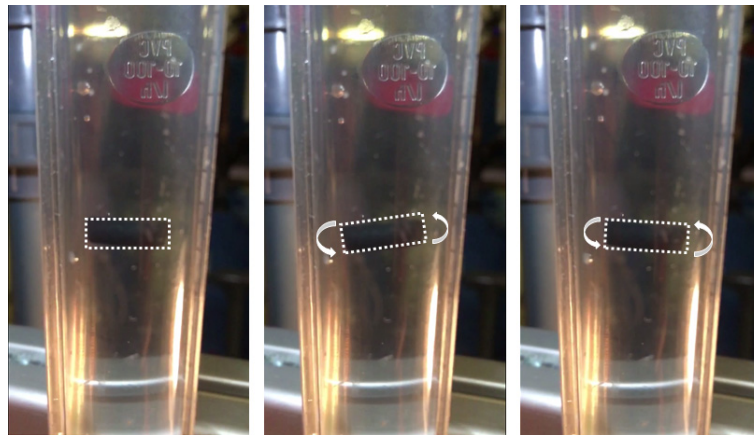


Figure 25 – Rod oscillation observations.

In order to understand how these individual particles settle, the flow was taken down increasingly to zero, the particle maintains a horizontal orientation but the wobbly settling trajectory follows a falling leaf-like behavior. The flow regimes of these experiments are summarized in Table 14.

Table 14 – Overview of single particle observations.

Flow [L/h]	Flow Velocity [m/h]	Re_p^* [-]	Hydraulic Regime**	Angle [Deg]
65	490	439	Transition	88-90
66	497	445	Transition	88-90
63	475	425	Transition	88-90
59	445	398	Transition	88-90
56	422	378	Transition	88-90
55	414	371	Transition	85-90
150	1,130	1,012	Transition	48-75-88

*Particle Reynolds number as defined in equation (4).

**Hydraulic Regime determined values based on Table 1.

To obtain further insights, the expression developed by (Hölzer & Sommerfeld, 2008) was applied to the single particle experiments using the d_{10} , d_{50} and d_{90} particle sizes and representative Reynolds numbers for every flow regime ($Re_p=10$, $Re_p=90$ and $Re_p=5,000$) according to Table 1, presented in Figure 26 to Figure 28. For this case, when the angle is 0 [deg] the rod particle is completely horizontal and when it is 90 [deg] the rod particle is completely vertical.

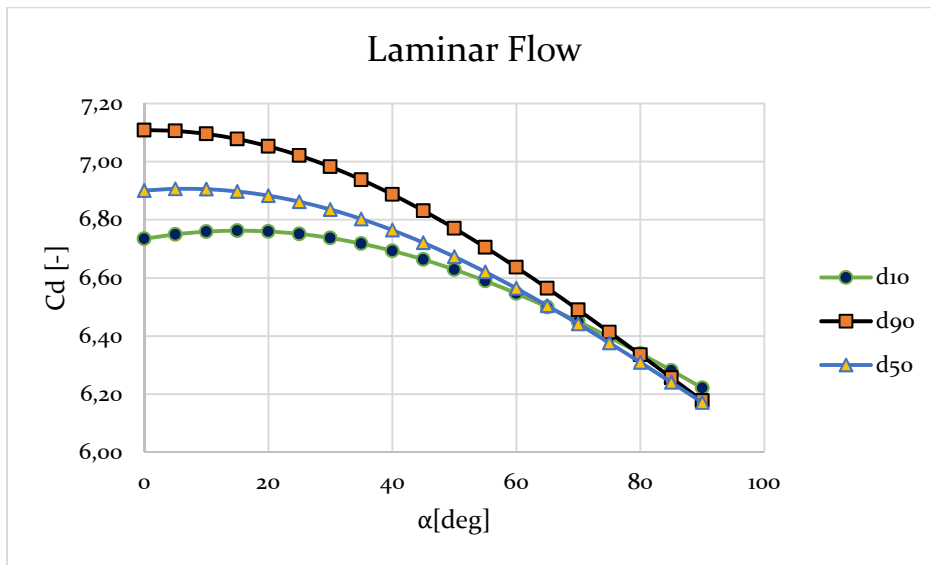


Figure 26 - Holzer-Sommerfeld drag coefficient (Laminar Flow).

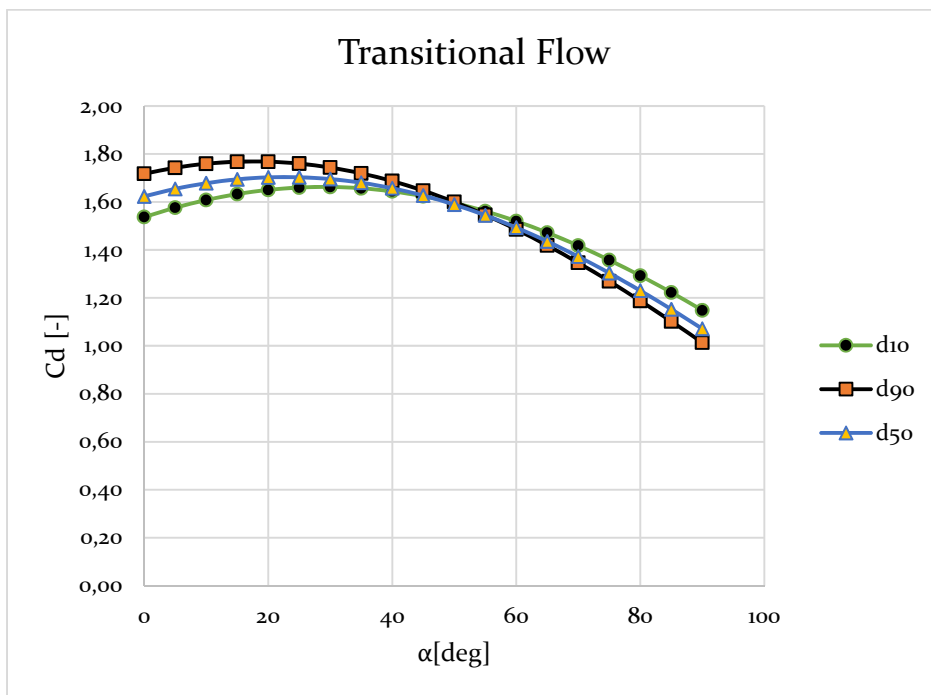


Figure 27 - Holzer-Sommerfeld drag coefficient (Transitional Flow).

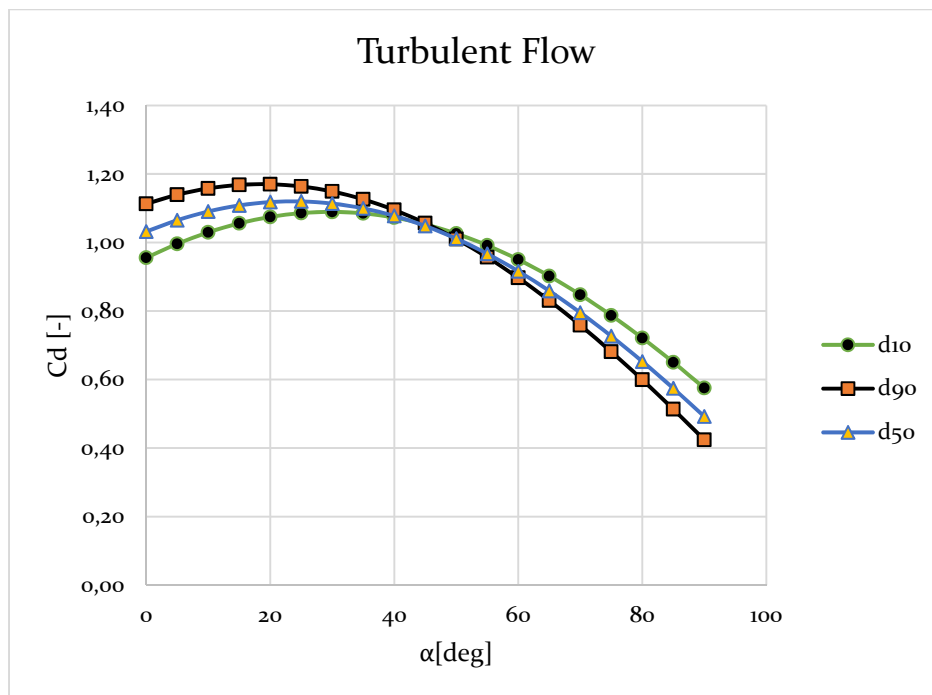


Figure 28 – Holzer-Sommerfeld drag coefficient (Turbulent Flow).

The single particle orientation experiment provides great qualitative insights to understand the behavior of the bed with thousands of particles. For the performed experiments, the particle was only in the transitional regime (particle Reynolds number from 60-306). When the flow velocity was increased abruptly, the particle tended to fluidize firstly at an angle and then arrive into an equilibrium at a horizontal orientation. The particle maintained a predominantly horizontal orientation in flow velocities of 414 through 490 [m/h]. When in equilibrium and in settling, the particle showed wobbling oscillations with a certain frequency, this is attributed to vortex shedding⁶; the shedding of these alternating vortices performs a pressure gradient on the rod, promoting motion towards the side with the lowest pressure. In addition, when the particle settles it does not settle in a straight line but in a pendulum movement that is in agreement with the minimum energy dissipation principle. The particle also showed some slow spins around the z-axis in a clockwise direction, this is attributed to the presence of a slight hydrodynamic torque.

When seeing the Holzer-Sommerfeld (H-S) plots, one can infer that in the laminar, transitional and turbulent flow, the highest drag coefficient is at an orientation between 0-15, 20-30 and 20-30 degrees, respectively. In the transitional regime (where most of particle fluidization occurs), the governing term of the H-S equation is the fourth term,

⁶ An oscillating flow phenomenon where vortices are created on the back of the body of an object and then detached. The fluid flow creates low pressure vortices on the downstream of the object. (https://en.wikipedia.org/wiki/Vortex_shedding)

representing the newton region, followed by the third term, dependent on the sphericity of the rod-like particle.

4.3.2 Multiple-particle orientation

After the single particle density experiment, a bed with hundreds of particles was observed to further understand the role of orientation in the fluidization of these particles. An overview of the main findings of the observations is presented in the following paragraph.

The Norit RB₄C rods start out in the packed orientation, which is mostly horizontal (0-35 degrees), refer to Figure A8.1. When flows increase to 203-560 [L/h] (80-95 [m/h]), the particles tend to have more inclined angles due to some preferential flows in the middle/sides of the bed, refer to Figure A8.2. These preferential flows cause particles near the water path change their orientation (0-45-75 degrees). This change in orientation creates particle-to-particle interaction, which increases the angle of surrounding particles. Finally, when the flow velocity is high ($Re_p > 250$), the increase in porosity creates enough space for particles to fluidize freely and have a tendency to behave as the single particle with a predominantly horizontal position as seen in figures A8.7 and A8.8. A more detailed description for each flow velocity analyzed is presented in Appendix A8, an overview of the measured parameters is presented in Table 15. In Figure 29, the main phases of multiple particle orientation are illustrated and briefly explained.

The parameters used were the following:

- Fixed bed height= 55 [cm]
- Water temperature= 13 [°C]
- Water density= 999 [kg/m³]
- Dynamic viscosity= 0.0012 [kg/m/s]
- Kinematic viscosity= 1.19 (10⁻⁶) [m²/s]
- Column diameter = 5.7 [cm]
- Particle diameter (width, length)= 3.865 [mm], 12.552 [mm]
- Particle wet density= 1,407 [kg/m³]
- Bulk density= 434 [kg/m³]
- Initial porosity (ϵ_0)= 69%

Table 15 – Overview of orientation observations.

Flow [L/h]	Flow Velocity [m/h]	Re_p^* [-]	Hydraulic Regime**	Bed height [cm]	Bed Expansion [%]	Porosity (Pe) [-]	Angle [Deg]
172-196	67-76	60-69	Transition	56-57	3-4	0.69-0.70	0-35
203-243	80-95	71-85	Transition	60-63	8-15	0.72-0.73	0-45-75
266-383	104-150	93-134	Transition	66-82	19-49	0.74-0.79	0-40-85
463-510	181-200	162-179	Transition	92-103	67-87	0.82-0.84	0-60-85
560	220	197	Transition	114	106	0.85	0-45-85
709	278	249	Transition	155	182	0.89	0-30-60
733-843	287-330	257-296	Transition	162-205	195-273	0.90-0.92	0-35-65
873	341	306	Transition	210	282	0.92	0-35

*Particle Reynolds number as defined in equation (4).

**Hydraulic Regime determined values based on Table 1.

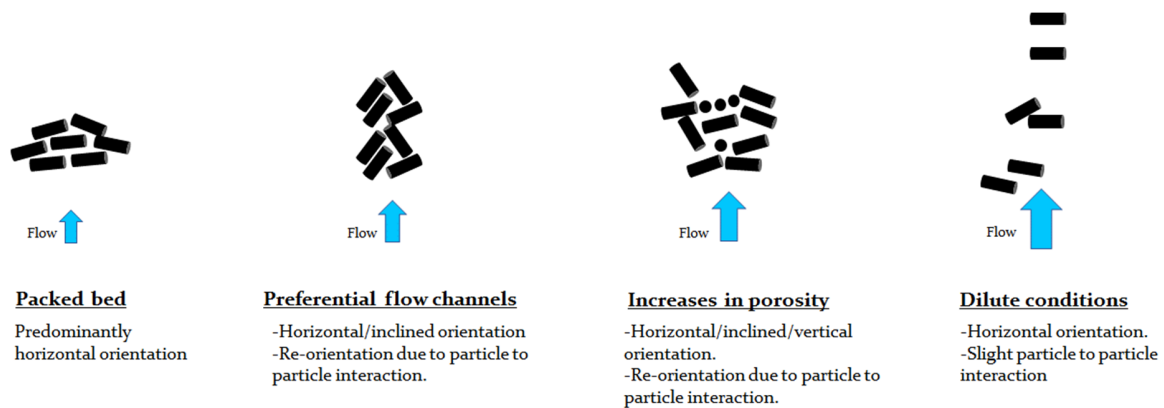


Figure 29 – Identified phases of orientation for multiple particles

For the case of the multi-particle bed, some similarities with the single particle behavior can be observed. In laminar flow and start of the transitional flow ($Re_p < 70$), particles tend to be predominantly horizontal (0-35 degrees), as originally packed. On the other extreme, at $250 < Re_p < 306$, there is also a tendency to follow the same behavior as a single particle as particles have enough space to freely flow, there are some slight inclinations of particles due to brief particle-to-particle interaction. In flow velocities between 200-500 [m/h] ($70 < Re_p < 200$), there are first preferential flows caused in the middle of the bed that causes the inclination of particles, this causes particle-to-particle interaction influencing

inclination of surrounding particles. The other identified phase was the presence of changes in porosity in different parts of the bed. These open spaces also create preferential flows in which particles either flow through this channel (if small enough) or interlock other particles, again influencing both of their orientations.

It is important to mention that all of the particle orientation insights are only based on observations. In the recommendations section of this report, some suggestions for a quantitative analysis of the particle orientation are made.

4.4 Fluidization experiments and models

As mentioned in the materials and methods section, the data of the performed fluidization experiments were used in combination with an existing fluidization model in order to compare porosity predictions of six classical models. In addition, the combination of the AquaGAC model with several morphological parameters made it possible to obtain sixteen data driven models (DDMs). This subsection will first present the obtained data of the expansion experiments, then present the results of the classical models output and finally present the results of the DDMs.

4.4.1 Expansion Experiments

In Appendix A10, two graphs per expansion experiment (30 experiments performed in total) are presented. The first graph illustrates the water flow versus the differential pressure measurements. The second graph illustrates the water flow versus the porosity, where both the data (yellow dots) and the Carman-Kozeny (C-K) model porosity prediction (dashed orange line) are compared.

It is interesting to see that the data of the graphs (see Appendix A10, Figures A10.31 to A10.60) a consistent fit with this classical model (when using the hydraulic C-K diameter), with one exception. For the case of the RB₄C sample (Figures A10.46 to A10.48), deviations are found in the porosity graphs. This is attributed to the particle-to-particle interaction that was observed in the orientation experiments. This interaction inhibits the free flow of surrounding particles, which results in an interlocking-like behavior that functions as an obstacle for particles to fluidize. It is also important to keep in mind that the Carman-Kozeny equation is based on the theory of capillary flow applied to a packed bed of particles, this implies that perfectly round spheres can freely fluidize. Due to this interlocking phenomenon, the flow patterns are much different for rod-like particles than for perfectly round spheres, explaining the observed deviations in the Carman-Kozeny prediction model.

Observations concerning the particle stratifications are considered a relevant part of the expansion experiments. Before starting the expansion experiment measurements, the GAC samples were fluidized for at least 40% expansion for several minutes. This promoted a size classification of the particles, having the smallest particles in the top of the bed and the largest ones in the bottom. A pre-classification of particles by size could already be

observed when the particles were initially introduced in the reactor, although fluidizing the particles was still required to have a fully stratified bed. A final remark on particle stratification was the formation of slugs due to particle cohesion. For the case of the Aquasorb KGA sample for example, the combination of small and big particles formed a cohesive structure that fluidized as a complete block. After several fluidization attempts, the bed finally stratified based on size.

4.4.2 Classical model outputs

The combination of the AquaGAC and FBI models (existing fluidization model), provided an output porosity that was then compared with six classical models. Several porosity prediction simulation results were performed to find out which diameter and classical model described better the collected experimental data, the absolute relative errors of these simulations are presented in Appendix A10.

The overview of the average relative error in porosity found between the different diameter inputs using all the particle sizing methods, and the classical models is presented in Figure 30, the numerical values are presented in Table 16. The d_{90} values were ignored as the smaller particles tend to control the overall expansion of the bed.

Table 16 – Average relative error in porosity for the different methods and diameters.

Model name	Average Relative Errors [%]							
	d_{50}				d_{10}			
	Microscope	ImageJ	Camsizer	Sieve	Microscope	ImageJ	Camsizer	Sieve
Kozeny⁷	N/A	N/A	N/A	N/A	N/A	N/A	N/A	N/A
Carman-Kozeny	12%	15%	9%	14%	9%	9%	9%	8%
Ergun	13%	17%	11%	16%	10%	10%	9%	9%
van Dijk	14%	16%	10%	15%	10%	9%	11%	9%
Richardson-Zaki (1954)	21%	26%	18%	25%	15%	17%	10%	14%
Richardson-Zaki (2018)	12%	15%	10%	15%	9%	9%	10%	8%

N/A – Not valid for boundary conditions

⁷ Boundary conditions exceeded for almost every case.

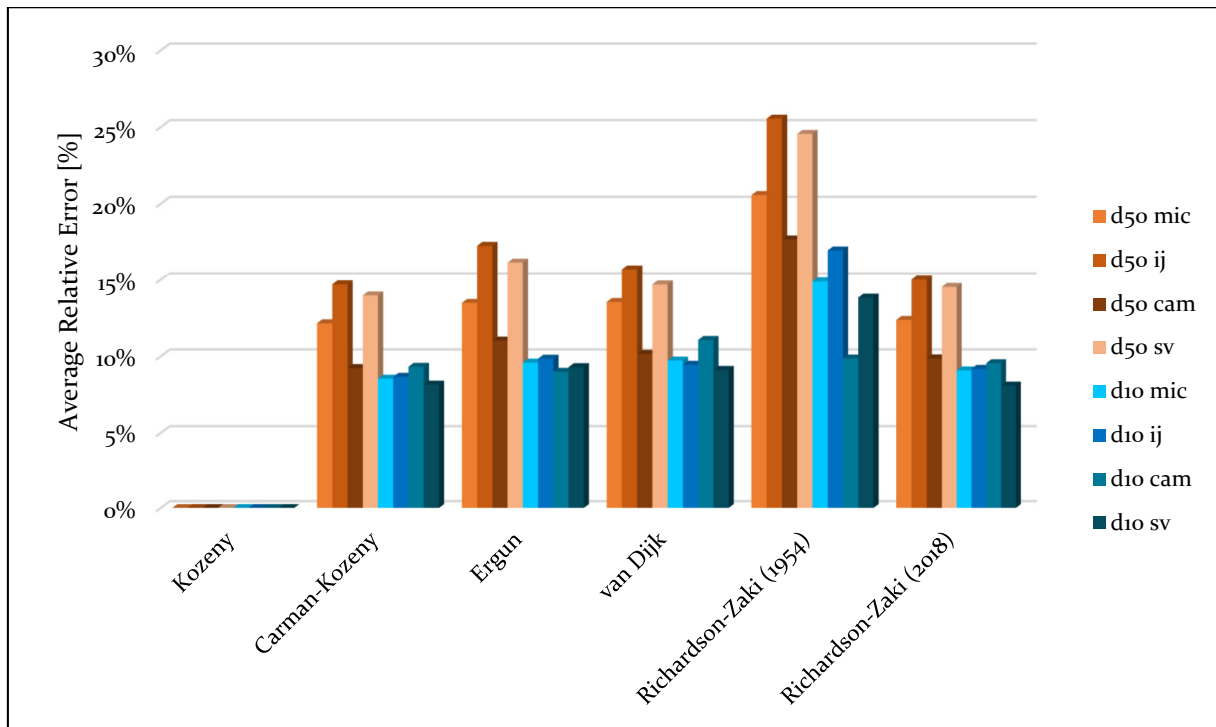


Figure 30 – Average relative error in porosity for the different methods and diameters.

Analyzing Figure 30, the first relevant finding is that all five classical models are able to predict the porosity relatively well, finding errors between 9-11%. Another relevant finding is that using the d10 diameter delivers more accurate results than the commonly used d50, this was found to be true for all of the particle measuring methods. This can easily be identified if the orange bars are compared with the blue bars in Figure 30). The Kozeny model was not applicable, as it exceeded the boundary conditions when evaluated with the corrected particle Reynolds number (Re_c).

- Best fitting diameter

In Table 17, the calculated Carman-Kozeny hydraulic diameter is presented. The average calculated C-K hydraulic diameter for each sample was compared with the d10, d50 and d90 of all the particle size measurement methods to determine the diameter (and method) with the minimum error, findings are presented on

Table 18.

Table 19 illustrates the overall best fitting diameter per method based again on the diameter that in compared with the hydraulic diameter delivers the minimum error.

Table 17 – Calculated Carman-Kozeny hydraulic diameter.

Sample Name	Experiment	$d_{p,CK}$ [mm]	Average $d_{p,CK}$ [mm]
Filtrisorb 300C	001	1.15	1.2
	002	1.12	
	003	1.26	
	004	1.27	
Aquasorb KGA	005	0.66	0.65
	006	0.65	
	007	0.64	
	008	0.66	
Saratech	009	0.34	0.3
	010	0.31	
	011	0.28	
	012	0.28	
Norit ROW o.8 S	013	0.89	0.91
	014	0.89	
	015	0.94	
Norit RB4C	016	3.32	3.55
	017	3.58	
	018	3.75	
Filtrisorb TL830	019	1.51	1.47
	020	1.47	
	021	1.43	
Aquasorb K-6300	022	1.16	1.16
	023	1.12	
	024	1.19	
Resorb HC	025	0.81	0.79
	026	0.78	
	027	0.78	
Norit GAC 830S	028	0.66	0.65
	029	0.66	
	030	0.63	

Table 18 – Diameter with the least error in comparison to the C-K calculated diameter.

Sample	Minimum error [%]	Best method and diameter		
		Percentile d _{10,50,90}	Diameter	Method employed
Filtrisorb 300 C	10.3%	d ₅₀	Maximum	Camsizer
Aquasorb K-GA 830	3.1%	d ₁₀	Minimum	Camsizer
Saratech Spherical	22.4%	d ₁₀	Minimum	ImageJ
Norit ROW o.8 Supra	0.7%	d ₅₀	Minimum	ImageJ
Norit RB 4C	4.8%	d ₁₀	Minimum	Camsizer
Filtrisorb TL830	0.1%	d ₅₀	Minimum	Camsizer
Aquasorb K-6300	0.5%	d ₁₀	Maximum	Camsizer
Resorb HC	6.5%	d ₁₀	Minimum	Microscope
Norit GAC 830 S	1.0%	d ₁₀	Minimum	Camsizer

Table 19 – Best overall fitting diameter.

Method	Minimum error [%]	Best diameter per method	
		Percentile d _{10,50,90}	Diameter*
Sieve	21.12%	d ₁₀	-
Microscope	27.02%	d ₅₀	Minimum
ImageJ	20.87%	d ₁₀	Minimum
Camsizer	21.38%	d ₅₀	Minimum

* Minimum diameter refers to the width of the particles, refer to Appendix A2 for additional information.

In

Table 18 one can observe that there is not one method nor diameter that delivers the lowest error in comparison to the Carman-Kozeny hydraulic diameter. However, the d_{10} best describes the majority of the experiments followed by the d_{50} . In general, the overall lowest errors are found using the Camsizer and ImageJ measurements.

Table 19 illustrates that similar errors ($\sigma=3\%$) are found in all four methods. If only one diameter should be picked as an input for the hydraulic model, the best option is the d_{10} diameter using the ImageJ method. This choice was made as it is the diameter that delivers the lowest relative error in comparison with the Carman-Kozeny hydraulic diameter. However, if the d_{10} of the sieve or d_{50} minimum diameter of the Camsizer are used very similar results in terms of accuracy should be expected.

4.5 Data driven modelling

In order to understand the governing parameters in the fluidization behavior of the different GAC samples, sixteen empirical equations were obtained using the Eureka commercial software. The output porosity from the FBI model was combined with different particle morphological parameters of all methods to obtain an empirical expression with relatively high correlation factors. The functions and coefficients of correlation (r^2) obtained are summarized in Table 20, the complete correlation expressions and nomenclature are presented in Appendix A11. The relative error found between the calculated porosity with the data driven models and output porosity of the FBI file are presented in Figure 31. The suffixes seen in Figure 31 refer to the particle sizing method used to obtain the morphological parameters: sv=sieve analysis, cam=Camsizer, ij=ImageJ and mic=microscope.

Table 20 – Output Eureka correlations

Model ID	Porosity function	r^2			
		Microscope	ImageJ	Camsizer	Sieve
DDM1	$\varepsilon(v_s, v, \rho_{wet}, d_{50})$	0.846	0.725	0.937	0.757
DDM2	$\varepsilon(v_s, \rho_c, \rho_{bulk}, \rho_{wet}, \rho_p, d_{10}, d_{90})$	0.981	0.982	0.987	0.987
DDM3	$\varepsilon(v_s, v, \rho_{wet}, u_{Cmin}, u_{Cmax}, d_{10,min}, d_{90,max}, d_{50,min}, d_{50,max})$	0.880	0.964	0.960	0.960
DDM4	$\varepsilon(v_s, v, \rho_{wet}, d_{max}, 2M_{ang}, AR, Circ)$	0.934	-	-	-
DDM5	$\varepsilon(v_s, v, \rho_{wet}, 2M_{ang}, Dia_w)$	0.930	-	-	-
DDM6	$\varepsilon(v_s, v, \rho_{wet}, rnd, Min_{Fer}, AR, UC_{min})$	-	0.960	-	-
DDM7	$\varepsilon(v_s, v, \rho_{wet}, rnd, Min_{Fer}, d_{ceq}, Fer, AR)$	-	0.977	-	-
DDM8	$\varepsilon(v_s, v, d_p, \rho_{wet}, bl_0, spht_0, UCx_0)$	-	-	0.945	-
DDM9	$\varepsilon(v_s, v, x_{c,min}, \rho_{wet}, bl_0, spht_0)$	-	-	0.963	-
DDM10	$\varepsilon(v_s, v, d_p, \rho_{wet}, spht_0)$	-	-	0.956	-
DDM11	$\varepsilon(v_s, v, x_{c,min}, \rho_{wet}, spht_0, spht_1)$	-	-	0.915	-
DDM12	$\varepsilon(v_s, v, x_{c,min}, \rho_{wet}, spht_0)$	-	-	0.945	-
DDM13	$\varepsilon(v_s, v, x_{c,min}, \rho_{wet}, sph, spht_0, spht_1)$	-	-	0.960	-

Model ID	Porosity function	r ²			
		Microscope	ImageJ	Camsizer	Sieve
DDM14	$\varepsilon(v_s, v, d_p, \rho_{wet}, d_{10}, d_{90}, d_{50}, UC)$	-	-	-	0.837
DDM15	$\varepsilon(v_s, v, d_p, \rho_{wet}, d_{10}, d_{90}, UC)$	-	-	-	0.971
DDM16	$\varepsilon(v_s, v, d_p, \rho_{wet}, d_{10}, d_{90}, d_{50})$	-	-	-	0.838

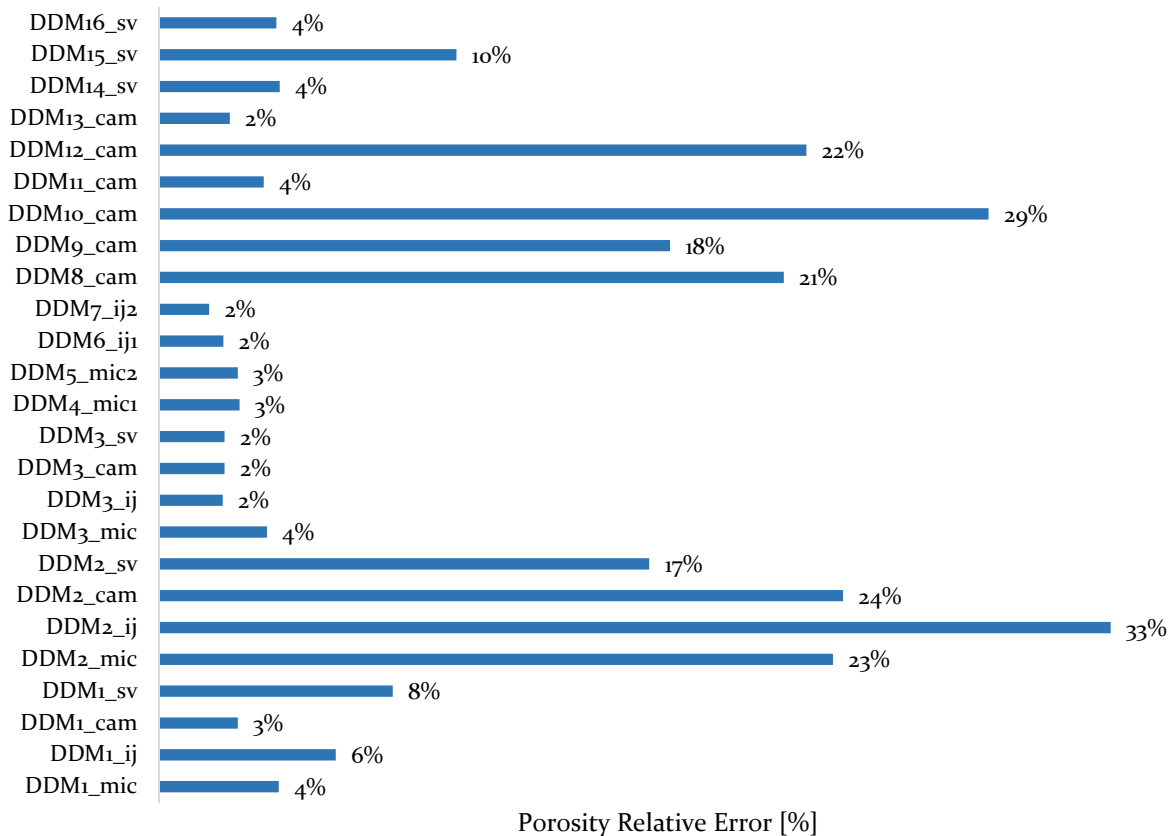


Figure 31 –Relative error of porosity in data driven models.

As illustrated in Table 20, two main sets of data compose the DDMs: hydraulic and morphological parameters. For the selection of the hydraulic parameters, it was well known from experiments using non-porous media that the governing hydraulic parameters of fluidization were the particle diameter, fluid and particle density, superficial flow velocity and kinematic viscosity. Since obtaining insights into what is the influence of the morph in the fluidization behavior of GAC was the main purpose of developing these data driven model, the selection of morphological parameters was performed by trial and error. The initial selection of morphological parameters was based in what was considered to be the most influential factors in the hydraulic behavior of GAC. From this initial selection, several combinations were tried to compare and obtain a correlation that delivered accurate results.

The lowest porosity prediction errors (illustrated in Figure 31) found were using the DDM7, DDM_{3_ij}, and DDM6; they delivered a 1.71%, 2.18% and 2.20% respectively. The morphological parameters used in the DDM7 were the roundness, minimum Feret diameter, circular equivalent diameter, Feret diameter and aspect ratio. For the case of the DDM6, the minimum Feret diameter, roundness, aspect ratio and minimum uniformity coefficient was the combination of morphological parameters that worked. Finally for the case of the DDM_{3_ij}, a combination of the $d_{10_{min}}$, $d_{90_{max}}$ $d_{50_{min,max}}$ and uniformity coefficients were able to describe well the data.

Some similarities can be found between DDM7 and DDM6 as they involve the same combination of morphological parameters with the exception of the Uniformity coefficient. In addition, DDM_{3_ij} delivered a very good accuracy using only a combination of diameters and uniformity coefficients. It is important to mention that not all combinations of morphological parameters were evaluated and it is encouraged to explore other combinations for future research. Another point of interest it that DDMs strongly depend on the amount of data analyzed and only data of 30 experiments were included in this modelling exercise.

Even though the DDMs deliver quite good correlation coefficient values, for some carbon samples they output very high, unrealistic porosities. This is attributed to the big range between the particle sizes of the samples and the fact that no boundary conditions were provided during the modelling exercise. Close attention should be payed to the validity of data driven models and classical models could be used to corroborate conclusions.

5 Conclusions

In this section of the report, the main conclusions concerning the model prediction accuracy and some of the model inputs are discussed. The presented results in this report has led to the discovery of further insights concerning the fluidization behavior of GAC in water.

Three main contributions to science have been identified in this project. The first one is a good data set of experimental data, where thirty expansion experiments at different temperatures were performed using nine GAC samples. The second one is the AquaGAC input model, which can be used as an input to use classical models to predict the porosity of porous media and as a tool to check for the consistency of the input data. The third contribution is several empirical equations that describe well the data set of experimental data.

Three main contributions to the drinking water treatment practice were also identified. The first one was the reduction potential of operational expenses due to diminishing of particle washout and an increased process control. The second one is unit process resilience and sustainability, where the unit process can be robust enough to change to sustainable material and adapting to changing process conditions. Consequently, a positive impact on the image of water utilities is expected due to an increase in the business performance. The findings of this report are expected to contribute to the improvement of current fluidization models and help towards closing the previously stated knowledge gap.

5.1 Particle size

It is advisable to use the minimum diameter d_{10} of the ImageJ analysis if only one diameter had to be used for fluidization experiments. The main reason for this choice is that it delivered the lowest error for the analyzed data set. When the d_{10} minimum diameter is employed, it was found that classical hydraulic models describe relatively well the data. The absolute relative error in the prediction of the porosity for the 30 performed expansion experiments was ranging from 9-11%.

5.2 Particle densities determination

Due to the porous nature of GAC particles, typically used methods (like the water displacement pycnometer) to determine the wet density delivered deviations from 10-15%. The irregularly shaped and polydispersity of the particles posed a challenge to accurately measure the particle volume and thus the particle envelope density. The uncertainties caused by these measurement methods were overcome by using the different equations developed in the AquaGAC model as checks for data consistency. Unrealistic parameter values from the output calculations were revised using different expressions for consistency. Recommendations for the improvement of the density measurement methods can be found in section 6 of the report.

5.3 Models and expansion experiments

The AquaGAC model approach integrated an existing fluidization model, experimental data and a data driven model. This approach in combination with the existing fluidization model proved to deliver promising results in terms of porosity prediction and even though the continuous improvement of this approach is recommended, it is considered a good foundation that towards closing the studied knowledge gap.

Data driven models, product of different morphological parameters (for example: Aspect Ratio, Circularity, Uniformity Coefficient, among others) and expansion data provide correlation coefficients (R^2) above 0.9 and porosity prediction errors below 3%. However, caution should be used in establishing adequate boundary conditions that are strictly not exceeded to ensure the reliability of the results. Classical hydraulic models, for instance the widely used Carmen-Kozeny model, have deviations while predicting the fluidization of rod-like particles with high aspect ratios. Observations indicate that the interlocking between particles (caused by particle-to-particle interaction) influence their expansion capacity, which is not considered in the models assumptions.

5.4 Particle orientation

The flow velocity and the interlocking between the particles, caused by preferential flow channels in different parts of the bed as the porosity increases, influence the positioning /reorientation of GAC particles. By studying the single particle, it was determined that rod like particles (RB₄C sample) maintain an equilibrium when in a horizontal position. This was also seen in the multi-particle bed when there was enough space for particles to fluidize. When analyzing the H-S drag coefficient in the transitional region, it is possible to observe that, based on the sphericities and particle Reynolds number, the highest drag coefficient is not completely horizontal. However, further information is required for a more quantitative analysis; recommendations to have a more comprehensive understanding of particle orientation are presented in the section 6 of this report.

5.5 Particle sizing methods

Sieve analysis is highly unadvisable for particles with high aspect ratios, as can be seen in the poor estimation of this method in the maximum diameters of the analyzed rod-like particles. The static image analysis methods are very accurate (as illustrated in the coin experiments in Table 23 and Table 26), but only applicable if a representative sample can be obtained using a limited amount of particles. The Camsizer data has the accuracy of the static image analysis methods and can process thousands of particles providing a more representative and accurate result of the particle size of the material. One can conclude that even though sieving analysis is widely used, it is unable to measure all the size characteristics for the case of non-spherical particles. This because particles with high aspect ratios tend to reorient themselves to the smallest diameter when they go through the mesh.

6 Recommendations

6.1 Densities determination

In the present research, we encountered difficulties in formulating the prediction model due to several uncertainties. These uncertainties can be solved either using alternative methods or performing additional checks in the performed experiments.

In order to decrease the uncertainty of the particle envelope density, a method that can accurately determine the exact volume of the particle density is required. Three main methods are proposed: alumina pycnometry, non-wetting fluid pycnometry and advanced image analysis. The first method proposed by (Mauget et al., 2005), consists in using a solid powder of alumina with specific particle size range to determine the volume of the analyzed GAC particles. The second method consists in using a non-wetting fluid with enough surface tension that prevents its flow into the GAC pores, then using standard fluid displacement pycnometry. Although hazardous, if used in a safe and controlled environment, mercury can provide accurate particle density results in a timely manner. The third and final method is using advanced image analysis methods, these consist in taking many pictures of the object and then process them using a photogrammetry free software, these will deliver a point cloud that can be easily processed in a CAD software with great accuracy. Using the VHX microscope and taking several pictures from different angles of a sample is also a possibility that can be explored in future research. Other density measurement methods to be considered are recommended by (Soyer & Akgiray, 2016).

If the envelope particle volume is accurately determined, by wetting the same analyzed particles for 6 days and weighing the wet mass in a microbalance, a more reliable wet density measurement can be obtained. One should notice that there is an increase in the reliability of the results as more mass is used in the measurements, as there is a lower error provided by the instruments. This measurement can later be compared with the calculated wet density experiments using the differential pressure measurements. Measuring the pressure difference with both a hand pressure meter and the differences in height can provide an extra check and increase the reliability of the measurements.

6.2 Particle size and orientation experiments

The orientation was only measured in a fixed point in time, it could be interesting to use existing algorithms, for example the one developed by (Kruggel-Emden & Vollmari, 2016), using a special camera setup in order to track and detect all particles and have the complete distribution of particle orientation in all the faces of the bed. Other options obtain more detailed information and get a better understanding of the particle orientation are to create detailed models using CFD-DEM analysis or, if possible, use more specialized measuring methods for example X-ray tomography. These approaches allow us to look inside the reactor and obtain a dynamic orientation distribution. Currently there is much work concerning these aspects, but they are mainly focused on GLS fluidized beds. It is important

to mention that observations are not enough to provide a comprehensive understanding of the behavior of particles with high aspect ratios.

In terms of the particle size, all of the image analysis methods deliver adequate measurement accuracy, but it is recommended to use the Camsizer measurements due to its capabilities of analyzing thousands of particles in a short amount of time and overall lower errors when compared with the C-K hydraulic diameter. If a low budget analysis is required, ImageJ could serve the same purpose although a representative sample would have to consist on around 700 particles, depending on the particle size.

6.3 Experimental set-up

The experimental set-up is a great way to perform fluidization experiments for a wide range of temperatures, nevertheless, a few improvements are recommended. The first improvement is to use a more sensitive flow meter and a smaller pump or by-pass when experimenting with GAC particles, some of the fixed bed flows had to be assumed because the flow was not detectable by the flow meter. A more accurate differential pressure sensor can also be implemented for the increased reliability of measurements and serve as a check for other measurements. It is recommended to measure the wet mass before introducing it into the column in a more controlled environment as it is difficult to remove the wet GAC from the column without losing any mass. It is also advisable to first perform an experiment with calcite pellets or other non-porous material (such as glass beads) where one can easily determine the expansion parameters to corroborate that there are no problems with the set-up.

6.4 Modelling aspects

The modelled morphs using symbolic regression were only using the tenth percentile measurements for every method, increasing the complexity of the morph matrix could provide additional insights to further understand the influence of the morph in the fluidization of GAC particles. Multiple combinations are possible with the obtained morphological parameters using the different percentiles, focusing on the lower percentiles could lead to better correlations.

For both the classical and data driven modelling it is recommended to evaluate the different samples by classifying them by their shape (granular, spheres and rods) and finding further insights and correlations. This can lead to models with increased accuracy based on the morphological parameters.

6.5 Future research

In practice, there are three additional dynamic phenomena identified that can affect the fluidization of GAC particles. The first one is the biofilm formation, which changes both the density and the size of the GAC particles. The second one are changes in size of GAC particles due to particle-to-particle interaction and GAC reactivation, the work of (Shpirt & Alben, 2018) points out that the changes in size are not uniform throughout the bed and

the decrease in size is a very slow process. The changes in size not only play an important role in the fluidization of GAC but also on water quality, (Fukuhara, Yoshinaka, Katsu, & Abe, 2018) found that a possible cause of GAC adsorption capacity deterioration was the stronger fluidization on smaller particles. The third one is air scouring, typical backwashing procedures include a combination of air, water and air, and water, for better removal of caught particles in the filter media. Even though there are many similarities in the fluidization of the two fluids, this definitely influences how particles are fluidizing in the full-scale filters. The present investigation only focused on the fluidization of virgin or reactivated carbon with particles with a constant particle density and size. The impacts of the effects on fluidization of these three phenomena should be evaluated and included in future modelling exercises. These three phenomena are considered to increase the robustness of the model and contribute towards making the GAC unit process even more resilient to changes.

The degree of wetting of the GAC particles is a crucial factor in the fluidization behavior, but not completely investigated in this project. Even though it was found in the report that particles should be wetted for at least 144 hours (6 days), future research concerning the degree of wetting is recommended.

For future research, it is also recommended to evaluate the expansion behavior of mixtures of GAC with particles of different morphology and aspect ratios. In practice, GAC mixtures of different shapes, uniformity coefficients and raw materials are found, but the expansion of mixtures and the possible negative effects have not been clearly evaluated. This research serves a good basis on the calculations and implications of the work required to deliver further understanding and insights using mixes.

References

- Akkoyunlu, A. (2003). Expansion of Granular Water Filters During Backwash. *Environmental Engineering Science*, 20(6), 655–665.
<https://doi.org/10.1089/109287503770736168>
- Awange, J., & Paláncz, B. (2016). *Geospatial Algebraic Computations* (Third).
- AWWA. (2011). *Water Quality & Treatment*. (J. K. Edzwald, Ed.) (6th editio).
- Barbosa, M. O., Moreira, N. F. F., Ribeiro, A. R., & Silva, M. F. . (2015). Pollutants from the EU Watch List : a review of their occurrence and water-treatment options. *European Commission -Science for Environment Policy*, (August 2013).
[https://doi.org/10.1016/j.watres.2016.02.047.Contact](https://doi.org/10.1016/j.watres.2016.02.047>Contact)
- Briens, L. A., Briens, C. L., Margaritis, A., & Hay, J. (1997). Minimum liquid fluidization velocity in gas-liquid-solid fluidized beds of low-density particles, 52(97).
- Burke, S. P., & Plummer, W. B. (1928). Gas Flow through Packed Columns, 20(11), 1196–1200. <https://doi.org/10.1021/ie50227a025>
- Carman, P. C. (1937). Fluid flow through granular beds. *Chemical Engineering Research and Design*, 75, S32–S48. [https://doi.org/10.1016/S0263-8762\(97\)80003-2](https://doi.org/10.1016/S0263-8762(97)80003-2)
- CEFIC. (1986). Test methods for activated carbon. *European Council of Chemical Manufacturers Federation/ European Chemical Industry Council*, (9), 43.
- Chen, X., Zhong, W., & Heindel, T. J. (2017). Fluidization of cylinder particles in a fluidized bed. *Advanced Powder Technology*, 28(3), 820–835.
<https://doi.org/10.1016/j.appt.2016.12.008>
- Dabrowski, W., Spaczyńska, M., & Mackie, R. I. (2008). A model to predict granular activated carbon backwash curves. *Clean - Soil, Air, Water*, 36(1), 103–110.
<https://doi.org/10.1002/clen.200600033>
- Dijk, Van, J., & Wilms, D. A. (1991). Water treatment without waste material fundamentals and state of the art pellet softening.
- Ergun, S., & Orning, A. A. (1949). Fluid Flow through Randomly Packed Columns and Fluidized Beds. *Industrial & Engineering Chemistry*, 41(6), 1179–1184.
<https://doi.org/10.1021/ie50474a011>
- Fukuhara, T., Yoshinaka, M., Katsu, S., & Abe, I. (2018). Deterioration of granular activated carbon collected from post-ozonation upflow fluidized bed contactor — influence of particle diameter, (November), 465–470.
<https://doi.org/10.2166/aqua.2008.104>
- Hölzer, A., & Sommerfeld, M. (2008). New simple correlation formula for the drag coefficient of non-spherical particles, 184, 361–365.
<https://doi.org/10.1016/j.powtec.2007.08.021>

- Kozeny, J. (1927). Über kapillare Leitun g des Wassers im Boden.
- Kramer, O. J. I., Moel, P. J. De, Baars, E. T., Vugt, W. H. Van, Padding, J. T., & Hoek, J. P. Van Der. (2018). Improvement of the Richardson-Zaki liquid-solid fluidisation model on the basis of hydraulics.
- Kruggel-Emden, H., & Vollmari, K. (2016). Flow-regime transitions in fluidized beds of non-spherical particles. *Particuology*, 29, 1–15.
<https://doi.org/10.1016/j.partic.2016.01.004>
- Kunii, Daizo; Levenspiel, O. (1991). *Fluidization Engineering*. (H. Brenner, Ed.) (2nd Editio). Butterworth-Heinemann.
- Livingston, J. V. (2005). Trends in Water Pollution Research, 2005.
- Ljung, L. (2001). Black-box models from input-output measurements. *IMTC*.
<https://doi.org/10.1109/IMTC.2001.928802>
- Ma, H., Xu, L., & Zhao, Y. (2017). CFD-DEM simulation of fluidization of rod-like particles in a fluidized bed. *Powder Technology*, 314, 355–366.
<https://doi.org/10.1016/j.powtec.2016.12.008>
- Mahajan, V. V., Nijssen, T. M. J., Kuipers, J. A. M., & Padding, J. T. (2018). Non-spherical particles in a pseudo-2D fluidised bed: Modelling study. *Chemical Engineering Science*, 192, 1105–1123. <https://doi.org/10.1016/j.ces.2018.08.041>
- Mauget, M. C., Montillet, A., & Comiti, J. (2005). Macrostructural characterization of granular activated carbon beds. *Journal Material Science*, 40(3), 747–755.
<https://doi.org/10.1007/s10853-005-6316-7>
- Mcnown, J. S., & Malaika, J. (1950). Effects of Particle Shape in Settling Velocity at Low Reynolds Numbers. *Transactions, American Geophysical Union*, 31(1), 74–82.
- Micrometrics. (2010). Determining Volume and Density for Particle Technologists. Retrieved from <https://www.azonano.com/article.aspx?ArticleID=2637>
- Richardson, J. F. (1954). SEDIMENTATION AND FLUIDISATION : PART I. *Chemical Engineering Research and Design*, 75(3), S82–S100. [https://doi.org/10.1016/S0263-8762\(97\)80006-8](https://doi.org/10.1016/S0263-8762(97)80006-8)
- Shpirt, E. A., & Alben, K. T. (2018). CHANGES IN PARTICLE SIZE DISTRIBUTIONS ON A FIXED BED OF GRANULAR ACTIVATED CARBON, 18(November), 31–42.
- Soyer, E., & Akgiray, O. (2016). Characterization of Granular Materials with Internal Pores for Hydraulic Calculations Involving Fixed and Fluidized Beds Selda Yig i. <https://doi.org/10.1021/acs.iecr.6b00953>
- Sutera, S., & Skalak, R. (1993). THE HISTORY OF POISEUILLE ' S LAW.
- van Lier, W. C. (1984). The Influence of Particle Shape and Particle Size Distribution on fluidisation behaviour of granular activated carbon in the aqueous phase. *Particle &*

Particle Systems Characterization, 1(1-4), 143-152.
<https://doi.org/10.1002/ppsc.19840010125>

Yang, W.-C. (2003). *Handbook of Fluidization and Fluid-particle Systems*. Marcel Dekker.

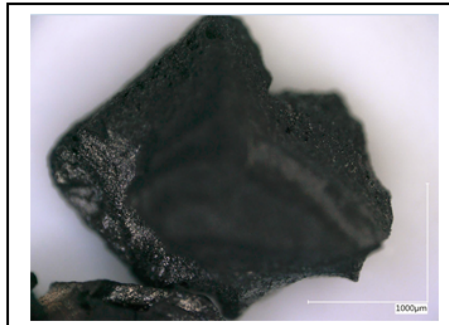
Appendix

Appendix A1 - Main characteristics of activated carbon samples

The following figures provide a basic overview of the nine GAC samples used in this research. Every GAC is referred to by their commercial name in every part of the present report. For further density and particle size characteristics refer to the results of the particle characterization section of this report.



Commercial Name	Filtrasorb 300C
Manufacturer	Calgon
Raw Material	Fossil
Bulk density	575 [kg/m ³]
d10	0.66 [mm]
d90	2.24 [mm]
d50	1.16 [mm]



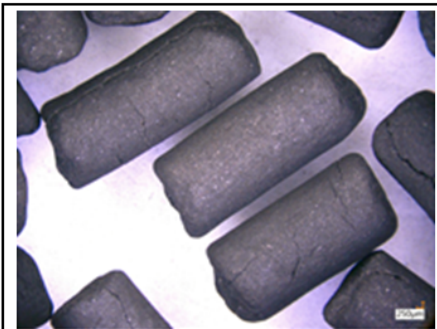
Commercial Name	Aquasorb K-GA
Manufacturer	Jacobi Carbons
Raw Material	Coconut Shells
Bulk density	450 [kg/m ³]
d10	0.67 [mm]
d90	2.62 [mm]
d50	1.33 [mm]



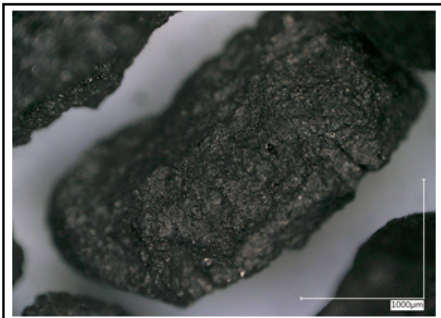
Commercial Name	Saratech Spherical
Manufacturer	BLÜCHER
Raw Material	Synthetic polymer
Bulk density	250-800 [kg/m ³]
d10	0.41 [mm]
d90	0.53 [mm]
d50	0.47 [mm]



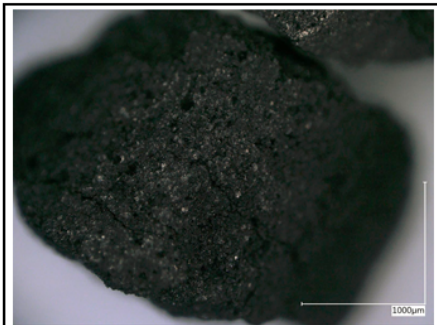
Commercial Name	Norit ROW o.8 Supra
Manufacturer	Cabot Corporation
Raw Material	Wood
Bulk density	390 [kg/m ³]
d10 (width)	0.81 [mm]
d90 (length)	2.72 [mm]
d50	1.33 [mm]



Commercial Name	Norit RB 4C
Manufacturer	Cabot Corporation
Raw Material	Wood*
Bulk density	400-500 [kg/m ³]
d ₁₀	3.73 [mm]
d ₉₀	9.36 [mm]
d ₅₀	5.41 [mm]



Commercial Name	Filtrasorb TL830
Manufacturer	Calgon
Raw Material	Fossil
Bulk density	515 [kg/m ³]
d ₁₀	0.99 [mm]
d ₉₀	2.77 [mm]
d ₅₀	1.78 [mm]



Commercial Name	Aquasorb K-6300
Manufacturer	Jacobi Carbons
Raw Material	Fossil
Bulk density	445 [kg/m ³]
d ₁₀	0.77 [mm]
d ₉₀	3.10 [mm]
d ₅₀	1.81 [mm]



Commercial Name	Resorb HC
Manufacturer	Jacobi Carbons
Raw Material	Fossil
Bulk density	450 [kg/m ³]
d ₁₀	0.60 [mm]
d ₉₀	2.64 [mm]
d ₅₀	1.34 [mm]



Commercial Name	Norit GAC 830 Supra
Manufacturer	Cabot Corporation
Raw Material	Fossil*
Bulk density	480 [kg/m ³]
d ₁₀	0.64 [mm]
d ₉₀	2.73 [mm]
d ₅₀	1.31 [mm]

Additional Notes:
* Assumed based on material properties
d ₁₀ - is the tenth percentile of the minimum diameter measured with the camsizer
maximum diameter measured with the camsizer
d ₅₀ - is the average fiftieth percentile of the maximum and minimum diameter measured with the camsizer

Appendix A2 - Instruments specifications & morphological parameters

In this appendix, the specs of the different instruments as well as their output morphological parameters are presented. For the case of the microscope and ImageJ, a validation of their measurements using a coin is also presented.

- Microscope

Table 21 – Microscope specifications (Keyence VHX-5000 user's manual).

VHX-5000 – Specifications		
Model		VHX-5000
Camera	Image sensor	1/1.8-inch, CMOS image sensor Virtual pixels: 1600 (H) × 1200 (V)
	Scanning system	Progressive
	Frame rate	50 frames/sec. (max.)
	High Dynamic Range	16-bit resolution through RGB data from each pixel
	Gain	AUTO, MANUAL, PRESET
	Electronic shutter	AUTO, MANUAL, 1/60, 1/120, 1/250, 1/500, 1/1000, 1/2000, 1/5000, 1/9000, 1/19000
	Supercharge shutter	0.02 sec. to 4 sec.
	White balance	AUTO, MANUAL, ONE-PUSH SET, PRESET (2700K, 3200K, 5600K, 9000K)
	Back-focus adjustment	Not required
	LCD monitor	Size
Panel size		509.184 (H) × 286.416 (V) mm 20.05 ^{''} (H) × 11.28 ^{''} (V)*1
Pixel pitch		0.2652 mm (H) × 0.2652 mm (V) 0.01 ^{''} (H) × 0.01 ^{''} (V)*1
Number of pixels		1920 (H) × 1080 (V) (FHD)*1
Display colors		Approx. 16,770,000 colors*2*1
Brightness		300 cd/m2 (Center 1 Point, typical)*1
Contrast ratio		1000:1 (typical)*1
Field of view	±89° (typical, horizontal), ±89° (typical, vertical)*1	
CD-R/CD-RW/DVD drive unit	Unit	DVD-ROM super-multi drive unit
	Applicable disk	CD-R/CD-RW/DVD±R/DVD±R DL/DVD±RW/DVD-RAM

VHX-5000 – Specifications		
Hard disk drive unit	Storage capacity	8.7 GB (when DVD±R DL is used)
		500 GB (including 165 GB reserved area) Approx. 1680000 images (When a 2 million-pixel image is compressed) to approx. 55000 images (When a 2 million-pixel image is not compressed)
Image format		JPEG (With compression), TIFF (No compression)
Observable image size		20000 (H) pixels × 20000 (V) pixels (when stitched)
Light source	Lamp	High brightness LED
	Lamp life	40000 hours (reference)
	Color temperature	5700K (typical)
Video output	Output method	DVI-I (1920 × 1080 pixels)
	Scanning frequency	Special LCD monitor
		External monitor
		66 kHz (H), 60 Hz (V)
Input	Mouse input	USB mouse supported
	Keyboard input	USB keyboard supported
	External remote input	Pause/Recording, Non-voltage input (Contact/Noncontact)
Interface	LAN	RJ-45 (10BASE-T/100BASE-TX/1000BASE-T)
	USB 2.0 Series A	6 types
	USB 3.0 Series A	2 types
Software	Video recording software	Allows recording/playing back moving images.
	High quality depth composition software	Captures multiple images focused on different heights and composes a single image from them.
	Area measurement software	Measures an area of a 2D image.
	Time-lapse software	Captures images automatically at specified time intervals.
	Screen splitting software	Displays vertical, horizontal, or 4-part split screens.

VHX-5000 – Specifications		
	Comment input software	Allows inputting and displaying comments such as characters and markers on the observation image.
	Image improvement software	Provides image-processing functions for modifying images to make observation easier.
Power supply	Power voltage	100 to 240 VAC, 50/60 Hz
	Power consumption	280 VA
Environmental resistance	Ambient temperature	+5 to +40 °C 41 to 104 °F
	Relative humidity	35 to 80 % RH (No condensation)
Weight	Controller	Approx. 12.5 kg
	Camera unit	Approx. 1.10 kg (VHX-5100), Approx.1.00 kg (VHX-5020)
	Console	Approx. 0.4 kg
Dimensions (Excluding the projected areas)		550 (W) × 470 (H) × 200 (D) 21.65"(W) × 18.50"(H) × 7.87"(D) (when stored)
<p>*₁ The LCD monitor provided in the VHX Series is based on extremely advanced technology. Rarely, an unlit pixel (black spot) or lit pixel (bright spot) may exist on the monitor screen. However, this is not an indication of the LCD monitor being defective.</p> <p>*₂ Approximately 16,770,000 colors are realized with the FRC processing of the display controller.</p>		

Table 22 – Microscope output morphological parameters

Measurement	Unit	Description
Max diameter	μm	The maximum length between any two points that lie on the inner perimeter of the figure
Area	μm ²	The area of the figure
Circularity	-	When the figure is a perfect circle, the maximum value is one. As it becomes long and thin, this value approaches zero.
Gravity center (Y)	-	The Y coordinate of the center of gravity of the figure.
Area ratio	%	The area ratio of the figure within the screen
Perimeter	μm	The length of the perimeter of the figure. This is calculated as the length of the line that passes through the center of the pixels that make up the inner perimeter.
Diagonal width	μm	This is the distance between two parallel lines that sandwich the particle and are parallel to the line along the maximum diameter. It is calculated as the distance between the pixels that each of the two lines touches.

Measurement	Unit	Description
Feret diameter (Horizontal)	μm	The horizontal length (number of pixels) of a rectangle circumscribed around the figure
Gravity 2nd moment (X-axis)	-	This is the center of gravity secondary moment of the figure on the X-axis. G is the center of gravity of the figure
Circle equivalent dia	μm	This is the diameter of a circle with the same area as the figure. It is sometimes referred to as the Heywood diameter.
Min diameter	μm	This is the minimum possible distance between two parallel lines on either side of the particle. It is calculated as the distance between the pixels that each of the two lines touches.
Feret diameter (Vertical)	μm	The vertical length (number of pixels) of a rectangle circumscribed around the figure.
Max diameter angle	Deg	The angle between a line along the maximum diameter and the x-axis.
Min diameter angle	Deg	The angle between a line along the minimum diameter and the x-axis.
Gravity center (X)	-	The X coordinate of the center of gravity of the figure.
Envelope curve (Perimeter)	-	This is the ratio between the perimeter of the figure and its convex envelope perimeter. This approaches one as the figure is less bumpy.
Envelope curve (Area)	-	This is the ratio between the area of the figure and its convex envelope area. This approaches one as the figure is less bumpy.
1st moment (X-axis)	μm^3	The primary moment of the figure on the X-axis.
1st moment (Y-axis)	μm^3	The primary moment of the figure on the Y-axis.
2nd moment (X-axis)	μm^4	The secondary moment of the figure on the X-axis.
2nd moment (Y-axis)	μm^4	The secondary moment of the figure on the Y-axis.
Product of inertia	μm^4	The product of inertia of the figure on the X and Y axes.
Inertial moment	μm^4	The moment of inertia of the specified particle
Gravity 2nd moment (Y-axis)	μm^4	This is the center of gravity secondary moment of the figure on the Y-axis. G is the center of gravity of the figure.
Gravity product of inertia	μm^4	The center of gravity product of inertia of the figure on the X and Y axes. G is the center of gravity of the figure.
2nd moment major axis	μm^4	This is the length of the figure's secondary moment major axis. Normalization is achieved by dividing by the area.
2nd moment minor axis	μm^4	This is the length of the figure's secondary moment minor axis. Normalization is achieved by dividing by the area.

Measurement	Unit	Description
2nd moment angle	Deg	The figure's secondary moment major axis angle

In Figure A2.1, an illustration of the coin test validation experiment is illustrated. Table 23, presents an overview of the real coin diameter and the measured diameter.

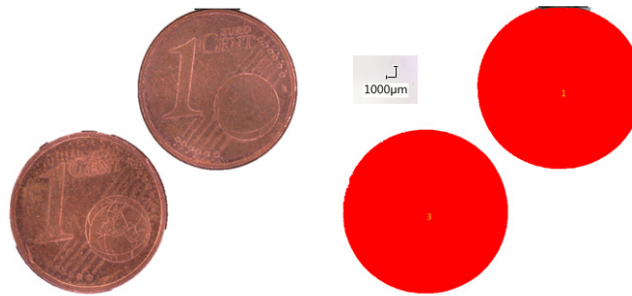


Figure A2.1 – Coin test for microscope measurements validation

Table 23 – Coin test for microscope measurements validation

Type of coin	Real Diameter	Measured Diameter							
	Coin diameter [mm]	Max diameter [mm]	Error [%]	Diag. width [mm]	Error [%]	Circular Eq. diameter [mm]	Error [%]	Min diameter [mm]	Error [%]
1 Euro cent	16.25	16.37	0.71	16.35	0.63	16.30	0.30	16.13	0.77
1 Euro cent	16.25	16.40	0.92	16.31	0.38	16.33	0.49	16.33	0.49

- Scanner (used for Image J processing)

Table 24 – Scanner specifications

EPSON V550 SCANNER SPECS.			
Optical Resolution	6400 dpi x 9600 dpi	Max V-Document Size	11.7 m
Interpolated Resolution	12800 dpi x 12800 dpi	Grayscale Depth	16-bit (64K gray levels)
Automatic Duplexing	none	Grayscale Depth (External)	16-bit (64K gray levels)

Table 25 –
 morphological
 description

Type	flatbed scanner	Color Depth	48-bit color
Scanner Speed Details	21 ms/line black&white (back) 21 ms/line color (back)	Color Depth (External)	48-bit color
Interface Type	USB 2.0	Max H-Optical Resolution	6400 dpi
Form Factor	desktop	Max V-Optical Resolution	9600 dpi
Scan Element Type	CCD	Max H-Interpolated Resolution	12800 dpi
Document Size Class	A4/Letter	Max V-Interpolated Resolution	12800 dpi
Max Supported Document Size	8.5 in x 11.7 in	Scan Density Range	3-4D
Max H-Document Size	8.5 m	Scanner Features	Digital ICE Technology, EPSON ReadyScan LED Technology

 ImageJ
 parameters

Measurement	Unit	Description
Area	mm ²	Area in mm2 (calibrated that way by the user)
Mean	-	Mean gray value --> sum of gray values of all the pixels divided by the number of pixels
StdDev	-	Standard deviation of gray values used to generate the mean gray value
Mode	-	Modal gray value --> most frequently occurred gray value from selection (highest peak in histogram)
Min	-	Minimum gray level --> min gray value of selection
Max	-	Maximum gray level --> max gray value of selection
X	-	Centroid (x coordinate)
Y	-	Centroid (y coordinate)

Measurement	Unit	Description
XM	-	Center of mass (x coordinate)
YM	-	Center of mass (y coordinate)
Perim.	mm	Length of the outside boundary of the selection
BX	-	X-coordinate of upper left corner of rectangle
BY	-	Y-coordinate of upper left corner of rectangle
Width	mm	Width of rectangle
Height	mm	Height of rectangle
Major	mm	Primary axis of ellipse
Minor	mm	Secondary axis of ellipse
Angle	Deg	The angle between the primary axis and a line parallel to the x-axis of the image
Circ.	-	$Circularity = 4\pi * area / perimeter^2$
Feret	mm	Feret diameter (maximum caliper) --> The longest distance between any two points along the selection boundary
IntDen	-	Integrated Density= Area*mean gray value
Median	-	The median value of the pixels in the image or selection
Skew	-	Skewness-->The third order moment about the mean
Kurt	-	Kurtuosis--> The fourth order moment about the mean.
%Area	%	The percentage of pixels in the image or selection that have been highlighted in red
RawIntDen	-	Sum of the values of the pixels in the image selection. RawIntden=IntDen if image is uncalibrated
Slice	-	Current position in the stack
FeretX	-	The starting x -coordinate of the Feret's diameter
FeretY	-	The starting y -coordinate of the Feret's diameter
FeretAngle	Deg	The angle between the Feret's diameter and a line parallel to the x-axis of the image
MinFeret	mm	Minimum feret (calliper) diameter
AR	-	Aspect ratio= major axis/minor axis
Round	-	$Roundness = 4 * area / (\pi * major_axis^2) = inverse\ of\ AR$
Solidity	-	area/convex area

The ImageJ workflow followed was the following:

1. Turn the image into an HSB (hue-saturation-brightness) stack. Since the predominant color of GAC grains is black, the brightness layer of the HSB stack is found to give a very acceptable threshold that allows an accurate identification most of the grains in the image.
2. Make the HSB stack binary. The software assigns pixels a value of either zero (white) or 255 (black).

3. Set measurements. All of the morphological outputs that ImageJ offers were selected, they will be part of a morph matrix input in the symbolic regression modelling part of this research.
4. Set scale. The scale was set based on the pixel size of the image. 2,400 dpi in distance pixels was chosen and the known distance inputed was 25.4 (1 in to mm). The units to be used are millimeters.
5. Analyze the particles choosing the following parameter ranges:
 - a. Size of particles: 0.10 to infinity (this will leave out very fine particles and any other noise that is not of interest).
 - b. Circularity: 0.20-1.00 (the carbon grains are mostly in between this range, including the rods).
 - c. Include holes: Yes. This command includes the internal gaps (if any) of the analyzed particles.
6. Process only the brightness layer: The last decision is to process one or all the images in the HSB stack. It is important to only select the brightness layer as it delivers the most accurate results.
7. Revert the process image to the original to revise that the analyzed contours match the scanned particles.

It is important to mention that this workflow was product of several trial and error attempts. Several workflows were tested and the one above resulted in a good balance between processing time and reliable results. Even though the workflow was considered satisfactory, other approaches can also work for other specific cases. It is also advisable to keep high parameter ranges so that the software identifies all the scanned particles, then when processing all the particles one can simply exclude particles based on a size or circularity range.

In Table 26, the measured diameter and the real diameters are compared.

Table 26 – Coin test for ImageJ validation.

Type of coin	Real Diameter	Measured Diameter					
	Coin diameter [mm]	Max diameter [mm]	Error [%]	Feret diameter [mm]	Error [%]	Min diameter [mm]	Error [%]
Penny	19.05	18.59	2.42	18.63	2.18	18.57	2.50
1 Euro cent	16.25	15.87	2.36	15.92	2.04	15.82	2.67
10 Euro cent	19.75	19.09	3.34	19.25	2.52	19.06	3.52

Table 27 – Pycnometer Specifications (Particle and Surface Sciences, 2010)

ACCUPYC specifications	
Sample Chamber	Small, 1-cm model: 1.2 cm I.D. x 1.1 cm long (with insert: 0.9 cm I.D x 0.8 cm long) Standard, 10-cm Model: 1.82cm I.D. x 3.93 cm long (0.72 in. I.D. x 1.57 in. long) Large, 100-cm Model: 6.8 cm I.D. x 6.31 cm long (1.92 in I.D. x 2.48 in. long)
Precision:	Typical reproducibility to within (0.01% of the nominal full-scale sample chamber volume. Guaranteed reproducibility to within) 0.02% of the nominal full-scale volume on clean, dry, thermally equilibrated samples.
Accuracy:	Accurate to within 0.03% of reading plus 0.03% of nominal full-scale sample chamber volume.
Gases:	Research grade helium is recommended. If unavailable, use helium with a dew point of 67 °C - 88 °F or lower. Carbon dioxide, dry air, nitrogen, etc. can also be used for specific applications.
Electrical:	Voltage: 90 to 264 VAC Power: 30 VA Frequency: 50/60 Hz
Physical:	Width: 53 cm (12 in.) Height 18 cm (7 in.) Depth: 36 cm (14 in.) Weight 19 kg (38 lbs.)
Miscellaneous:	ISO 9001 manufacturer CE certified

Table 28 – Camsizer specifications (Retsch Technology)

Camsizer specifications	
Measuring principle	Dynamic Image Analysis (ISO 13322-2)
Measuring range	0.8 μm to 8 mm 10 μm to 8 mm (gravity dispersion) 0.8 μm to 5 mm (air pressure dispersion) 0.8 μm to 1 mm (wet dispersion)
Type of analysis	dry and wet analysis

Camsizer specifications	
Measuring time	~ 1 to 3 min (depends on desired measuring statistics)
Number of cameras	2
Sample volume	< 20 mg - 500 g (depends on sample type and measurement mode)
Measuring methods	> 300 images/s, each with approx. 4.2 MPixel

Table 29 – Camsizer morphological parameter description

Symbol	Measurement	Unit	Description
Xarea	Particle diameter	mm	Equivalent diameter of the particle calculated by the diameter of a circle having the same projection area A. Suitable for comparison with laser diffraction analysis. (Xarea)
SPHTo	Sphericity	-	Sphericity calculated from the perimeter P and area A of the particle projection. (Xarea)
Symmo	Symmetry	-	Depending on the software configuration, the particle projection is scanned in up to 64 directions. For each direction, the distances r ₁ and r ₂ between the center of area C to the particle projection borders are recorded to calculate the symmetry. (Xarea)
b/lo	Aspect ratio	-	Aspect (width-to-length) ratio of xc min and xFe max. (Xarea)
B/L_rec o	Minimum aspect ratio	-	Depending on the software configuration, the particle projection is scanned in up to 64 directions. For each pair of Feret diameters xFe ₁ and xFe ₂ being perpendicular to each other, the aspect ratio is calculated. The smallest of all aspect ratios is given by B/Lreco. (Xarea)

Conv	Convexity	-	Square root ratio of the real area Areal of the particle projection and its convex area Aconvex. (Xarea)
Tran	Transparency	-	Ratio of the area A ₁ within the particle projection having a brightness > Threshold ₁ to the overall area A of the particle projection. (Xarea)
UC Xarea	Uniformity coefficient	-	d ₆₀ /d ₁₀ based on Xarea
Xc min	Inner width	mm	Particle diameter determined from the smallest of all maximum chords of the particle projection. Also referred to as width of the particle projection. Suitable for comparison with sieve analysis.
		-	d ₆₀ /d ₁₀ based on Xmin
Xfe max	Longest direct length	mm	Particle diameter determined from the longest of all measured Feret diameters of the particle projection. Also referred to as length of the particle projection. Particularly suitable for measuring straight extrudates/fibres or rice grains. (Xfemin)
Xc	Maximum chord	mm	Depending on the software configuration, the particle projection is scanned in up to 64 directions. For each direction, the maximum chord xc perpendicular to the scanning direction (maximum distance between two boundary points) is recorded.
XFe	Feret diameter	mm	Depending on the software configuration, the particle projection is scanned in up to 64 directions. For each direction, the distance xFe between two tangents placed parallel to the scanning direction (calliper measurement) is recorded.

p_o	Fraction	%	Fraction of particles with size x in the range from $> x_1$ and $\leq x_2$. $p(x_1, x_2) = Q(x_2) - Q(x_1)$
Q_o	Cumulative distribution	%	Proportion of particles smaller than or equal to size x with respect to the total amount.
1-Q_o	Cumulative distribution of residue	%	Proportion of particles larger than size x with respect to the total amount
q_o	Frequency distribution	%/m m	The frequency distribution $q_{o,2,3}(x)$ is defined as first derivation of $Q_{o,2,3}(x)$.
NOTE:			The indices "o, 2, or 3" indicate whether the presented distribution is based on number, area or volume, respectively

Appendix A3 – Particle size results

▪ Sieving

The following figures illustrate the frequency and cumulative distributions of the sieving analysis measurements performed:

→ *Filtrisorb 300c*

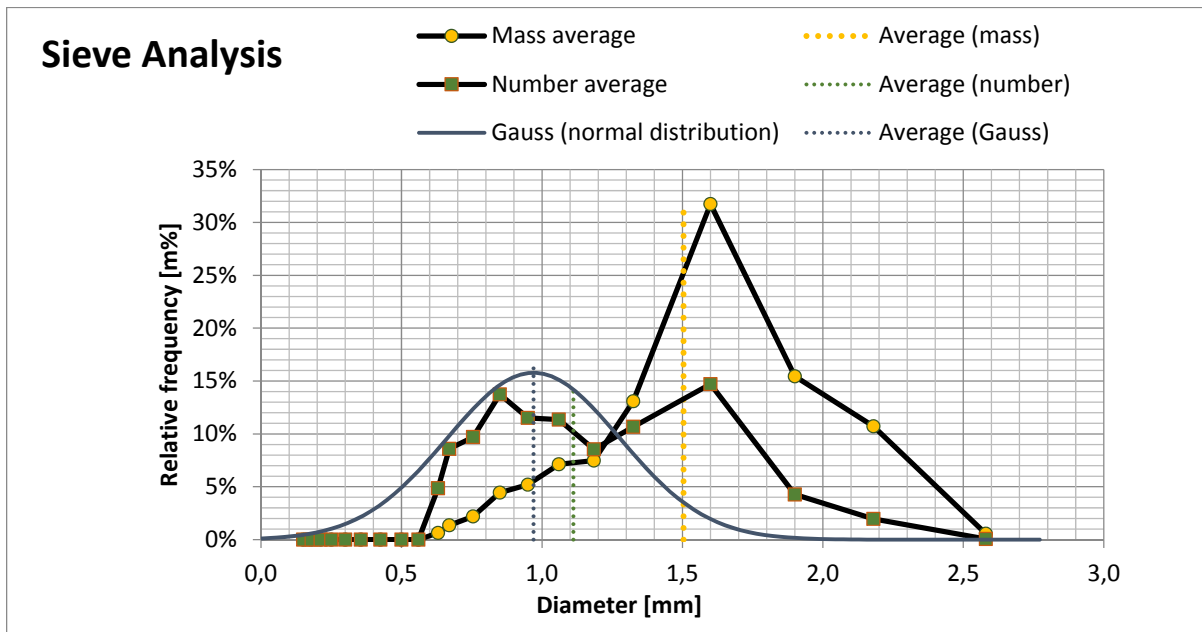


Figure A3.1 - Frequency distribution Filtrisorb 300C

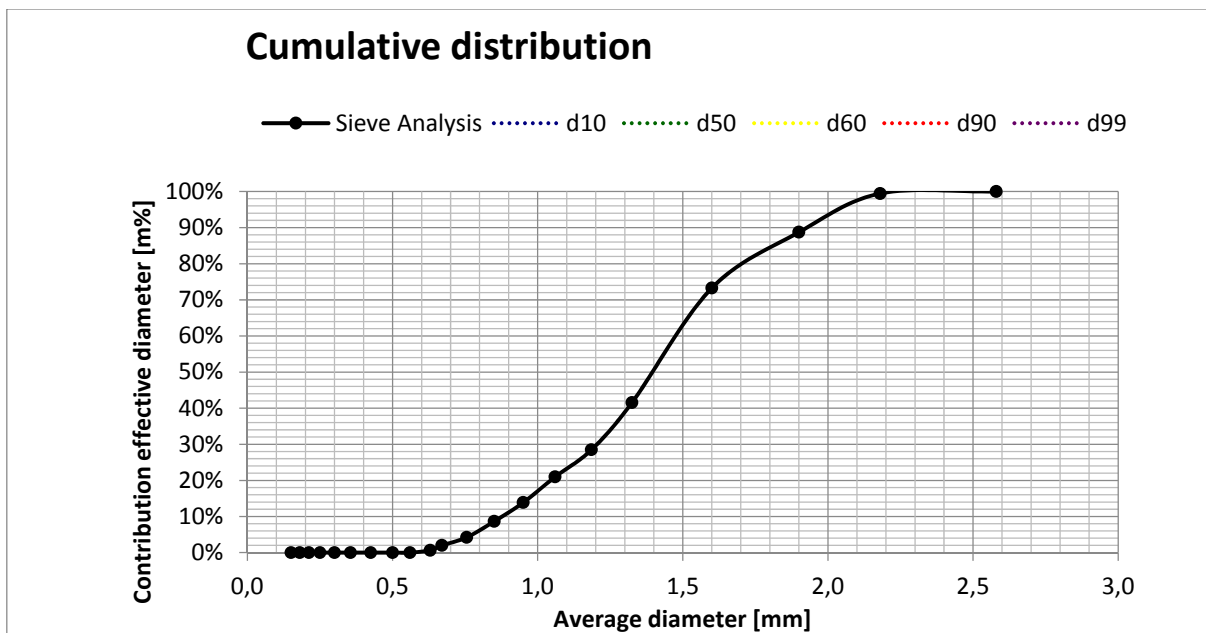


Figure A3.2 - Cumulative distribution Filtrisorb 300C

→ Aquasorb KGA

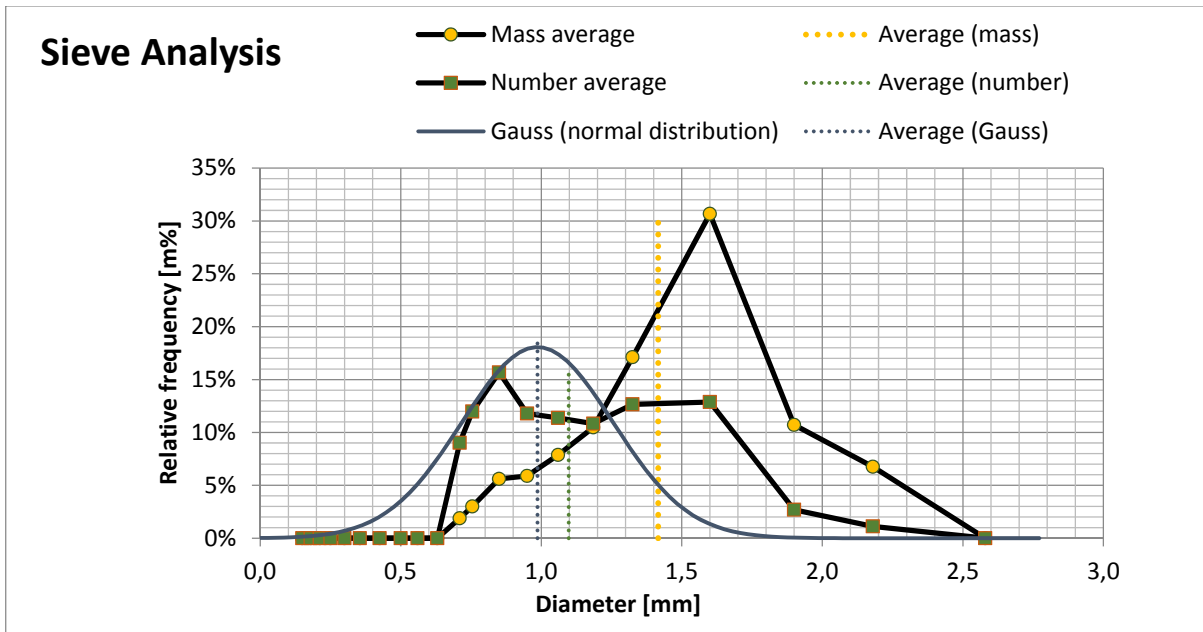


Figure A3.3 - Frequency distribution Aquasorb KGA

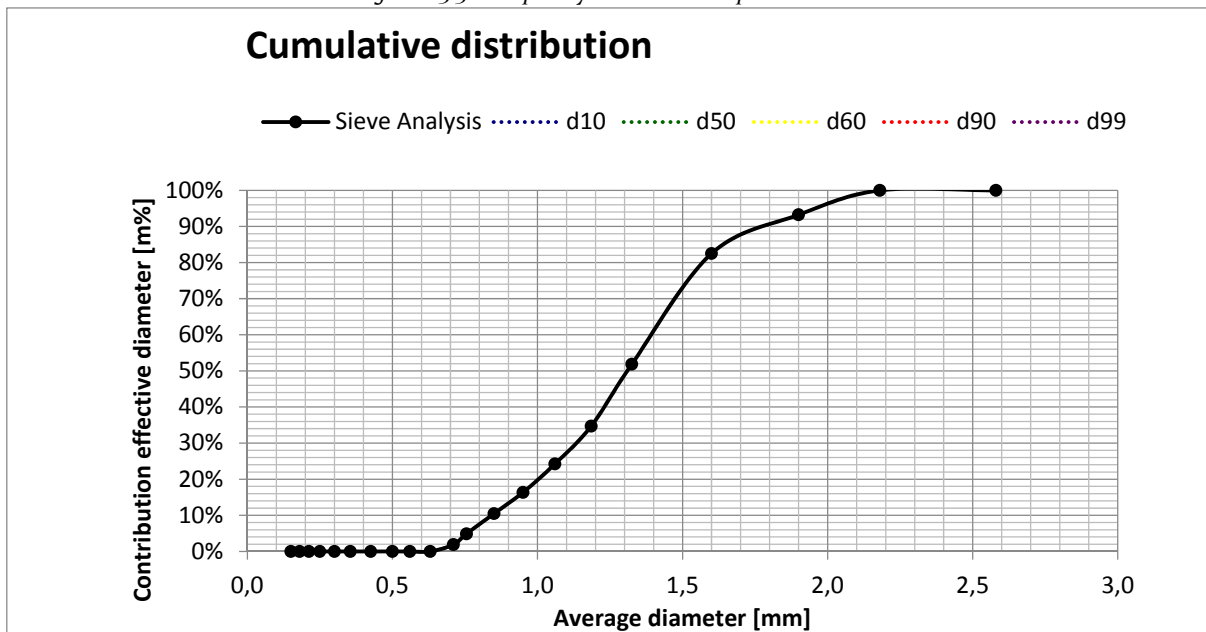


Figure A3.4 - Cumulative distribution Aquasorb KGA

→ Saratech spherical

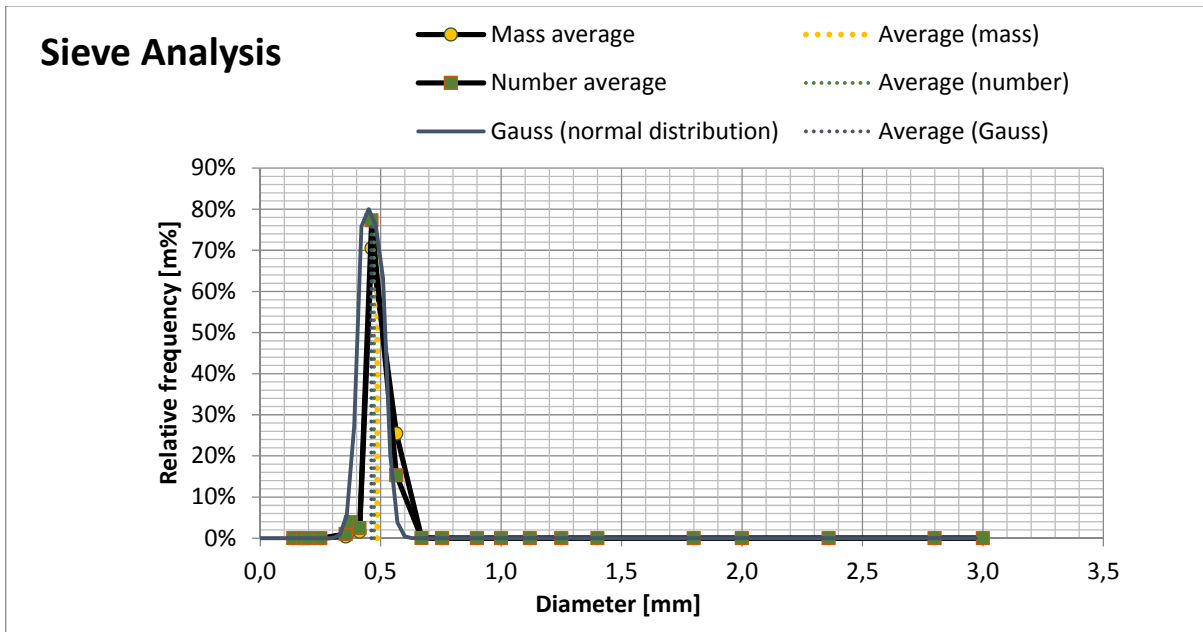


Figure A3.5 - Frequency distribution Saratech spherical

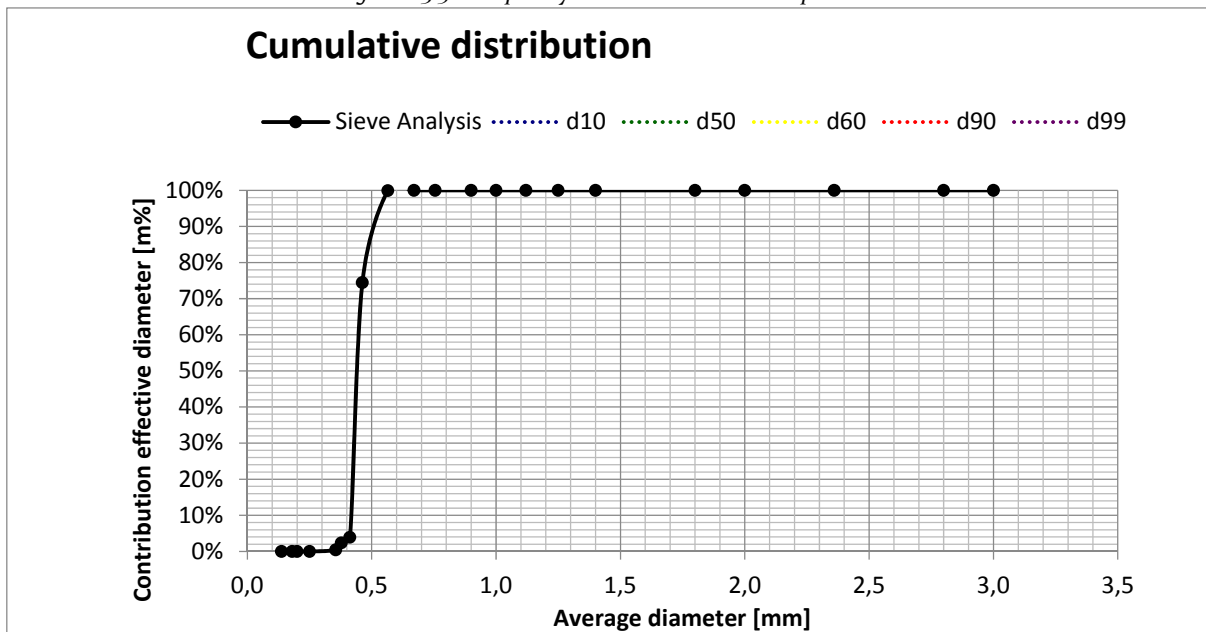


Figure A3.6 - Cumulative distribution Saratech spherical

→ROW o.8 Supra

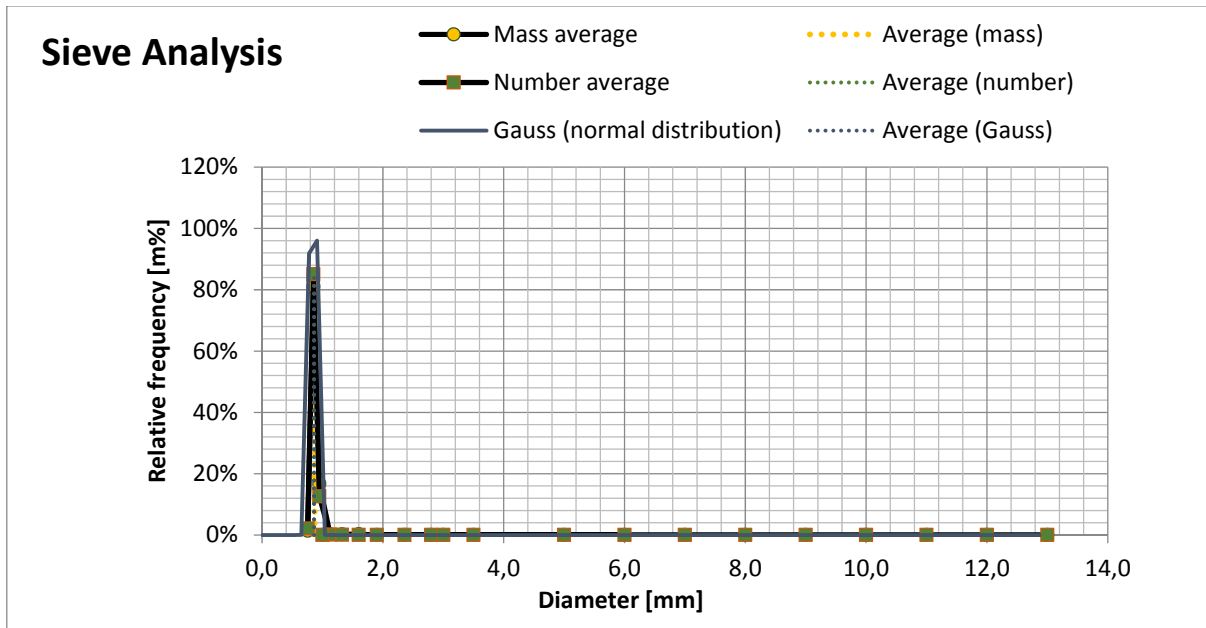


Figure A3.7 - Frequency distribution ROW o.8 Supra

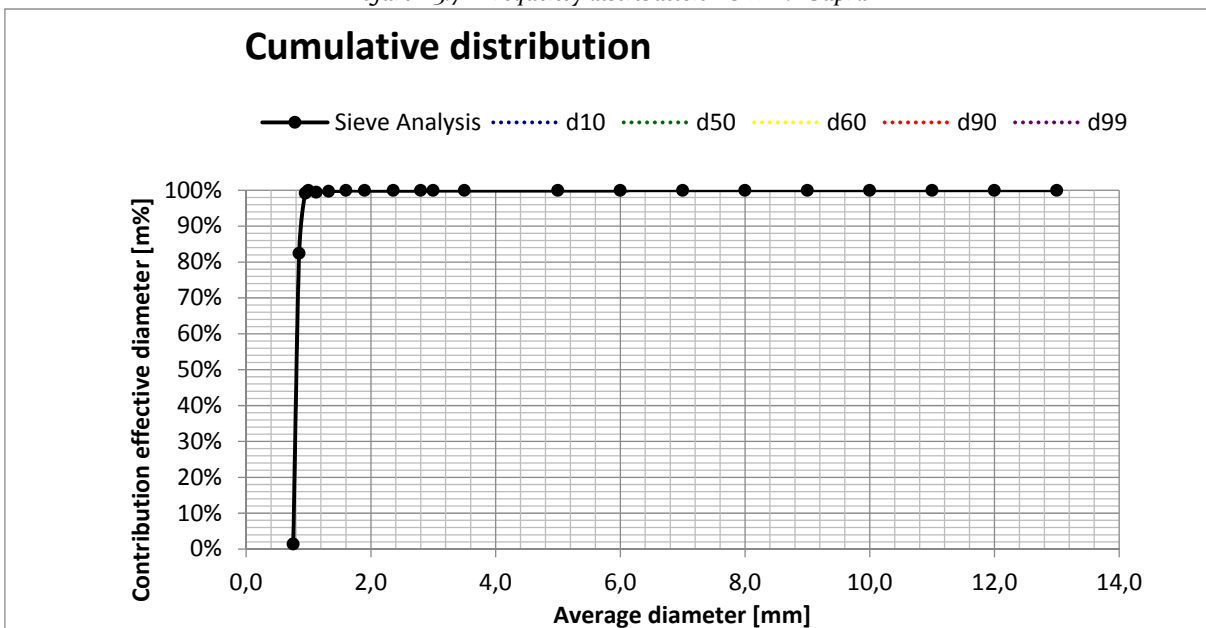


Figure A3.8 - Cumulative distribution ROW o.8 Supra

→ RB₄C

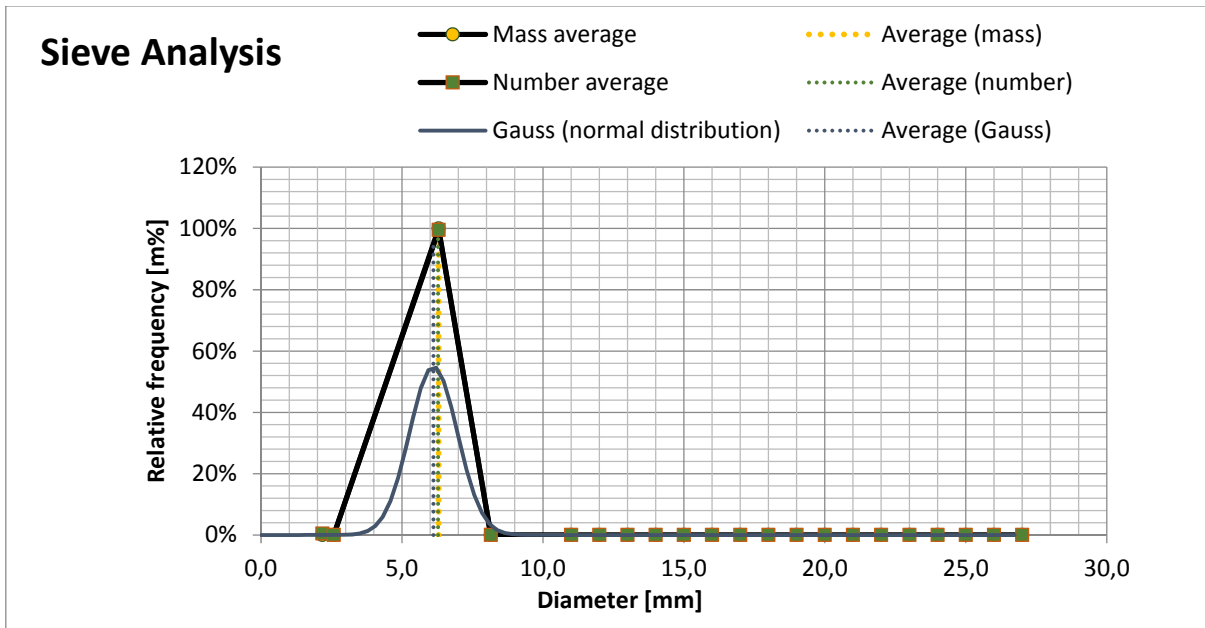


Figure A3.9 - Frequency distribution RB₄C

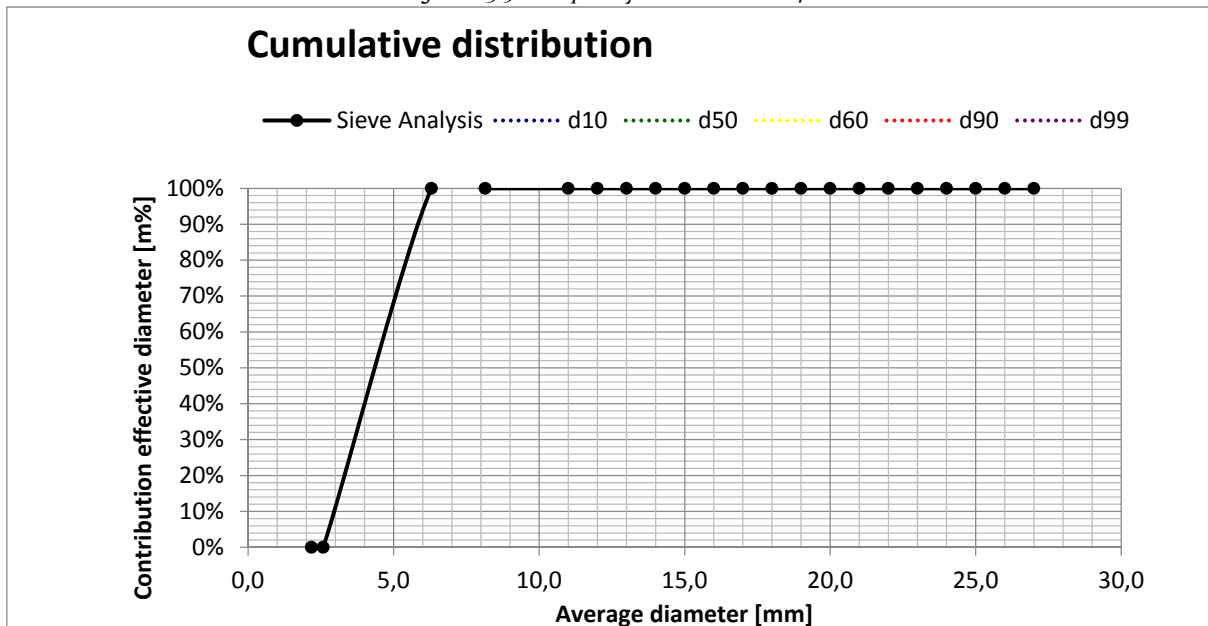


Figure A3.10 - Cumulative distribution RB₄C

→ Filtrasorb TL830

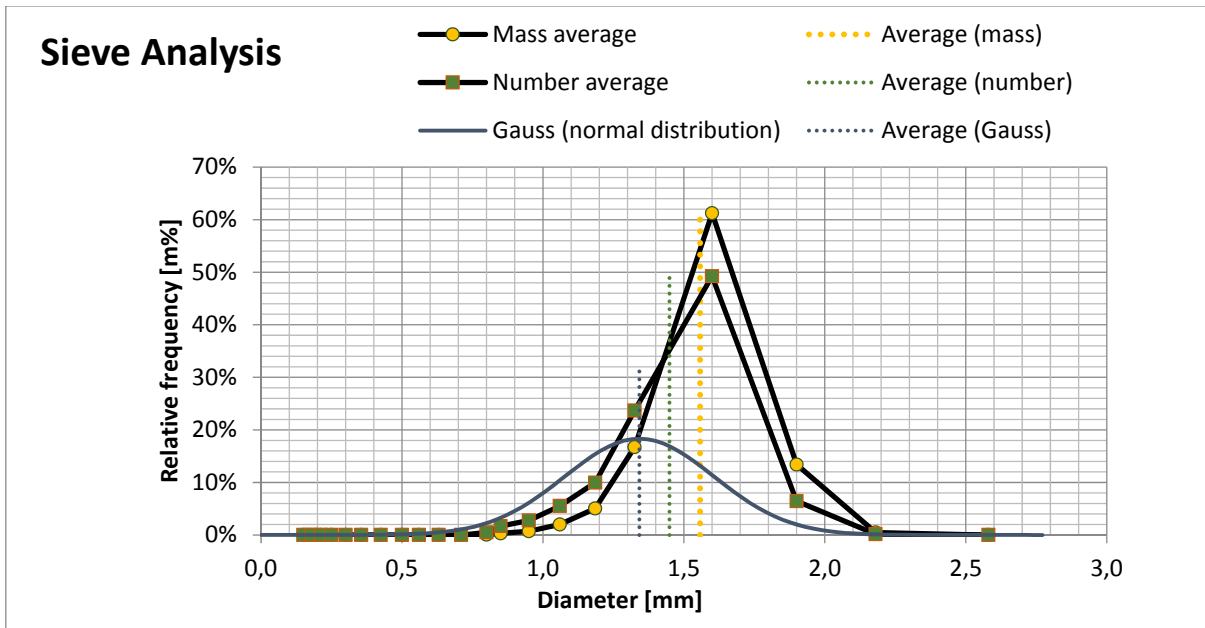


Figure A3.11 - Frequency distribution Filtrasorb TL830

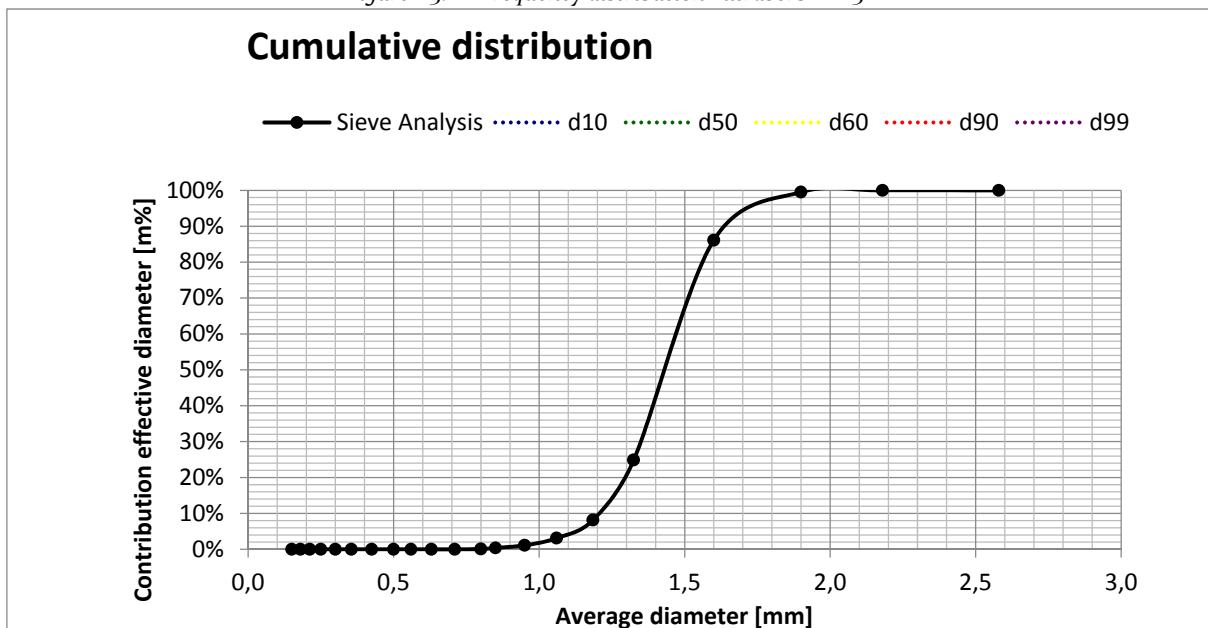


Figure A3.12 - Cumulative distribution Filtrasorb TL830

→ Aquasorb K-6300

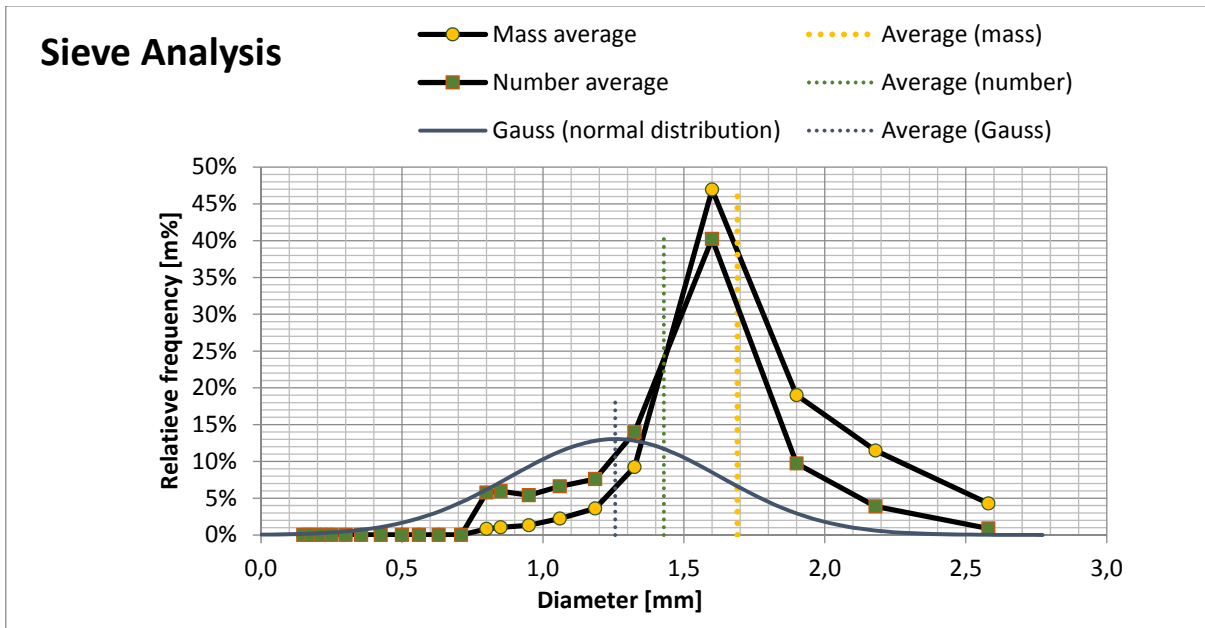


Figure A3.13 - Frequency distribution Aquasorb K-6300

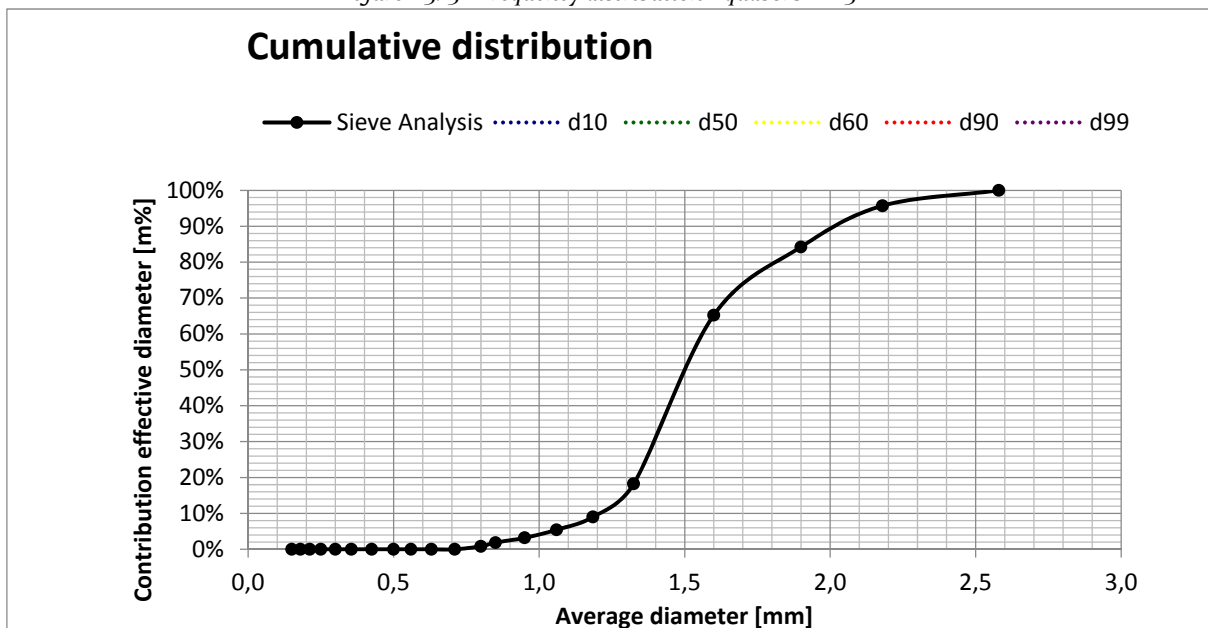


Figure A3.14 - Cumulative distribution Aquasorb K-6300

→ Resorb HC

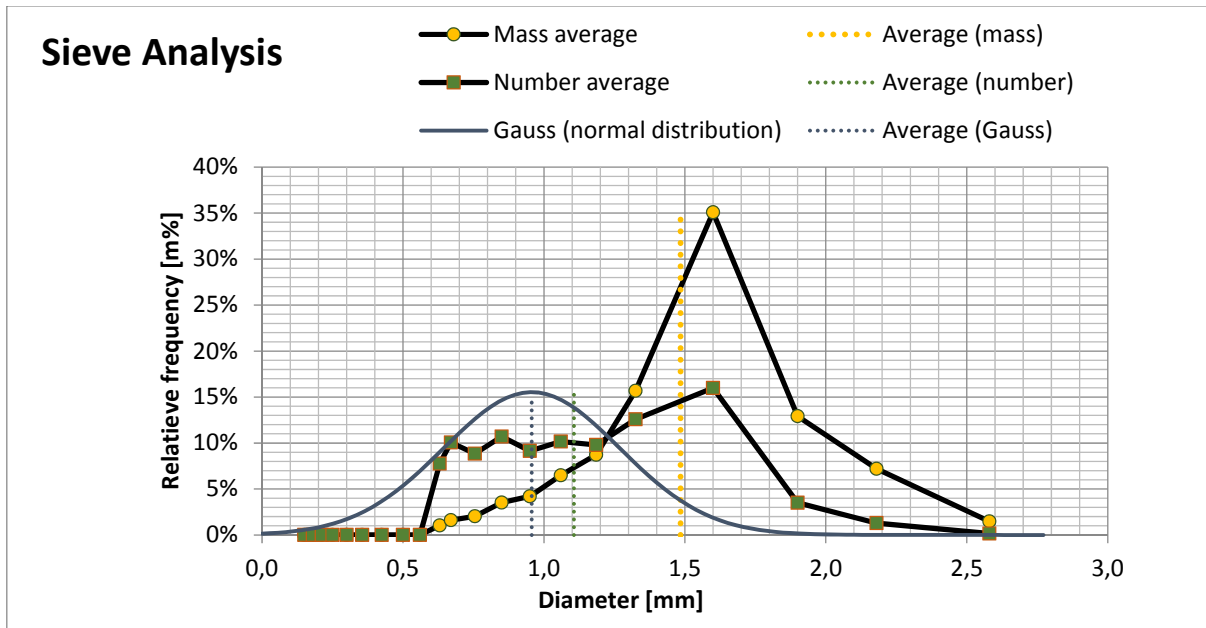


Figure A3.15 - Frequency distribution Resorb HC

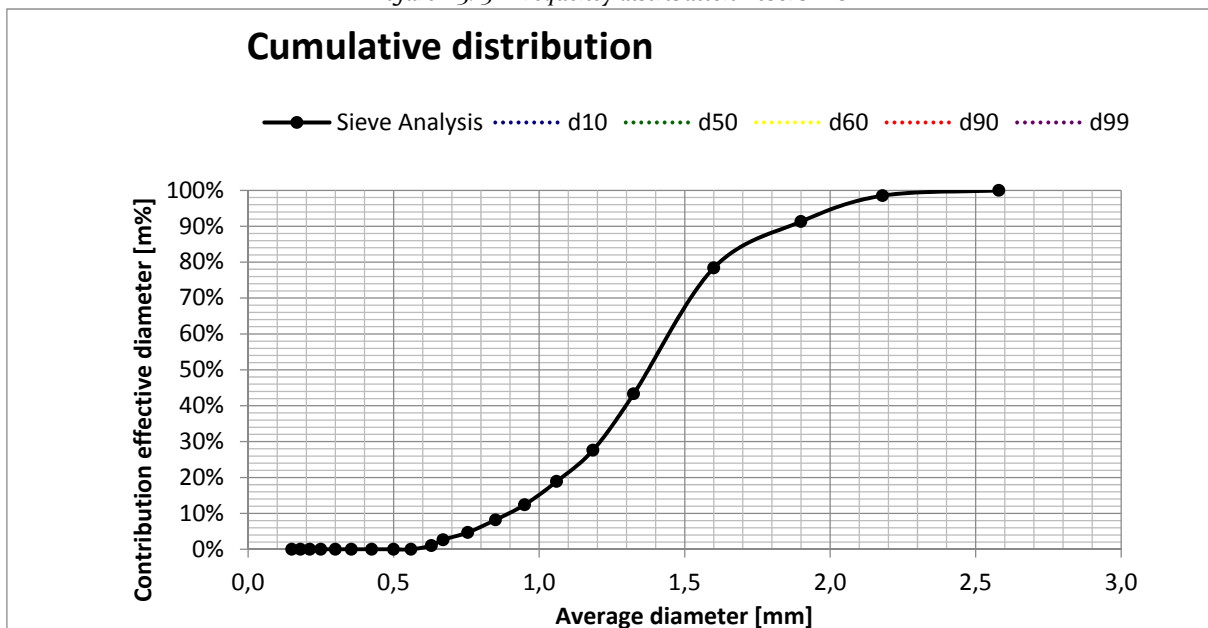


Figure A3.16 - Cumulative distribution Resorb HC

→ GAC 830 SUPRA

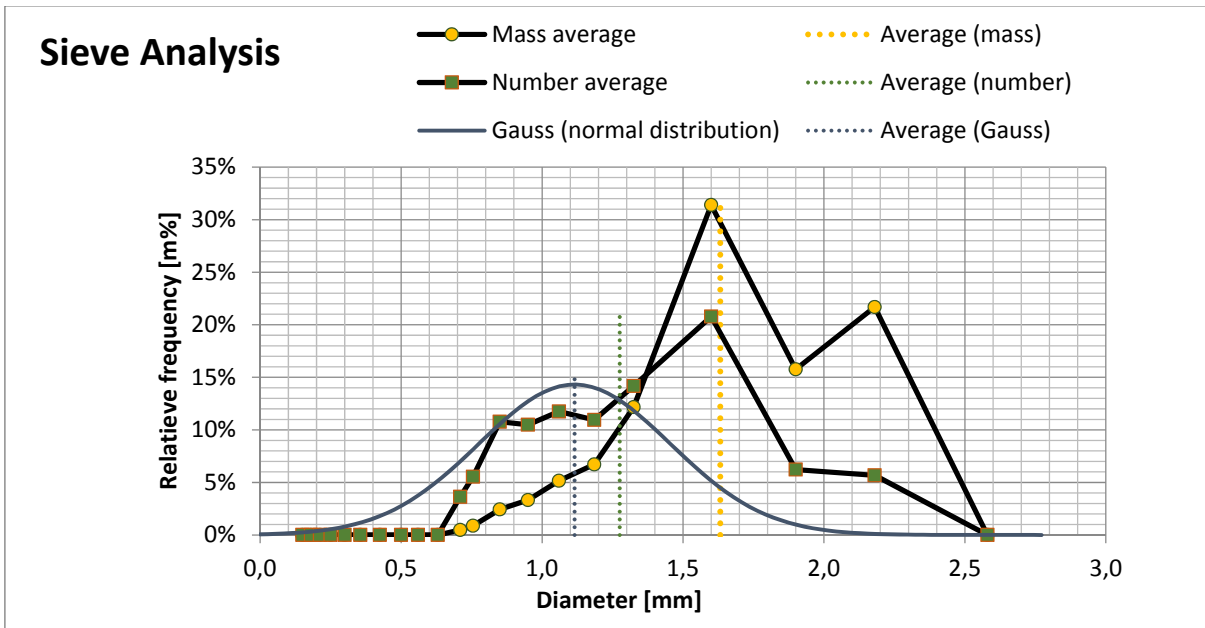


Figure A3.17- Frequency distribution GAC 830 Supra

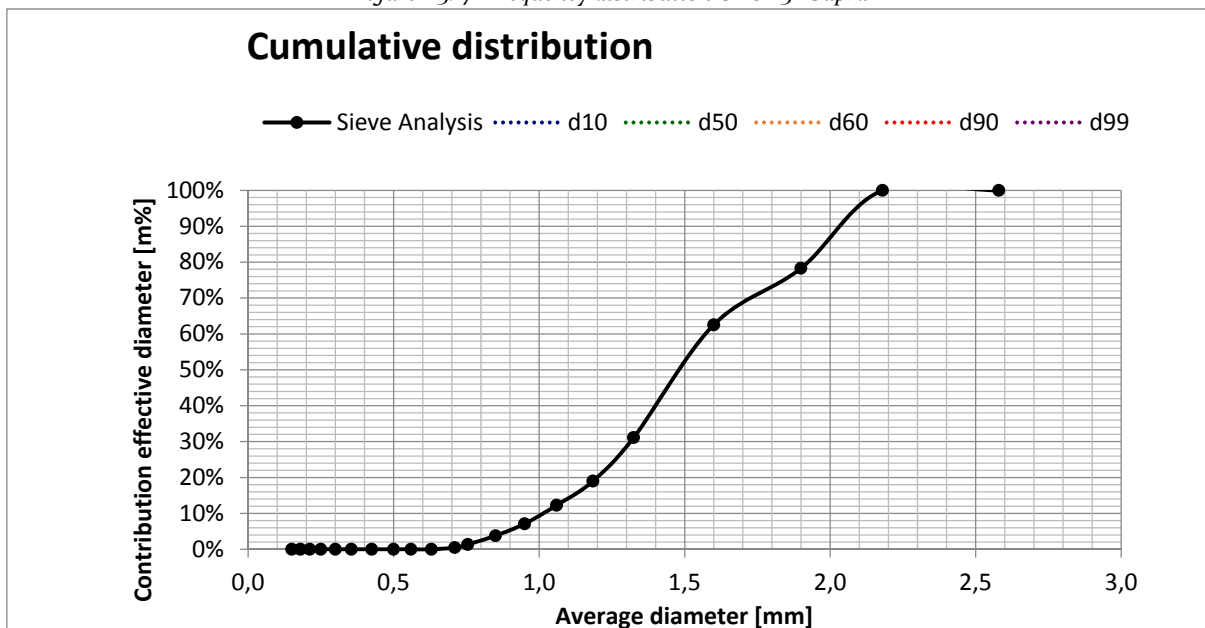


Figure A3.18 - Cumulative distribution GAC 830 Supra

- Microscope VHX 5000

The average cumulative distribution of minimum and maximum diameter measurements of the Microscope VHX 5000 analysis for all carbon samples is presented in the following figures:

→ *Filtrisorb 300c*

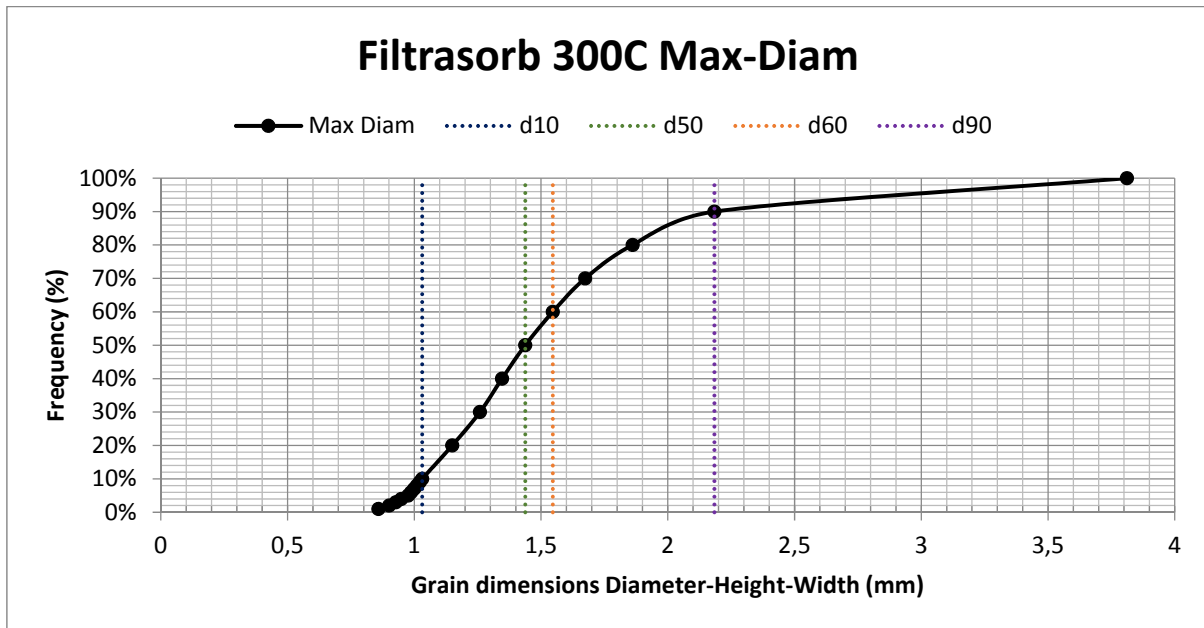


Figure A3.19 – Average cumulative distribution maximum diameter Filtrisorb 300C

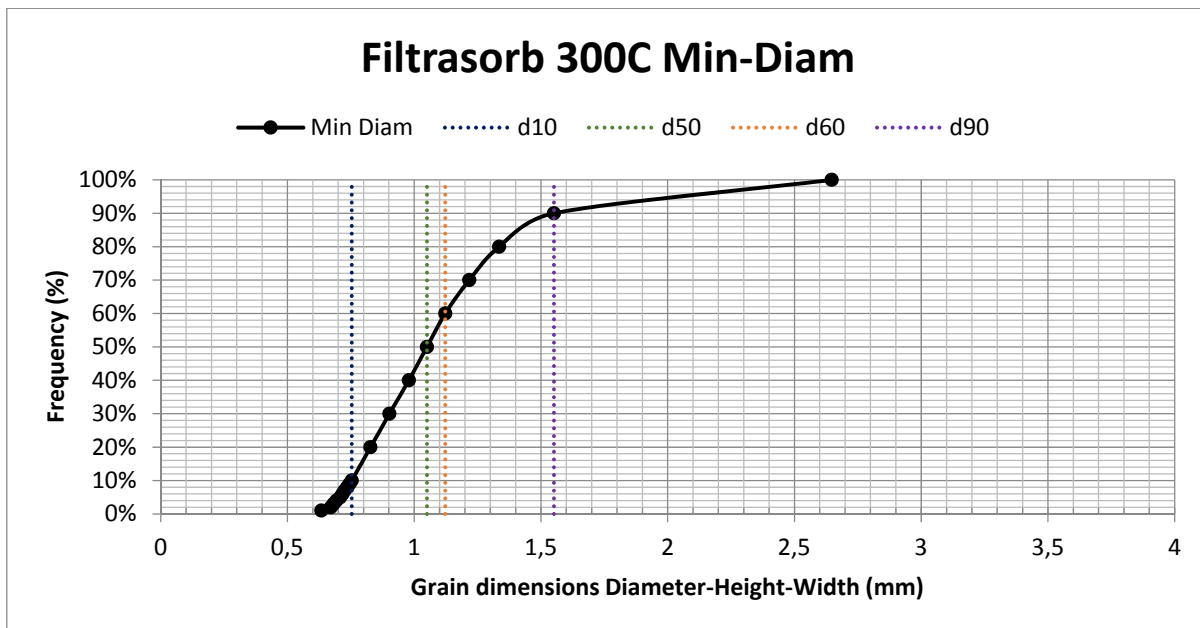


Figure A3.20 - Average cumulative distribution minimum diameter Filtrisorb 300C

→ Aquasorb KGA

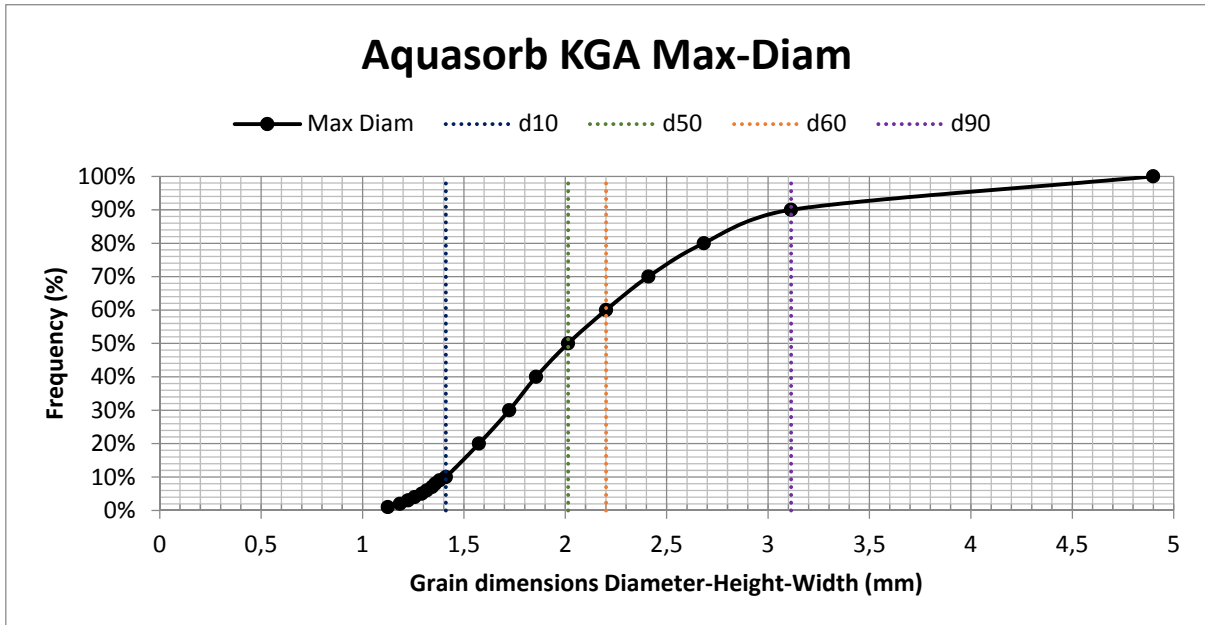


Figure A3.21 - Average cumulative distribution maximum diameter Aquasorb KGA

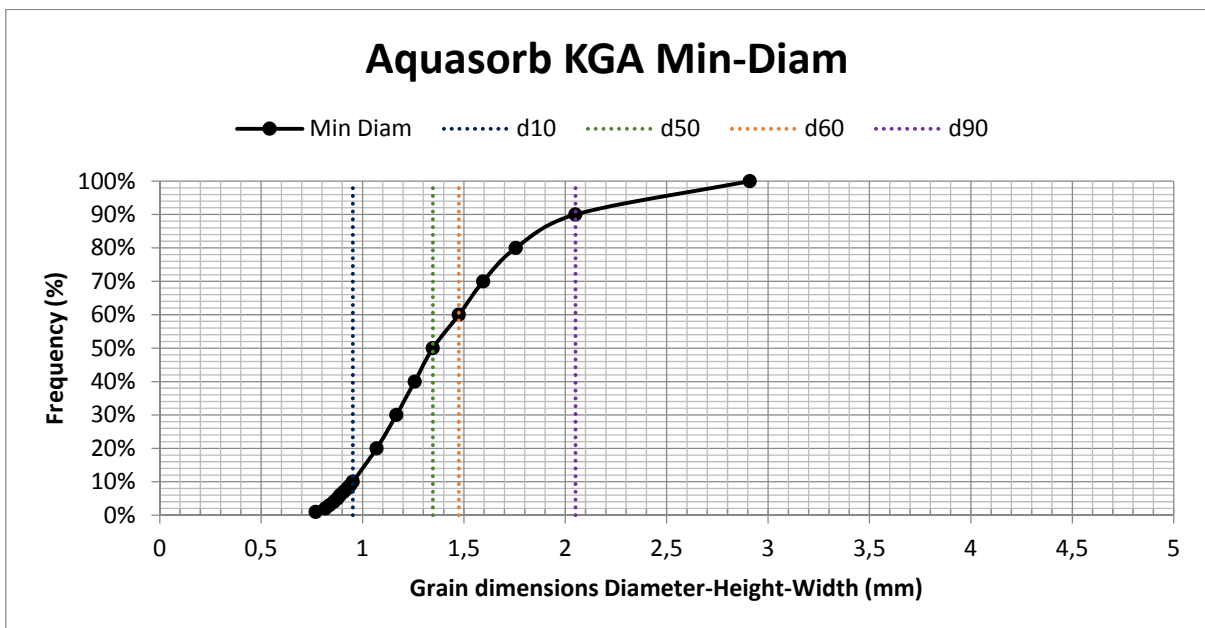


Figure A3.22 - Average cumulative distribution minimum diameter Aquasorb KGA

→ Saratech spherical

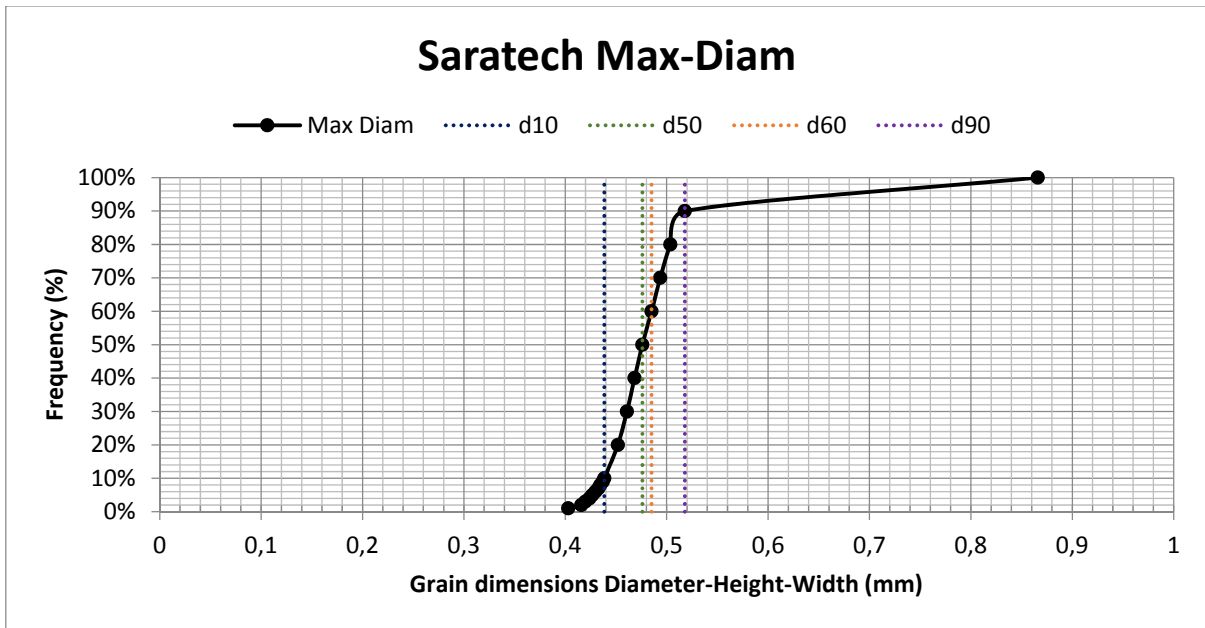


Figure A3.23 - Average cumulative distribution maximum diameter Saratech spherical

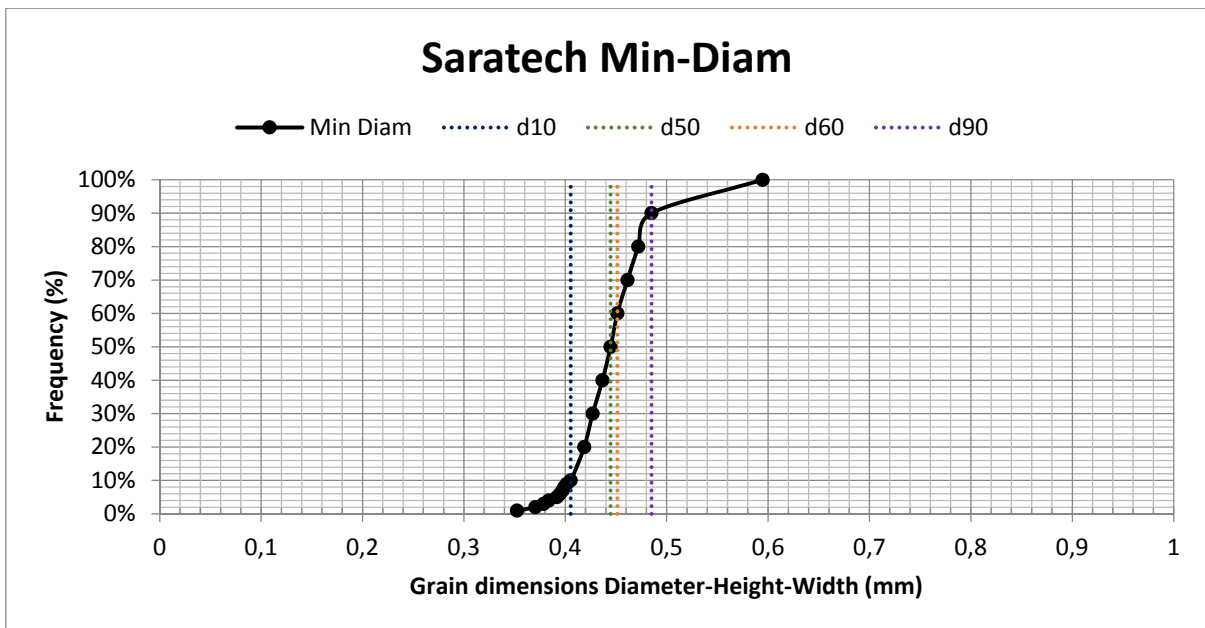


Figure A3.24 - Average cumulative distribution minimum diameter Saratech spherical

→ROW o.8 Supra

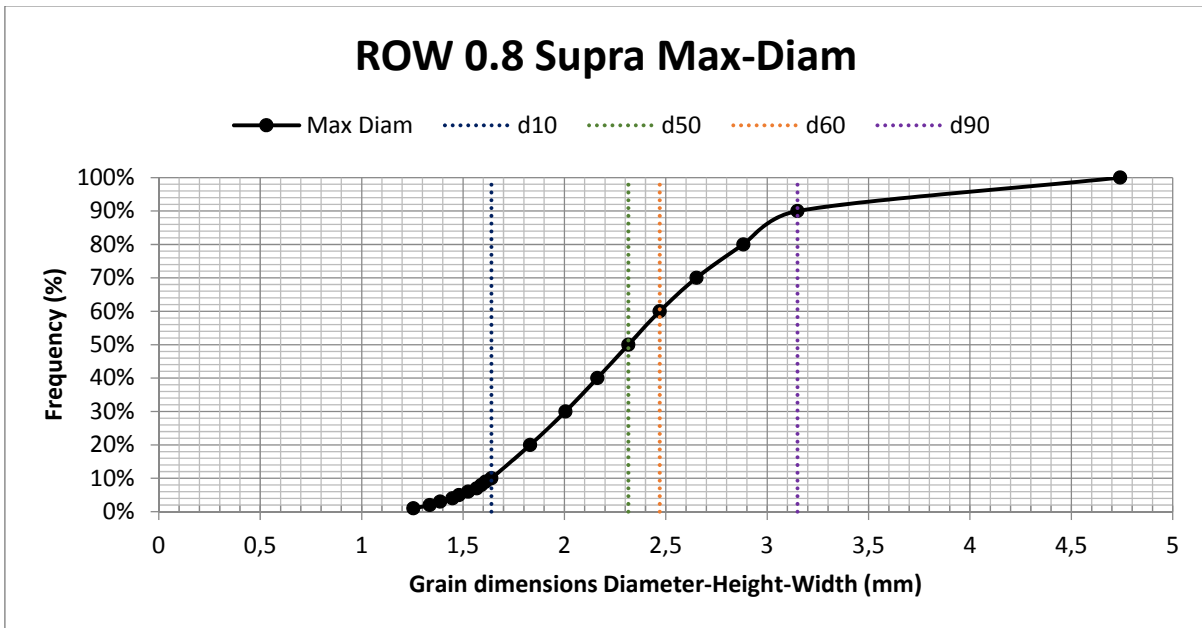


Figure A3.25 - Average cumulative distribution maximum diameter ROW 0.8 Supra

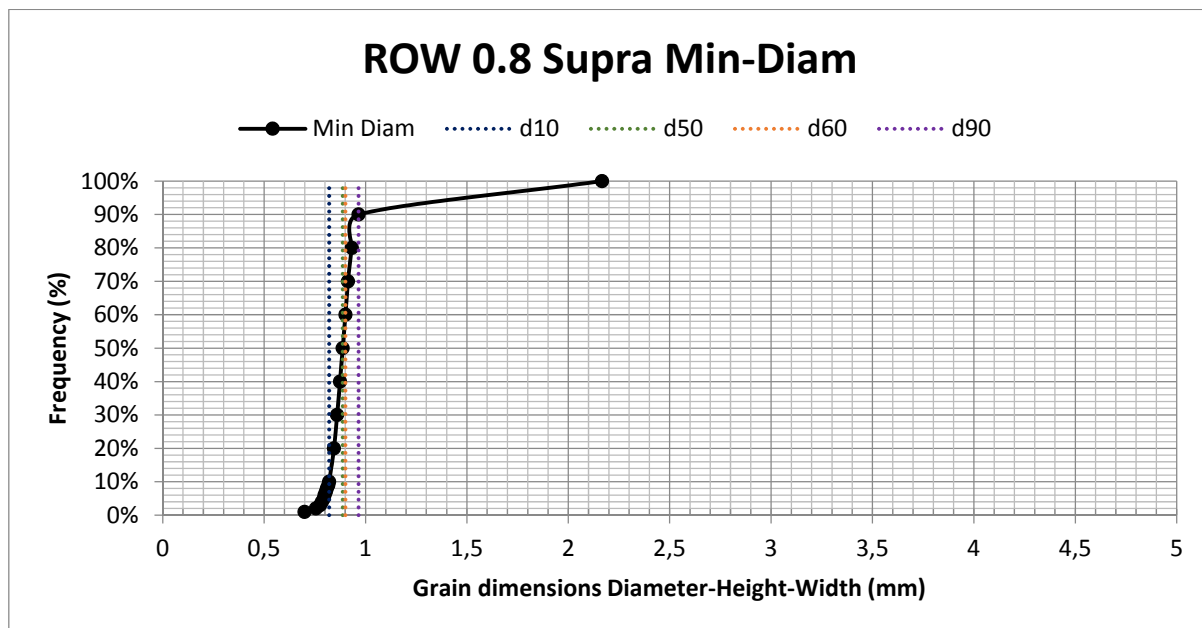


Figure A3.26 - Average cumulative distribution minimum diameter ROW 0.8 Supra

→ RB₄C

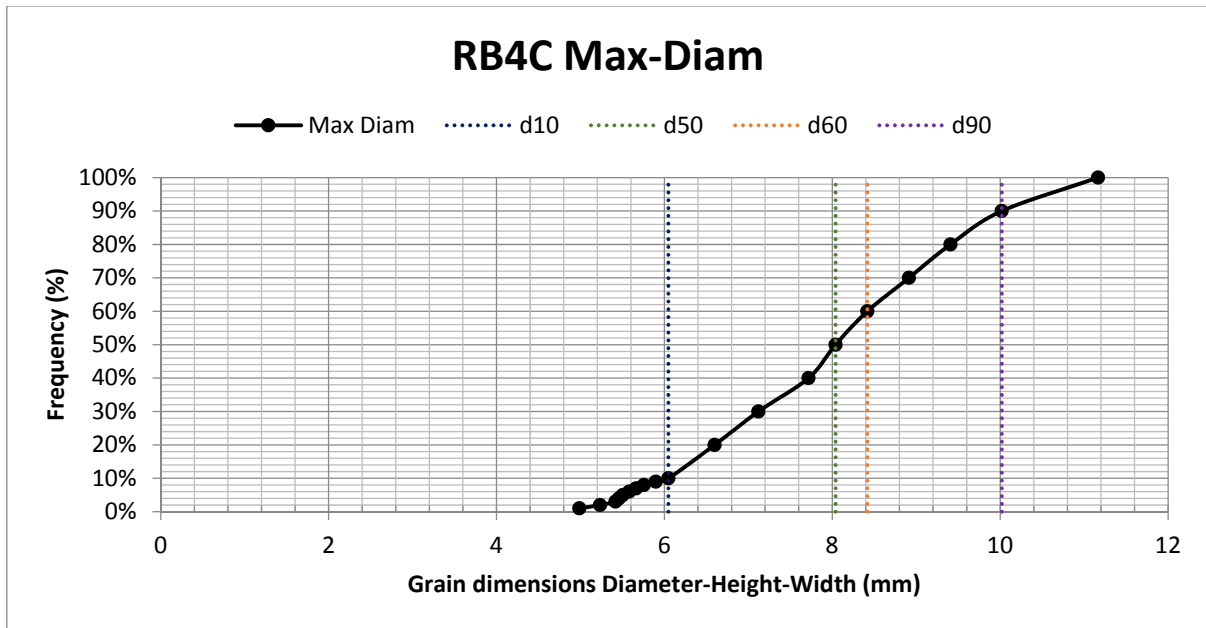


Figure A3.27 - Average cumulative distribution maximum diameter RB₄C

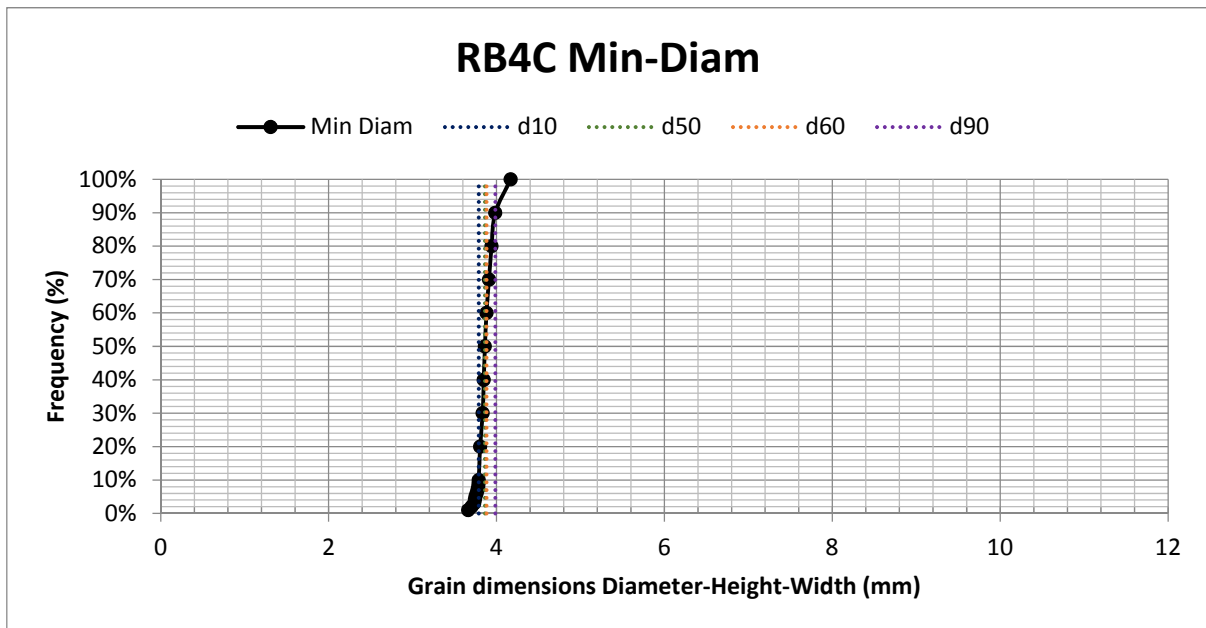


Figure A3.28 - Average cumulative distribution minimum diameter RB₄C

→ Filtrasorb TL830

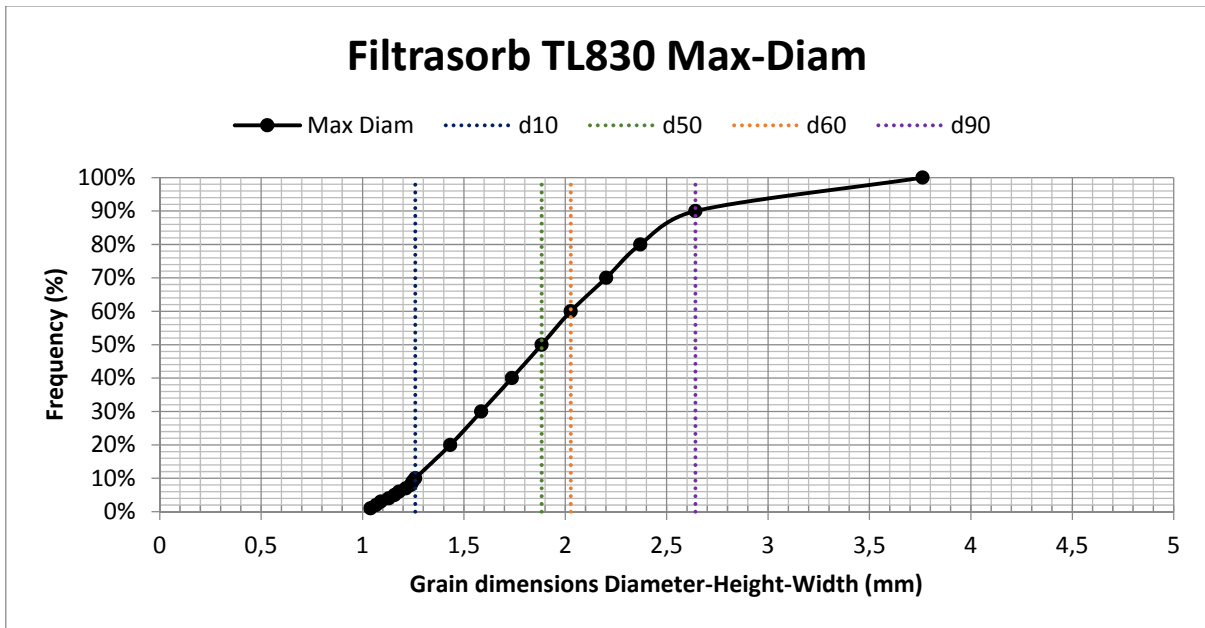


Figure A3.29 - Average cumulative distribution maximum diameter Filtrasorb TL830

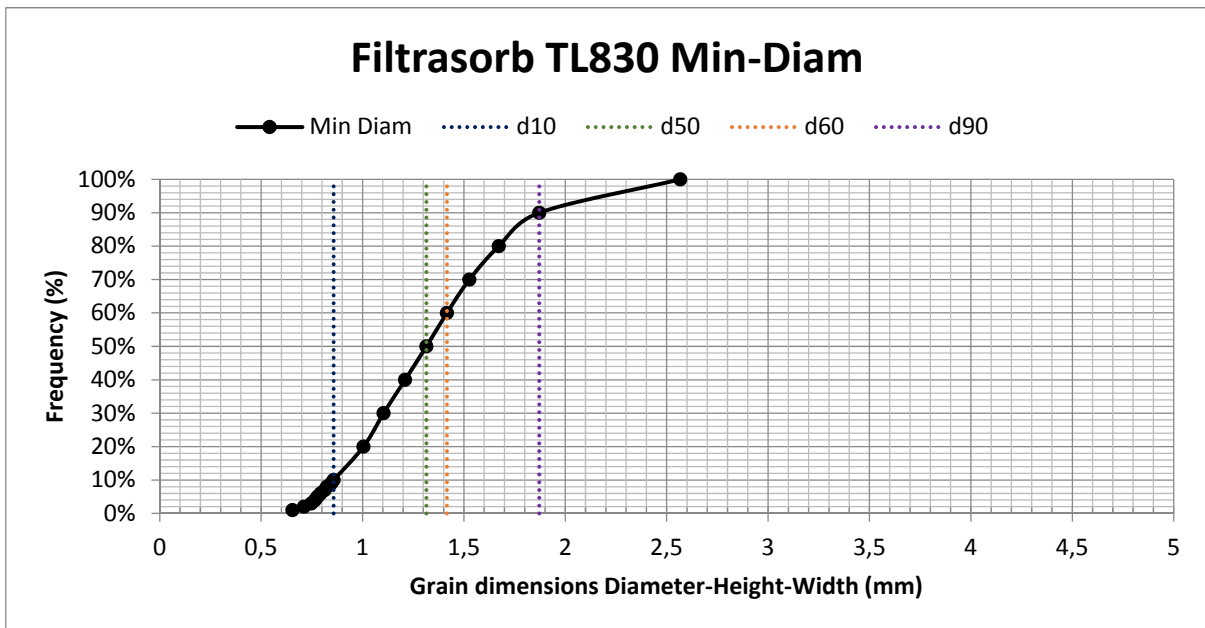


Figure A3.30 - Average cumulative distribution minimum diameter Filtrasorb TL830

→ Aquasorb K-6300

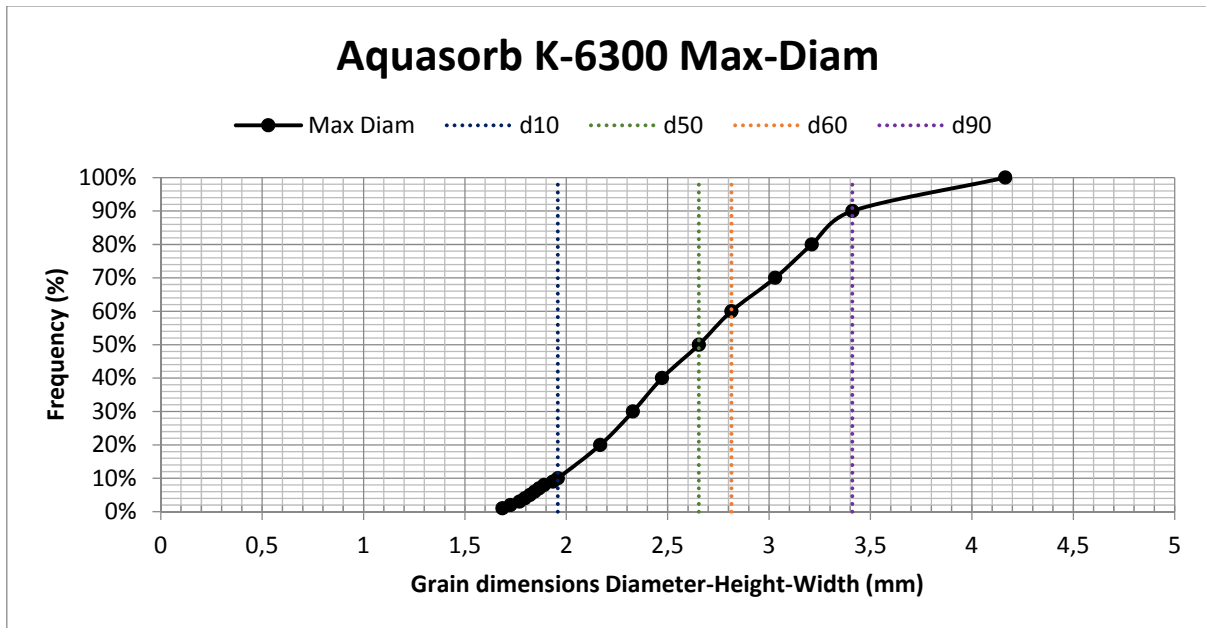


Figure A3.31 - Average cumulative distribution maximum diameter Aquasorb K-6300

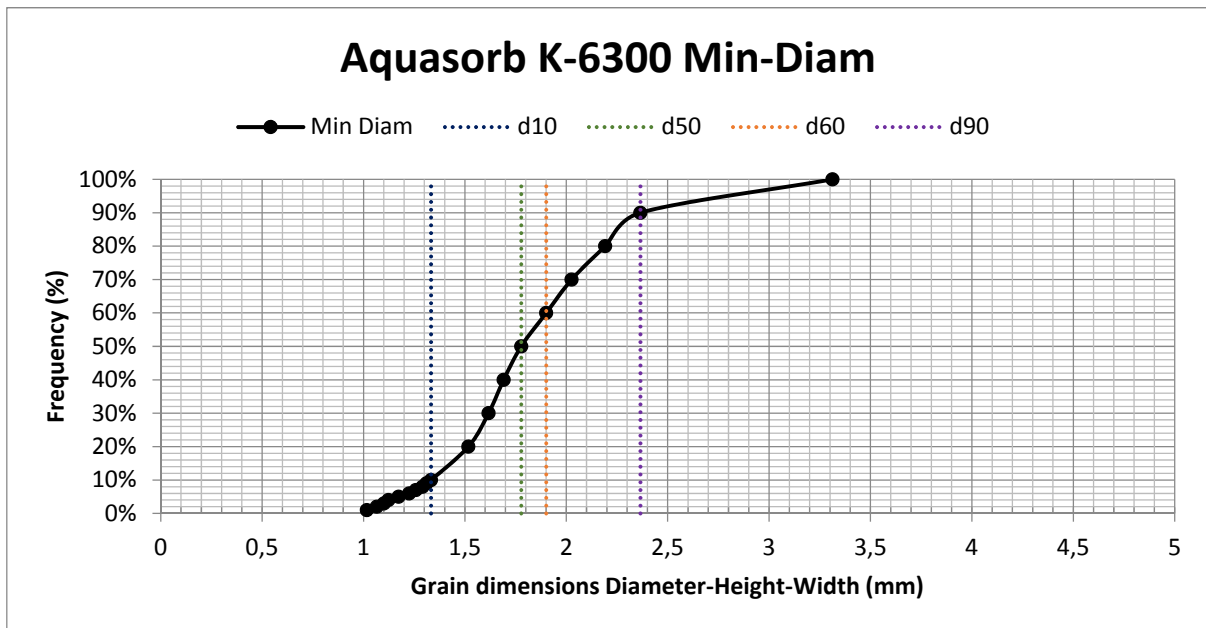


Figure A3.32 - Average cumulative distribution minimum diameter Aquasorb K-6300

→ Resorb HC

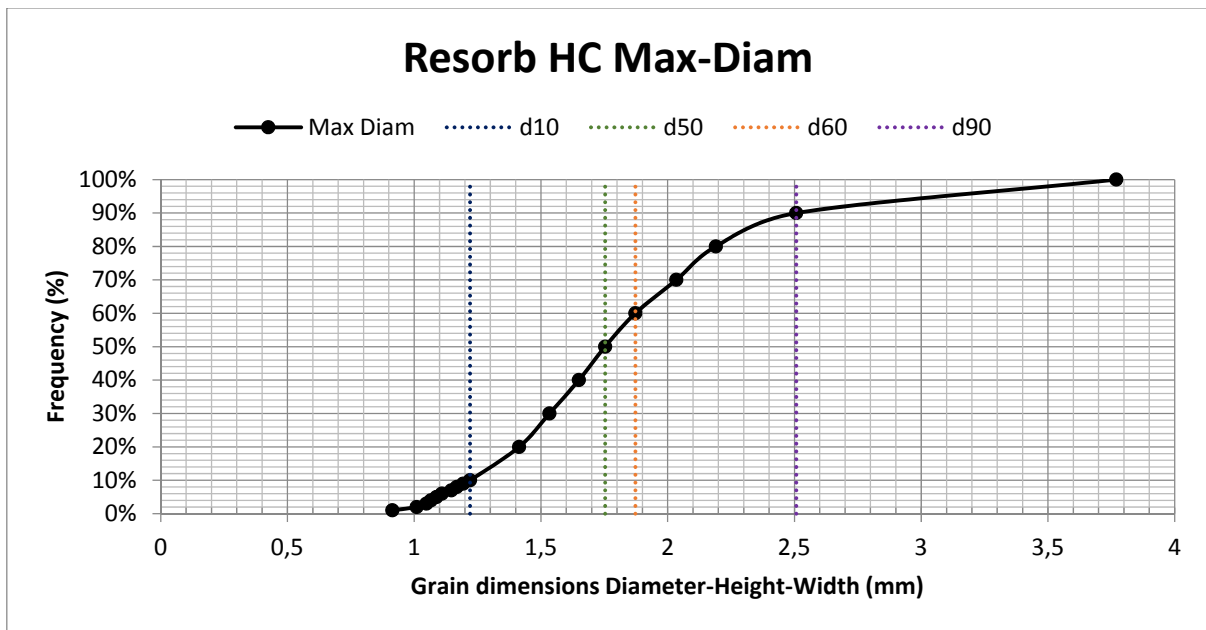


Figure A3.33 - Average cumulative distribution maximum diameter Resorb HC

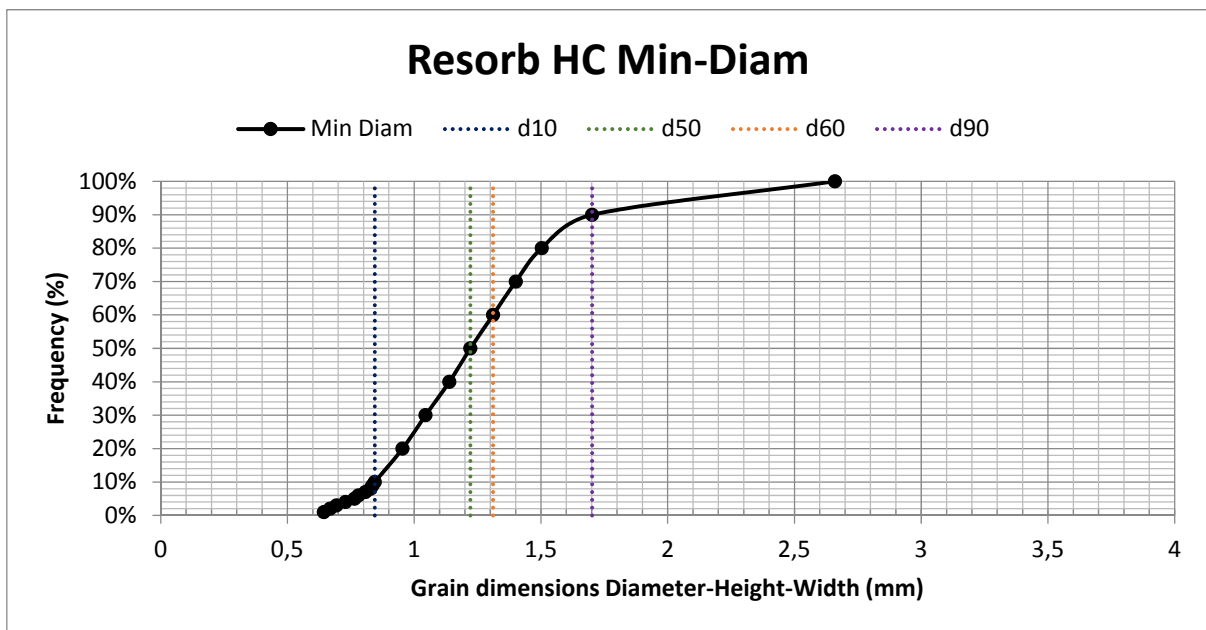


Figure A3.34 - Average cumulative distribution minimum diameter Resorb HC

→ GAC 830 SUPRA

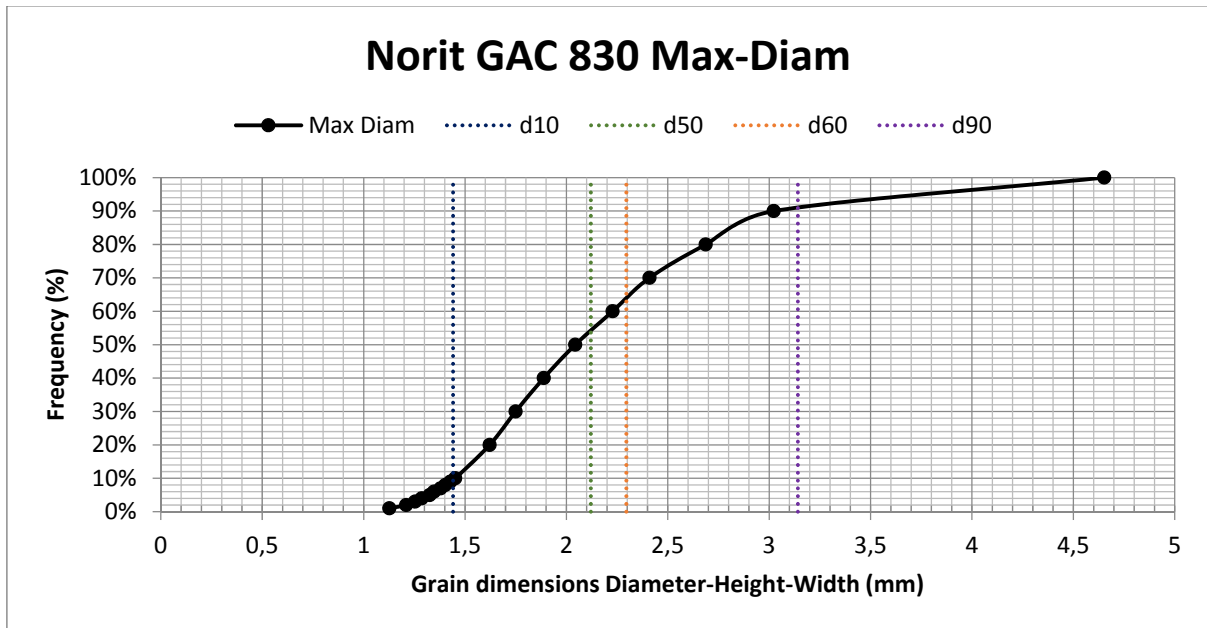


Figure A3.35- Average cumulative distribution maximum diameter GAC 830 Supra

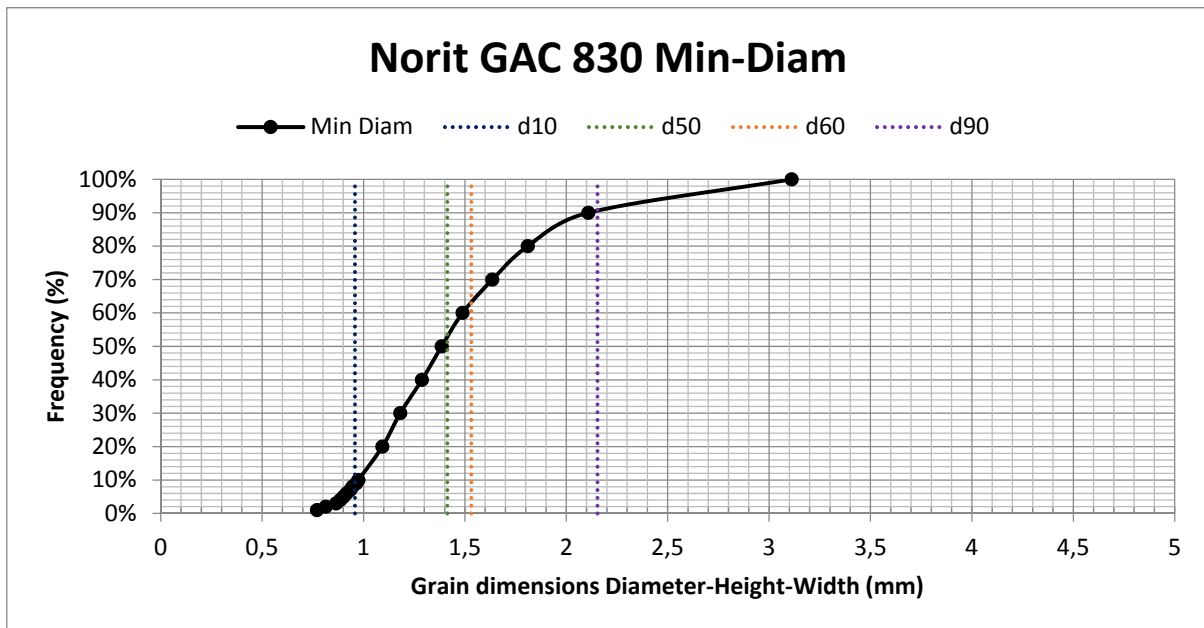


Figure A3.36 - Average cumulative distribution minimum diameter GAC 830 Supra

- ImageJ

The cumulative distribution of minimum (minor axis of ellipse) and maximum (major axis of ellipse) diameter measurements of the ImageJ analysis for all carbon samples is presented in the following figures:

→ Filtrasorb 300c

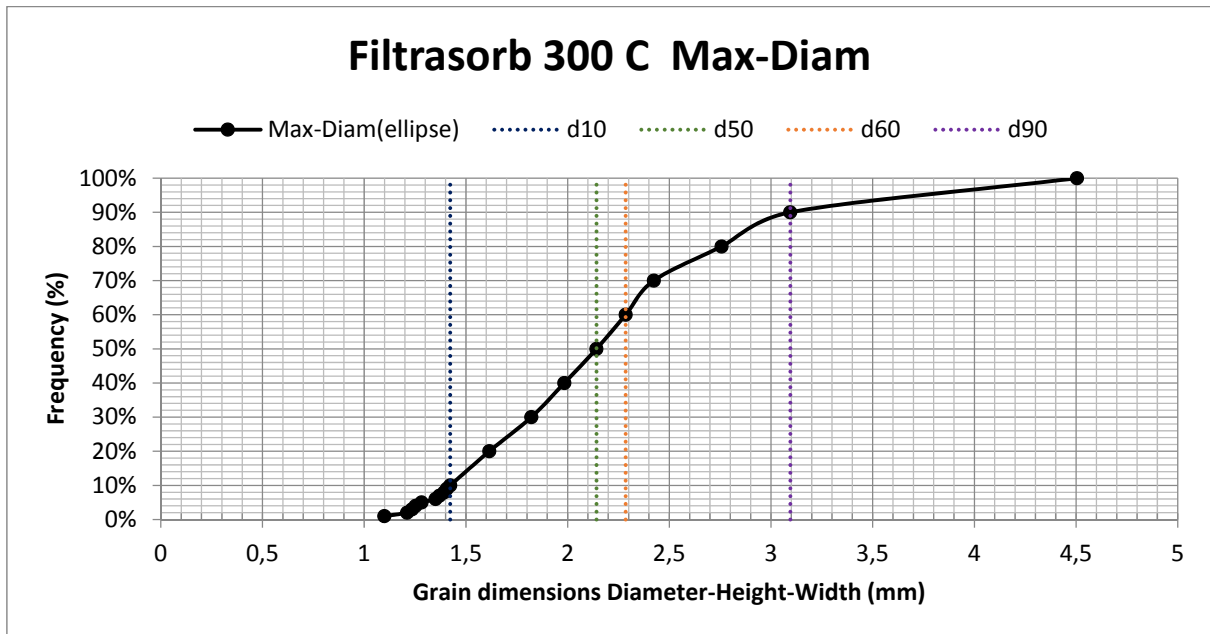


Figure A3.37 - Cumulative distribution maximum diameter (ellipse) Filtrasorb 300C

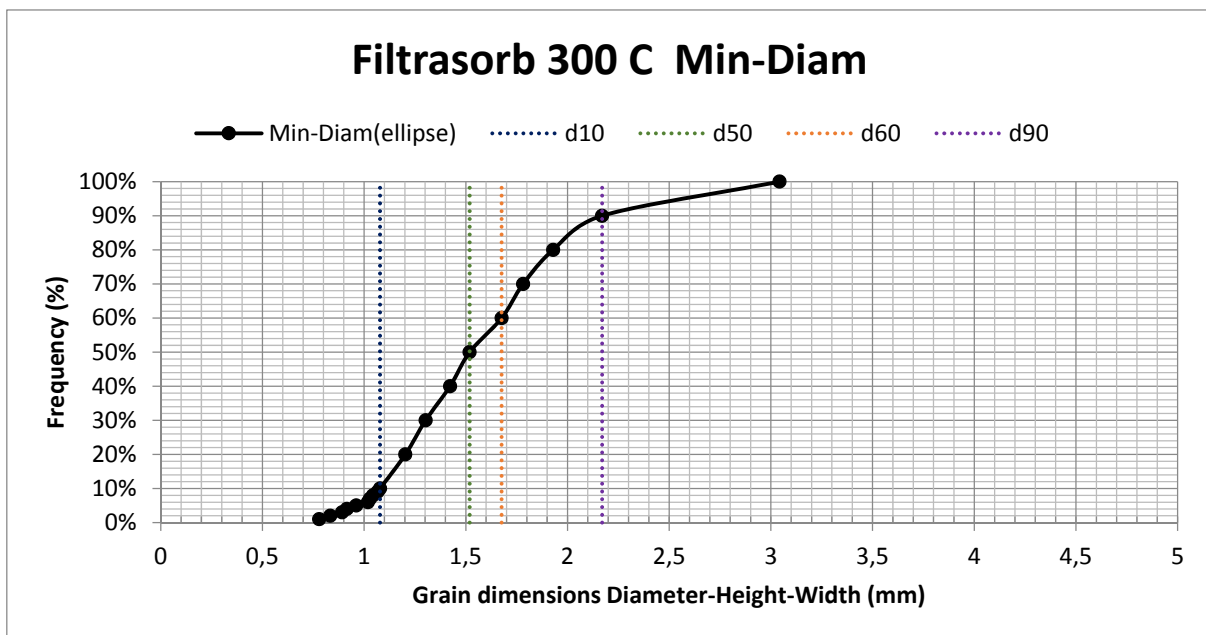


Figure A3.38 - Cumulative distribution minimum diameter (ellipse) Filtrasorb 300C

→ Aquasorb KGA

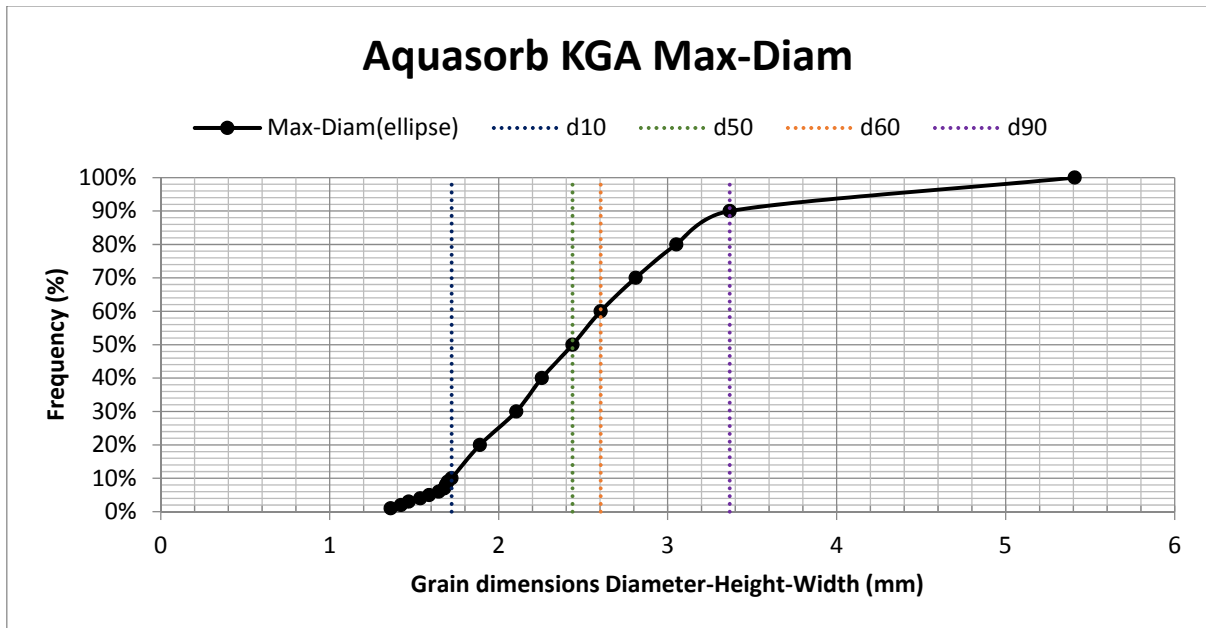


Figure A3.39 - Cumulative distribution maximum diameter (ellipse) Aquasorb KGA

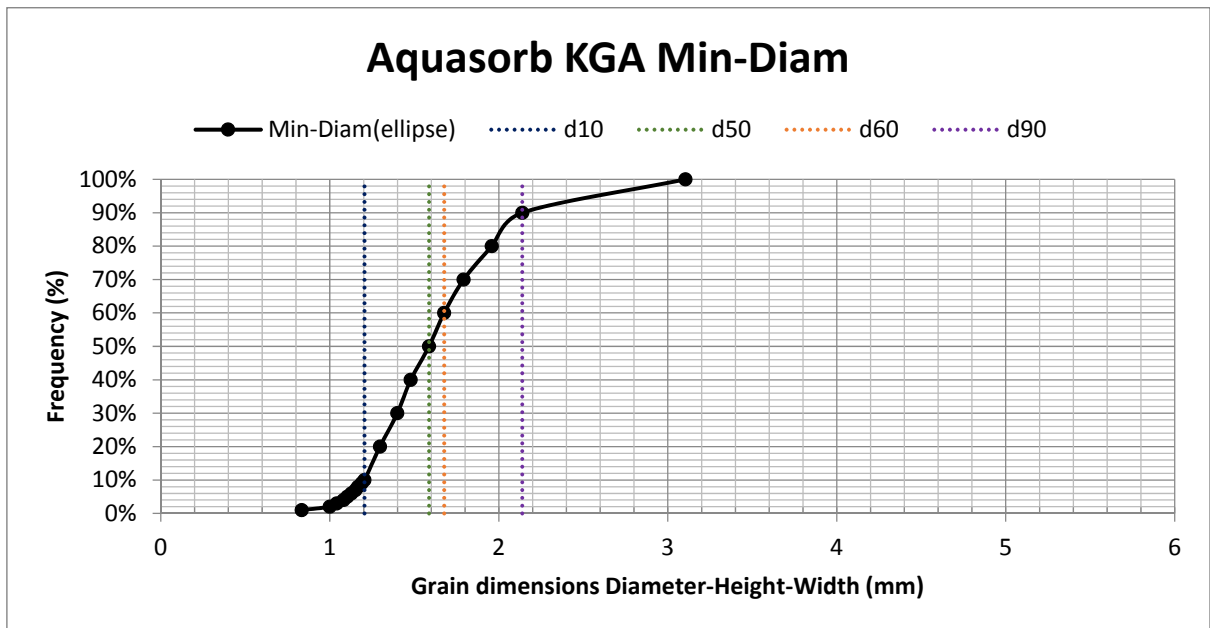


Figure A3.40 - Cumulative distribution minimum diameter (ellipse) Aquasorb KGA

→ Saratech spherical

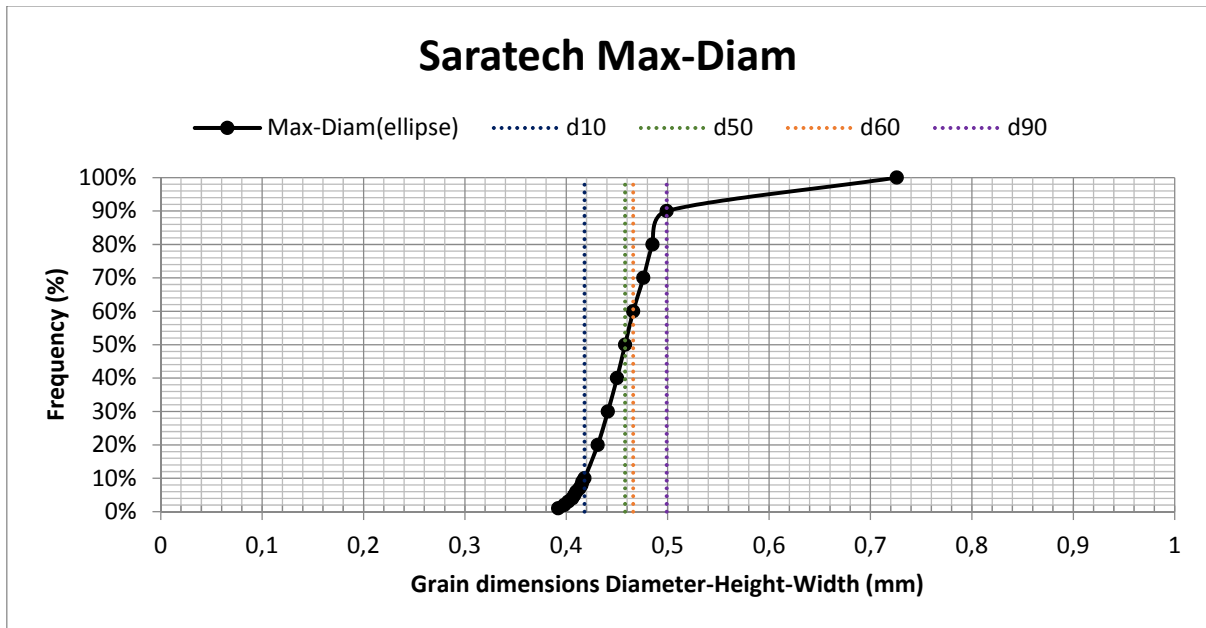


Figure A3.41 - Cumulative distribution maximum diameter (ellipse) Saratech spherical

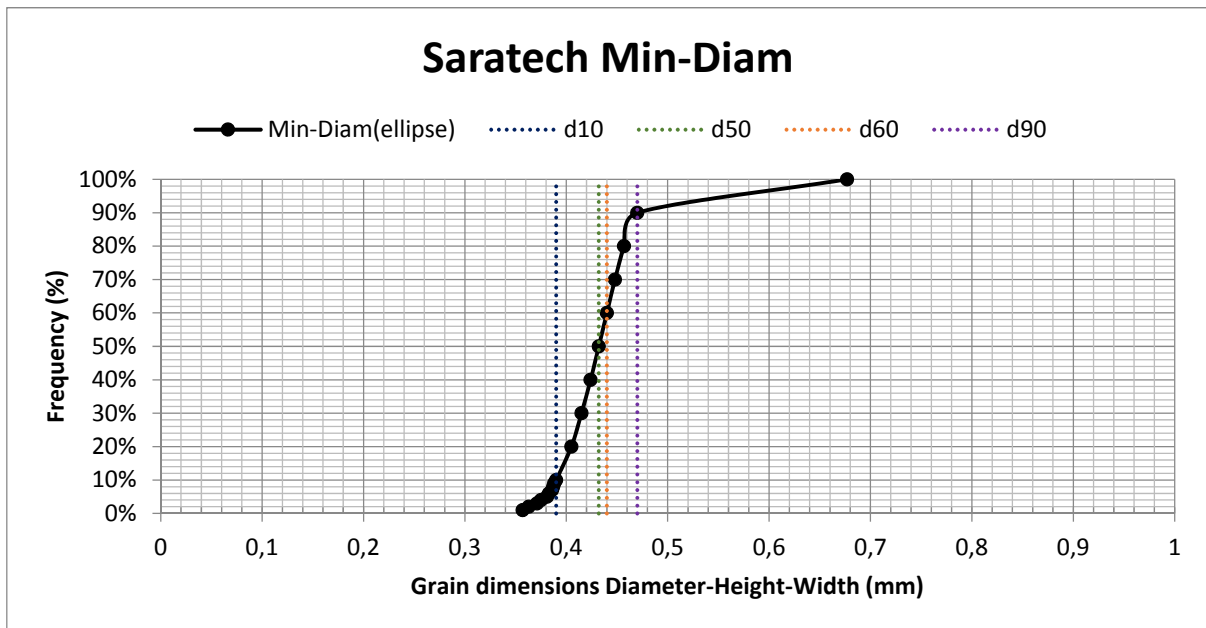


Figure A3.42 - Cumulative distribution minimum diameter (ellipse) Saratech spherical

→ROW 0.8 Supra

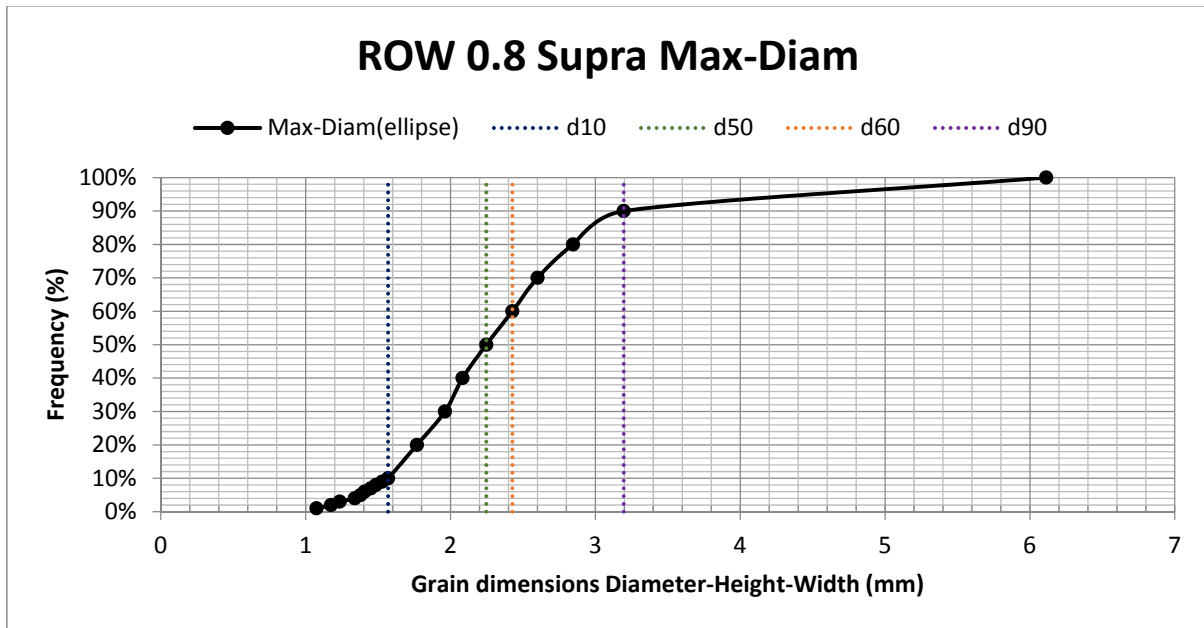


Figure A3.43 - Cumulative distribution maximum diameter (ellipse) ROW 0.8 Supra

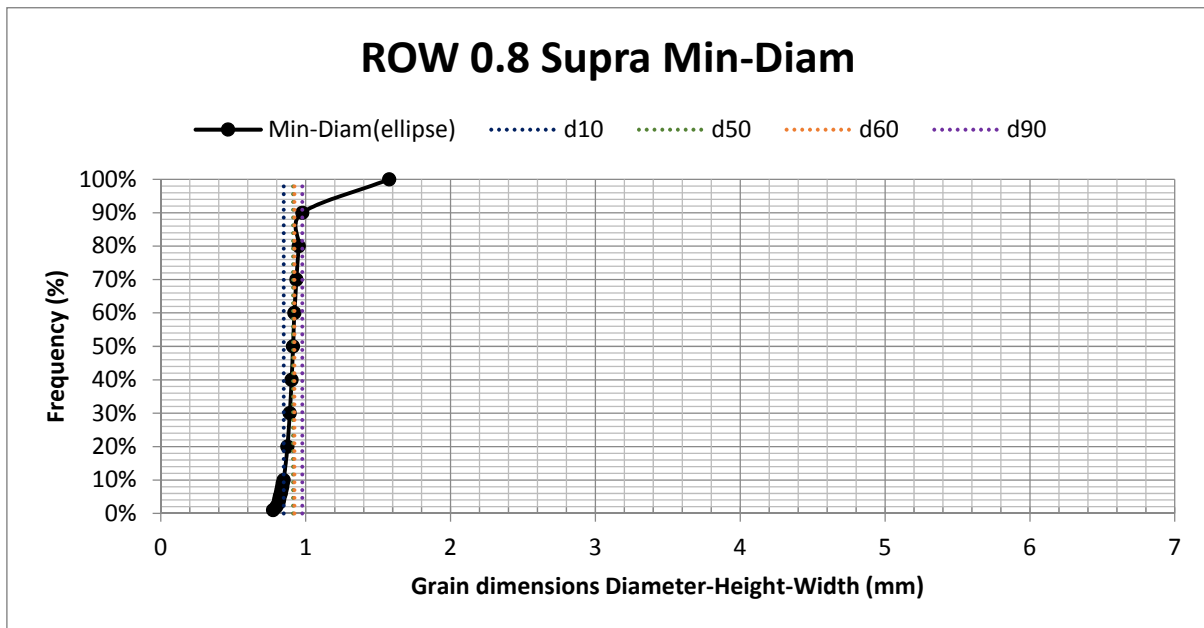


Figure A3.44 - Cumulative distribution minimum diameter (ellipse) ROW 0.8 Supra

→ RB₄C

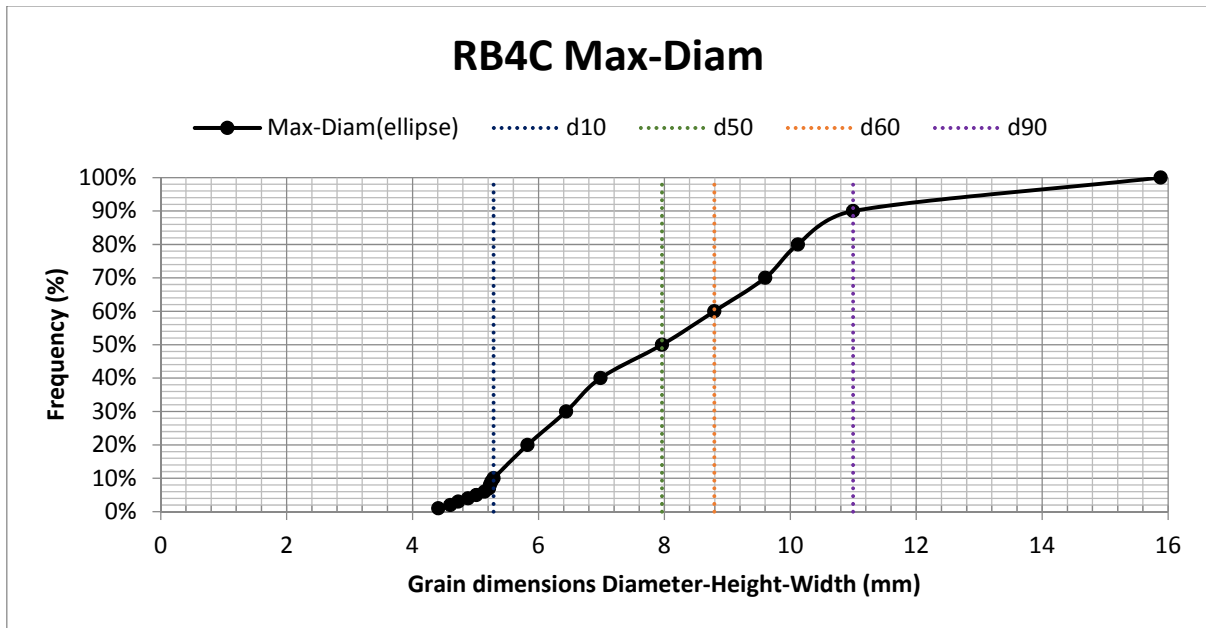


Figure A3.45 - Cumulative distribution maximum diameter (ellipse) RB₄C

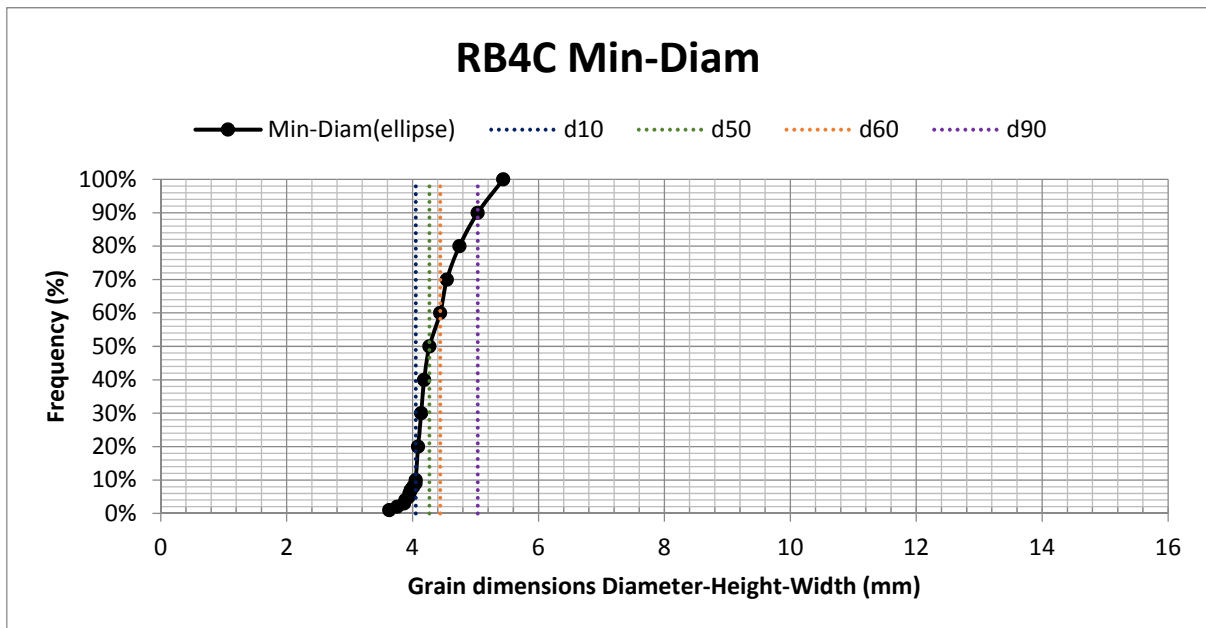


Figure A3.46 - Cumulative distribution minimum diameter (ellipse) RB₄C

→ Filtrasorb TL830

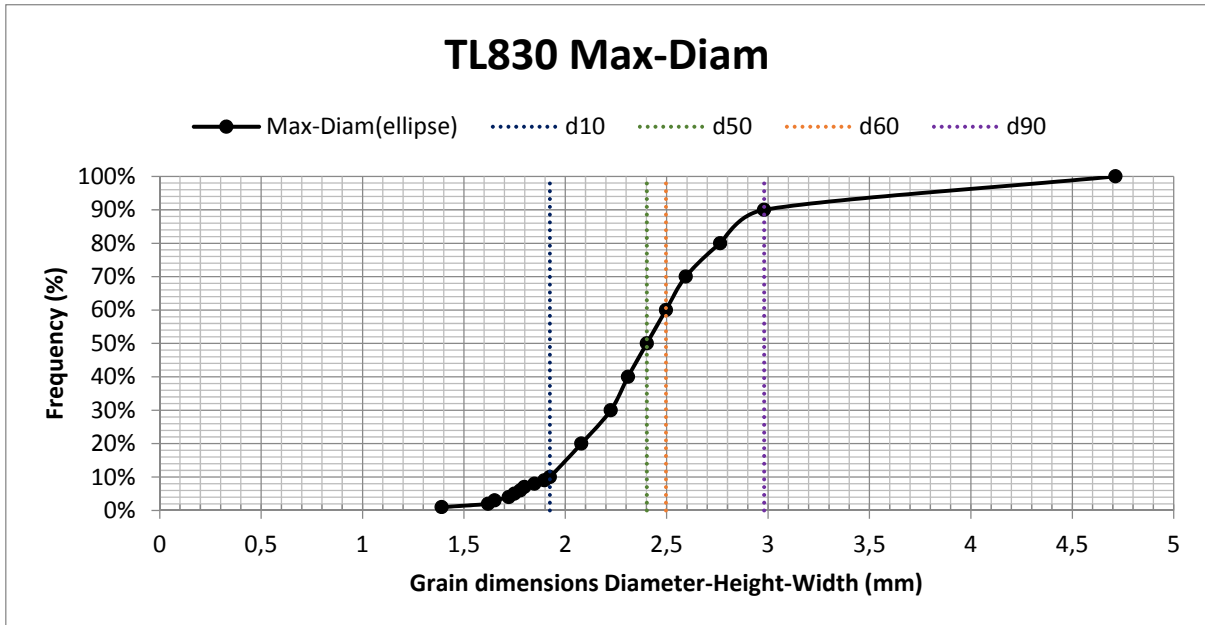


Figure A3.47 - Cumulative distribution maximum diameter (ellipse) Filtrasorb TL830

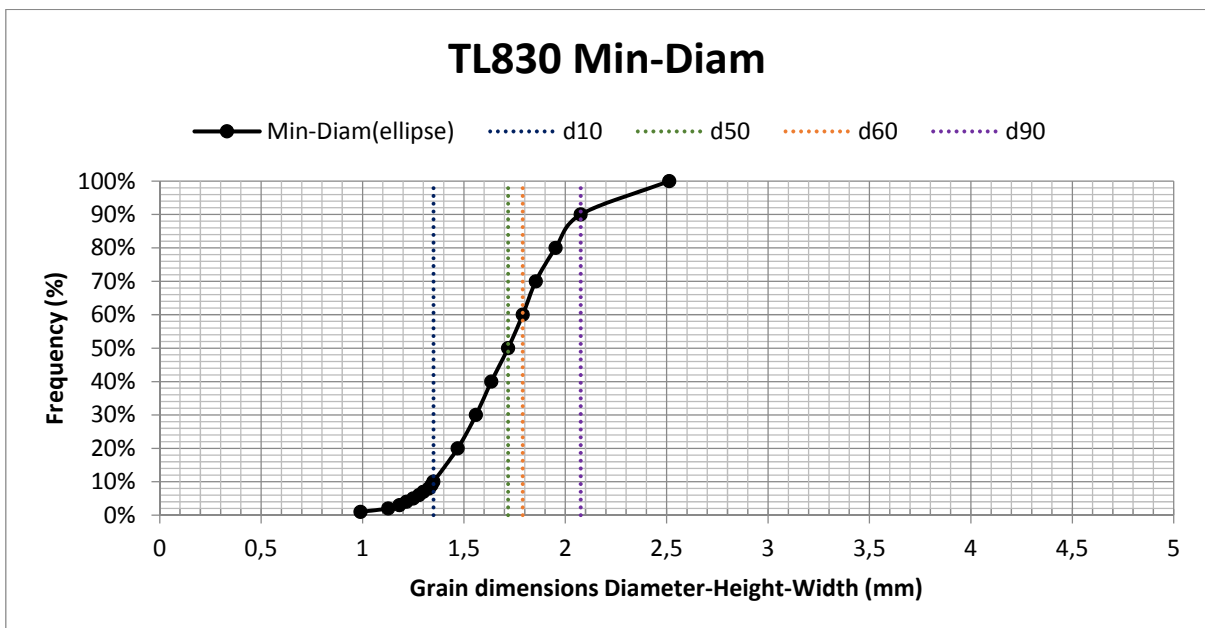


Figure A3.48 - Cumulative distribution minimum diameter (ellipse) Filtrasorb TL830

→ Aquasorb K-6300

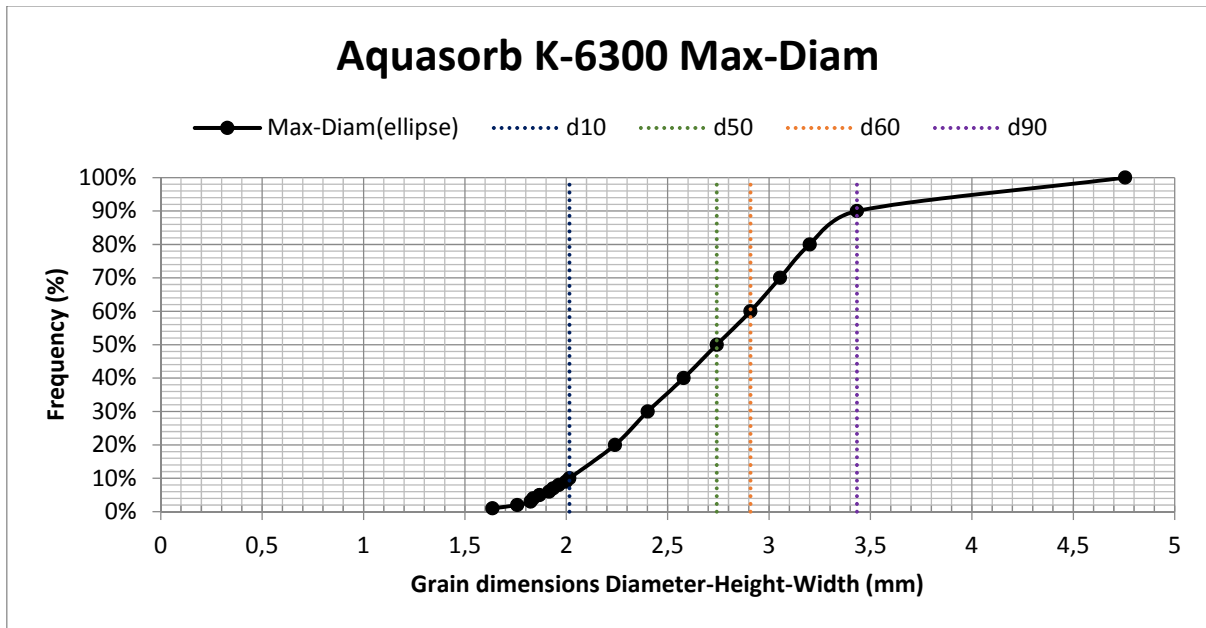


Figure A3.49 - Cumulative distribution maximum diameter (ellipse) Aquasorb K-6300

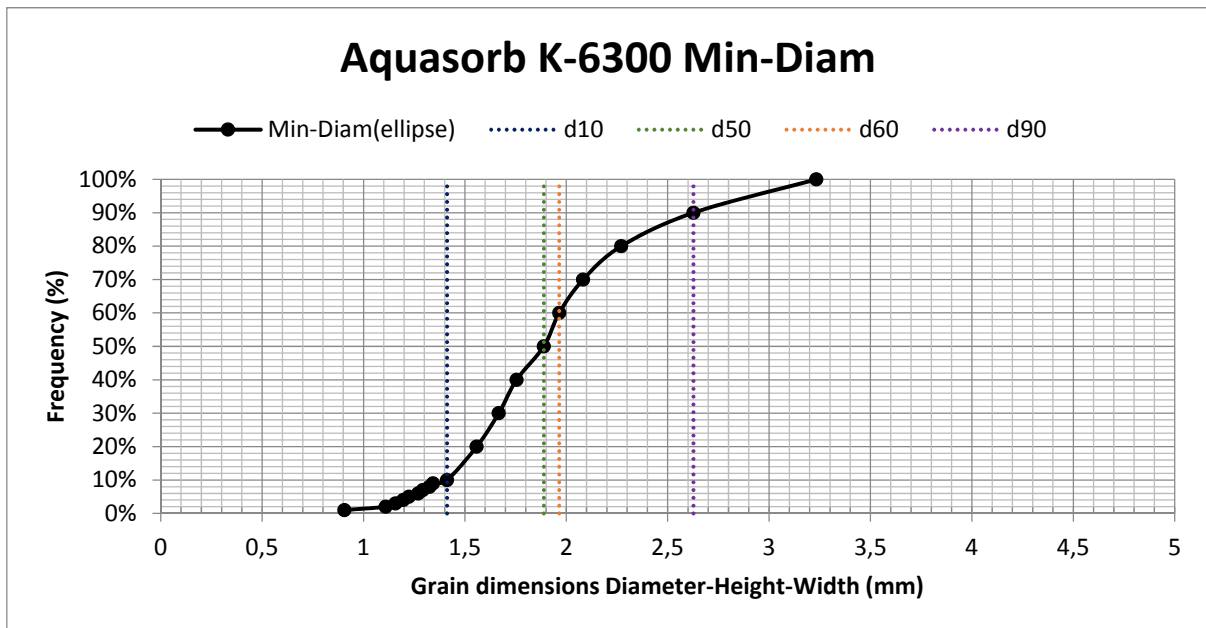


Figure A3.50 - Cumulative distribution minimum diameter (ellipse) Aquasorb K-6300

→ Resorb HC

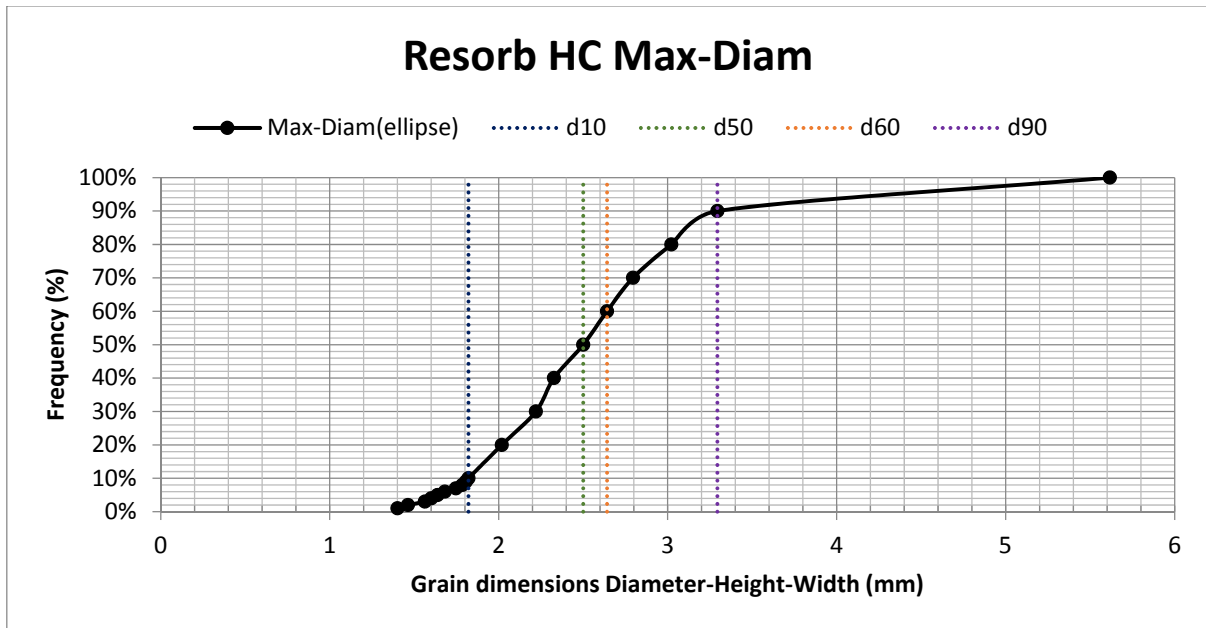


Figure A3.51 - Cumulative distribution maximum diameter (ellipse) Resorb HC

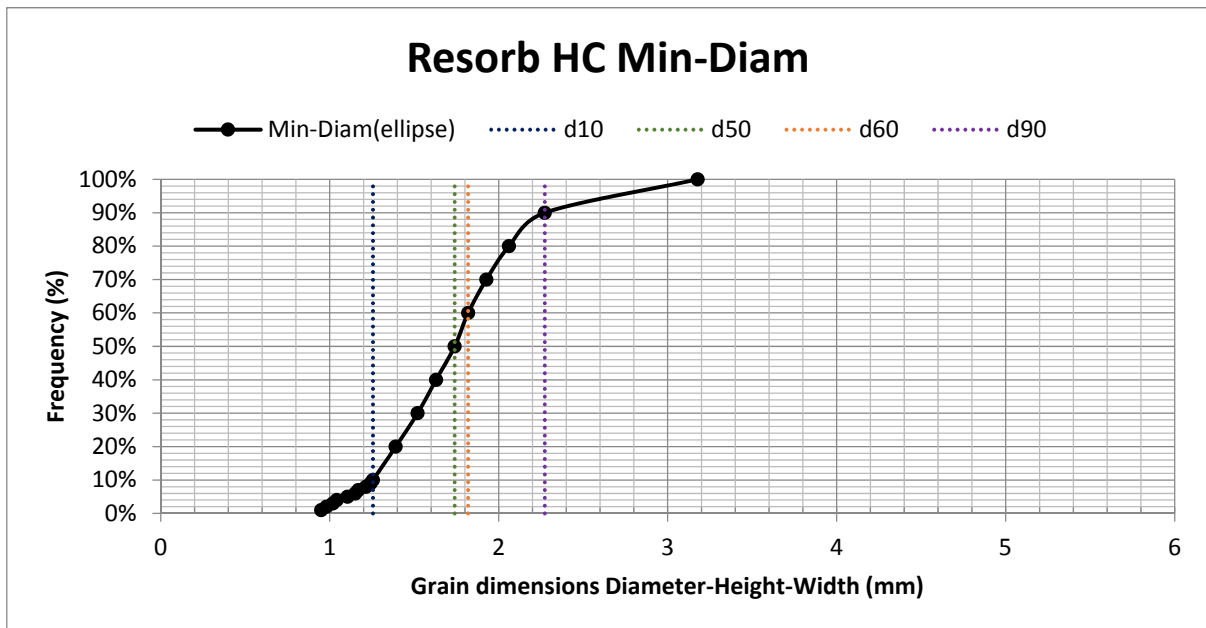


Figure A3.52 - Cumulative distribution minimum diameter (ellipse) Resorb HC

→ GAC 830 SUPRA

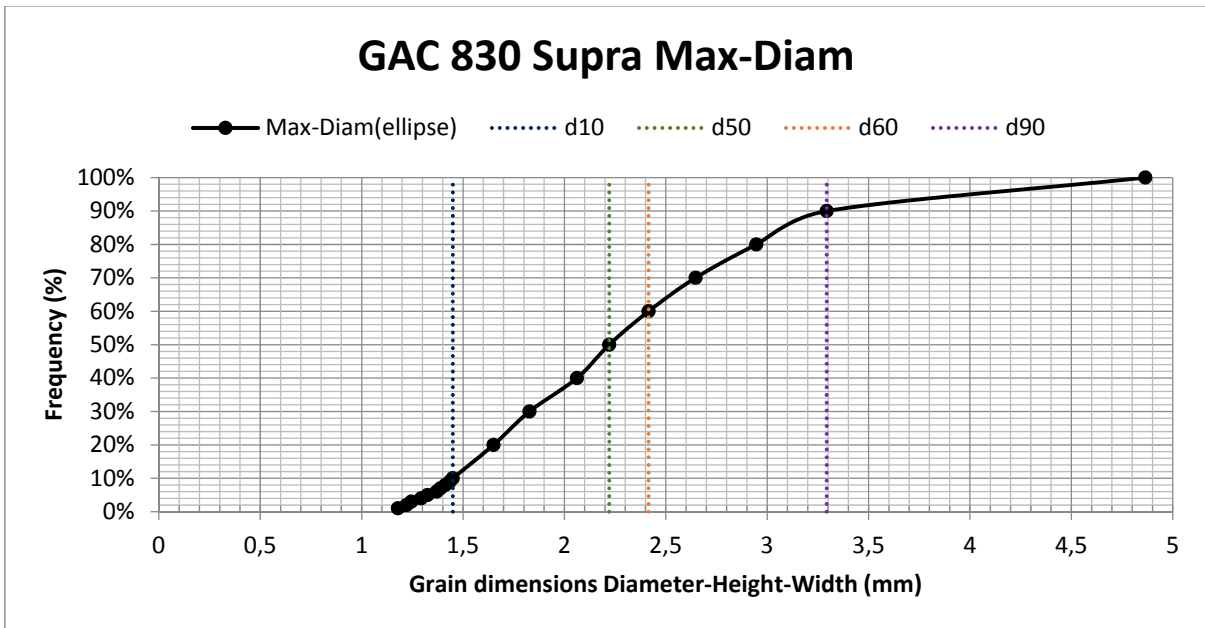


Figure A3.53- Cumulative distribution maximum diameter (ellipse) GAC 830 Supra

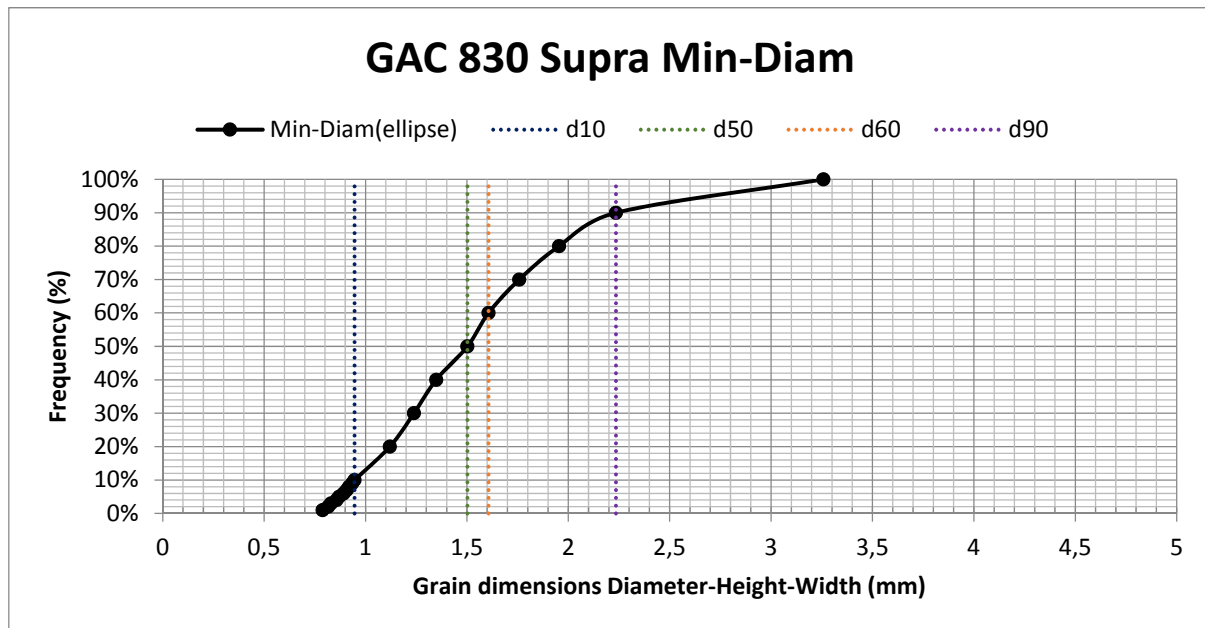


Figure A3.54 - Cumulative distribution minimum diameter (ellipse) GAC 830 Supra

- Camsizer

The measurements of the Camsizer analysis for all carbon samples is presented in the following figures:

→ *Filtrisorb 300c*

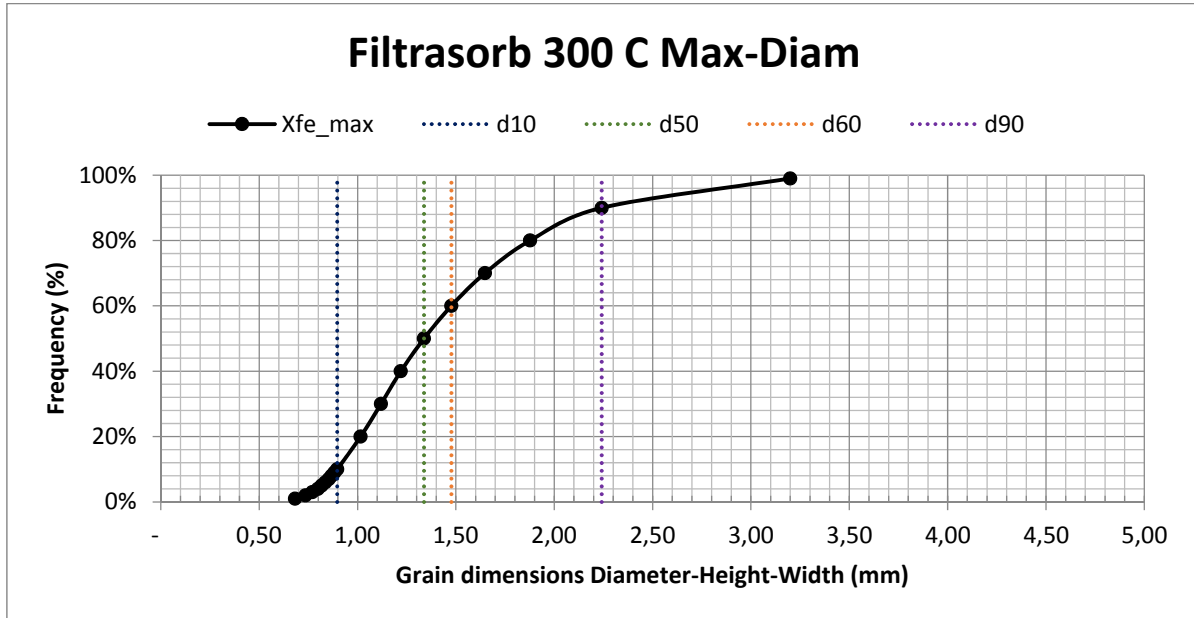


Figure A3.55 - Cumulative distribution maximum diameter Filtrisorb 300C

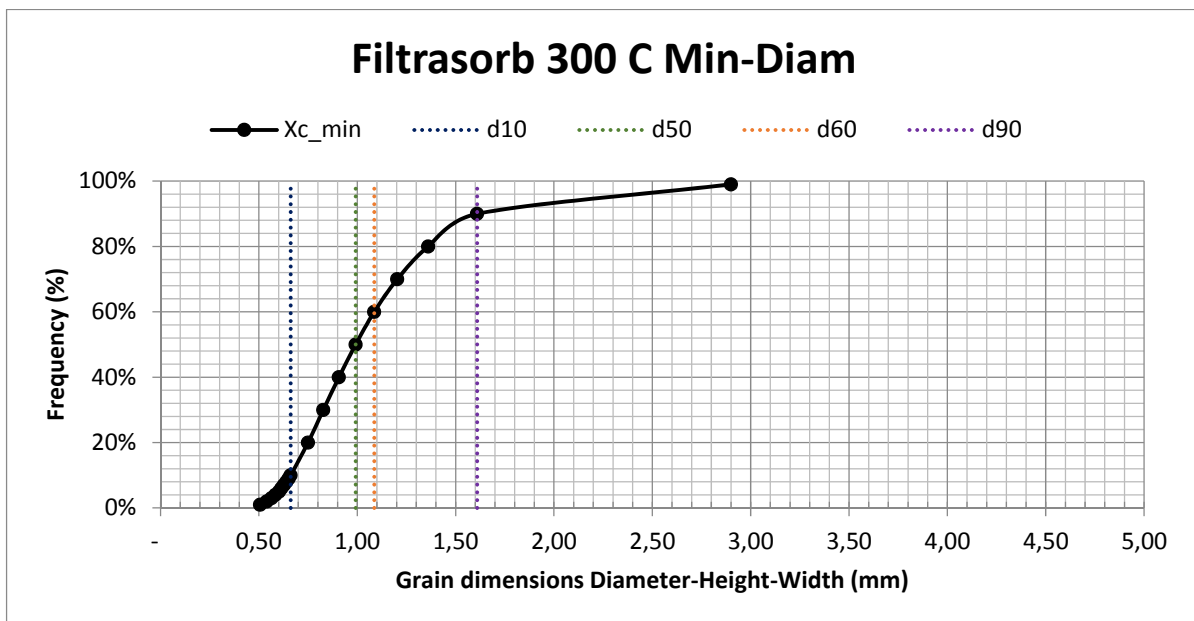


Figure A3.56 - Cumulative distribution minimum diameter Filtrisorb 300C

→ Aquasorb KGA

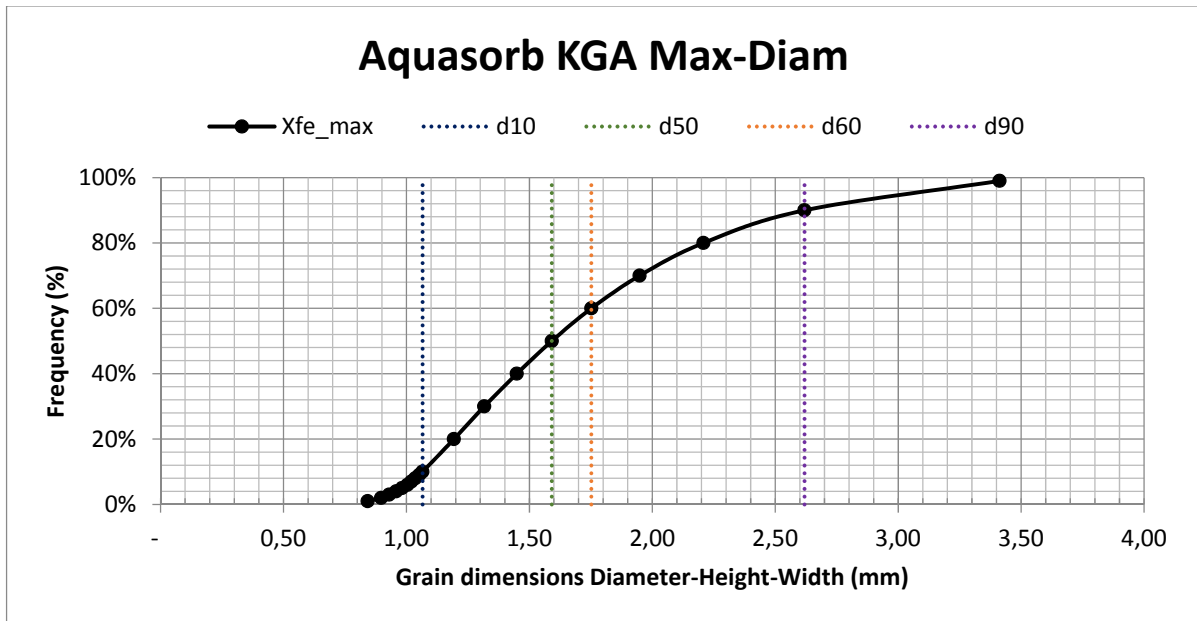


Figure A3.57 - Cumulative distribution maximum diameter Aquasorb KGA

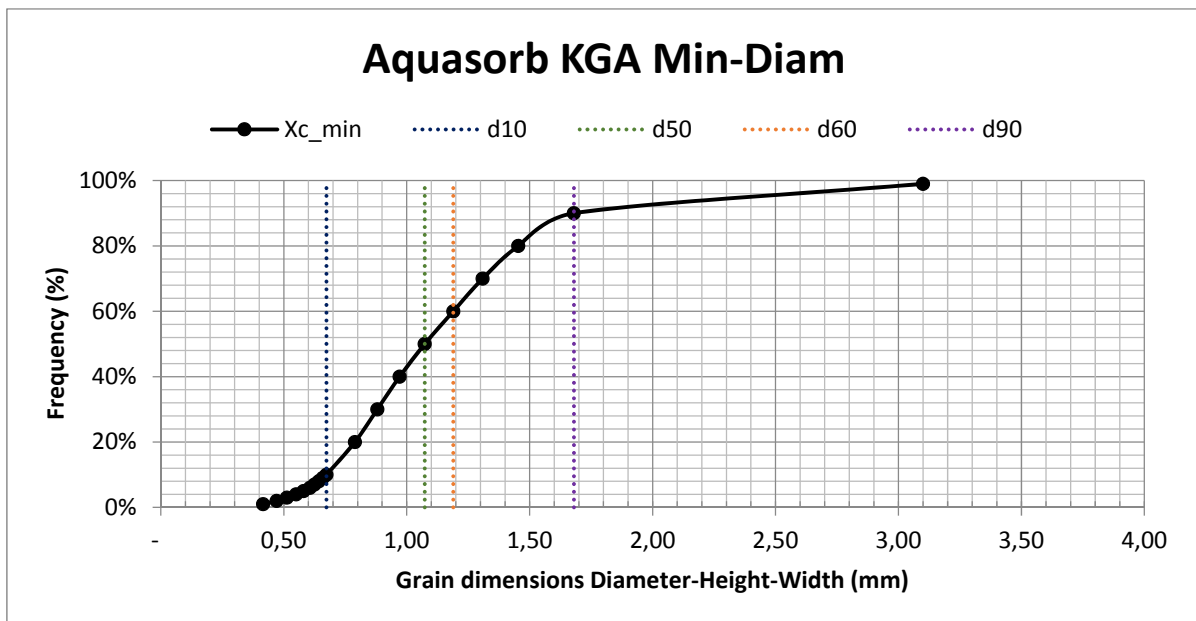


Figure A3.58 - Cumulative distribution minimum diameter Aquasorb KGA

→ Saratech spherical

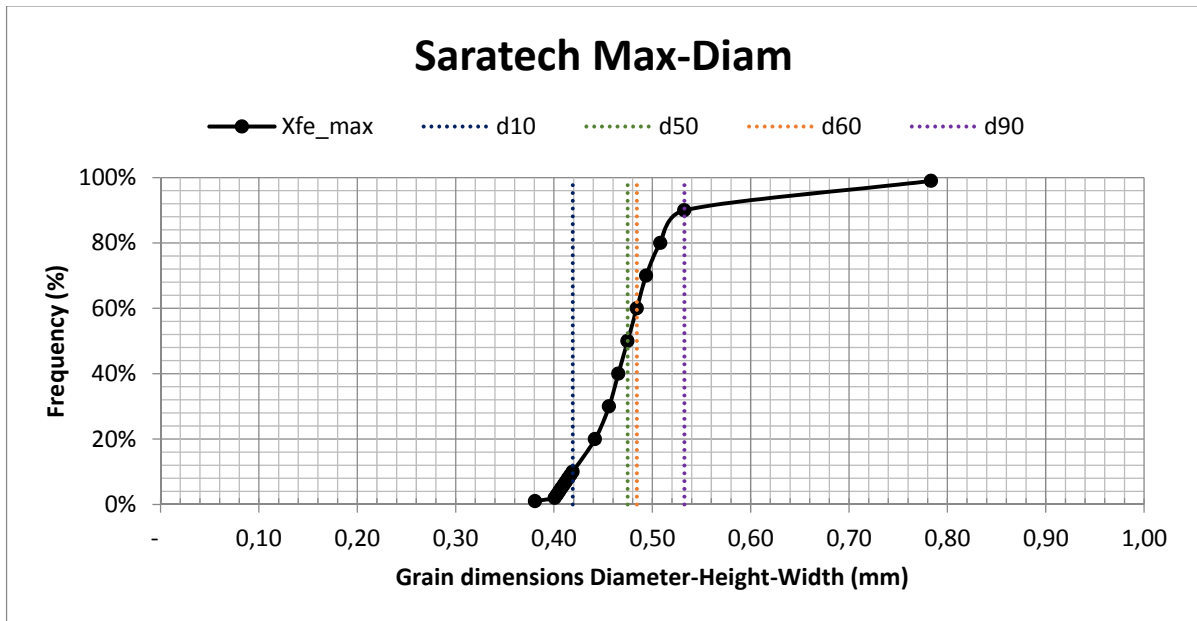


Figure A3.59 - Cumulative distribution maximum diameter Saratech spherical

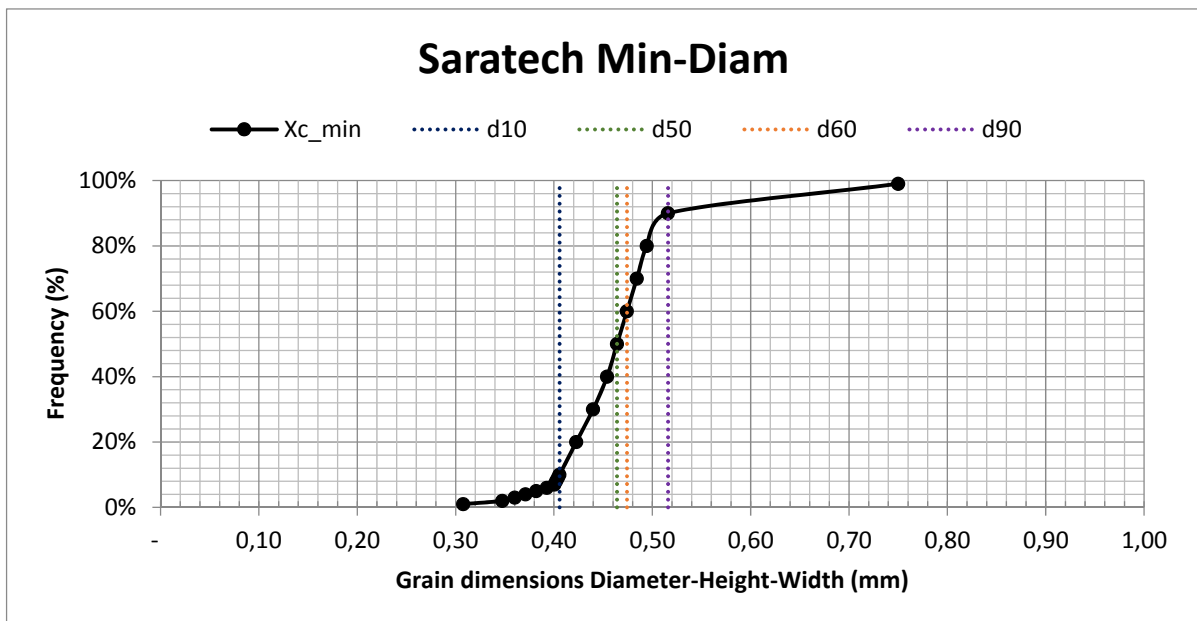


Figure A3.60 - Cumulative distribution minimum diameter Saratech spherical

→ROW 0.8 Supra

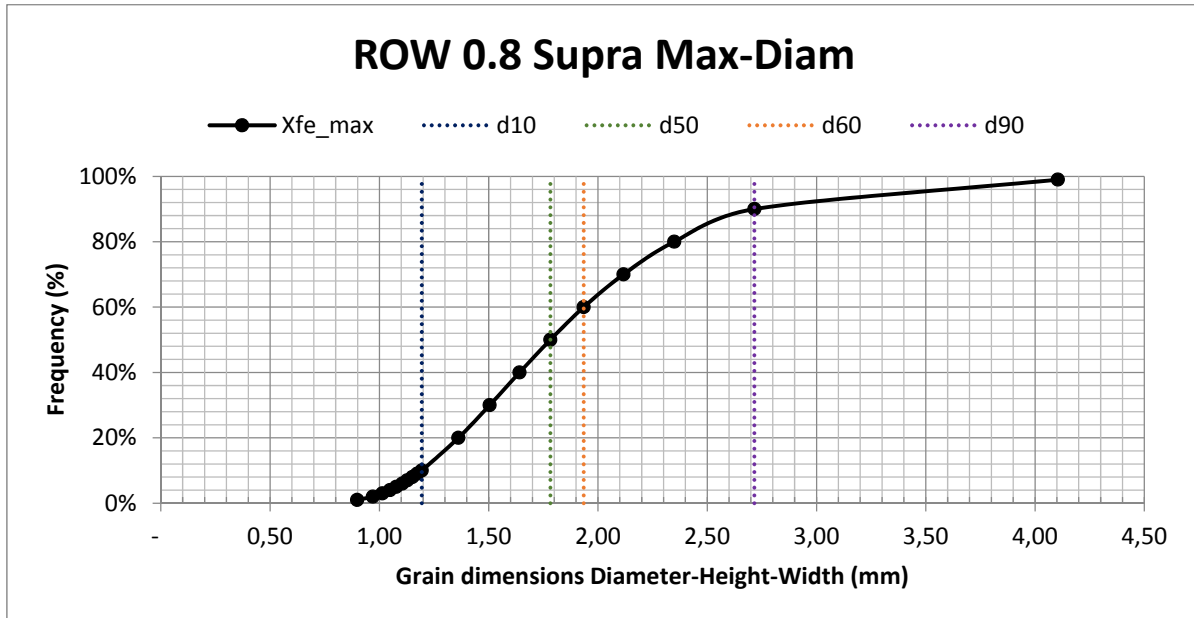


Figure A3.61 - Cumulative distribution maximum diameter ROW 0.8 Supra

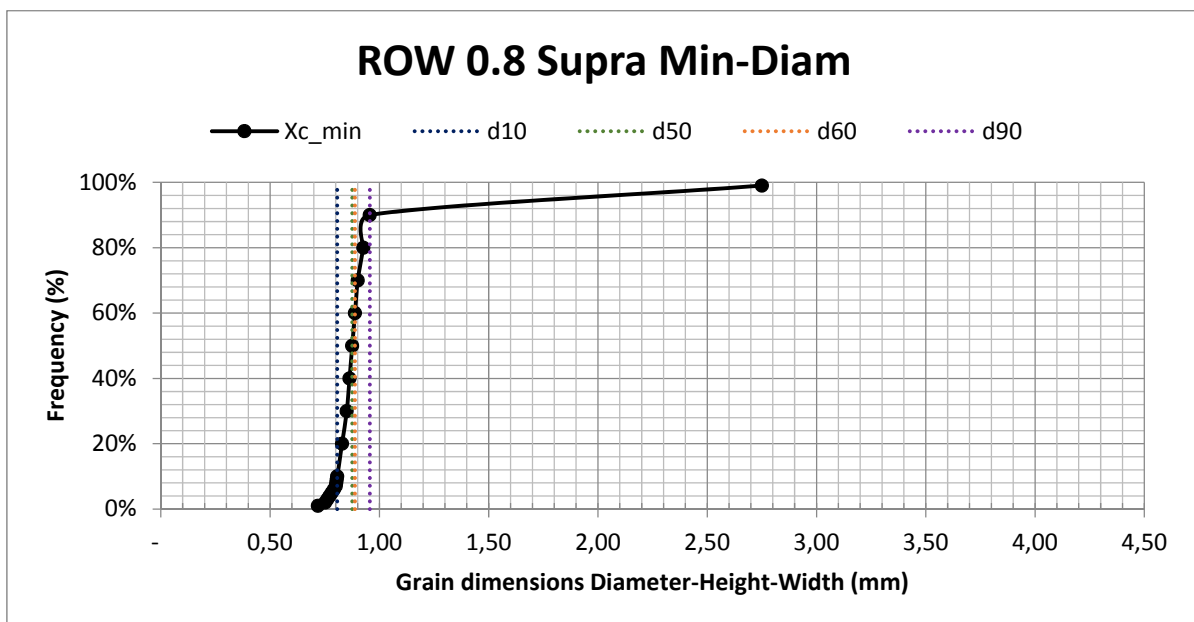


Figure A3.62 - Cumulative distribution minimum diameter ROW 0.8 Supra

→ RB₄C

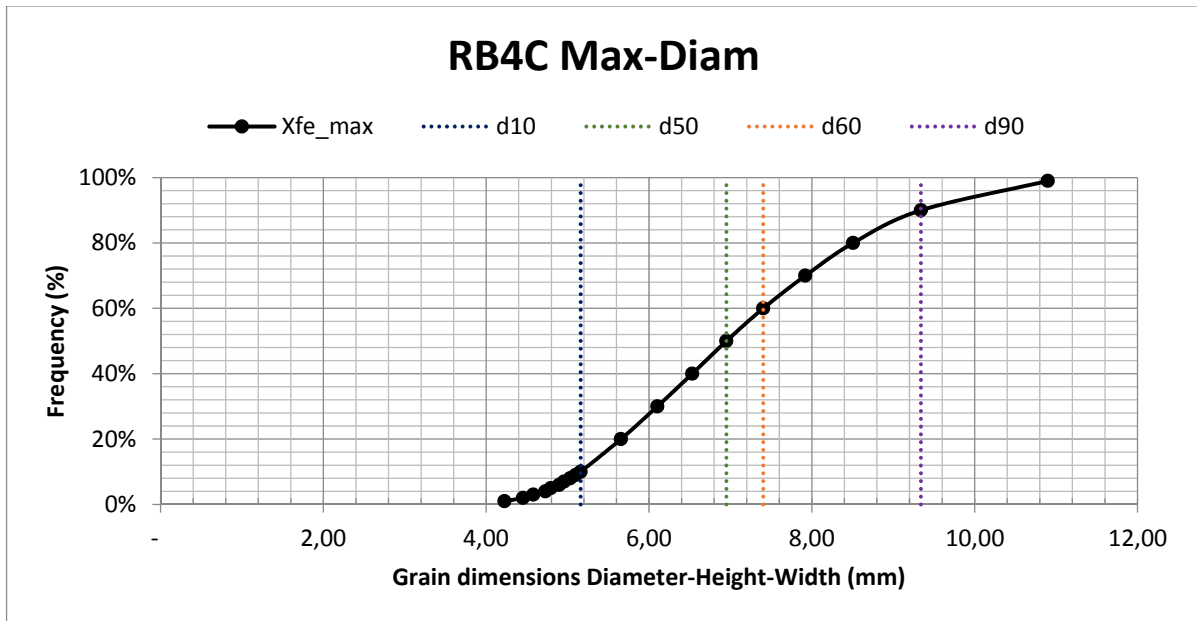


Figure A3.63 - Cumulative distribution maximum diameter RB₄C

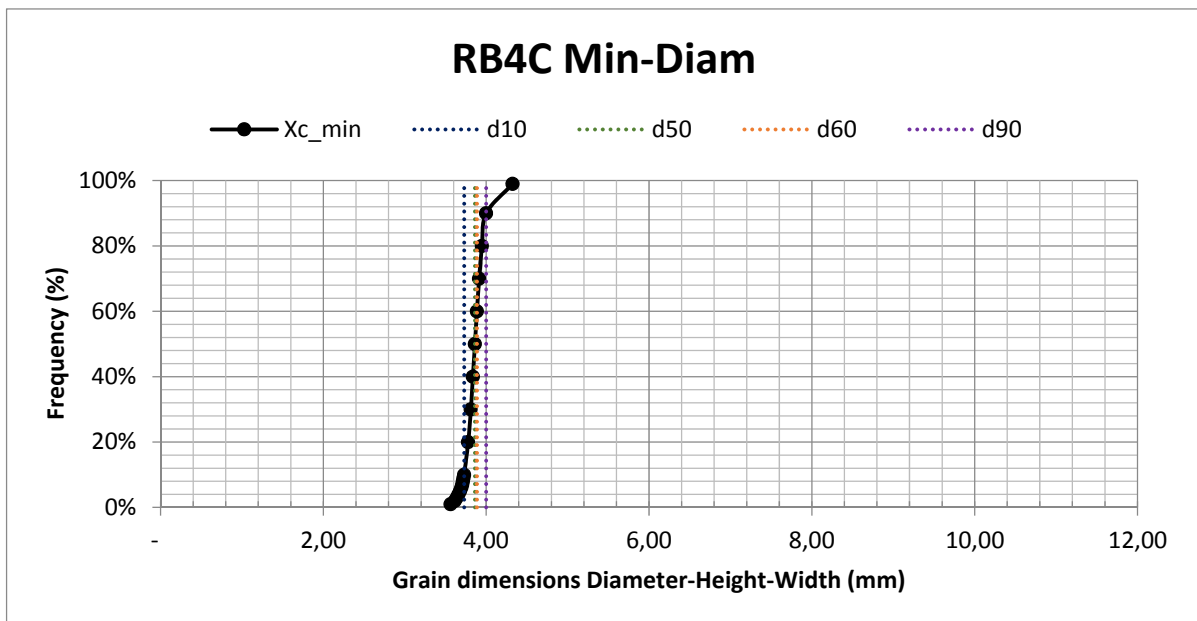


Figure A3.64 - Cumulative distribution minimum diameter RB₄C

→ Filtrasorb TL830

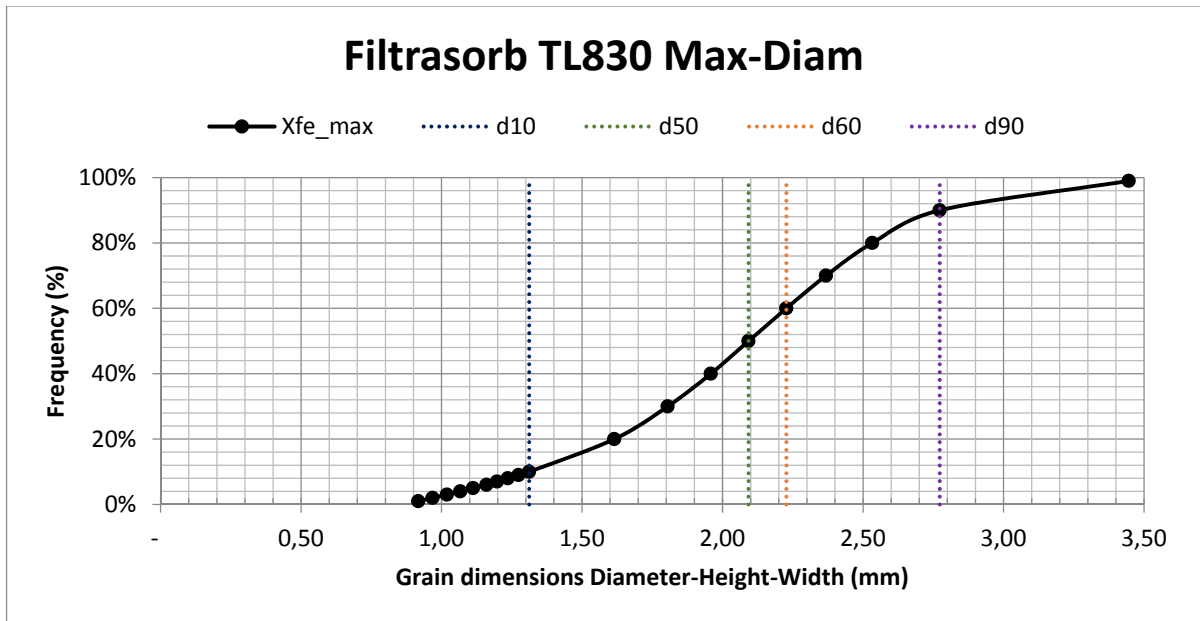


Figure A3.65 - Cumulative distribution maximum diameter Filtrasorb TL830

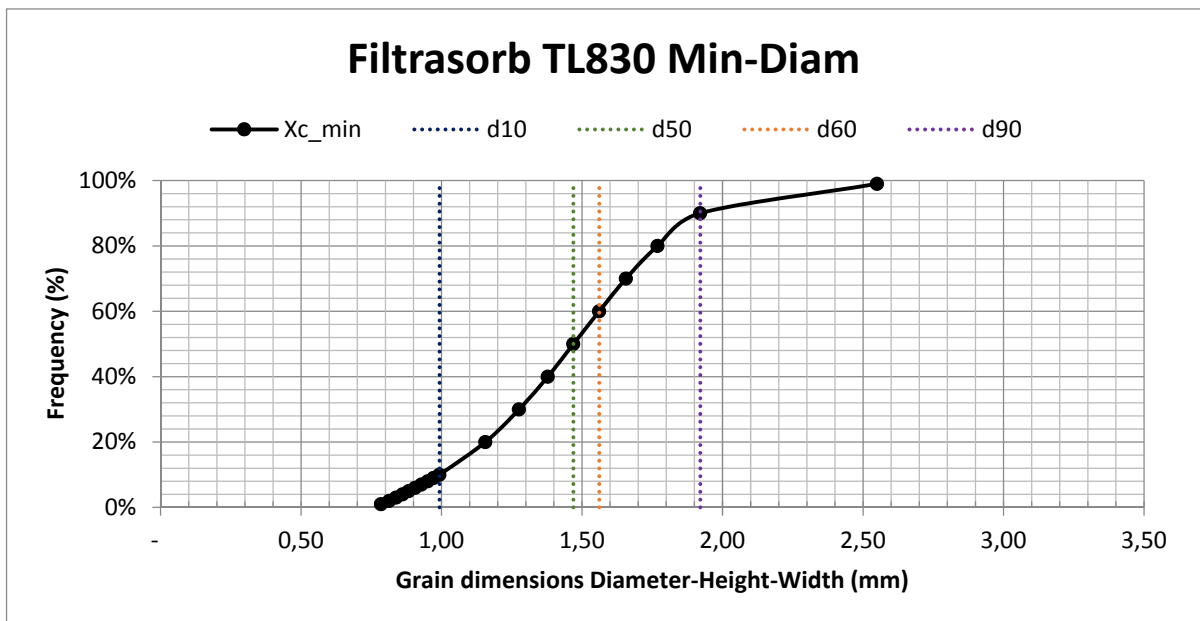


Figure A3.66 - Cumulative distribution minimum diameter Filtrasorb TL830

→ Aquasorb K-6300

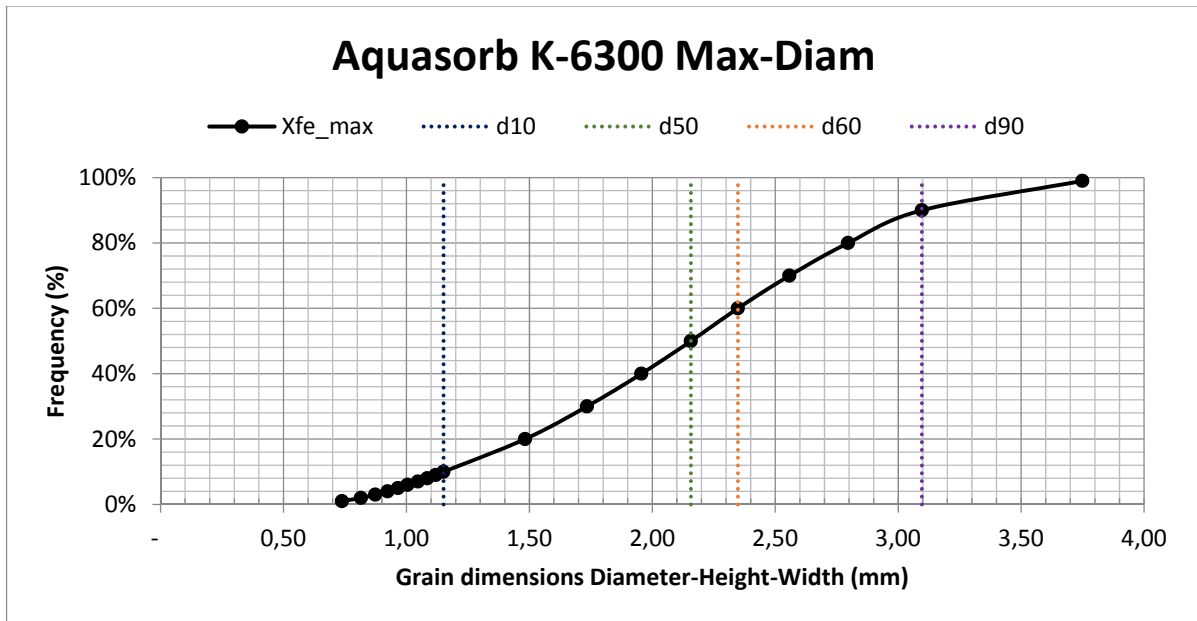


Figure A3.67 - Cumulative distribution maximum diameter Aquasorb K-6300

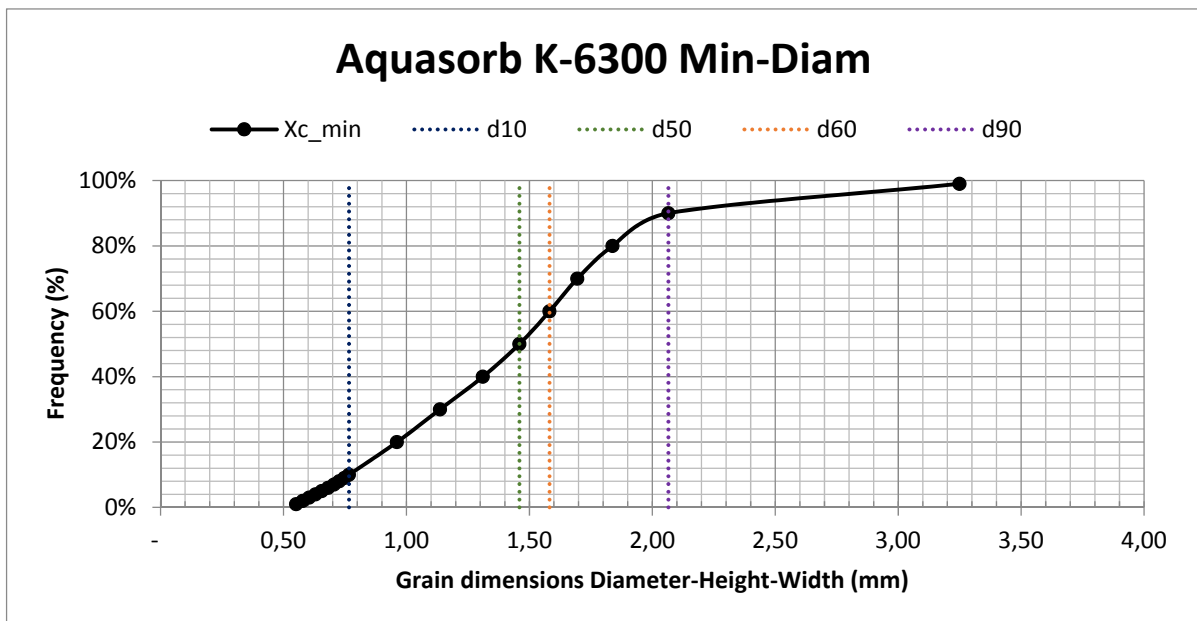


Figure A3.68 - Cumulative distribution minimum diameter Aquasorb K-6300

→ Resorb HC

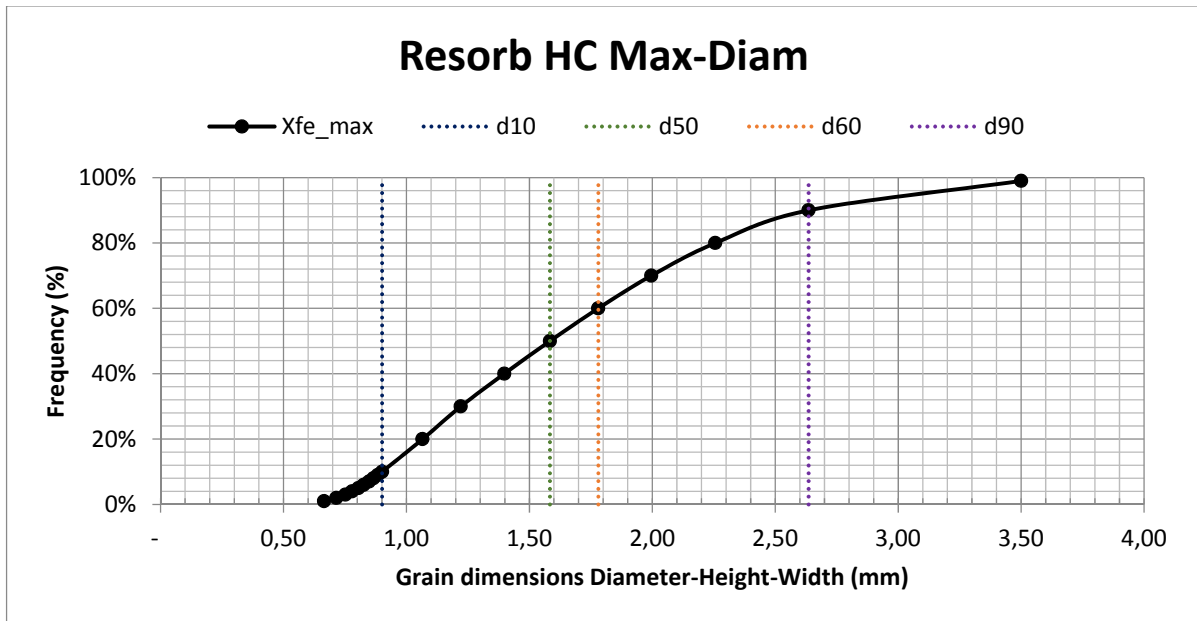


Figure A3.69 - Cumulative distribution maximum diameter Resorb HC

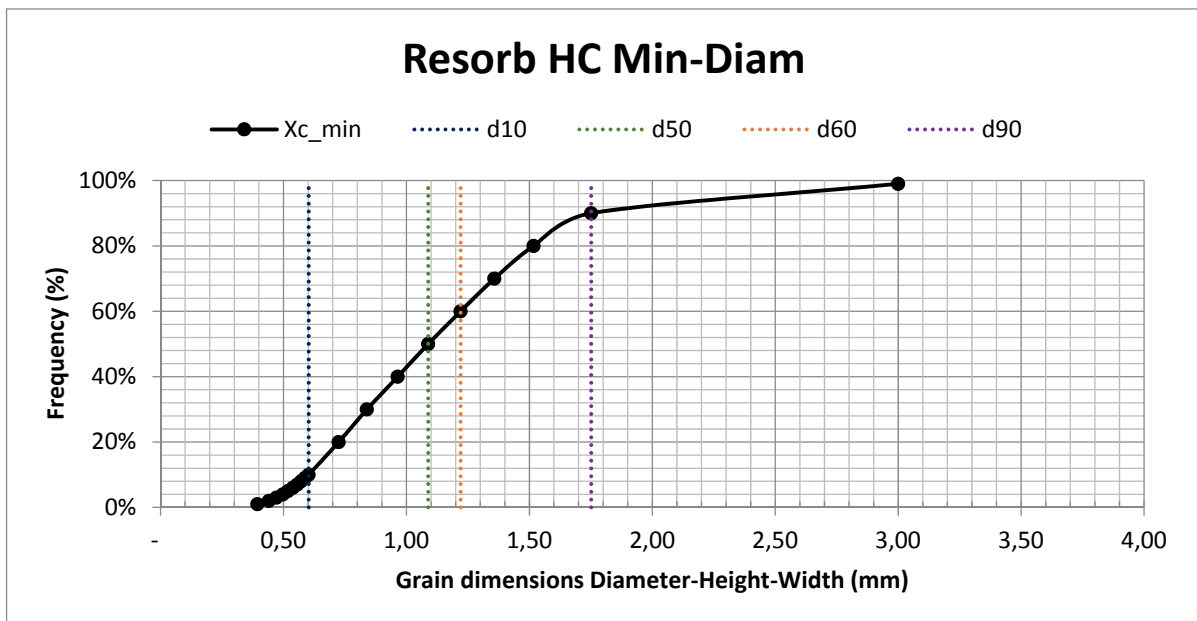


Figure A3.70 - Cumulative distribution minimum diameter Resorb HC

→ GAC 830 SUPRA

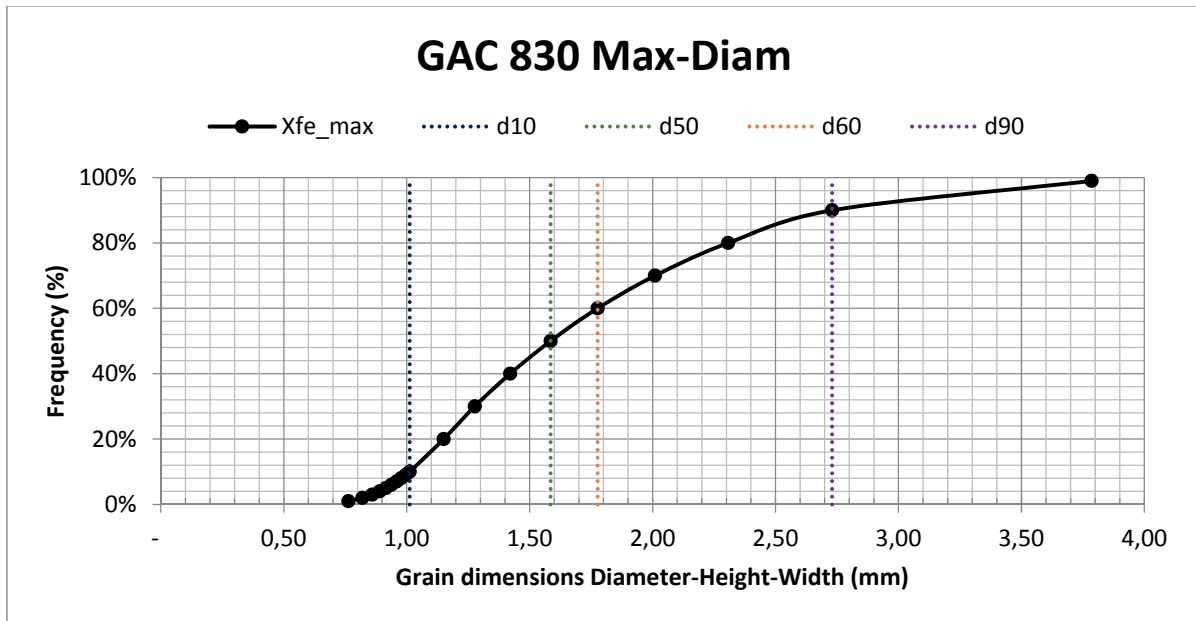


Figure A3.71- Cumulative distribution maximum diameter GAC 830 Supra

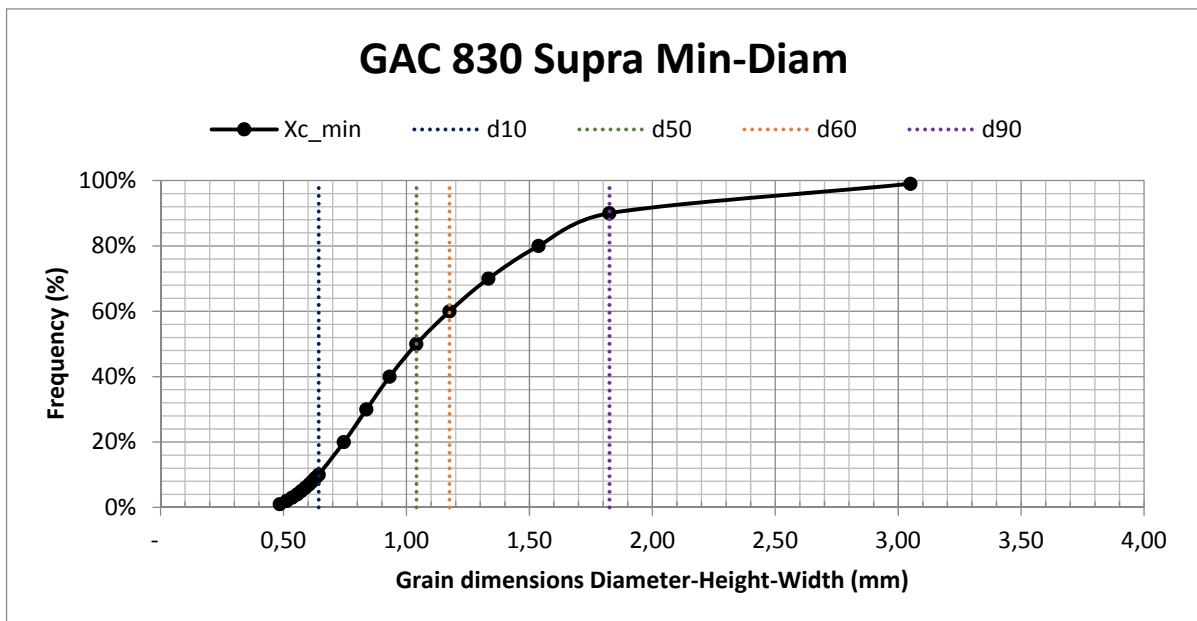


Figure A3.72 - Cumulative distribution minimum diameter GAC 830 Supra

Appendix A4 – Comparison between different particle measurement methods

A comparison of all particle size measurements are presented in this appendix.

→ *Filtrisorb 300c*

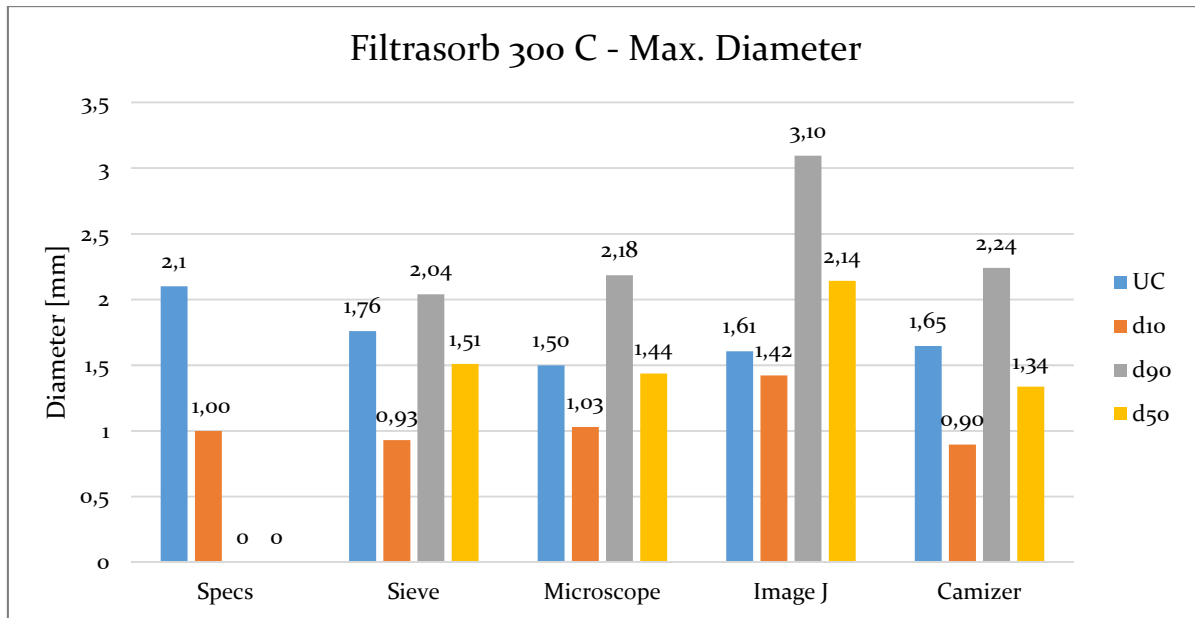


Figure A4.1 – Particle size comparison maximum diameter Filtrisorb 300C

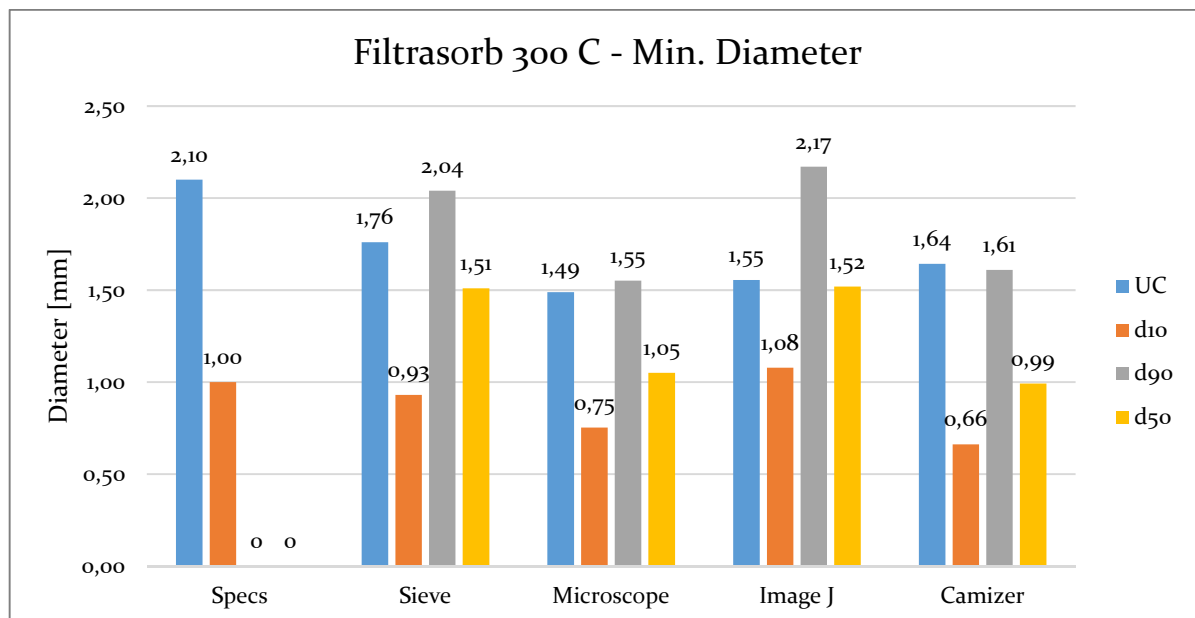


Figure A4.2 - Particle size comparison minimum diameter Filtrisorb 300C

→ Aquasorb KGA

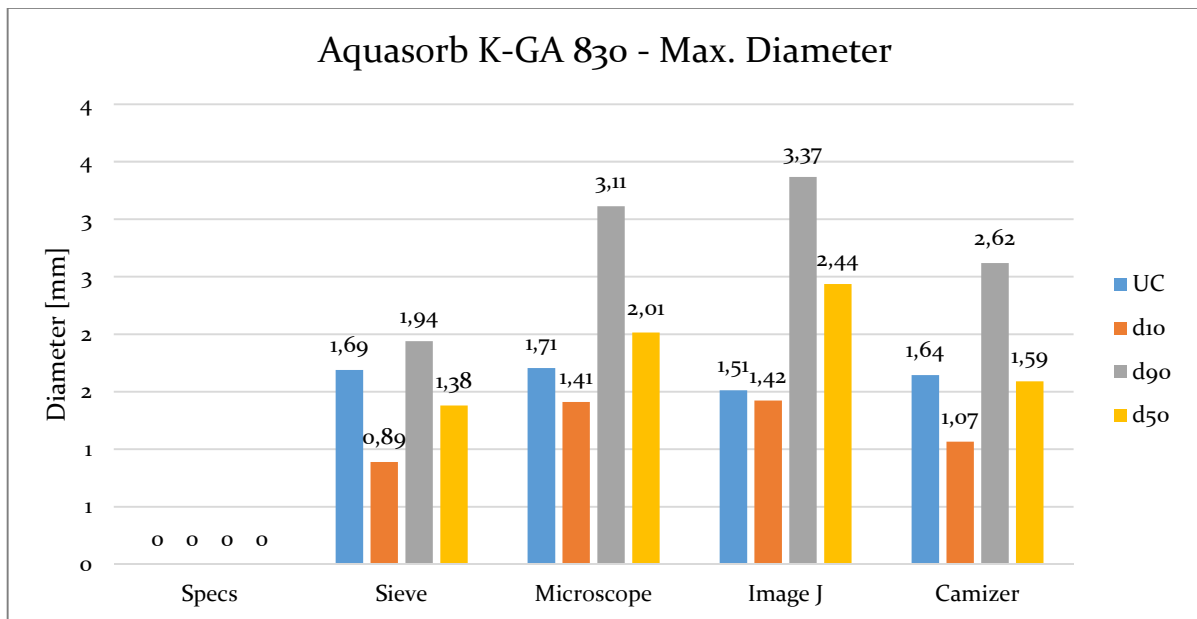


Figure A4.3 - Particle size comparison maximum diameter Aquasorb KGA

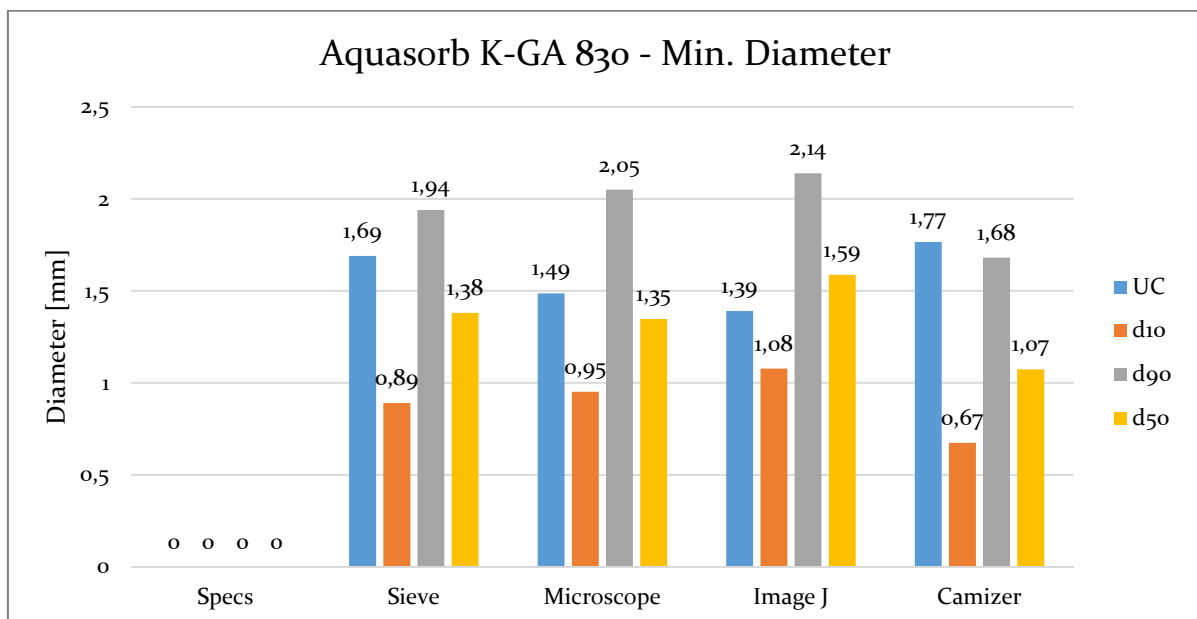


Figure A4.4 - Particle size comparison minimum diameter Aquasorb KGA

→ Saratech spherical

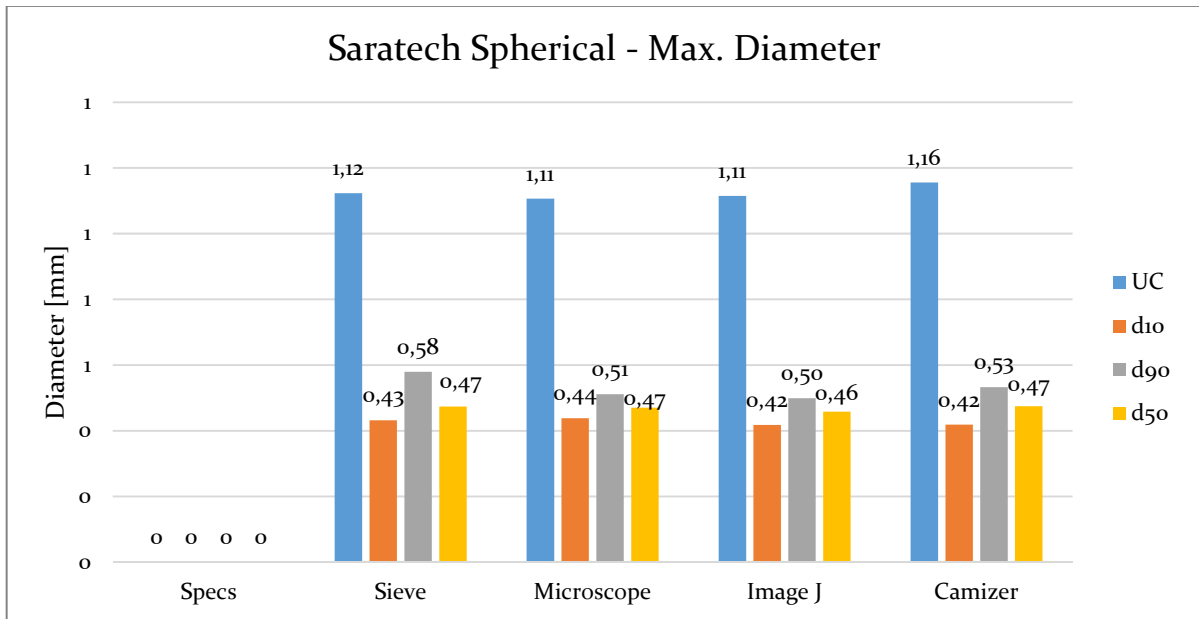


Figure A4.5 - Particle size comparison maximum diameter Saratech spherical

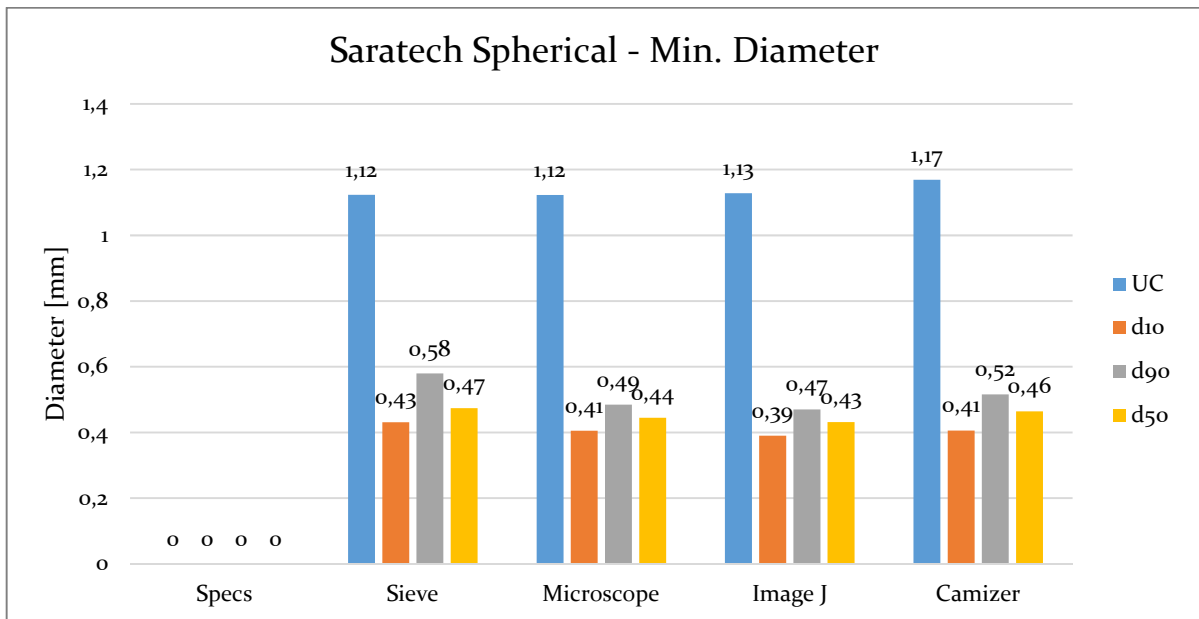


Figure A4.6 - Particle size comparison minimum diameter Saratech spherical

→ROW o.8 Supra

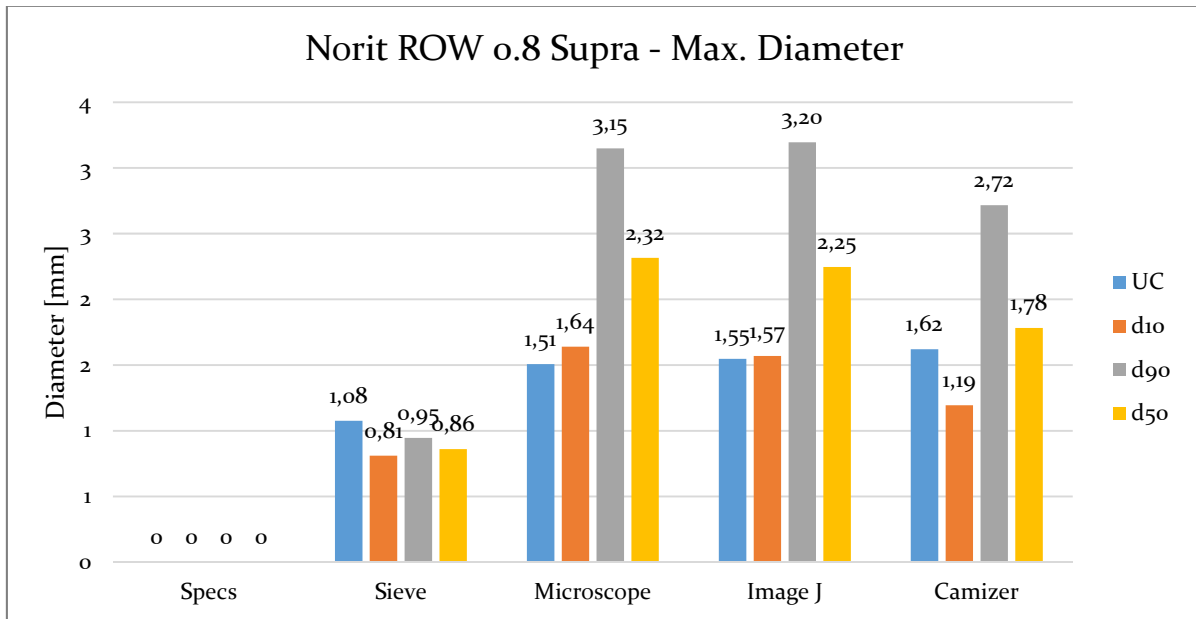


Figure A4.7 - Particle size comparison maximum diameter ROW o.8 Supra

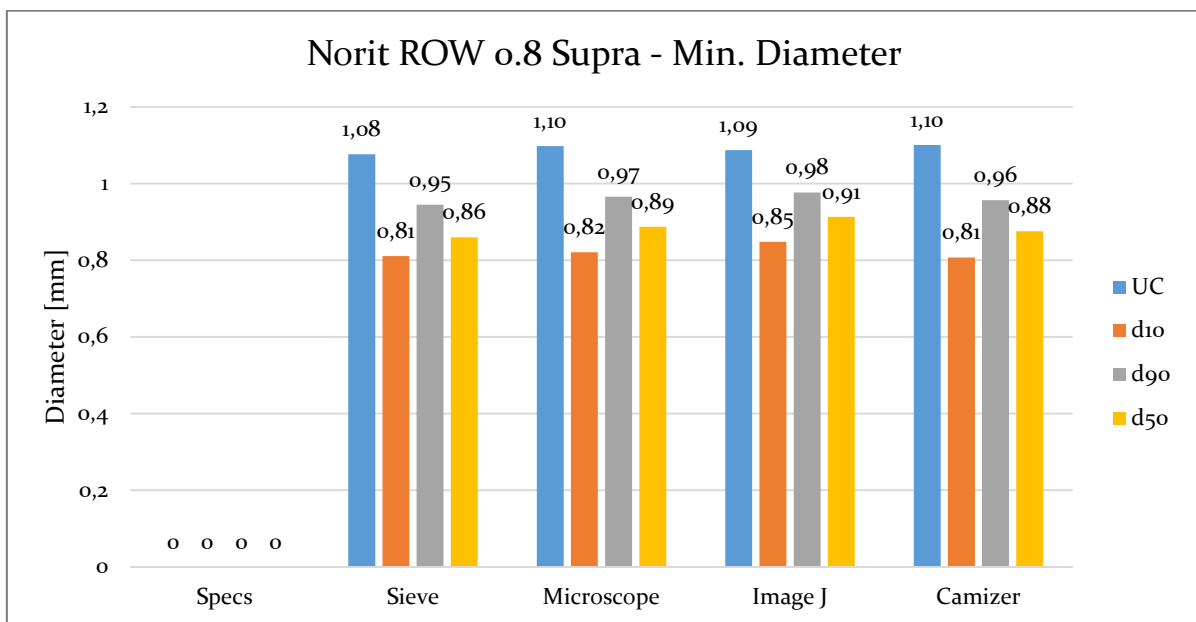


Figure A4.8 - Particle size comparison minimum diameter ROW o.8 Supra

→ RB₄C

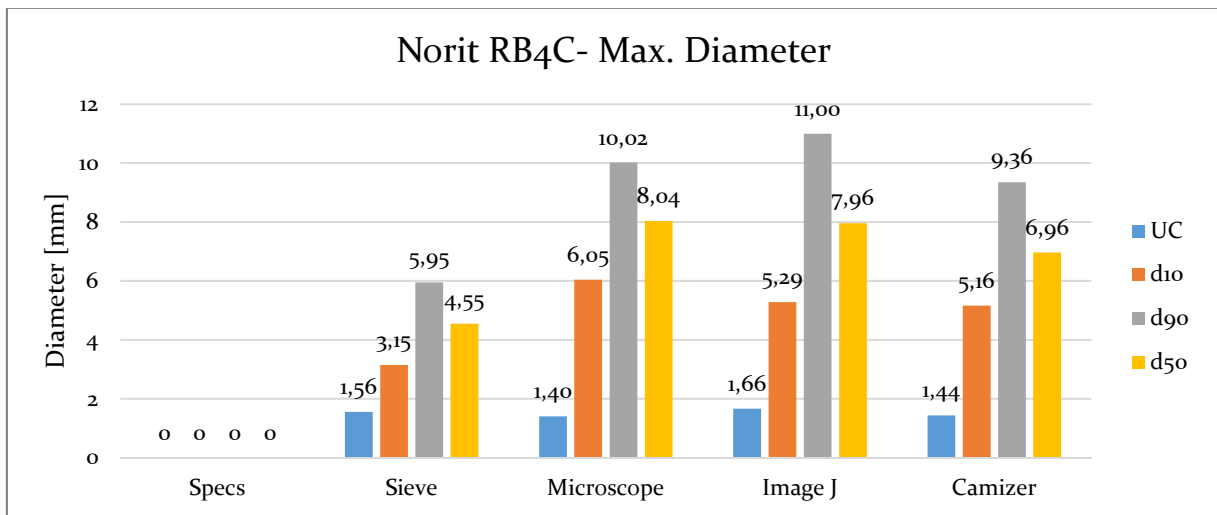


Figure A4.9 - Particle size comparison maximum diameter RB₄C

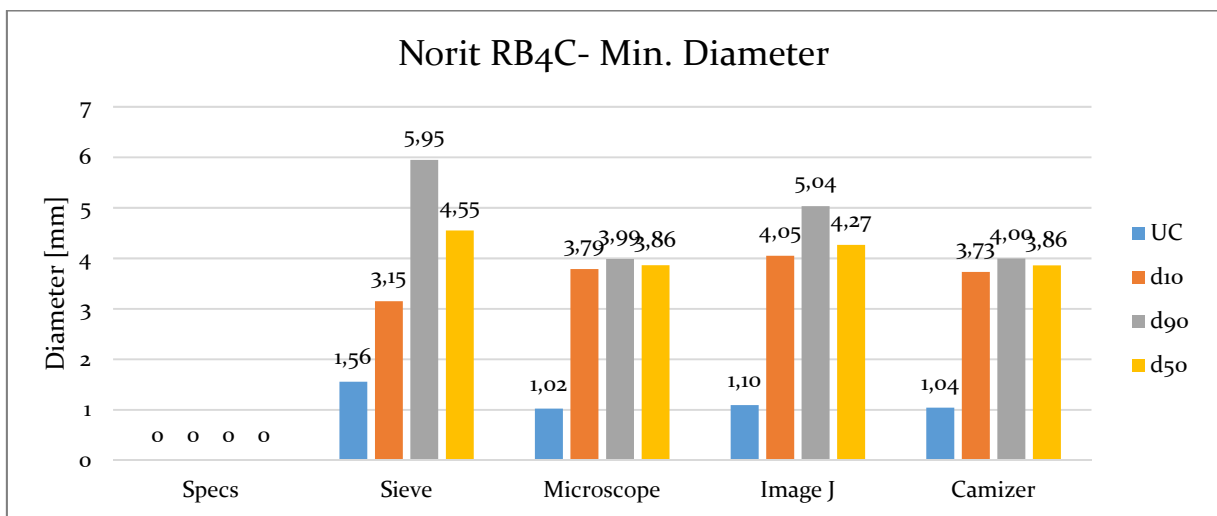


Figure A4.10 - Particle size comparison minimum diameter RB₄C

→ Filtrasorb TL830

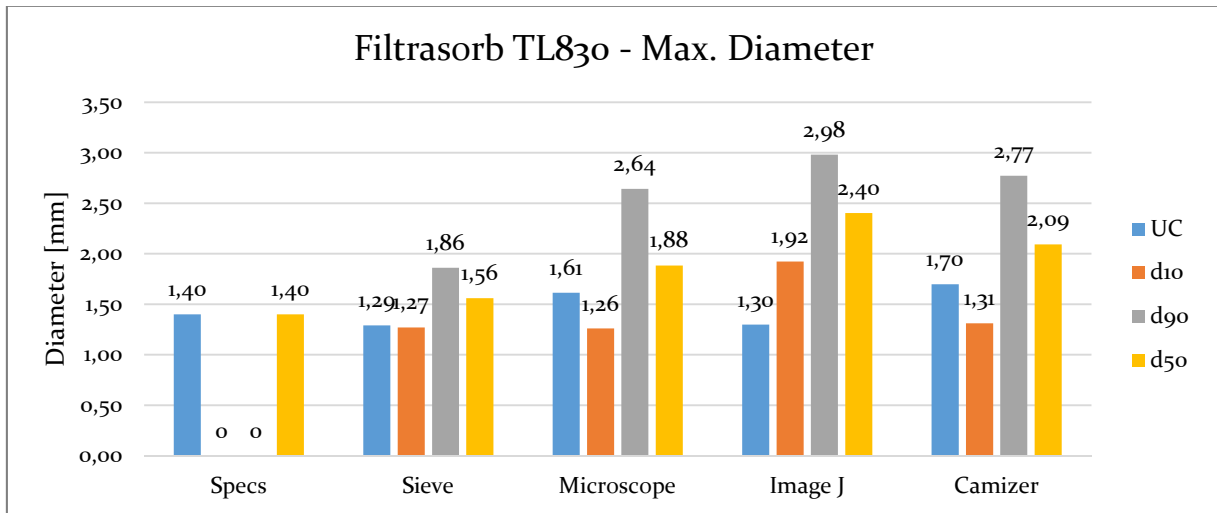


Figure A4.11 - Particle size comparison maximum diameter Filtrasorb TL830

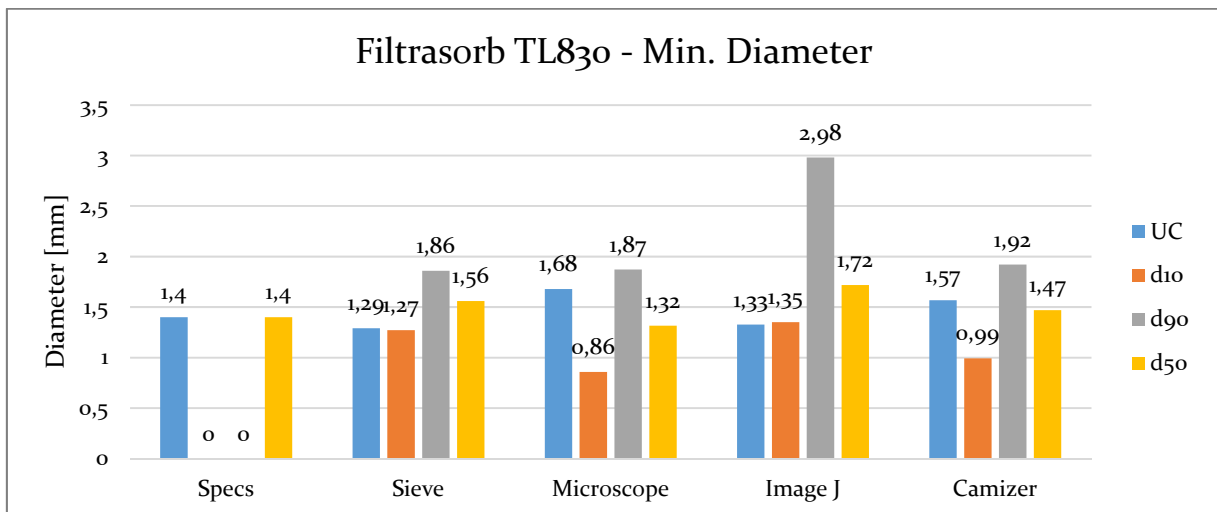


Figure A4.12 - Particle size comparison minimum diameter Filtrasorb TL830

→ Aquasorb K-6300

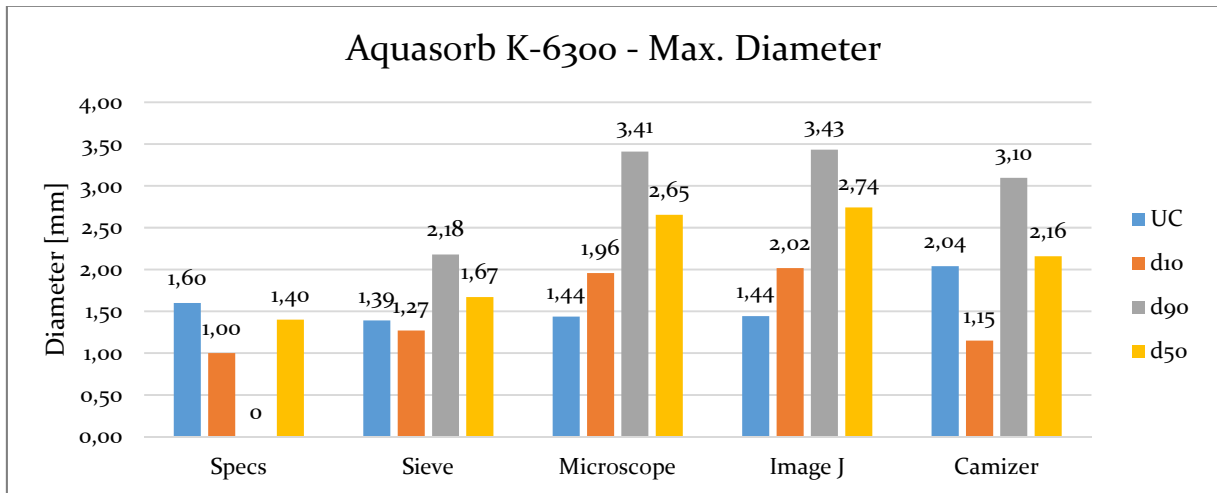


Figure A4.13 - Particle size comparison maximum diameter Aquasorb K-6300

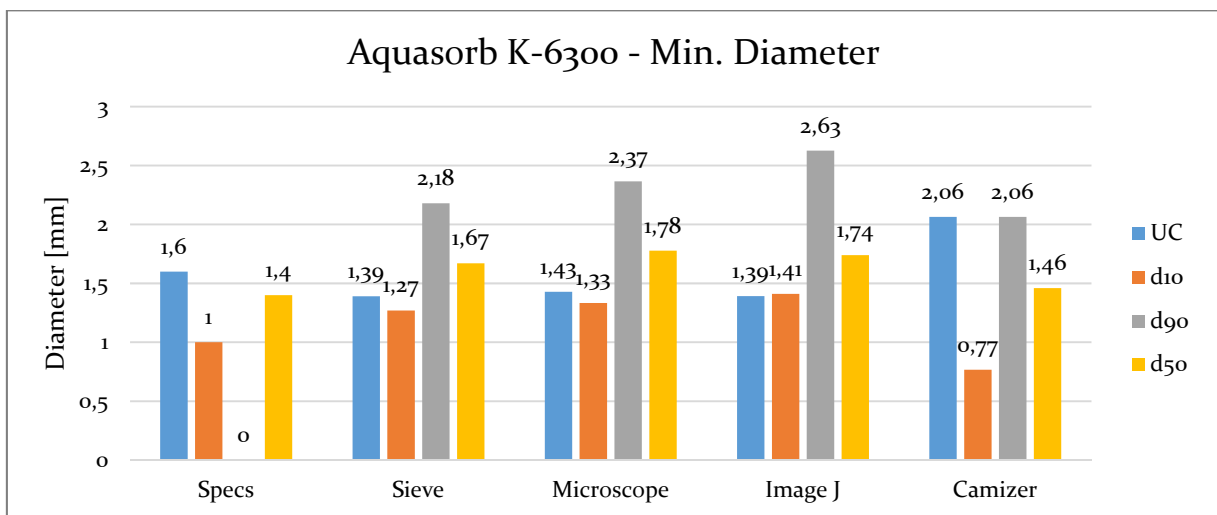


Figure A4.14 - Particle size comparison minimum diameter Aquasorb K-6300

→ Resorb HC

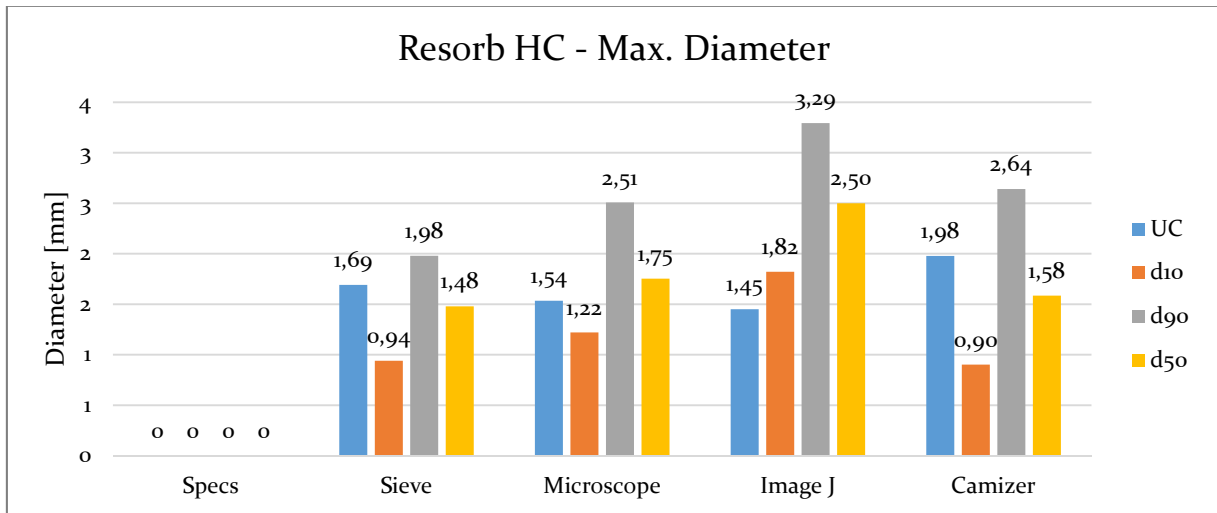


Figure A4.15 - Particle size comparison maximum diameter Resorb HC

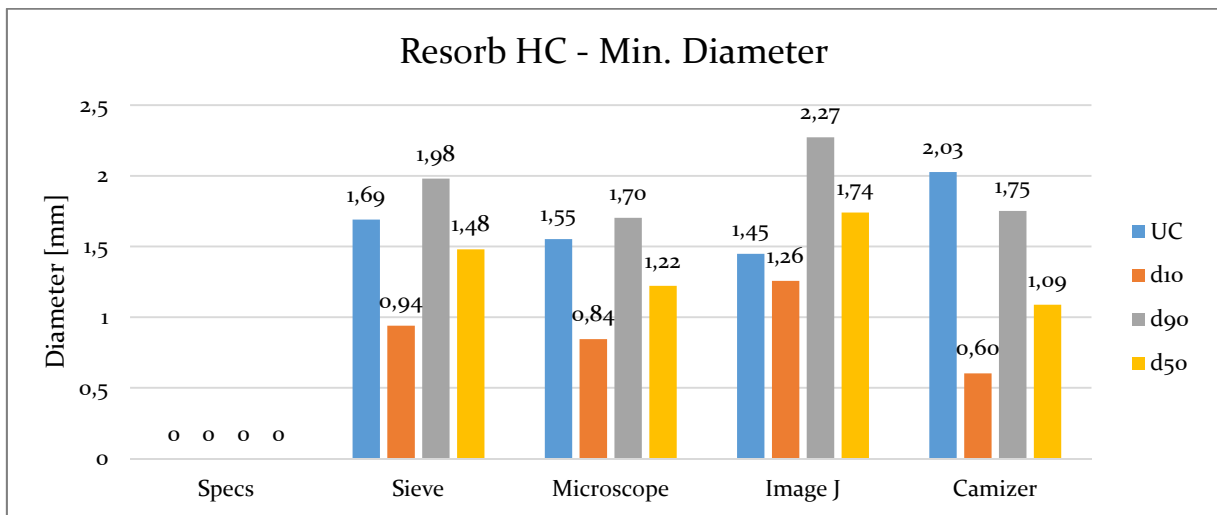


Figure A4.16 - Particle size comparison minimum diameter Resorb HC

→ GAC 830 SUPRA

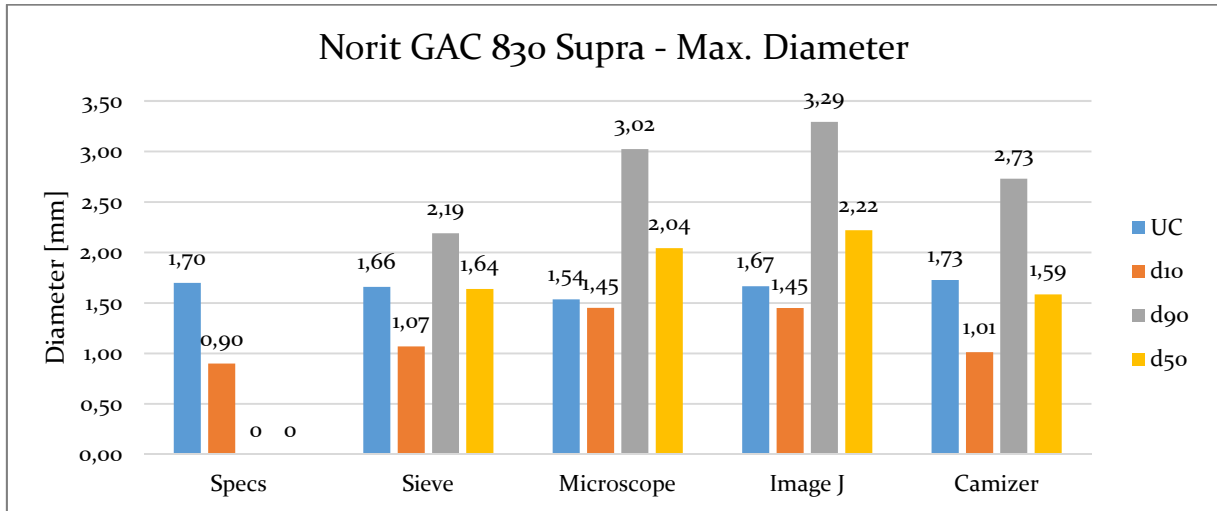


Figure A4.17- Particle size comparison maximum diameter GAC 830 Supra

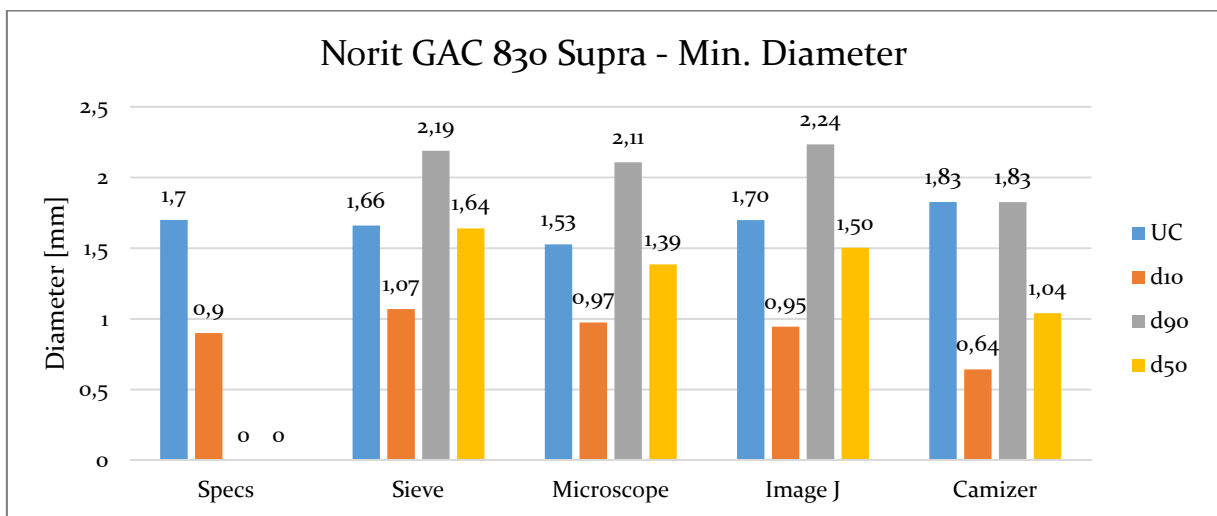


Figure A4.18 - Particle size comparison minimum diameter GAC 830 Supra

Appendix A5 - Density measurements.

- Skeletal density complete measurement runs.

Table 30 – Skeletal density measurement runs.

Sample	Run 1	Run 2	Run 3	Run 4	Run 5	Run 6	Run 7	Run 8	Run 9	Run 10
Filtrisorb_300C	1,636	1,634	1,637	1,636	1,641	1,637	1,640	1,636	1,637	1,635
Aquasorb KGA	2,043	2,036	2,036	2,029	2,027	2,026	2,024	2,018	2,025	2,016
Saratech Spherical	2,213	2,211	2,206	2,202	2,201	2,193	2,196	2,195	2,198	2,192
Norit ROW o.8 Supra	2,159	2,158	2,154	2,154	2,151	2,153	2,151	2,151	2,150	2,154
Norit_RB4C	2,210	2,213	2,203	2,204	2,204	2,207	2,183	2,200	2,195	2,200
Filtrisorb_TL830	1,646	1,646	1,648	1,648	1,648	1,648	1,647	1,648	1,648	1,648
Aquasorb K-6300	1,786	1,799	1,200	1,795	1,790	1,793	1,797	1,791	1,796	1,796
Resorb HC	1,927	1,929	1,928	1,924	1,930	1,929	1,927	1,931	1,929	1,930
Norit GAC 830 Supra	2,102	2,095	2,093	2,092	2,092	2,087	2,087	2,081	2,084	2,088

- Wet density mass conservation inputs and detailed calculations.

Table 31 – Wet density mass conservation calculations – Run 1 (1/3)

Sample Name	Weight of flask	Wdry [g]	Wcarbon+Wwater+Wflask [g]	Wcarbon+Wwater	Wwater before [g]
Filtrisorb 300C (F300)	144.38	1.00	232.12	87.74	84.12
Aquasorb KGA	144.86	1.00	230.4	85.54	84.12
Saratech spheres	144.54	1.00	227.1	82.56	84.12
Norit ROW o.8 Supra	147.00	1.00	230.12	83.12	84.12
Norit RB 4C	146.4	1.00	227.1	80.7	84.12
Filtrisorb TL830	145.06	1.00	230.12	85.06	84.12
Aquasorb K-6300	147.66	1.00	228.68	81.02	84.12
Resorb HC	145.2	1.00	224.78	79.58	84.12
Norit GAC 830 Supra	145.02	1.00	227.4	82.38	84.12

Table 32 – Wet density mass conservation calculations – Run 1 (2/3)

Sample Name	Wcarbonwet(with flask)	Wcarbon wet	Wwater after	Wwet/Wdry	Vwater [mL]
-------------	------------------------	-------------	--------------	-----------	-------------

Filtrisorb 300C (F300)	146.26	1.88	85.74	1.9	100
Aquasorb KGA	147.66	2.8	82.38	2.8	100
Saratech spheres	147.3	2.76	79.88	2.8	100
Norit ROW o.8 Supra	150.34	3.34	79.66	3.3	100
Norit RB 4C	148.88	2.48	79.64	2.5	100
Filtrisorb TL830	147.04	1.98	77.48	2.0	100
Aquasorb K-6300	150.18	2.52	77.02	2.5	100
Resorb HC	148	2.8	83.7	2.8	100
Norit GAC 830 Supra	147.56	2.54	81.94	2.5	100

Table 33 – Wet density mass conservation calculations – Run 1 (3/3)

Sample Name	Wdry+Wwbefore	Wwet+Wwafter	ERROR (%)	Dry Density [kg/m ³]	Wet Density [kg/m ³]
Filtrisorb 300C (F300)	85.12	87.62	-3%	787	1,479
Aquasorb KGA	85.12	85.18	0%	489	1,368
Saratech spheres	85.12	82.64	3%	702	1,937
Norit ROW o.8 Supra	85.12	83	2%	675	2,253
Norit RB 4C	85.12	82.12	4%	764	1,894
Filtrisorb TL830	85.12	79.46	7%	647	1,280
Aquasorb K-6300	85.12	79.54	7%	493	1,242
Resorb HC	85.12	86.5	-2%	498	1,394
Norit GAC 830 Supra	85.12	84.48	1%	492	1,251

Table 34 – Wet density mass conservation calculations – Run 2 (1/3)

Sample Name	Weight of flask	Wdry [g]	Wcarbon+Wwater+Wflask [g]	Wcarbon+Wwater	Wwater before [g]

Filtrisorb 300C (F300)	144.38	6	235.62	91.24	85.24
Aquasorb KGA	144.86	10	243.1	98.24	88.24
Saratech spheres	144.54	6	233.56	89.02	83.02
Norit ROW o.8 Supra	147.00	6	237.24	90.24	84.24
Norit RB 4C	146.4	6	233.6	87.2	81.2
Filtrisorb TL830	145.06	10	240.84	95.78	85.78
Aquasorb K-6300	147.66	6.02	239.38	91.72	85.7
Resorb HC	145.2	6	239.24	94.04	88.04
Norit GAC 830 Supra	145.02	6.04	234.04	89.02	82.98

Table 35 – Wet density mass conservation calculations – Run 2 (2/3)

Sample Name	Wcarbonwet(w ith flask)	Wcarbon wet	Wwater after	Wwet/Wdry	Vwater [mL]
Filtrisorb 300C (F300)	155.04	10.66	79.66	1.8	100
Aquasorb KGA	171.08	26.22	70.58	2.6	100
Saratech spheres	159.94	15.4	72.32	2.6	100
Norit ROW o.8 Supra	165.68	18.68	70.36	3.1	100
Norit RB 4C	158.38	11.98	74.02	2.0	100
Filtrisorb TL830	163.02	17.96	76.34	1.8	100
Aquasorb K-6300	161.86	14.2	76.46	2.4	100
Resorb HC	160.36	15.16	77.94	2.5	100
Norit GAC 830 Supra	159.02	14	73.84	2.3	100

Table 36 – Wet density mass conservation calculations – Run 2 (3/3)

Sample Name	Wdry+Wwbefore	Wwet+W wafter	ERROR (%)	Dry Density [kg/m³]	Wet Density [kg/m³]
--------------------	----------------------	----------------------	------------------	---------------------------------------	---------------------------------------

Filtrisorb 300C (F300)	91.24	90.32	1.0%	787	1,397
Aquasorb KGA	98.24	96.8	1.5%	489	1,281
Saratech spheres	89.02	87.72	1.5%	702	1,801
Norit ROW o.8 Supra	90.24	89.04	1.3%	675	2,100
Norit RB 4C	87.2	86	1.4%	764	1,525
Filtrisorb TL830	95.78	94.3	1.5%	647	1,161
Aquasorb K-6300	91.72	90.66	1.2%	493	1,162
Resorb HC	94.04	93.1	1.0%	498	1,258
Norit GAC 830 Supra	89.02	87.84	1.3%	492	1,141

Table 37 – Wet density mass conservation calculations – Run 3 (1/3)

Sample Name	Weight of flask	Wdry [g]	Wcarbon+Wwater+Wflask [g]	Wcarbon+Wwater	Wwater before [g]
Filtrisorb 300C (F300)	101.24	1	140.4	39.16	38.16
Aquasorb KGA	102.02	1.02	145.66	43.64	42.62
Saratech spheres	102.8	1	141.86	39.06	38.06
Norit ROW o.8 Supra	101.20	1	139.56	38.36	37.36
Norit RB 4C	97.02	1	144.7	47.68	46.68
Filtrisorb TL830	102.36	1.02	141.2	38.84	37.82
Aquasorb K-6300	100.98	1.02	145.44	44.46	43.44
Resorb HC	105.62	1.02	144.08	38.46	37.44
Norit GAC 830 Supra	101.9	1	142.96	41.06	40.06

Table 38 – Wet density mass conservation calculations – Run 3 (2/3)

Sample Name	Wcarbonwet(with flask)	Wcarbon wet	Wwater after	Wwet/Wdry	Vwater [mL]
--------------------	-------------------------------	--------------------	---------------------	------------------	--------------------

Filtrisorb 300C (F300)	103.14	1.9	35.85	1.9	100
Aquasorb KGA	105	2.98	39.56	2.9	100
Saratech spheres	105.62	2.82	35.01	2.8	100
Norit ROW o.8 Supra	104.4	3.2	33.88	3.2	100
Norit RB 4C	99.52	2.5	43.74	2.5	100
Filtrisorb TL830	104.42	2.06	35.28	2.0	100
Aquasorb K-6300	103.7	2.72	40.58	2.7	100
Resorb HC	108.34	2.72	34.52	2.7	100
Norit GAC 830 Supra	104.38	2.48	37.42	2.5	100

Table 39 – Wet density mass conservation calculations – Run 3 (3/3)

Sample Name	Wdry+Wwbefore	Wwet+Wwafter	ERROR (%)	Dry Density [kg/m³]	Wet Density [kg/m³]
Filtrisorb 300C (F300)	39.16	37.75	3.60%	787	1,494
Aquasorb KGA	43.64	42.54	2.52%	489	1,427
Saratech spheres	39.06	37.83	3.15%	702	1,979
Norit ROW o.8 Supra	38.36	37.08	3.34%	675	2,159
Norit RB 4C	47.68	46.24	3.02%	764	1,909
Filtrisorb TL830	38.84	37.34	3.86%	647	1,306
Aquasorb K-6300	44.46	43.3	2.61%	493	1,314
Resorb HC	38.46	37.24	3.17%	498	1,328
Norit GAC 830 Supra	41.06	39.9	2.83%	492	1,221

- Particle (envelope) density 3D models and sample profiles

→ Filtrasorb 300C

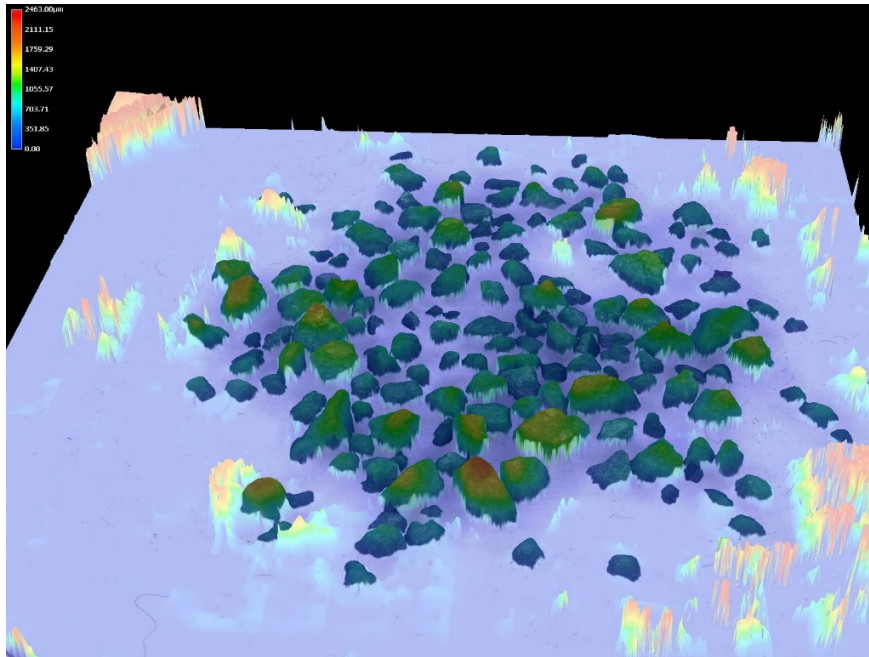


Figure A5.1 – Filtrasorb 300C generated 3D model

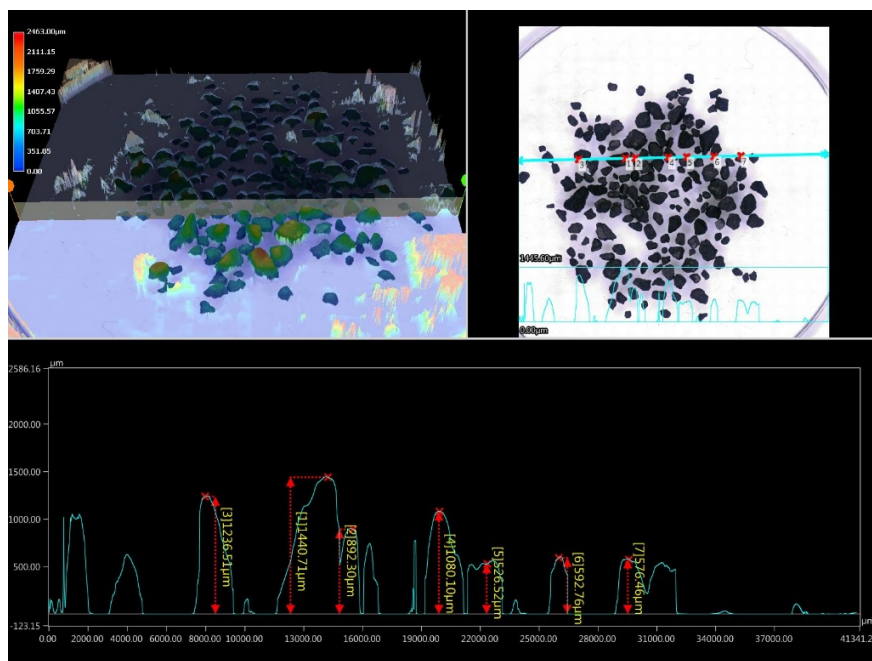


Figure A5.2 – Profile sample of 3D model Filtrasorb 300C

→ Aquasorb KGA

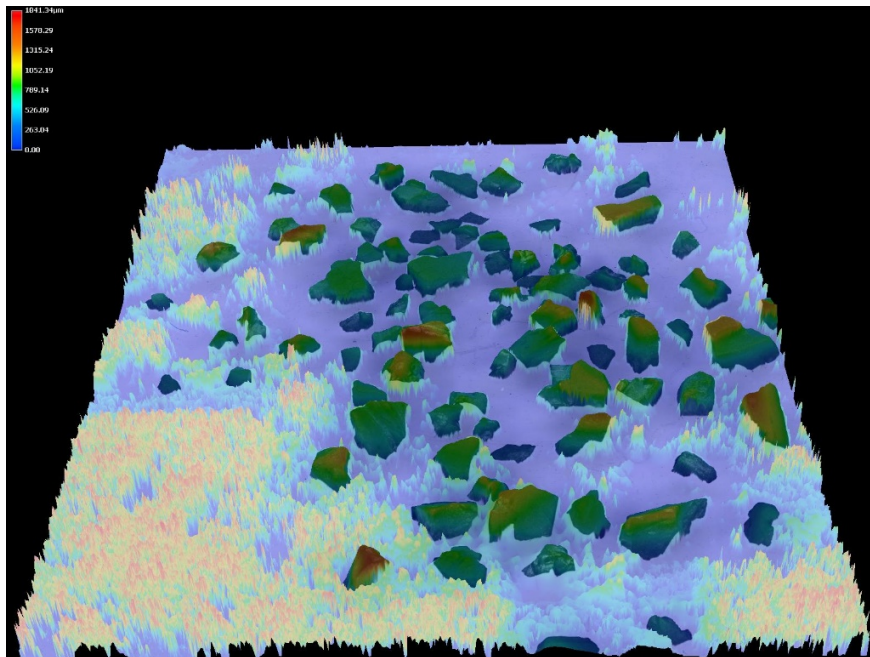


Figure A5.3 - Aquasorb KGA generated 3D model

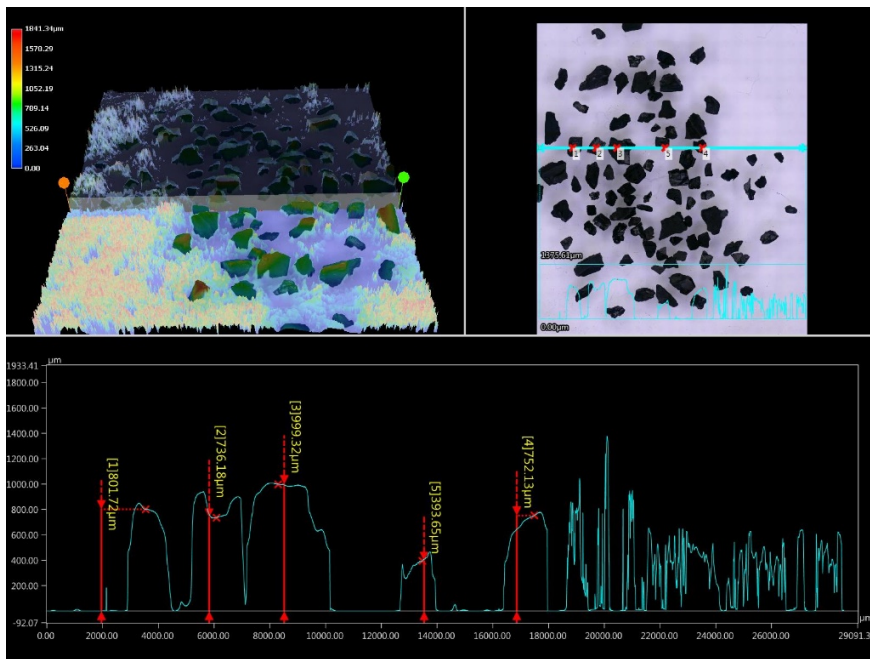


Figure A5.4 - Profile sample of 3D model Aquasorb KGA

→ROW 0.8 Supra

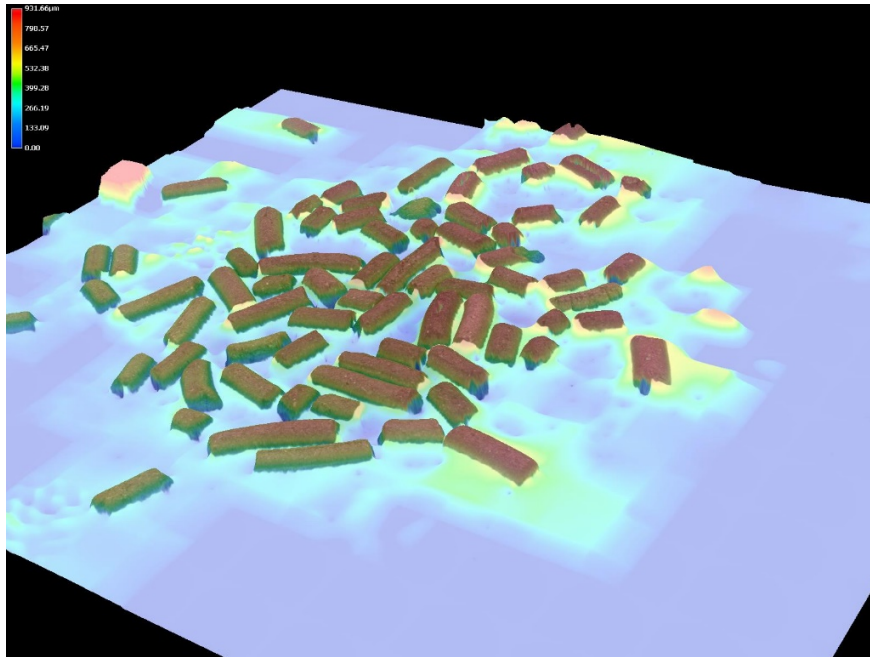


Figure A5.5 - ROW 0.8 Supra generated 3D model

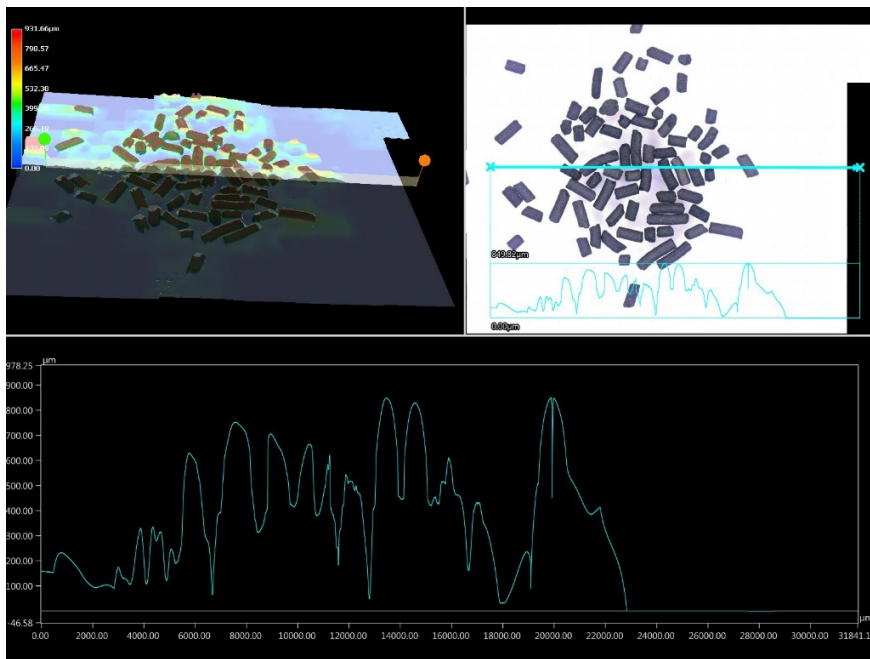


Figure A5.6 - Profile sample of 3D model ROW 0.8 Supra

→ RB₄C

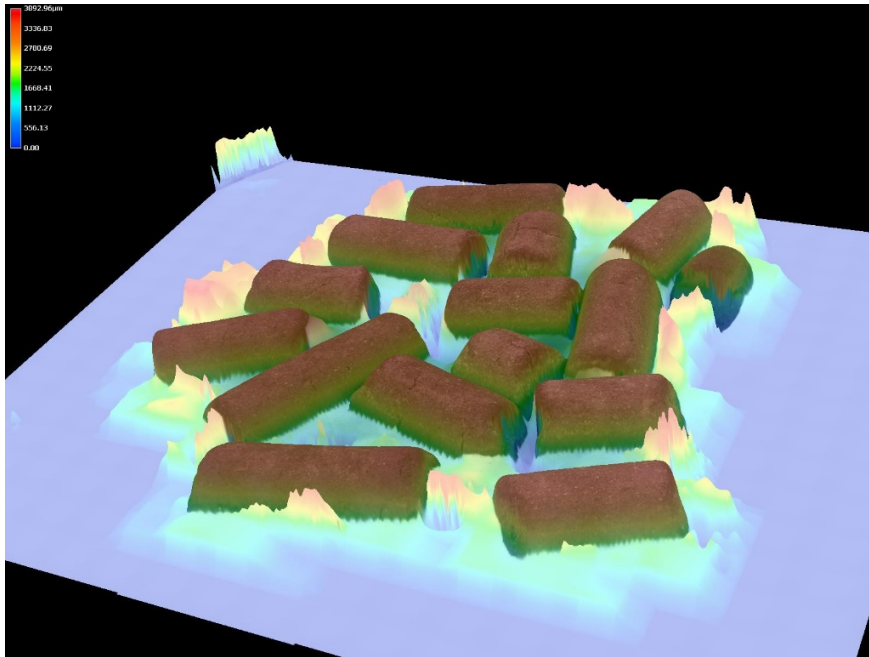


Figure A5.7 - RB₄C generated 3D model

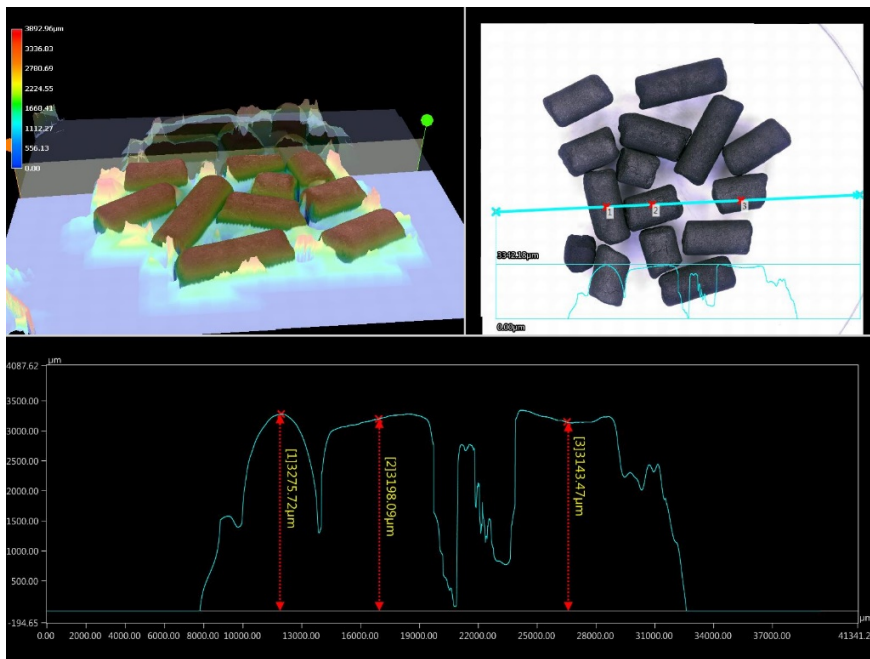


Figure A5.8 - Profile sample of 3D model RB₄C

→ Filtrasorb TL830

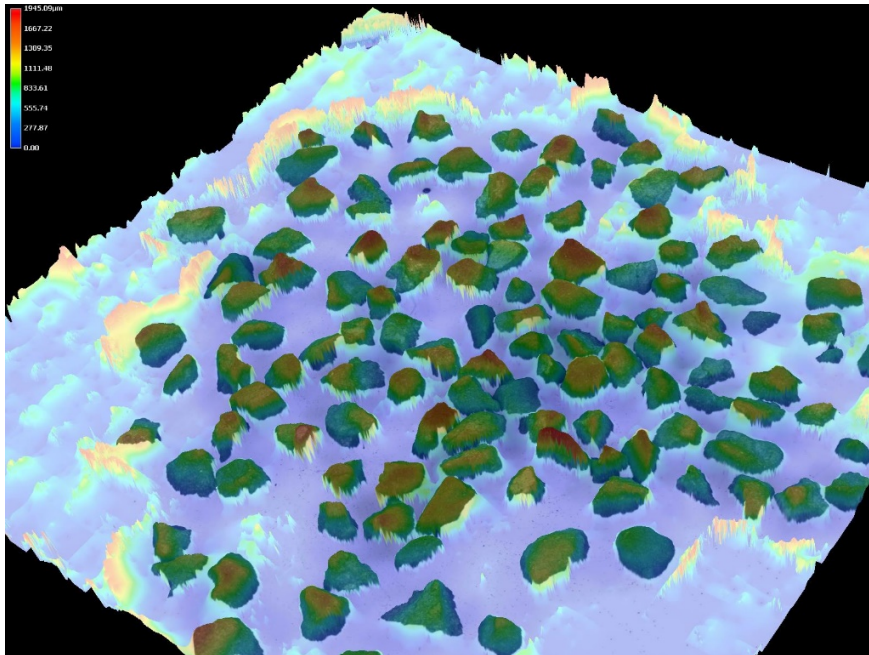


Figure A5.9 - Filtrasorb TL830 generated 3D model

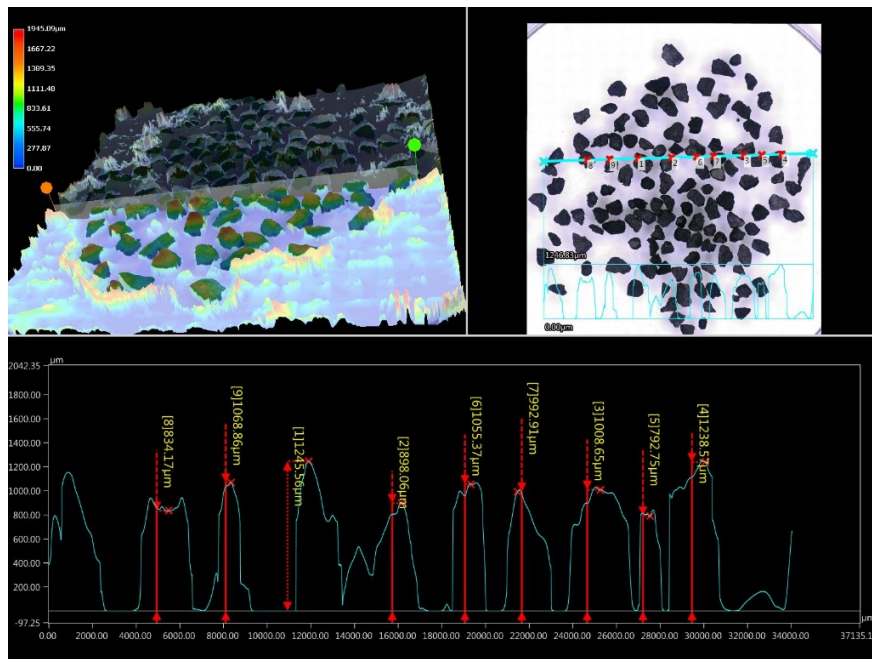


Figure 5.10 - Profile sample of 3D model Filtrasorb TL830

→ Aquasorb K-6300

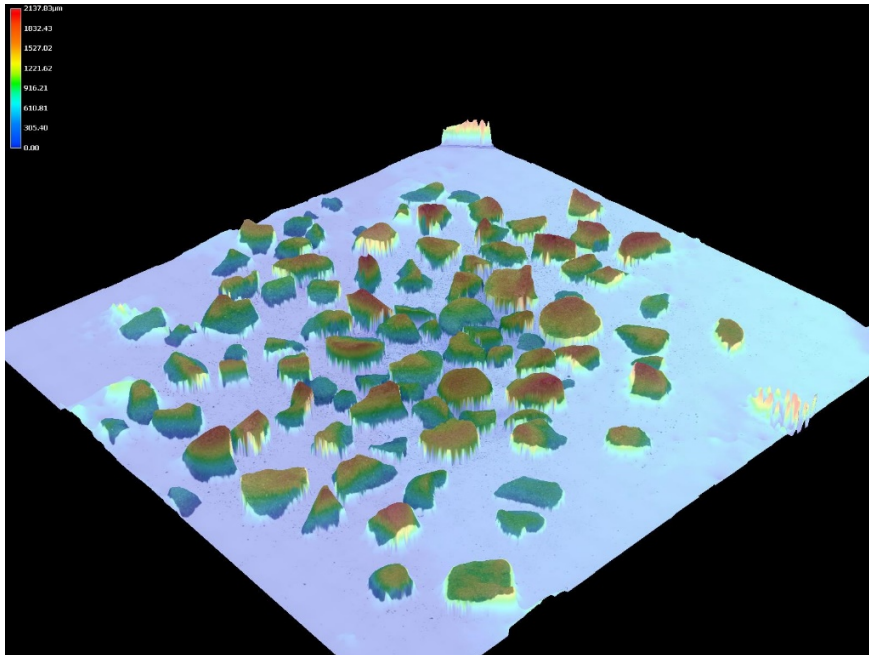


Figure A5.11 - Aquasorb K-6300 generated 3D model

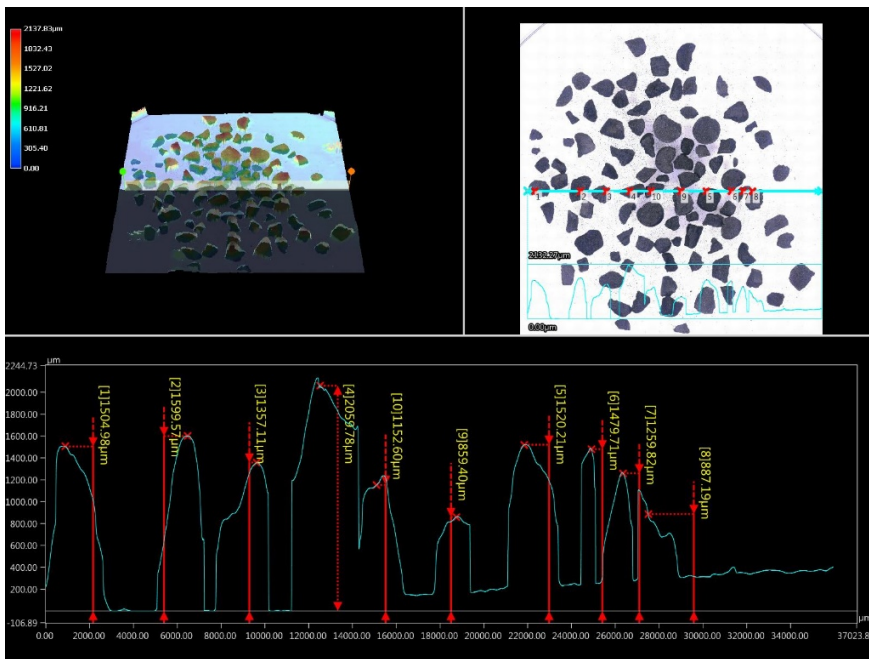


Figure A5.12 - Profile sample of 3D model Aquasorb K-6300

→ Resorb HC

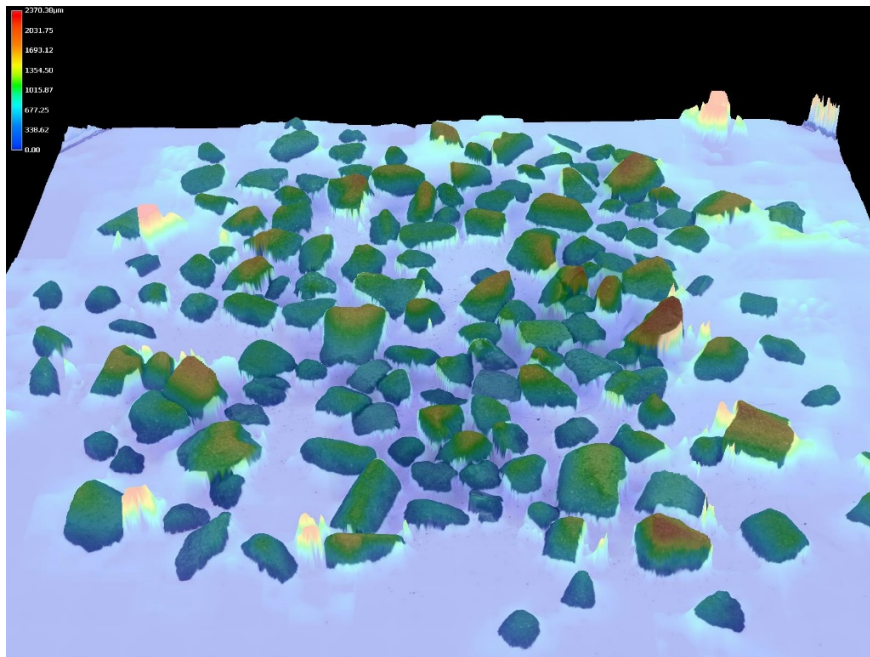


Figure A5.13 - Resorb HC generated 3D model

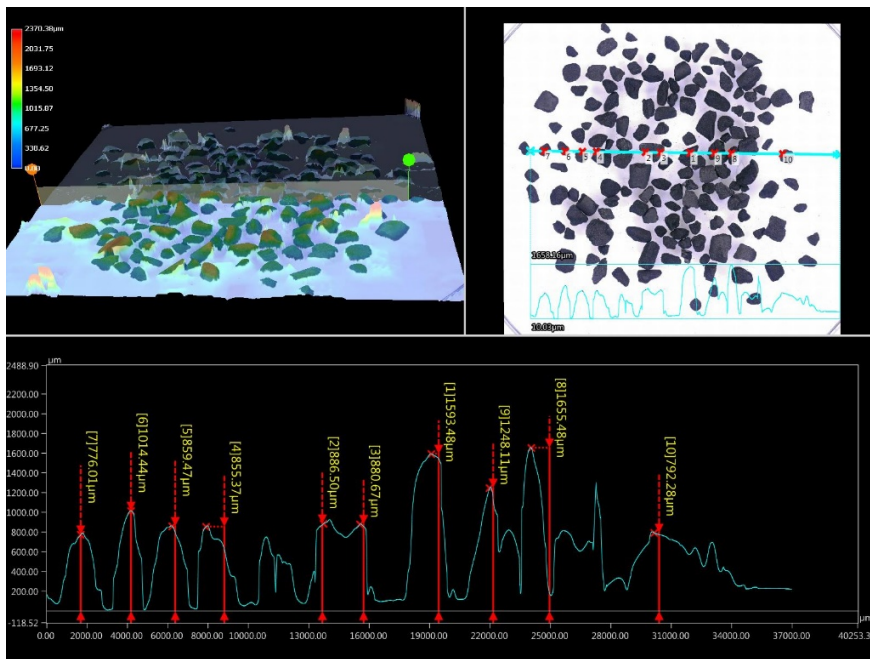


Figure A5.14 - Profile sample of 3D model Resorb HC

→ GAC 830 SUPRA

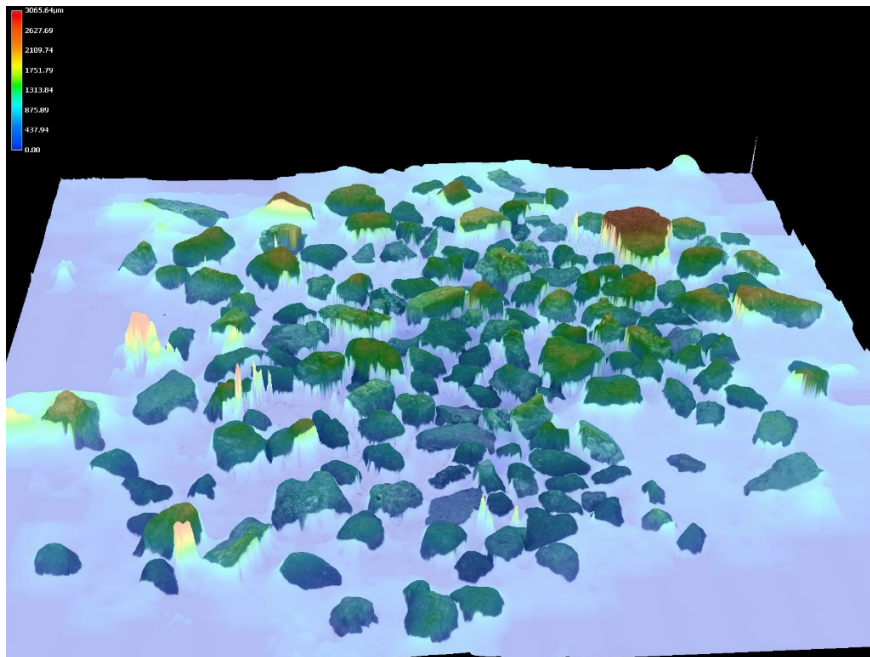


Figure A5.15- GAC 830 Supra generated 3D model

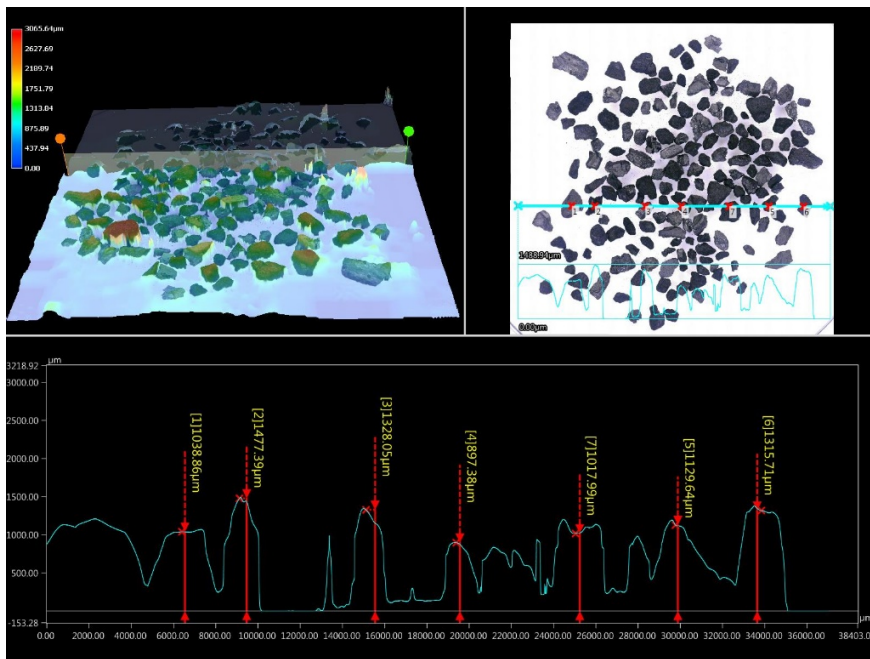


Figure A5.16 - Profile sample of 3D model GAC 830 Supra

Appendix A6 – Morphological parameters of the particles

Microscope morph measurements

	Percentile	Max diameter	Area	Circularity	Gravity center (Y)	Perimeter	Diagonal width	Fore diameter (Horizontal)	Circle equivalent dia	Min diameter	Fore diameter (Vertical)	Max diameter angle	Min diameter angle	Gravity center (X)	1st moment (X-axis)	1st moment (Y-axis)	2nd moment (X-axis)	2nd moment (Y-axis)	Product of inertia	Gravity 2nd moment (Y-axis)	Gravity product of inertia	2nd moment major axis	2nd moment minor axis	2nd moment angle	Aspect Ratio
0.01	0.86	0.44	1.00	233.79	2.67	0.67	0.74	0.75	0.63	0.74	3.33	0.00	462.00	2.57E+06	1.26E+06	1.65E+09	3.52E+08	1.49E+09	5.49E+05	-1.22E+07	3.34E+03	1.86E+03	2.86	1.35	
0.02	0.90	0.48	1.00	313.69	2.80	0.70	0.77	0.78	0.67	0.76	5.40	0.29	591.55	3.04E+06	1.77E+06	2.33E+09	7.76E+08	2.55E+09	6.27E+05	-7.30E+06	3.67E+03	2.13E+03	4.00	1.34	
0.03	0.93	0.50	1.00	387.64	2.86	0.72	0.80	0.80	0.68	0.79	7.00	2.60	656.49	3.30E+06	2.16E+06	2.70E+09	1.05E+09	3.15E+09	6.83E+05	-5.66E+06	3.92E+03	2.24E+03	5.67	1.36	
0.04	0.95	0.52	1.00	450.00	2.91	0.73	0.81	0.81	0.69	0.81	8.95	4.79	754.60	3.83E+06	2.52E+06	3.26E+09	1.26E+09	3.97E+09	7.34E+05	-4.43E+06	4.07E+03	2.32E+03	7.67	1.37	
0.05	0.98	0.53	1.00	498.13	2.98	0.74	0.83	0.82	0.71	0.82	10.33	7.18	823.10	4.07E+06	2.87E+06	4.02E+09	1.54E+09	4.68E+09	8.06E+05	-3.97E+06	4.24E+03	2.38E+03	8.53	1.38	
0.06	0.99	0.54	1.00	538.24	3.02	0.75	0.84	0.83	0.72	0.85	11.51	9.11	883.10	4.59E+06	3.15E+06	4.90E+09	1.86E+09	5.06E+09	8.60E+05	-3.19E+06	4.40E+03	2.44E+03	10.71	1.38	
0.07	1.00	0.56	1.00	580.53	3.05	0.77	0.87	0.84	0.73	0.86	13.40	11.95	937.44	5.02E+06	3.40E+06	5.77E+09	2.15E+09	5.73E+09	9.14E+05	-2.87E+06	4.56E+03	2.49E+03	13.07	1.38	
0.08	1.01	0.57	1.00	629.25	3.08	0.78	0.88	0.85	0.74	0.87	15.00	14.85	981.79	5.48E+06	3.68E+06	6.76E+09	2.61E+09	6.53E+09	9.75E+05	-2.63E+06	4.66E+03	2.54E+03	14.67	1.37	
0.09	1.02	0.58	1.00	679.15	3.12	0.78	0.89	0.86	0.75	0.88	17.33	16.80	1039.46	5.95E+06	3.97E+06	7.63E+09	2.94E+09	7.14E+09	1.01E+06	-2.38E+06	4.83E+03	2.63E+03	15.67	1.37	
0.10	1.03	0.60	1.00	720.37	3.16	0.79	0.90	0.87	0.75	0.89	18.73	19.07	1113.43	6.15E+06	4.16E+06	8.38E+09	3.34E+09	7.81E+09	1.06E+06	-2.17E+06	4.91E+03	2.67E+03	19.20	1.37	
0.12	1.15	0.71	1.00	1081.13	3.47	0.88	1.01	0.95	0.83	1.00	37.67	36.80	1519.27	8.72E+06	6.56E+06	1.44E+10	7.91E+09	1.20E+10	1.54E+06	-9.04E+05	6.09E+03	3.27E+03	35.47	1.39	
0.30	1.26	0.84	1.00	1409.50	3.78	0.96	1.09	1.04	0.90	1.09	55.67	53.20	1845.43	1.07E+07	8.77E+06	2.20E+10	1.37E+10	1.75E+10	2.26E+06	-4.15E+05	7.21E+03	3.87E+03	54.87	1.40	
0.40	1.35	0.97	1.00	1741.87	4.05	1.04	1.18	1.11	0.98	1.18	74.27	71.33	2109.73	1.31E+07	1.06E+07	3.04E+10	2.08E+10	2.32E+10	3.01E+06	-1.69E+05	8.34E+03	4.52E+03	73.73	1.38	
0.50	1.44	1.11	1.00	2024.17	4.37	1.11	1.29	1.19	1.05	1.26	93.67	88.33	2372.17	1.55E+07	1.26E+07	3.78E+10	2.76E+10	2.92E+10	3.97E+06	-4.86E+03	9.51E+03	5.23E+03	91.50	1.37	
0.60	1.55	1.30	1.00	2285.07	4.69	1.19	1.39	1.28	1.12	1.35	112.33	105.47	2647.60	1.82E+07	1.50E+07	4.64E+10	3.47E+10	3.58E+10	5.10E+06	-1.66E+05	1.10E+04	6.03E+03	111.07	1.38	
0.70	1.67	1.48	1.00	2561.93	5.03	1.29	1.49	1.37	1.22	1.47	128.47	123.43	2916.27	2.17E+07	1.87E+07	6.11E+10	4.62E+10	4.41E+10	7.19E+06	-3.65E+05	1.30E+04	7.01E+03	130.57	1.38	
0.80	1.86	1.81	1.00	2830.07	5.57	1.42	1.64	1.52	1.34	1.66	148.00	141.40	3215.93	2.62E+07	2.38E+07	7.90E+10	5.93E+10	5.50E+10	1.10E+07	-6.83E+05	1.61E+04	8.48E+03	147.00	1.39	
0.90	2.18	2.36	1.00	3111.53	6.40	1.65	1.92	1.73	1.55	1.89	164.00	160.03	3638.50	3.63E+07	3.11E+07	1.14E+11	8.64E+10	7.76E+10	1.93E+07	-1.66E+06	2.20E+04	1.12E+04	161.70	1.41	
1.00	3.81	6.72	1.00	3555.67	11.37	2.76	3.71	2.92	2.65	3.19	178.67	179.00	4432.67	1.21E+08	9.99E+07	4.87E+11	2.90E+11	2.92E+11	1.39E+08	-3.96E+07	7.35E+04	3.22E+04	179.67	1.44	

Figure A6.1 – Filtrasorb 300 C microscope morph measurements

	Percentile	Max diameter	Area	Circularity	Gravity center (Y)	Perimeter	Diagonal width	Fore diameter (Horizontal)	Circle equivalent dia	Min diameter	Fore diameter (Vertical)	Max diameter angle	Min diameter angle	Gravity center (X)	1st moment (X-axis)	1st moment (Y-axis)	2nd moment (X-axis)	2nd moment (Y-axis)	Product of inertia	Gravity 2nd moment (Y-axis)	Gravity product of inertia	2nd moment major axis	2nd moment minor axis	2nd moment angle	Aspect Ratio
0.01	1.12	0.67	0.18	125.25	3.42	0.82	0.89	0.92	0.77	0.91	3.67	0.96	196.73	1.81E+06	1.48E+06	4.48E+08	2.43E+08	1.53E+09	1.52E+06	-5.12E+07	5.68E+03	2.90E+03	1.01	1.46	
0.02	1.18	0.72	0.33	172.56	3.59	0.86	0.95	0.96	0.82	0.99	5.00	2.62	258.32	2.37E+06	2.10E+06	6.37E+08	4.80E+08	1.76E+09	1.88E+06	-2.82E+07	3.18E+03	3.18E+03	2.33	1.45	
0.03	1.22	0.77	0.72	237.58	3.76	0.89	0.99	0.98	0.84	1.01	6.76	6.04	323.90	3.00E+06	2.44E+06	1.09E+09	6.93E+08	2.45E+09	2.08E+06	-2.14E+07	6.81E+03	3.34E+03	3.56	1.46	
0.04	1.26	0.81	1.00	263.29	3.86	0.90	1.02	1.01	0.86	1.04	9.67	7.39	393.04	3.53E+06	2.87E+06	1.37E+09	9.14E+08	2.90E+09	2.42E+06	-1.78E+07	7.19E+03	3.61E+03	5.57	1.46	
0.05	1.29	0.84	1.00	302.42	3.95	0.94	1.04	1.03	0.88	1.06	11.50	9.67	413.42	3.96E+06	3.24E+06	2.05E+09	1.33E+09	3.38E+09	2.54E+06	-1.50E+07	7.56E+03	3.80E+03	7.00	1.47	
0.06	1.32	0.88	1.00	338.20	4.01	0.96	1.07	1.05	0.89	1.09	13.33	10.49	469.65	4.66E+06	3.98E+06	2.48E+09	1.53E+09	3.80E+09	2.74E+06	-1.34E+07	7.93E+03	3.91E+03	9.67	1.48	
0.07	1.34	0.90	1.00	371.97	4.06	0.98	1.09	1.07	0.91	1.11	14.50	12.67	502.13	5.13E+06	4.34E+06	2.86E+09	1.82E+09	4.21E+09	2.84E+06	-1.13E+07	8.16E+03	4.04E+03	11.32	1.48	
0.08	1.36	0.93	1.00	413.21	4.14	1.00	1.12	1.08	0.93	1.13	16.71	14.77	534.48	5.37E+06	4.65E+06	3.30E+09	2.14E+09	4.86E+09	3.16E+06	-1.01E+07	8.59E+03	4.12E+03	12.71	1.47	
0.09	1.38	0.96	1.00	446.75	4.18	1.02	1.15	1.10	0.94	1.14	17.62	15.33	579.13	5.85E+06	4.98E+06	3.70E+09	2.33E+09	5.49E+09	3.35E+06	-8.52E+06	8.83E+03	4.25E+03	14.62	1.47	
0.10	1.41	0.98	1.00	478.30	4.25	1.03	1.17	1.11	0.95	1.17	18.67	17.43	615.80	6.11E+06	5.29E+06	4.08E+09	2.63E+09	6.04E+09	3.53E+06	-7.78E+06	9.18E+03	4.38E+03	15.77	1.48	
0.20	1.57	1.20	1.00	855.87	4.73	1.16	1.32	1.23	1.07	1.34	33.60	35.33	1100.07	1.18E+07	9.71E+06	1.38E+10	9.35E+09	1.28E+10	5.39E+06	-3.20E+06	1.16E+04	5.51E+03	35.20	1.47	
0.30	1.72	1.43	1.00	1234.63	5.20	1.25	1.47	1.34	1.17	1.47	53.00	53.33	1526.77	1.76E+07	1.31E+07	2.88E+10	1.79E+10	2.05E+10	8.25E+06	-1.56E+06	1.40E+04	6.60E+03	51.07	1.48	
0.40	1.86	1.65	1.00	1558.60	5.57	1.38	1.60	1.44	1.26	1.58	69.87	73.33	1908.80	2.24E+07	1.70E+07	4.63E+10	2.63E+10	3.16E+10	1.05E+07	-6.16E+05	1.60E+04	7.79E+03	68.27	1.48	
0.50	2.01	1.97	1.00	1824.83	6.09	1.49	1.75	1.58	1.35	1.72	86.33	89.17	2283.83	2.73E+07	2.07E+07	6.73E+10	3.85E+10	4.21E+10	1.38E+07	-4.79E+04	1.89E+04	9.13E+03	86.50	1.50	
0.60	2.20	2.26	1.00	2123.47	6.50	1.60	1.90	1.69	1.48	1.85	107.07	104.47	2633.40	3.40E+07	2.55E+07	9.07E+10	5.61E+10	5.67E+10	1.98E+07	-7.09E+05	2.30E+04	1.05E+04	106.80	1.49	
0.70	2.41	2.73	1.00	2443.37	7.19	1.75	2.07	1.85	1.60	2.03	127.43	124.60	3091.07	4.43E+07	3.07E+07	1.37E+11	7.41E+10	7.35E+10	2.87E+07	-1.90E+06	2.75E+04	1.25E+04	125.33	1.51	
0.80	2.68	3.25	1.00	2737.73	7.88	1.94	2.36	2.02	1.76	2.26	146.33	139.87	3546.13	5.74E+07	4.08E+07	1.83E+11	9.80E+10	1.02E+11	4.09E+07	-4.35E+06	3.41E+04	1.49E+04	143.00	1.53	
0.90	3.11	4.43	1.00	3115.70	9.36	2.24	2.74	2.37	2.05	2.63	163.73	161.53	3974.97	7.35E+07	5.91E+07	2.52E+11	1.54E+11	1.50E+11	6.74E+07	-1.20E+07	4.61E+04	1.97E+04	163.87	1.52	
1.00	4.90	9.21	1.00	3521.00	13.73	3.21	4.64	3.42	2.91	4.39	179.00	178.33	4635.00	1.92E+08	1.52E+08	8.05E+11	4.81E+11	4.99E+11	3.72E+08	-1.55E+08	1.20E+05	4.10E+04	180.00	1.68	

Figure A6.2 – Aquasorb KGA microscope morph measurements

	Percentile	Max diameter	Area	Circularity	Gravity center (Y)	Perimeter	Diagonal width	Fore diameter (Horizontal)	Circle equivalent dia	Min diameter	Fore diameter (Vertical)	Max diameter angle	Min diameter angle	Gravity center (X)	1st moment (X-axis)	1st moment (Y-axis)	2nd moment (X-axis)	2nd moment (Y-axis)	Product of inertia	Gravity 2nd moment (Y-axis)	Gravity product of inertia	2nd moment major axis	2nd moment minor axis	2nd moment angle	Aspect Ratio
0.01	0.40	0.12	1.00	117.60	1.29	0.37	0.39	0.38	0.35	0.38	6.00	0.00	175.16	2.05E+05	1.11E+05	4.01E+07	1.74E+07	1.02E+08	4.61E+04	-8.96E+03	8.16E+02	6.67E+02	2.14	1.14	
0.02	0.42	0.12	1.00	194.04	1.33	0.38	0.40	0.40	0.37	0.40	8.00	0.00	262.01	2.80E+05	1.88E+05	1.00E+08	4.39E+07	1.57E+08	5.21E+04	-5.94E+03	8.64E+02	7.31E+02	4.33	1.12	
0.03	0.42	0.13	1.00	230.84	1.36	0.39	0.41	0.40	0.38	0.41	10.08	0.00	299.74	3.15E+05	2.43E+05	1.27E+08	6.55E+07	2.01E+08	5.66E+04	-4.85E+03					

	Perceivable	Max diameter	Area	Circularity	Gravity center (Y)	Perimeter	Diagonal width	Foret diameter (Horizontal)	Circle equivalent dia	Min diameter	Foret diameter (Vertical)	Max diameter angle	Min diameter angle	Gravity center (X)	1st moment (X-axis)	1st moment (Y-axis)	2nd moment (X-axis)	2nd moment (Y-axis)	Product of inertia	Gravity 2nd moment (Y-axis)	Gravity product of inertia	2nd moment major axis	2nd moment minor axis	Aspect Ratio
0.01	1.26	0.78	0.00	69.86	3.88	0.76	0.85	0.99	0.70	0.84	3.03	1.23	154.48	1.83E-03	5.90E-04	3.05E-04	5.12E-05	4.34E-04	1.88E-06	-5.32E-05	7.40E-09	2.58E-09	2.26	1.80
0.02	1.34	0.90	0.00	94.27	4.11	0.83	0.89	1.07	0.75	0.89	4.89	3.15	312.32	2.87E-03	8.69E-04	9.73E-04	1.13E-04	1.04E-03	2.39E-06	-4.25E-05	8.90E-09	3.17E-09	4.00	1.77
0.03	1.39	0.95	0.00	123.53	4.24	0.85	0.91	1.10	0.77	0.92	6.30	4.00	432.98	3.97E-03	1.26E-03	2.00E-03	1.91E-04	1.30E-03	2.78E-06	-3.42E-05	9.80E-09	3.44E-09	5.59	1.79
0.04	1.45	1.01	0.00	150.63	4.36	0.86	0.94	1.14	0.78	0.94	7.71	5.41	490.04	5.31E-03	1.55E-03	3.58E-03	3.05E-04	1.79E-03	2.99E-06	-3.10E-05	1.06E-08	3.57E-09	7.33	1.85
0.05	1.48	1.04	0.00	192.23	4.43	0.88	0.96	1.15	0.79	0.96	9.00	7.83	568.33	6.24E-03	2.07E-03	4.10E-03	4.50E-04	2.49E-03	3.16E-06	-2.79E-05	1.15E-08	3.68E-09	8.97	1.87
0.06	1.53	1.07	0.00	219.40	4.57	0.88	0.99	1.17	0.80	0.98	9.84	8.84	649.75	6.72E-03	2.47E-03	4.95E-03	5.89E-04	3.18E-03	3.33E-06	-2.52E-05	1.21E-08	3.74E-09	9.73	1.91
0.07	1.57	1.11	0.00	262.12	4.64	0.89	1.00	1.19	0.80	1.00	12.30	10.15	741.05	7.28E-03	2.90E-03	5.65E-03	8.09E-04	3.94E-03	3.50E-06	-2.37E-05	1.27E-08	3.80E-09	11.19	1.95
0.08	1.59	1.15	0.00	309.27	4.68	0.90	1.02	1.21	0.81	1.02	13.75	11.67	802.83	7.88E-03	3.41E-03	6.85E-03	1.15E-03	4.65E-03	3.65E-06	-2.16E-05	1.36E-08	3.85E-09	13.13	1.97
0.09	1.61	1.16	0.00	337.05	4.75	0.90	1.04	1.22	0.82	1.03	15.33	12.77	863.61	8.49E-03	3.83E-03	7.65E-03	1.35E-03	5.30E-03	3.82E-06	-2.01E-05	1.40E-08	3.90E-09	15.23	1.97
0.10	1.64	1.19	0.00	354.20	4.85	0.91	1.06	1.23	0.82	1.05	16.93	14.33	949.33	9.07E-03	3.98E-03	8.81E-03	1.55E-03	5.71E-03	3.91E-06	-1.88E-05	1.45E-08	3.94E-09	17.60	2.00
0.20	1.83	1.38	0.67	723.00	5.24	0.97	1.25	1.32	0.84	1.26	36.20	35.00	1310.27	1.45E-02	8.02E-03	1.96E-02	6.03E-03	1.23E-02	5.53E-06	-9.29E-06	1.88E-08	4.22E-09	36.73	2.17
0.30	2.01	1.53	0.67	1048.27	5.67	1.02	1.45	1.39	0.86	1.44	56.20	51.53	1649.40	1.85E-02	1.15E-02	3.14E-02	1.21E-02	1.90E-02	7.42E-06	-5.28E-06	2.27E-08	4.39E-09	57.80	2.33
0.40	2.16	1.67	0.67	1343.87	6.00	1.07	1.62	1.46	0.87	1.61	75.93	68.00	1965.27	2.24E-02	1.48E-02	4.47E-02	2.02E-02	2.63E-02	9.75E-06	-2.20E-06	2.71E-08	4.52E-09	75.67	2.47
0.50	2.32	1.78	1.00	1633.67	6.35	1.12	1.78	1.51	0.89	1.79	92.33	85.67	2276.00	2.60E-02	1.85E-02	6.23E-02	3.18E-02	3.75E-02	1.35E-05	-3.88E-07	3.14E-08	4.66E-09	93.00	2.61
0.60	2.45	1.94	1.00	1905.00	6.72	1.17	1.95	1.57	0.90	1.98	109.33	101.13	2597.07	3.01E-02	2.23E-02	7.74E-02	4.25E-02	4.93E-02	1.86E-05	-1.57E-06	3.61E-08	4.79E-09	109.00	2.74
0.70	2.67	2.12	1.00	2194.60	7.17	1.22	2.16	1.64	0.91	2.18	126.33	122.33	2901.93	3.43E-02	2.66E-02	9.94E-02	5.81E-02	6.05E-02	2.54E-05	-4.28E-06	4.16E-08	4.90E-09	128.53	2.90
0.80	2.88	2.32	1.00	2573.13	7.64	1.27	2.40	1.72	0.93	2.43	144.13	143.47	3237.80	3.95E-02	3.16E-02	1.23E-01	8.17E-02	7.65E-02	3.56E-05	-7.97E-06	5.01E-08	5.05E-09	145.00	3.09
0.90	3.15	2.60	1.00	3073.13	8.18	1.35	2.71	1.82	0.97	2.75	162.00	161.13	3580.60	4.69E-02	3.94E-02	1.58E-01	1.13E-01	1.06E-01	5.54E-05	-1.64E-05	6.04E-08	5.31E-09	163.33	3.26
1.00	4.74	4.99	1.67	3542.00	13.77	2.48	4.65	2.51	2.17	4.14	178.67	179.00	4564.33	8.75E-02	7.92E-02	3.27E-01	2.52E-01	2.51E-01	1.99E-04	1.00E-04	1.44E-07	2.38E-08	179.00	2.19

Figure A6.4 - ROW o.8 Supra microscope morph measurements

	Perceivable	Max diameter	Area	Circularity	Gravity center (Y)	Perimeter	Diagonal width	Foret diameter (Horizontal)	Circle equivalent dia	Min diameter	Foret diameter (Vertical)	Max diameter angle	Min diameter angle	Gravity center (X)	1st moment (X-axis)	1st moment (Y-axis)	2nd moment (X-axis)	2nd moment (Y-axis)	Product of inertia	Gravity 2nd moment (Y-axis)	Gravity product of inertia	2nd moment major axis	2nd moment minor axis	Aspect Ratio
0.01	3.51	14.98	0.78	313.99	15.68	4.08	4.11	4.35	3.66	3.87	5.39	7.90	727.09	1.18E+08	5.30E+07	9.27E+10	2.12E+10	8.90E+10	7.27E+08	-5.24E+09	1.16E+05	7.69E+04	3.56	0.96
0.02	3.74	15.97	0.89	335.31	16.36	4.11	4.15	4.49	3.70	3.91	6.44	13.14	752.85	1.21E+08	5.52E+07	1.00E+11	2.48E+10	1.04E+11	8.14E+08	-4.42E+09	1.31E+05	7.84E+04	4.45	1.01
0.03	3.90	16.69	1.00	368.75	16.94	4.14	4.21	4.59	3.73	3.95	7.32	17.31	777.45	1.24E+08	5.82E+07	1.07E+11	2.95E+10	1.18E+11	8.76E+08	-3.84E+09	1.41E+05	8.00E+04	5.63	1.05
0.04	3.93	16.88	1.00	417.00	17.35	4.16	4.29	4.61	3.74	3.97	7.76	18.33	794.11	1.32E+08	6.62E+07	1.14E+11	3.59E+10	1.25E+11	8.89E+08	-3.62E+09	1.44E+05	8.11E+04	7.39	1.05
0.05	3.95	17.06	1.00	465.08	17.77	4.17	4.38	4.64	3.75	3.99	8.20	19.33	810.63	1.39E+08	7.43E+07	1.22E+11	4.22E+10	1.33E+11	9.02E+08	-3.39E+09	1.46E+05	8.22E+04	9.15	1.05
0.06	3.98	17.62	1.00	487.85	18.07	4.21	4.45	4.72	3.76	4.01	9.53	20.55	843.25	1.45E+08	7.94E+07	1.29E+11	4.71E+10	1.37E+11	9.24E+08	-3.24E+09	1.53E+05	8.36E+04	10.57	1.06
0.07	4.01	18.21	1.00	505.50	18.18	4.24	4.53	4.80	3.77	4.03	10.59	22.03	870.02	1.47E+08	8.10E+07	1.40E+11	4.99E+10	1.47E+11	9.42E+08	-2.96E+09	1.61E+05	8.46E+04	11.74	1.06
0.08	4.04	18.69	1.00	537.88	18.34	4.28	4.62	4.86	3.78	4.06	11.49	23.44	895.60	1.48E+08	8.35E+07	1.51E+11	5.20E+10	1.56E+11	9.60E+08	-2.66E+09	1.67E+05	8.55E+04	12.89	1.07
0.09	4.11	19.07	1.00	582.57	18.62	4.32	4.74	4.91	3.79	4.09	12.04	25.34	923.68	1.50E+08	8.77E+07	1.61E+11	5.31E+10	1.70E+11	9.76E+08	-2.30E+09	1.74E+05	8.60E+04	14.16	1.09
0.10	4.19	19.38	1.00	629.77	18.98	4.36	4.83	4.95	3.79	4.12	12.67	27.00	959.37	1.56E+08	9.13E+07	1.64E+11	5.38E+10	1.80E+11	1.00E+09	-2.15E+09	1.80E+05	8.65E+04	15.83	1.11
0.20	4.57	21.70	1.00	886.20	20.43	4.79	5.55	5.25	3.80	4.54	22.67	52.33	1322.47	2.41E+08	1.59E+08	3.49E+11	1.40E+11	2.95E+11	1.28E+09	-1.22E+09	2.31E+05	8.84E+04	37.33	1.20
0.30	4.88	24.11	1.00	1223.97	21.76	5.07	6.17	5.54	3.83	4.98	37.60	67.40	1750.50	2.98E+08	1.88E+08	5.46E+11	2.54E+11	4.32E+11	1.52E+09	-3.37E+08	2.76E+05	8.99E+04	46.23	1.27
0.40	5.31	26.06	1.00	1468.87	22.67	5.24	6.56	5.76	3.85	5.53	60.00	73.27	2146.33	3.33E+08	2.46E+08	6.68E+11	3.88E+11	5.26E+11	1.85E+09	-6.96E+07	3.26E+05	9.10E+04	72.47	1.38
0.50	5.53	27.40	1.00	1807.33	23.33	5.36	7.08	5.90	3.86	6.18	83.83	91.00	2530.00	4.11E+08	2.96E+08	1.14E+12	5.49E+11	6.45E+11	2.17E+09	-1.13E+08	3.53E+05	9.18E+04	84.50	1.43
0.60	5.83	29.07	1.00	2074.73	24.16	5.47	7.49	6.08	3.88	6.62	102.73	99.67	2862.00	4.71E+08	3.88E+08	1.43E+12	7.44E+11	7.24E+11	2.55E+09	-2.70E+08	4.05E+05	9.27E+04	110.93	1.50
0.70	6.19	30.97	1.00	2388.63	25.28	5.56	8.18	6.28	3.91	7.07	141.13	113.43	3154.47	5.59E+08	4.23E+08	1.64E+12	1.10E+12	9.04E+11	3.22E+09	-6.33E+08	4.65E+05	9.33E+04	139.97	1.58
0.80	6.55	32.70	1.00	2671.00	26.14	5.67	8.54	6.43	3.94	7.45	151.13	127.20	3535.80	6.27E+08	4.74E+08	1.96E+12	1.29E+12	1.13E+12	4.00E+09	-1.19E+09	5.22E+05	9.42E+04	151.93	1.66
0.90	6.98	34.75	1.00	2975.83	27.72	5.82	9.29	6.65	3.99	8.66	166.70	147.70	3805.40	7.30E+08	5.58E+08	2.73E+12	1.61E+12	1.51E+12	6.81E+09	-2.13E+09	5.93E+05	9.54E+04	165.33	1.75
1.00	7.59	38.60	1.00	3290.33	30.29	6.01	10.71	7.01	4.17	10.30	177.67	173.00	4169.33	8.60E+08	6.49E+08	3.38E+12	1.98E+12	2.22E+12	1.16E+10	4.53E+09	7.39E+05	9.91E+04	179.00	1.82

Figure A6.5 - RB4C microscope morph measurements

	Perceivable	Max diameter	Area	Circularity	Gravity center (Y)	Perimeter	Diagonal width	Foret diameter (Horizontal)	Circle equivalent dia	Min diameter	Foret diameter (Vertical)	Max diameter angle	Min diameter angle	Gravity center (X)	1st moment (X-axis)	1st moment (Y-axis)	2nd moment (X-axis)	2nd moment (Y-axis)	Product of inertia	Gravity 2nd moment (Y-axis)	Gravity product of inertia	2nd moment major axis	2nd moment minor axis	Aspect Ratio
0.01	1.04	0.54	0.58	92.94	3.19	0.71	0.78	0.83	0.65	0.80	2.55	0.79	184.81	1.46E+06	9.14E+05	3.91E+08	1.24E+08	7.50E+08	9.48E+05	-2.44E+07	1.97E+03	1.91	1.59	
0.02	1.07	0.59	1.00	179.43	3.26	0.75	0.85	0.86	0.71	0.85	4.67	2.20	257.96	2.04E+06	1.37E+06	6.56E+08	3.27E+08	1.47E+09	1.17E+06	-1.59E+07	5.40E+03	2.43E+03	3.33	1.50
0.03	1.09	0.61	1.00	235.77	3.37	0.79	0.90	0.88	0.75	0.90	6.32	4.79	311.15	2.54E+06	1.72E+06	8.77E+08	4.71E+08	1.95E+09	1.31E+06	-1.27E+07	5.70E+03	2.71E+03	5.93	1.46
0.04	1.13	0.63	1.00	275.43																				

	Percentile	Max diameter	Area	Circularity	Gravity center (Y)	Perimeter	Diagonal width	Fore diameter (Horizontal)	Circle equivalent dia	Min diameter	Fore diameter (Vertical)	Max diameter angle	Min diameter angle	Gravity center (X)	1st moment (X-axis)	1st moment (Y-axis)	2nd moment (X-axis)	2nd moment (Y-axis)	Product of inertia	Gravity 2nd moment (Y-axis)	Gravity product of inertia	2nd moment major axis	2nd moment minor axis	Aspect Ratio
0.01	0.91	0.46	0.33	168.13	2.89	0.67	0.80	0.77	0.64	0.76	2.18	0.17	218.00	1.89E+06	1.48E+06	5.87E+08	3.34E+08	1.39E+09	6.83E+05	-1.86E+07	4.03E+03	2.06E+03	2.74	1.42
0.02	1.01	0.53	1.00	235.33	3.12	0.71	0.84	0.82	0.67	0.81	4.00	2.67	297.71	2.63E+06	1.94E+06	9.97E+08	6.32E+08	2.11E+09	8.80E+05	-1.30E+07	4.84E+03	2.15E+03	4.03	1.51
0.03	1.05	0.59	1.00	313.30	3.24	0.74	0.87	0.86	0.69	0.86	5.33	5.18	366.06	3.19E+06	2.41E+06	1.48E+09	8.86E+08	2.49E+09	1.14E+06	-1.04E+07	5.08E+03	2.36E+03	5.74	1.51
0.04	1.07	0.61	1.00	344.75	3.34	0.78	0.91	0.88	0.73	0.91	6.48	6.68	424.31	3.79E+06	3.16E+06	2.18E+09	1.22E+09	2.94E+09	1.39E+06	-9.35E+06	5.43E+03	2.57E+03	7.81	1.46
0.05	1.09	0.65	1.00	392.08	3.42	0.81	0.93	0.91	0.76	0.94	7.78	8.27	479.40	4.54E+06	3.62E+06	2.71E+09	1.70E+09	3.52E+09	1.53E+06	-7.67E+06	5.64E+03	2.79E+03	9.00	1.42
0.06	1.11	0.68	1.00	458.26	3.48	0.83	0.95	0.93	0.78	0.96	9.72	10.43	571.46	4.98E+06	3.94E+06	3.51E+09	2.05E+09	3.85E+09	1.69E+06	-7.21E+06	5.89E+03	3.01E+03	10.43	1.42
0.07	1.15	0.71	1.00	500.24	3.52	0.84	0.97	0.95	0.81	0.98	11.23	14.81	601.24	5.20E+06	4.47E+06	4.13E+09	2.33E+09	4.33E+09	1.85E+06	-6.61E+06	6.29E+03	3.12E+03	12.01	1.42
0.08	1.17	0.73	1.00	540.33	3.58	0.85	0.99	0.96	0.83	1.01	13.13	16.72	646.12	5.65E+06	4.94E+06	5.11E+09	2.79E+09	5.01E+09	2.00E+06	-5.76E+06	6.67E+03	3.29E+03	13.33	1.41
0.09	1.19	0.75	1.00	563.62	3.68	0.86	1.00	0.97	0.84	1.02	15.12	19.58	695.66	6.02E+06	5.19E+06	5.79E+09	3.38E+09	5.65E+09	2.08E+06	-5.15E+06	6.85E+03	3.38E+03	15.33	1.43
0.10	1.22	0.78	1.00	604.40	3.76	0.88	1.01	0.99	0.84	1.04	16.80	21.50	760.27	6.48E+06	5.57E+06	6.43E+09	3.92E+09	6.66E+09	2.28E+06	-4.56E+06	7.20E+03	3.49E+03	17.00	1.44
0.20	1.41	1.01	1.00	933.33	4.27	1.01	1.16	1.13	0.95	1.19	32.40	40.73	1207.13	9.65E+06	8.65E+06	1.38E+10	9.18E+09	1.25E+10	3.87E+06	-2.00E+06	9.55E+03	4.51E+03	34.00	1.48
0.30	1.53	1.20	1.00	1225.07	4.68	1.10	1.30	1.23	1.04	1.30	50.57	59.73	1555.93	1.34E+07	1.13E+07	2.16E+10	1.52E+10	1.92E+10	5.44E+06	-8.35E+05	1.12E+04	5.42E+03	52.33	1.47
0.40	1.65	1.37	1.00	1486.47	5.02	1.21	1.44	1.31	1.14	1.41	70.20	75.87	1860.13	1.67E+07	1.38E+07	3.16E+10	2.21E+10	2.50E+10	7.06E+06	-3.31E+05	1.31E+04	6.45E+03	69.67	1.45
0.50	1.75	1.58	1.00	1724.67	5.34	1.30	1.54	1.41	1.22	1.49	85.67	91.83	2150.83	2.06E+07	1.63E+07	4.27E+10	3.08E+10	3.19E+10	9.07E+06	3.59E+04	1.49E+04	7.41E+03	87.67	1.44
0.60	1.87	1.79	1.00	2019.07	5.74	1.40	1.65	1.50	1.31	1.62	106.53	110.20	2432.27	2.48E+07	1.98E+07	5.82E+10	3.87E+10	4.14E+10	1.14E+07	5.85E+05	1.69E+04	8.44E+03	106.60	1.43
0.70	2.03	2.05	1.00	2290.07	6.13	1.49	1.77	1.61	1.40	1.72	124.63	128.33	2713.10	2.98E+07	2.35E+07	7.71E+10	4.92E+10	5.22E+10	1.52E+07	1.29E+06	1.99E+04	9.83E+03	126.00	1.45
0.80	2.19	2.39	1.00	2581.80	6.68	1.64	1.94	1.73	1.50	1.92	143.87	143.93	3119.33	3.74E+07	2.85E+07	1.10E+11	6.63E+10	6.78E+10	2.25E+07	2.49E+06	2.32E+04	1.14E+04	145.67	1.46
0.90	2.51	2.96	1.00	2916.87	7.42	1.82	2.20	1.93	1.70	2.17	162.47	161.63	3674.73	5.14E+07	3.68E+07	1.74E+11	9.18E+10	9.34E+10	3.59E+07	5.37E+06	3.05E+04	1.45E+04	162.67	1.47
1.00	3.77	6.85	1.00	3519.33	11.46	2.94	3.67	2.95	2.66	3.35	179.00	178.67	4635.33	1.47E+08	1.14E+08	5.60E+11	3.62E+11	3.58E+11	1.78E+08	6.19E+07	7.13E+04	3.68E+04	179.67	1.42

Figure A6.7 - Aquasorb K-6300 microscope morph measurements

	Percentile	Max diameter	Area	Circularity	Gravity center (Y)	Perimeter	Diagonal width	Fore diameter (Horizontal)	Circle equivalent dia	Min diameter	Fore diameter (Vertical)	Max diameter angle	Min diameter angle	Gravity center (X)	1st moment (X-axis)	1st moment (Y-axis)	2nd moment (X-axis)	2nd moment (Y-axis)	Product of inertia	Gravity 2nd moment (Y-axis)	Gravity product of inertia	2nd moment major axis	2nd moment minor axis	Aspect Ratio
0.01	0.91	0.46	0.33	168.13	2.89	0.67	0.80	0.77	0.64	0.76	2.18	0.17	218.00	1.89E+06	1.48E+06	5.87E+08	3.34E+08	1.39E+09	6.83E+05	-1.86E+07	4.03E+03	2.06E+03	2.74	1.42
0.02	1.01	0.53	1.00	235.33	3.12	0.71	0.84	0.82	0.67	0.81	4.00	2.67	297.71	2.63E+06	1.94E+06	9.97E+08	6.32E+08	2.11E+09	8.80E+05	-1.30E+07	4.84E+03	2.15E+03	4.03	1.51
0.03	1.05	0.59	1.00	313.30	3.24	0.74	0.87	0.86	0.69	0.86	5.33	5.18	366.06	3.19E+06	2.41E+06	1.48E+09	8.86E+08	2.49E+09	1.14E+06	-1.04E+07	5.08E+03	2.36E+03	5.74	1.51
0.04	1.07	0.61	1.00	344.75	3.34	0.78	0.91	0.88	0.73	0.91	6.48	6.68	424.31	3.79E+06	3.16E+06	2.18E+09	1.22E+09	2.94E+09	1.39E+06	-9.35E+06	5.43E+03	2.57E+03	7.81	1.46
0.05	1.09	0.65	1.00	392.08	3.42	0.81	0.93	0.91	0.76	0.94	7.78	8.27	479.40	4.54E+06	3.62E+06	2.71E+09	1.70E+09	3.52E+09	1.53E+06	-7.67E+06	5.64E+03	2.79E+03	9.00	1.42
0.06	1.11	0.68	1.00	458.26	3.48	0.83	0.95	0.93	0.78	0.96	9.72	10.43	571.46	4.98E+06	3.94E+06	3.51E+09	2.05E+09	3.85E+09	1.69E+06	-7.21E+06	5.89E+03	3.01E+03	10.43	1.42
0.07	1.15	0.71	1.00	500.24	3.52	0.84	0.97	0.95	0.81	0.98	11.23	14.81	601.24	5.20E+06	4.47E+06	4.13E+09	2.33E+09	4.33E+09	1.85E+06	-6.61E+06	6.29E+03	3.12E+03	12.01	1.42
0.08	1.17	0.73	1.00	540.33	3.58	0.85	0.99	0.96	0.83	1.01	13.13	16.72	646.12	5.65E+06	4.94E+06	5.11E+09	2.79E+09	5.01E+09	2.00E+06	-5.76E+06	6.67E+03	3.29E+03	13.33	1.41
0.09	1.19	0.75	1.00	563.62	3.68	0.86	1.00	0.97	0.84	1.02	15.12	19.58	695.66	6.02E+06	5.19E+06	5.79E+09	3.38E+09	5.65E+09	2.08E+06	-5.15E+06	6.85E+03	3.38E+03	15.33	1.43
0.10	1.22	0.78	1.00	604.40	3.76	0.88	1.01	0.99	0.84	1.04	16.80	21.50	760.27	6.48E+06	5.57E+06	6.43E+09	3.92E+09	6.66E+09	2.28E+06	-4.56E+06	7.20E+03	3.49E+03	17.00	1.44
0.20	1.41	1.01	1.00	933.33	4.27	1.01	1.16	1.13	0.95	1.19	32.40	40.73	1207.13	9.65E+06	8.65E+06	1.38E+10	9.18E+09	1.25E+10	3.87E+06	-2.00E+06	9.55E+03	4.51E+03	34.00	1.48
0.30	1.53	1.20	1.00	1225.07	4.68	1.10	1.30	1.23	1.04	1.30	50.57	59.73	1555.93	1.34E+07	1.13E+07	2.16E+10	1.52E+10	1.92E+10	5.44E+06	-8.35E+05	1.12E+04	5.42E+03	52.33	1.47
0.40	1.65	1.37	1.00	1486.47	5.02	1.21	1.44	1.31	1.14	1.41	70.20	75.87	1860.13	1.67E+07	1.38E+07	3.16E+10	2.21E+10	2.50E+10	7.06E+06	-3.31E+05	1.31E+04	6.45E+03	69.67	1.45
0.50	1.75	1.58	1.00	1724.67	5.34	1.30	1.54	1.41	1.22	1.49	85.67	91.83	2150.83	2.06E+07	1.63E+07	4.27E+10	3.08E+10	3.19E+10	9.07E+06	3.59E+04	1.49E+04	7.41E+03	87.67	1.44
0.60	1.87	1.79	1.00	2019.07	5.74	1.40	1.65	1.50	1.31	1.62	106.53	110.20	2432.27	2.48E+07	1.98E+07	5.82E+10	3.87E+10	4.14E+10	1.14E+07	5.85E+05	1.69E+04	8.44E+03	106.60	1.43
0.70	2.03	2.05	1.00	2290.07	6.13	1.49	1.77	1.61	1.40	1.72	124.63	128.33	2713.10	2.98E+07	2.35E+07	7.71E+10	4.92E+10	5.22E+10	1.52E+07	1.29E+06	1.99E+04	9.83E+03	126.00	1.45
0.80	2.19	2.39	1.00	2581.80	6.68	1.64	1.94	1.73	1.50	1.92	143.87	143.93	3119.33	3.74E+07	2.85E+07	1.10E+11	6.63E+10	6.78E+10	2.25E+07	2.49E+06	2.32E+04	1.14E+04	145.67	1.46
0.90	2.51	2.96	1.00	2916.87	7.42	1.82	2.20	1.93	1.70	2.17	162.47	161.63	3674.73	5.14E+07	3.68E+07	1.74E+11	9.18E+10	9.34E+10	3.59E+07	5.37E+06	3.05E+04	1.45E+04	162.67	1.47
1.00	3.77	6.85	1.00	3519.33	11.46	2.94	3.67	2.95	2.66	3.35	179.00	178.67	4635.33	1.47E+08	1.14E+08	5.60E+11	3.62E+11	3.58E+11	1.78E+08	6.19E+07	7.13E+04	3.68E+04	179.67	1.42

Figure A6.8 - Resorb HC microscope morph measurements

	Percentile	Max diameter	Area	Circularity	Gravity center (Y)	Perimeter	Diagonal width	Fore diameter (Horizontal)	Circle equivalent dia	Min diameter	Fore diameter (Vertical)	Max diameter angle	Min diameter angle	Gravity center (X)	1st moment (X-axis)	1st moment (Y-axis)	2nd moment (X-axis)	2nd moment (Y-axis)	Product of inertia	Gravity 2nd moment (Y-axis)	Gravity product of inertia	2nd moment major axis	2nd moment minor axis	Aspect Ratio
0.01	1.13	0.68	0.20	113.21	3.54	0.83	0.92	0.92	0.77	0.93	2.12	1.00	393.29	3.58E+06	1.24E+06	1.91E+09	1.68E+08	2.00E+09	2.00E+06	-4.60E+07	6.06E+03	2.98E+03	1.90	1.46
0.02	1.21	0.80	0.25	159.25	3.73	0.89	1.01	1.00	0.81	0.96	4.95	2.09	464.10	4.57E+06	2.00E+06	2.66E+09	3.62E+08	2.55E+09	2.42E+06	-3.69E+07	6.93E+03	3.41E+03	4.57	1.49
0.03	1.25	0.85	1.00	203.44	3.91	0.91	1.06	1.04	0.87	1.01	6.41	3.52	497.66	5.40E+06	2.54E+06	3.52E+09	8.45E+08	3.15E+09	2.68E+06	-2.97E+07	7.67E+03	3.71E+03	6.48	1.45
0.04	1.29	0.89	1.00	233.29	3.97	0.94	1.09	1.																

ImageJ morph measurements

	Perceivable	Area	Mean	X	Y	MM	WM	Perim	BK	BT	Width	Height	Major	Minor	Angle	Circ	Feret	lObbn	SArea	RawlRatio	FeretX	FeretY	FeretAngle	MinFeret	RR	Round	Solidity	Circ Equiv. diam
FILTRASORB 300 C	0.01	0.78	253.32	26.85	27.18	26.85	27.18	4.64	25.76	26.21	0.95	0.99	1.10	0.78	2.51	0.55	1.18	198.74	99.34	1774351.20	25.76	27.71	5.47	0.84	1.04	0.43	0.91	1.00
	0.02	0.86	253.81	28.45	38.74	28.45	38.74	3.73	27.75	37.95	1.06	1.06	1.21	0.83	5.12	0.58	1.26	220.48	99.53	1968467.40	28.05	39.26	6.59	0.89	1.05	0.45	0.91	1.05
	0.03	0.92	253.91	31.17	43.34	31.17	43.34	3.91	30.30	42.19	1.10	1.08	1.24	0.89	6.49	0.62	1.33	233.63	99.57	2085838.80	30.52	42.93	7.50	0.93	1.08	0.48	0.92	1.08
	0.04	0.97	254.18	33.34	44.58	33.34	44.58	4.04	32.60	43.39	1.13	1.12	1.25	0.92	8.95	0.63	1.35	248.40	99.68	2217694.20	32.92	44.96	8.53	0.95	1.10	0.51	0.93	1.11
	0.05	1.05	254.26	38.35	46.34	38.35	46.34	4.09	37.34	45.50	1.16	1.16	1.28	0.96	11.57	0.63	1.37	267.75	99.71	2390472.00	37.50	46.34	9.63	0.99	1.10	0.52	0.93	1.16
	0.06	1.08	254.30	39.15	47.68	39.14	47.68	4.20	38.21	46.60	1.19	1.20	1.35	1.02	12.45	0.64	1.39	275.59	99.73	2460444.00	38.49	47.36	11.10	1.05	1.12	0.53	0.93	1.17
	0.07	1.10	254.37	40.53	49.60	40.53	49.60	4.26	39.70	48.58	1.22	1.21	1.37	1.03	15.12	0.64	1.42	279.78	99.75	2497898.40	39.70	49.75	13.38	1.06	1.13	0.54	0.93	1.18
	0.08	1.13	254.42	43.64	50.69	43.64	50.69	4.34	43.06	49.73	1.25	1.23	1.39	1.04	16.10	0.66	1.45	288.32	99.77	2574112.80	43.14	50.74	14.33	1.07	1.13	0.55	0.94	1.20
	0.09	1.17	254.47	45.42	52.53	45.42	52.53	4.40	44.40	51.74	1.28	1.26	1.41	1.07	16.80	0.66	1.47	299.10	99.79	2670370.20	44.57	52.01	16.45	1.09	1.13	0.56	0.94	1.22
	0.10	1.20	254.50	47.63	54.12	47.63	54.12	4.46	46.60	53.16	1.32	1.27	1.42	1.08	18.67	0.67	1.52	306.03	99.80	2732274.00	46.61	53.77	18.90	1.10	1.14	0.57	0.94	1.24
	0.20	1.62	254.76	61.05	72.85	61.05	72.85	5.16	59.72	71.87	1.51	1.45	1.62	1.20	35.28	0.70	1.69	412.30	99.91	3680976.00	59.80	73.58	37.08	1.23	1.19	0.63	0.95	1.43
	0.30	1.91	254.87	75.06	100.96	75.06	100.96	5.67	74.01	100.21	1.64	1.61	1.82	1.30	52.18	0.73	1.92	487.44	99.95	4351830.00	74.24	100.94	55.90	1.35	1.25	0.68	0.95	1.56
	0.40	2.25	254.94	87.65	139.34	87.65	139.34	6.19	86.71	138.06	1.79	1.74	1.98	1.42	74.81	0.74	2.08	574.62	99.98	5130243.00	87.23	138.32	73.13	1.45	1.29	0.71	0.96	1.69
	0.50	2.59	254.98	104.59	174.10	104.59	174.10	6.61	103.74	172.46	1.91	1.89	2.14	1.52	94.03	0.76	2.24	660.58	99.99	5897640.00	104.08	175.02	96.67	1.57	1.34	0.75	0.96	1.82
	0.60	2.93	255.02	120.78	203.28	120.78	203.28	7.06	119.49	202.51	2.07	2.04	2.29	1.68	109.86	0.77	2.39	745.83	100.00	6658764.00	119.74	203.30	114.21	1.73	1.41	0.77	0.96	1.93
	0.70	3.42	255.00	137.61	225.21	137.61	225.21	7.61	136.74	224.65	2.22	2.25	2.42	1.78	132.41	0.78	2.58	871.19	100.00	7778010.00	136.76	225.21	131.63	1.81	1.48	0.80	0.97	2.09
	0.80	4.00	255.00	153.11	241.84	153.11	241.84	8.27	151.68	241.08	2.46	2.46	2.76	1.93	149.91	0.79	2.83	1019.54	100.00	9102429.00	151.75	241.94	146.40	1.98	1.60	0.84	0.97	2.26
	0.90	4.95	255.00	176.96	251.77	176.96	251.77	9.33	175.79	251.00	2.81	2.76	3.10	2.17	165.25	0.81	3.20	1262.69	100.00	11273295.00	176.13	251.37	163.47	2.23	1.76	0.88	0.97	2.51
	1.00	8.37	255.00	202.60	282.35	202.60	282.35	12.13	200.66	281.57	4.17	4.21	4.51	3.04	179.00	0.85	4.41	2133.05	100.00	19043910.00	200.66	283.05	177.47	3.06	2.96	0.99	0.98	3.26

Figure A6.10 – Filtrasorb 300 C ImageJ morph measurements

	Perceivable	Area	Mean	X	Y	MM	WM	Perim	BK	BT	Width	Height	Major	Minor	Angle	Circ	Feret	lObbn	SArea	RawlRatio	FeretX	FeretY	FeretAngle	MinFeret	RR	Round	Solidity	Circ Equiv. diam
AQUASORB KGA	0.01	1.02	247.56	27.27	26.75	27.27	26.75	4.36	25.97	25.61	1.16	1.16	1.36	0.83	3.26	0.47	1.46	258.75	97.08	2310147.00	25.97	26.31	2.72	0.91	1.04	0.34	0.83	1.14
	0.02	1.18	249.55	33.32	31.98	33.32	31.98	4.54	31.56	30.69	1.29	1.28	1.42	1.00	5.76	0.49	1.55	295.89	97.86	2641698.00	31.79	31.84	4.55	1.07	1.07	0.37	0.85	1.22
	0.03	1.30	252.06	35.88	34.73	35.88	34.73	4.80	34.61	33.54	1.35	1.31	1.47	1.04	6.81	0.50	1.59	331.08	98.85	2955909.00	34.78	34.84	6.55	1.11	1.08	0.38	0.86	1.29
	0.04	1.37	252.83	38.00	38.70	38.00	38.70	5.01	36.98	37.79	1.40	1.35	1.54	1.08	7.90	0.52	1.68	348.52	99.15	3111561.00	37.00	39.23	8.59	1.15	1.10	0.41	0.87	1.32
	0.05	1.47	253.32	40.25	42.40	40.25	42.40	5.20	39.01	41.40	1.45	1.37	1.59	1.10	9.67	0.54	1.74	370.36	99.34	3306585.00	39.30	42.24	10.86	1.16	1.10	0.42	0.87	1.37
	0.06	1.52	253.73	41.32	43.74	41.32	43.74	5.28	40.72	42.75	1.46	1.38	1.65	1.13	11.14	0.55	1.77	385.20	99.50	3439083.00	40.96	43.53	12.09	1.18	1.11	0.43	0.88	1.39
	0.07	1.56	253.93	44.55	46.24	44.55	46.24	5.34	43.67	45.38	1.49	1.41	1.68	1.15	14.19	0.56	1.79	392.79	99.58	3506811.00	43.72	46.72	14.86	1.20	1.13	0.44	0.88	1.41
	0.08	1.58	254.10	48.18	49.87	48.18	49.87	5.40	46.81	48.75	1.50	1.45	1.69	1.17	16.91	0.56	1.82	401.04	99.65	3580506.00	47.31	49.09	16.02	1.23	1.14	0.45	0.89	1.42
	0.09	1.63	254.33	50.38	50.89	50.38	50.89	5.48	49.11	50.03	1.52	1.48	1.70	1.19	19.71	0.57	1.84	414.32	99.74	3699055.00	49.61	51.51	17.21	1.25	1.15	0.46	0.89	1.44
	0.10	1.68	254.39	52.03	53.06	52.03	53.06	5.57	51.04	51.26	1.54	1.51	1.72	1.21	20.68	0.57	1.87	425.71	99.76	3800775.00	51.51	52.95	18.56	1.26	1.17	0.47	0.89	1.46
	0.20	2.07	254.78	66.07	73.97	66.07	73.97	6.20	65.00	72.89	1.72	1.68	1.89	1.30	35.98	0.60	2.07	526.71	99.91	4702455.00	65.54	73.12	36.20	1.37	1.25	0.55	0.91	1.62
	0.30	2.39	254.99	82.11	101.68	82.11	101.68	6.71	81.35	100.91	1.86	1.84	2.10	1.40	52.57	0.63	2.25	608.32	99.96	5490225.00	81.70	101.36	50.32	1.46	1.33	0.60	0.92	1.74
	0.40	2.71	254.95	98.44	125.51	98.44	125.51	7.14	97.47	124.73	2.03	2.02	2.25	1.48	67.56	0.66	2.45	691.82	99.98	6176610.00	97.62	125.86	66.78	1.55	1.40	0.64	0.93	1.86
	0.50	3.09	254.98	115.33	149.60	115.33	149.60	7.61	114.22	148.53	2.17	2.17	2.44	1.59	89.88	0.67	2.61	787.36	99.99	7029585.00	114.22	149.99	91.62	1.65	1.48	0.67	0.94	1.98
	0.60	3.44	255.00	127.62	178.14	127.62	178.14	8.13	126.46	177.32	2.35	2.35	2.60	1.68	109.25	0.70	2.79	875.28	100.00	7814475.00	126.87	178.12	107.86	1.75	1.55	0.72	0.94	2.09
	0.70	3.90	255.00	140.57	205.50	140.57	205.50	8.65	139.36	203.96	2.53	2.49	2.81	1.79	125.37	0.72	3.02	994.01	100.00	8874510.00	139.54	205.67	123.77	1.92	1.67	0.75	0.95	2.23
	0.80	4.48	255.00	157.09	230.14	157.09	230.14	9.30	156.04	229.06	2.77	2.77	3.05	1.96	147.90	0.73	3.26	1142.50	100.00	10200255.00	156.04	229.63	144.28	2.07	1.82	0.80	0.96	2.39
	0.90	5.10	255.00	170.80	248.18	170.80	248.18	10.27	169.70	246.77	3.11	3.14	3.37	2.14	164.35	0.76	3.60	1301.53	100.00	11620095.00	170.04	248.57	159.62	2.29	2.12	0.86	0.96	2.55
	1.00	11.61	255.00	200.50	281.29	200.50	281.29	14.43	199.04	280.69	4.77	4.60	5.41	3.11	179.92	0.84	5.37	2599.89	100.00	26425905.00	199.05	281.89	179.00	3.14	4.26	0.99	0.98	3.84

Figure A6.11 – Aquasorb KGA ImageJ morph measurements

	Perceivable	Area	Mean	X	Y	MM	WM	Perim	BK	BT	Width	Height	Major	Minor	Angle	Circ	Feret	lObbn	SArea	RawlRatio	FeretX	FeretY	FeretAngle	MinFeret	RR	Round	Solidity	Circ Equiv. diam
SARATECH SPHERICAL	0.01	0.11	233.80	34.96	30.58	34.96	30.58	1.25	34.75	30.37	0.38	0.37	0.39	0.36	0.42	0.59	0.41	27.88	81.69	248890.20	34.75	30.46	6.34	0.36	1.01	0.83	0.52	0.37
	0.02	0.12	235.72	35.00	39.23	35.00	39.23	1.27	38.99	34.78	0.39	0.37	0.40	0.36	0.85	0.41	0.41	28.94	82.44	258406.80	38.99	34.85	7.94	0.37	1.01	0.85	0.93	0.38
	0.03	0.12																										

	Perceivable		Area		Mean		X		Y		XM		YM		Perim		BX		BY		Width		Height		Major		Minor		Angle		Circ		Feret		InDen		SArea		RawInDen		Feret		FeretAngle		MidFeret		AR		Round		Solidity		Circ Equiv. diam	
	Area	Mean	X	Y	XM	YM	Perim	BX	BY	Width	Height	Major	Minor	Angle	Circ	Feret	InDen	SArea	RawInDen	Feret	FeretAngle	MidFeret	AR	Round	Solidity	Circ Equiv. diam																												
0.01	1.57	254.23	37.62	29.41	37.62	29.41	5.52	36.17	28.36	1.41	1.30	1.64	0.91	0.76	0.51	1.83	387.16	99.70	3456563.25	36.20	28.41	2.96	0.98	1.04	0.38	0.88	1.39																											
0.02	1.70	254.49	38.40	38.89	38.40	38.89	5.70	37.04	37.68	1.52	1.49	1.76	1.11	1.26	0.55	1.94	433.15	99.88	3867161.70	37.06	39.49	3.50	1.17	1.05	0.41	0.89	1.47																											
0.03	1.82	254.55	41.68	42.40	41.68	42.40	5.78	40.62	40.99	1.58	1.54	1.82	1.16	2.76	0.57	2.00	464.32	99.82	4145476.35	40.81	42.35	4.42	1.22	1.06	0.44	0.90	1.52																											
0.04	1.83	254.57	50.69	43.59	50.69	43.59	5.84	49.30	42.60	1.65	1.58	1.84	1.19	6.22	0.58	2.02	467.29	99.83	4171993.80	49.54	43.02	4.67	1.31	1.09	0.48	0.91	1.53																											
0.05	1.95	254.60	53.22	46.17	53.22	46.17	5.96	52.04	45.01	1.68	1.60	1.87	1.22	8.85	0.58	2.04	496.15	99.84	4429605.00	52.50	46.37	7.14	1.32	1.10	0.48	0.91	1.57																											
0.06	1.97	254.62	55.16	48.19	55.16	48.19	6.05	53.91	46.99	1.74	1.66	1.92	1.27	10.26	0.59	2.07	501.57	99.85	4478029.50	54.29	48.37	8.27	1.35	1.11	0.50	0.91	1.58																											
0.07	2.10	254.65	55.72	49.01	55.72	49.01	6.07	54.61	47.60	1.78	1.70	1.94	1.29	10.66	0.61	2.11	535.15	99.86	4777850.85	55.50	49.65	10.02	1.38	1.12	0.51	0.92	1.64																											
0.08	2.13	254.68	58.94	49.89	58.94	49.89	6.31	57.84	48.78	1.80	1.72	1.96	1.33	11.77	0.62	2.14	543.63	99.88	4853557.80	57.93	50.25	11.51	1.41	1.13	0.51	0.92	1.65																											
0.09	2.29	254.70	60.09	54.49	60.09	54.49	6.39	58.71	53.13	1.82	1.75	2.00	1.34	12.90	0.62	2.15	583.94	99.88	5213424.00	58.71	54.93	15.02	1.45	1.13	0.51	0.92	1.71																											
0.10	2.36	254.72	61.79	55.57	61.79	55.57	6.52	60.63	53.95	1.82	1.78	2.02	1.41	13.58	0.63	2.18	602.70	99.89	5380882.50	61.05	55.71	16.22	1.48	1.15	0.51	0.92	1.73																											
0.20	2.82	254.84	77.18	79.33	77.18	79.33	7.11	75.85	78.22	2.04	1.94	2.24	1.56	25.55	0.66	2.40	719.37	99.94	6422532.00	75.87	80.37	30.01	1.61	1.19	0.60	0.94	1.90																											
0.30	3.26	254.91	91.17	103.83	91.17	103.83	7.59	96.15	102.62	2.20	2.13	2.40	1.67	47.06	0.69	2.59	830.21	99.96	7412136.00	96.27	103.55	45.46	1.72	1.25	0.64	0.94	2.04																											
0.40	3.61	254.95	109.45	132.80	109.45	132.80	8.04	108.20	131.36	2.33	2.27	2.58	1.75	65.27	0.70	2.75	918.90	99.98	8203962.00	108.20	132.72	67.33	1.81	1.32	0.69	0.95	2.14																											
0.50	3.99	254.97	123.22	162.57	123.22	162.57	8.42	122.10	161.61	2.45	2.39	2.74	1.89	85.60	0.72	2.91	1017.56	99.99	9084757.50	122.68	162.76	85.03	1.92	1.38	0.72	0.96	2.25																											
0.60	4.34	254.99	133.83	179.63	133.83	179.63	8.87	132.48	178.52	2.66	2.60	2.91	1.97	109.01	0.73	3.04	1105.20	100.00	9867225.00	132.63	180.49	112.96	2.04	1.46	0.76	0.96	2.35																											
0.70	4.88	255.00	145.70	208.01	145.70	208.01	9.25	144.45	206.48	2.84	2.74	3.05	2.08	126.72	0.75	3.18	1243.97	100.00	11106168.00	144.75	208.33	129.79	2.15	1.56	0.80	0.96	2.49																											
0.80	5.66	255.00	159.29	226.91	159.29	226.91	9.93	158.16	225.66	3.06	2.96	3.20	2.27	149.98	0.76	3.33	1444.01	100.00	12892188.00	158.26	227.41	150.24	2.34	1.68	0.84	0.97	2.69																											
0.90	6.53	255.00	173.66	245.36	173.66	245.36	10.57	172.58	244.36	3.23	3.20	3.43	2.63	165.55	0.78	3.53	1665.22	100.00	14867088.50	172.59	244.97	166.40	2.62	1.96	0.87	0.97	2.88																											
1.00	9.70	255.00	198.17	279.39	198.17	279.39	12.97	197.08	278.05	4.56	4.56	4.76	3.23	178.74	0.88	4.58	2474.28	100.00	22090395.00	197.39	280.85	178.74	3.22	4.91	0.98	0.99	3.51																											

Figure A6.16 - Aquasorb K-6300 ImageJ morph measurements

	Perceivable		Area		Mean		X		Y		XM		YM		Perim		BX		BY		Width		Height		Major		Minor		Angle		Circ		Feret		InDen		SArea		RawInDen		Feret		FeretAngle		MidFeret		AR		Round		Solidity		Circ Equiv. diam	
	Area	Mean	X	Y	XM	YM	Perim	BX	BY	Width	Height	Major	Minor	Angle	Circ	Feret	InDen	SArea	RawInDen	Feret	FeretAngle	MidFeret	AR	Round	Solidity	Circ Equiv. diam																												
0.01	1.11	254.24	23.27	24.10	23.27	24.10	4.30	21.76	22.93	1.29	1.13	1.40	0.95	2.58	0.53	1.51	282.88	99.70	2525520.00	21.78	24.66	4.55	1.01	1.04	0.39	0.88	1.19																											
0.02	1.23	254.50	25.82	28.07	25.82	28.07	4.73	24.67	26.83	1.33	1.22	1.46	0.98	5.55	0.57	1.60	312.27	99.80	2787915.00	24.75	26.85	5.68	1.04	1.05	0.43	0.90	1.25																											
0.03	1.32	254.57	27.68	32.22	27.68	32.22	4.88	26.60	31.17	1.39	1.28	1.56	1.02	7.25	0.58	1.65	337.40	99.83	3012315.00	26.87	32.23	6.84	1.08	1.07	0.45	0.91	1.30																											
0.04	1.47	254.63	30.31	34.78	30.31	34.78	4.95	29.18	33.05	1.42	1.34	1.60	1.04	11.07	0.60	1.67	375.39	99.86	3351465.00	29.75	34.93	9.19	1.16	1.08	0.47	0.92	1.37																											
0.05	1.56	254.66	32.58	36.87	32.58	36.87	5.05	31.36	35.70	1.46	1.38	1.64	1.10	11.61	0.60	1.72	396.01	99.87	3535575.00	31.52	36.01	10.05	1.18	1.09	0.49	0.92	1.41																											
0.06	1.66	254.70	33.33	39.60	33.33	39.60	5.16	32.19	38.58	1.51	1.40	1.68	1.15	14.28	0.62	1.80	422.43	99.88	3771450.00	32.47	38.90	13.18	1.21	1.12	0.49	0.92	1.45																											
0.07	1.70	254.73	35.91	41.13	35.91	41.13	5.33	34.59	40.38	1.54	1.45	1.75	1.17	15.14	0.62	1.84	432.20	99.89	3858660.00	35.09	40.74	16.79	1.24	1.12	0.50	0.93	1.47																											
0.08	1.75	254.75	39.33	43.14	39.33	43.14	5.51	37.72	42.18	1.55	1.47	1.79	1.22	19.81	0.63	1.87	447.36	99.90	3994065.00	37.72	42.82	17.91	1.26	1.13	0.50	0.93	1.49																											
0.09	1.81	254.79	41.91	44.77	41.91	44.77	5.53	40.53	43.53	1.56	1.52	1.81	1.24	21.36	0.64	1.91	461.59	99.92	4121055.00	40.55	44.85	19.16	1.28	1.14	0.51	0.93	1.52																											
0.10	1.84	254.80	42.95	45.57	42.95	45.57	5.58	42.16	44.55	1.58	1.55	1.82	1.26	23.22	0.64	1.93	468.24	99.92	4180470.00	42.28	46.07	20.95	1.30	1.15	0.52	0.94	1.53																											
0.20	2.35	254.91	61.76	68.14	61.76	68.14	6.33	60.81	66.99	1.81	1.80	2.02	1.39	40.49	0.69	2.13	598.03	99.97	5339190.00	61.03	67.23	37.03	1.44	1.21	0.59	0.95	1.73																											
0.30	2.67	254.95	77.30	98.71	77.30	98.71	6.79	76.13	97.28	1.96	1.94	2.22	1.52	56.00	0.71	2.31	681.88	99.98	6087870.00	76.13	98.76	55.05	1.56	1.29	0.62	0.95	1.85																											
0.40	3.09	254.98	89.10	127.40	89.10	127.40	7.21	88.12	125.92	2.05	2.09	2.33	1.63	78.76	0.73	2.49	786.68	99.99	7023465.00	88.41	128.01	77.61	1.69	1.36	0.67	0.96	1.98																											
0.50	3.38	254.99	105.42	147.65	105.42	147.65	7.58	104.29	146.56	2.19	2.21	2.50	1.74	100.89	0.74	2.62	859.74	100.00	7675755.00	105.25	146.88	97.49	1.77	1.43	0.70	0.96	2.07																											
0.60	3.74	255.00	124.33	174.14	124.33	174.14	8.08	123.29	173.26	2.35	2.41	2.64	1.82	114.75	0.76	2.77	954.42	100.00	8521080.00	123.57	175.26	114.80	1.87	1.50	0.74	0.97	2.18																											
0.70	4.21	255.00	140.09	198.74	140.09	198.74	8.50	138.82	197.65	2.52	2.55	2.80	1.93	134.34	0.77	2.92	1074.09	100.00	9580605.00	139.64	197.88	130.55	1.97	1.61	0.78	0.97	2.32																											
0.80	4.63	255.00	155.82	230.20	155.82	230.20	9.00	154.69	229.25	2.74	2.76	3.02	2.06	152.39	0.78	3.15	1179.60	100.00	10531500.00	154.69	230.73	149.21	2.12	1.71	0.82	0.97	2.43																											
0.90	5.69	255.00	169.96	254.88	169.96	254.88	9.90	168.72	251.55	3.06	3.01	3.29	2.27	166.58	0.80	3.41	1446.88	100.00	12917900.00	169.15	253.30	163.39	2.34	1.93	0.87	0.98	2.69																											
1.00	12.80	255.00	200.53	285.51	200.53	285.51	16.40	199.51	284.40	5.90	4.45	5.62	3.18	179.94	0.85	5.93	3262.50	100.00	29127630.00	199.76	286.27	178.23	3.22	3.46	0.98	0.98	4.04																											

Figure A6.17 - Resorb HC ImageJ morph measurements

	Perceivable		Area		Mean		X		Y		XM		YM		Perim		BX		BY		Width		Height		Major		Minor		Angle		Circ		Feret		InDen		SArea		RawInDen		Feret		FeretAngle		MidFeret		AR		Round		Solidity		Circ Equiv. diam	
	Area	Mean																																																				

▪ Camsizer morph measurements

	Percentile	Particle size				Particle size				Particle size				Aspect ratio			
		SPHT0	Symm0	b/l0	B/L_rec0	SPHT0	Symm0	b/l0	B/L_rec0	SPHT0	Symm0	b/l0	B/L_rec0	Xf _{amax} /Xf _{cmin}			
FILTRASORB 300 C	0.01	0.56	0.83	0.88	0.69	0.73	0.51	0.80	0.89	0.61	0.64	0.68	0.80	0.87	0.66	0.69	1.35
	0.02	0.63	0.82	0.88	0.67	0.70	0.54	0.79	0.89	0.59	0.61	0.74	0.83	0.89	0.72	0.75	1.36
	0.03	0.67	0.83	0.89	0.69	0.71	0.56	0.79	0.89	0.59	0.62	0.77	0.86	0.90	0.76	0.79	1.36
	0.04	0.69	0.84	0.89	0.69	0.72	0.58	0.80	0.89	0.60	0.63	0.80	0.88	0.90	0.78	0.81	1.37
	0.05	0.71	0.84	0.90	0.70	0.72	0.60	0.80	0.89	0.61	0.64	0.82	0.89	0.90	0.79	0.81	1.36
	0.06	0.72	0.84	0.90	0.70	0.73	0.61	0.81	0.89	0.62	0.65	0.84	0.89	0.90	0.79	0.81	1.36
	0.07	0.74	0.84	0.90	0.71	0.74	0.63	0.81	0.89	0.63	0.66	0.85	0.89	0.90	0.78	0.81	1.36
	0.08	0.75	0.85	0.90	0.71	0.74	0.64	0.82	0.89	0.64	0.67	0.87	0.89	0.90	0.78	0.81	1.36
	0.09	0.76	0.85	0.90	0.71	0.74	0.65	0.82	0.90	0.65	0.67	0.88	0.89	0.90	0.78	0.81	1.35
	0.10	0.77	0.85	0.90	0.71	0.74	0.66	0.82	0.90	0.65	0.68	0.90	0.89	0.90	0.78	0.81	1.36
	0.20	0.86	0.87	0.89	0.73	0.76	0.75	0.84	0.90	0.69	0.72	1.02	0.88	0.90	0.75	0.78	1.35
	0.30	0.95	0.87	0.90	0.73	0.75	0.83	0.86	0.89	0.72	0.74	1.12	0.87	0.90	0.74	0.76	1.35
	0.40	1.04	0.87	0.90	0.73	0.75	0.91	0.87	0.90	0.73	0.76	1.22	0.87	0.89	0.73	0.76	1.35
	0.50	1.14	0.86	0.90	0.73	0.75	0.99	0.87	0.90	0.74	0.76	1.34	0.89	0.89	0.75	0.77	1.35
	0.60	1.24	0.86	0.90	0.72	0.75	1.09	0.87	0.90	0.74	0.77	1.48	0.88	0.89	0.73	0.75	1.36
	0.70	1.38	0.88	0.89	0.73	0.76	1.20	0.87	0.89	0.74	0.76	1.65	0.88	0.89	0.72	0.75	1.37
	0.80	1.56	0.88	0.89	0.73	0.75	1.36	0.89	0.89	0.75	0.78	1.88	0.87	0.89	0.71	0.73	1.38
0.90	1.84	0.87	0.89	0.72	0.75	1.61	0.88	0.89	0.75	0.78	2.24	0.86	0.89	0.70	0.72	1.39	
1.00	3.25	0.86	0.90	0.68	0.71	2.90	0.89	0.90	0.82	0.85	3.20	0.82	0.89	0.62	0.64	1.10	

Figure A6.19 – Filtrasorb 300 C Camsizer morph measurements

	Percentile	Particle size				Particle size				Particle size				Aspect ratio			
		SPHT0	Symm0	b/l0	B/L_rec0	SPHT0	Symm0	b/l0	B/L_rec0	SPHT0	Symm0	b/l0	B/L_rec0	Xf _{amax} /Xf _{cmin}			
AQUASORB KGA	0.01	0.67	0.66	0.86	0.46	0.49	0.42	0.56	0.87	0.32	0.34	0.84	0.85	0.86	0.72	0.75	2.03
	0.02	0.71	0.64	0.86	0.44	0.46	0.47	0.60	0.87	0.36	0.38	0.90	0.85	0.87	0.70	0.73	1.91
	0.03	0.73	0.69	0.87	0.49	0.52	0.51	0.64	0.87	0.39	0.41	0.93	0.85	0.87	0.69	0.72	1.81
	0.04	0.76	0.72	0.87	0.52	0.55	0.55	0.63	0.84	0.40	0.42	0.96	0.84	0.87	0.68	0.72	1.74
	0.05	0.78	0.72	0.87	0.53	0.56	0.58	0.67	0.85	0.45	0.47	0.98	0.84	0.87	0.69	0.73	1.69
	0.06	0.80	0.72	0.86	0.54	0.57	0.61	0.71	0.86	0.49	0.51	1.00	0.84	0.87	0.70	0.73	1.66
	0.07	0.81	0.74	0.86	0.55	0.58	0.62	0.71	0.87	0.50	0.53	1.02	0.84	0.87	0.69	0.73	1.63
	0.08	0.83	0.75	0.86	0.57	0.60	0.64	0.72	0.87	0.52	0.54	1.04	0.84	0.87	0.69	0.73	1.61
	0.09	0.84	0.77	0.86	0.59	0.62	0.66	0.73	0.87	0.52	0.55	1.05	0.83	0.87	0.68	0.72	1.60
	0.10	0.85	0.79	0.87	0.60	0.63	0.67	0.73	0.87	0.52	0.55	1.07	0.83	0.87	0.68	0.71	1.58
	0.20	0.96	0.80	0.87	0.63	0.66	0.79	0.76	0.87	0.60	0.63	1.19	0.80	0.87	0.65	0.68	1.51
	0.30	1.05	0.79	0.86	0.63	0.66	0.88	0.80	0.87	0.63	0.67	1.32	0.82	0.87	0.64	0.67	1.50
	0.40	1.15	0.79	0.87	0.63	0.67	0.97	0.80	0.87	0.65	0.68	1.45	0.82	0.87	0.64	0.67	1.49
	0.50	1.27	0.80	0.86	0.65	0.68	1.07	0.80	0.86	0.65	0.69	1.59	0.82	0.87	0.64	0.68	1.48
	0.60	1.39	0.82	0.87	0.66	0.69	1.19	0.79	0.86	0.66	0.69	1.75	0.81	0.87	0.64	0.68	1.47
	0.70	1.53	0.82	0.87	0.65	0.69	1.31	0.82	0.87	0.67	0.70	1.95	0.81	0.86	0.64	0.67	1.49
	0.80	1.71	0.81	0.87	0.64	0.68	1.45	0.83	0.87	0.67	0.71	2.21	0.80	0.87	0.62	0.65	1.52
0.90	1.99	0.79	0.87	0.62	0.66	1.68	0.82	0.87	0.68	0.71	2.62	0.78	0.87	0.59	0.63	1.56	
1.00	3.50	0.69	0.78	0.63	0.67	3.10	1.00	0.82	0.77	0.80	3.41	0.68	0.85	0.55	0.59	1.10	

Figure A6.20 – Aquasorb KGA Camsizer morph measurements

	Percentile	Particle size				Particle size				Particle size				Aspect ratio			
		SPH10	Symm0	b/l0	B/L_rec0	SPH10	Symm0	b/l0	B/L_rec0	SPH10	Symm0	b/l0	B/L_rec0	Xf_max	Xf_min		
SARATECH SPHERICAL	0.01	0.36	0.87	0.90	0.68	0.70	0.31	0.86	0.89	0.66	0.69	0.38	0.94	0.94	0.88	0.90	1.24
	0.02	0.37	0.90	0.91	0.74	0.76	0.35	0.91	0.91	0.74	0.77	0.40	0.96	0.95	0.92	0.93	1.15
	0.03	0.39	0.93	0.93	0.81	0.83	0.36	0.92	0.92	0.78	0.80	0.40	0.96	0.95	0.92	0.93	1.12
	0.04	0.40	0.95	0.94	0.86	0.87	0.37	0.93	0.92	0.81	0.83	0.41	0.97	0.96	0.92	0.94	1.09
	0.05	0.40	0.95	0.94	0.86	0.88	0.38	0.94	0.93	0.84	0.86	0.41	0.97	0.96	0.93	0.94	1.07
	0.06	0.40	0.95	0.94	0.87	0.88	0.39	0.95	0.94	0.87	0.89	0.41	0.97	0.96	0.93	0.94	1.04
	0.07	0.41	0.95	0.94	0.87	0.88	0.40	0.96	0.94	0.89	0.91	0.41	0.97	0.96	0.93	0.94	1.03
	0.08	0.41	0.95	0.94	0.87	0.89	0.40	0.96	0.95	0.89	0.91	0.41	0.97	0.96	0.93	0.94	1.03
	0.09	0.41	0.95	0.94	0.88	0.89	0.40	0.96	0.95	0.90	0.91	0.42	0.97	0.96	0.93	0.94	1.03
	0.10	0.41	0.95	0.94	0.88	0.90	0.41	0.96	0.95	0.90	0.91	0.42	0.97	0.96	0.94	0.95	1.03
	0.20	0.43	0.97	0.96	0.92	0.93	0.42	0.97	0.96	0.93	0.94	0.44	0.98	0.96	0.95	0.96	1.05
	0.30	0.45	0.98	0.97	0.96	0.97	0.44	0.98	0.96	0.95	0.96	0.46	0.98	0.97	0.96	0.97	1.04
	0.40	0.46	0.98	0.97	0.97	0.97	0.45	0.98	0.97	0.97	0.98	0.47	0.98	0.97	0.96	0.97	1.03
	0.50	0.47	0.98	0.97	0.97	0.98	0.46	0.98	0.97	0.97	0.98	0.47	0.98	0.97	0.97	0.97	1.02
	0.60	0.48	0.98	0.97	0.97	0.98	0.47	0.98	0.97	0.97	0.98	0.48	0.98	0.97	0.97	0.98	1.02
	0.70	0.49	0.98	0.97	0.97	0.98	0.48	0.98	0.97	0.97	0.98	0.49	0.98	0.97	0.97	0.98	1.02
	0.80	0.50	0.98	0.97	0.98	0.98	0.49	0.98	0.97	0.97	0.98	0.51	0.98	0.97	0.97	0.98	1.03
	0.90	0.52	0.98	0.97	0.98	0.99	0.52	0.98	0.97	0.97	0.98	0.53	0.98	0.97	0.97	0.98	1.03
1.00	0.85	0.54	0.64	0.53	0.61	0.75	0.84	0.84	0.90	0.92	0.78	0.84	0.91	0.65	0.66	1.04	

Figure A6.21 - Saratech Camsizer morph measurements

	Percentile	Particle size (Karea)				Particle size (Kcmin)				Particle size (Kfe_max)				Aspect ratio			
		SPH10	Symm0	b/l0	B/L_rec0	SPH10	Symm0	b/l0	B/L_rec0	SPH10	Symm0	b/l0	B/L_rec0	Xf_max	Xf_min		
NORIT ROW 0.8 SUPRA	0.01	0.81	0.84	0.87	0.70	0.72	0.72	0.78	0.91	0.56	0.58	0.25	0.58	0.77	0.45	0.49	0.35
	0.02	0.87	0.93	0.92	0.79	0.83	0.75	0.77	0.93	0.51	0.53	0.32	0.50	0.74	0.42	0.46	0.43
	0.03	0.90	0.94	0.93	0.81	0.84	0.76	0.77	0.93	0.51	0.53	0.36	0.48	0.75	0.37	0.41	0.48
	0.04	0.92	0.94	0.93	0.80	0.84	0.77	0.78	0.94	0.51	0.54	0.40	0.48	0.76	0.35	0.38	0.52
	0.05	0.95	0.94	0.94	0.80	0.83	0.78	0.78	0.94	0.52	0.54	0.43	0.51	0.78	0.34	0.36	0.55
	0.06	0.96	0.94	0.94	0.79	0.82	0.79	0.79	0.94	0.52	0.55	0.45	0.53	0.79	0.33	0.35	0.57
	0.07	0.97	0.94	0.94	0.78	0.81	0.80	0.79	0.94	0.53	0.55	0.48	0.53	0.80	0.33	0.35	0.60
	0.08	0.99	0.93	0.94	0.77	0.80	0.80	0.79	0.94	0.53	0.55	0.50	0.53	0.80	0.33	0.35	0.62
	0.09	1.00	0.93	0.94	0.76	0.79	0.80	0.79	0.94	0.53	0.55	0.52	0.51	0.80	0.32	0.33	0.65
	0.10	1.01	0.93	0.94	0.75	0.78	0.81	0.79	0.94	0.53	0.55	0.54	0.48	0.80	0.30	0.31	0.67
	0.20	1.10	0.90	0.94	0.66	0.69	0.83	0.80	0.94	0.52	0.55	0.71	0.58	0.83	0.40	0.42	0.86
	0.30	1.17	0.87	0.94	0.60	0.63	0.85	0.80	0.94	0.52	0.55	0.85	0.75	0.85	0.57	0.59	1.00
	0.40	1.24	0.84	0.94	0.56	0.58	0.86	0.80	0.94	0.52	0.54	0.99	0.94	0.94	0.83	0.86	1.15
	0.50	1.30	0.83	0.93	0.52	0.54	0.88	0.80	0.94	0.52	0.54	1.13	0.94	0.94	0.77	0.80	1.29
	0.60	1.36	0.80	0.93	0.48	0.50	0.89	0.80	0.94	0.52	0.54	1.28	0.93	0.93	0.69	0.72	1.44
	0.70	1.44	0.76	0.93	0.44	0.46	0.90	0.80	0.94	0.52	0.54	1.46	0.89	0.93	0.61	0.64	1.63
	0.80	1.53	0.72	0.92	0.40	0.42	0.93	0.80	0.94	0.52	0.54	1.70	0.84	0.93	0.53	0.56	1.83
	0.90	1.66	0.66	0.90	0.36	0.38	0.96	0.79	0.93	0.52	0.54	2.06	0.77	0.92	0.44	0.47	2.15
1.00	3.25	0.29	0.55	0.46	0.55	2.75	0.34	0.59	0.59	0.71	3.05	0.34	0.36	0.33	0.58	1.11	

Figure A6.22 - ROW 0.8 Supra Camsizer morph measurements

Percentile	Particle size		SPH10	Symm0	b/l0	B/L_rec0	Particle size		SPH10	Symm0	b/l0	B/L_rec0	Particle size		SPH10	Symm0	b/l0	B/L_rec0	Aspect ratio X_{fmax}/X_{cmin}
	SPH10	Symm0					SPH10	Symm0					SPH10	Symm0					
0.01	4.02	0.96	0.95	0.87	0.89	3.56	0.84	0.95	0.55	0.58	4.23	0.96	0.96	0.86	0.88	1.19			
0.02	4.15	0.96	0.96	0.83	0.87	3.61	0.82	0.95	0.55	0.57	4.45	0.97	0.97	0.86	0.88	1.23			
0.03	4.22	0.95	0.95	0.81	0.85	3.64	0.82	0.95	0.55	0.57	4.58	0.96	0.96	0.82	0.85	1.26			
0.04	4.28	0.95	0.96	0.81	0.85	3.66	0.82	0.95	0.54	0.57	4.73	0.95	0.95	0.81	0.84	1.29			
0.05	4.32	0.95	0.95	0.79	0.84	3.68	0.81	0.95	0.53	0.55	4.80	0.95	0.95	0.80	0.83	1.30			
0.06	4.38	0.94	0.95	0.78	0.83	3.70	0.81	0.95	0.52	0.54	4.90	0.95	0.96	0.79	0.83	1.33			
0.07	4.42	0.94	0.95	0.77	0.82	3.71	0.80	0.95	0.52	0.54	4.96	0.94	0.96	0.78	0.82	1.34			
0.08	4.45	0.93	0.96	0.76	0.81	3.71	0.80	0.96	0.51	0.54	5.03	0.94	0.96	0.77	0.81	1.35			
0.09	4.49	0.93	0.96	0.75	0.79	3.72	0.80	0.96	0.51	0.53	5.10	0.94	0.95	0.76	0.79	1.37			
0.10	4.52	0.93	0.96	0.75	0.79	3.73	0.80	0.96	0.50	0.53	5.16	0.93	0.95	0.75	0.79	1.38			
0.20	4.81	0.91	0.96	0.68	0.71	3.78	0.80	0.96	0.50	0.53	5.66	0.91	0.95	0.68	0.72	1.50			
0.30	5.04	0.89	0.95	0.63	0.66	3.81	0.82	0.96	0.53	0.55	6.10	0.90	0.96	0.64	0.66	1.60			
0.40	5.26	0.87	0.96	0.59	0.62	3.84	0.83	0.96	0.54	0.57	6.53	0.87	0.96	0.59	0.62	1.70			
0.50	5.45	0.85	0.96	0.56	0.58	3.86	0.84	0.96	0.56	0.58	6.95	0.85	0.96	0.56	0.58	1.80			
0.60	5.66	0.83	0.96	0.52	0.55	3.89	0.84	0.96	0.57	0.59	7.40	0.83	0.96	0.52	0.54	1.90			
0.70	5.87	0.80	0.96	0.49	0.51	3.91	0.85	0.96	0.58	0.61	7.92	0.80	0.96	0.49	0.51	2.02			
0.80	6.12	0.77	0.96	0.45	0.47	3.95	0.86	0.96	0.59	0.62	8.51	0.78	0.96	0.45	0.47	2.16			
0.90	6.42	0.74	0.96	0.41	0.43	4.00	0.87	0.96	0.61	0.64	9.34	0.73	0.96	0.41	0.43	2.34			
1.00	7.20	0.67	0.95	0.35	0.37	4.33	0.83	0.88	0.62	0.66	10.90	0.68	0.59	0.22	0.23	2.52			

Figure A6.23 - RB4C Camsizer morph measurements

Percentile	Particle size		SPH10	Symm0	b/l0	B/L_rec0	Particle size		SPH10	Symm0	b/l0	B/L_rec0	Particle size		SPH10	Symm0	b/l0	B/L_rec0	Aspect ratio X_{fmax}/X_{cmin}
	SPH10	Symm0					SPH10	Symm0					SPH10	Symm0					
0.01	0.60	0.79	0.87	0.67	0.71	0.78	0.78	0.87	0.64	0.67	0.92	0.83	0.87	0.66	0.68	1.17			
0.02	0.65	0.77	0.87	0.65	0.68	0.81	0.78	0.87	0.62	0.65	0.97	0.82	0.88	0.66	0.69	1.19			
0.03	0.69	0.78	0.87	0.64	0.68	0.84	0.80	0.88	0.62	0.65	1.02	0.82	0.88	0.67	0.70	1.22			
0.04	0.74	0.78	0.87	0.64	0.67	0.86	0.80	0.88	0.62	0.65	1.07	0.83	0.88	0.68	0.71	1.24			
0.05	0.78	0.76	0.86	0.64	0.67	0.88	0.81	0.88	0.63	0.66	1.11	0.82	0.88	0.67	0.70	1.26			
0.06	0.83	0.79	0.87	0.64	0.67	0.91	0.80	0.87	0.63	0.66	1.16	0.81	0.88	0.66	0.69	1.28			
0.07	0.87	0.82	0.88	0.65	0.68	0.93	0.79	0.87	0.62	0.65	1.20	0.82	0.88	0.67	0.70	1.29			
0.08	0.91	0.82	0.88	0.66	0.69	0.95	0.78	0.87	0.61	0.64	1.24	0.83	0.88	0.67	0.70	1.30			
0.09	0.94	0.82	0.88	0.65	0.68	0.97	0.79	0.87	0.61	0.64	1.27	0.84	0.88	0.67	0.70	1.31			
0.10	0.98	0.82	0.88	0.66	0.69	0.99	0.79	0.87	0.61	0.64	1.31	0.86	0.88	0.67	0.70	1.32			
0.20	1.27	0.82	0.87	0.65	0.69	1.16	0.79	0.87	0.61	0.65	1.61	0.86	0.88	0.69	0.73	1.40			
0.30	1.45	0.84	0.88	0.66	0.69	1.28	0.82	0.88	0.64	0.67	1.80	0.86	0.88	0.70	0.74	1.41			
0.40	1.58	0.84	0.88	0.67	0.70	1.38	0.83	0.88	0.65	0.68	1.96	0.86	0.88	0.70	0.73	1.42			
0.50	1.69	0.84	0.88	0.67	0.70	1.47	0.84	0.88	0.66	0.70	2.09	0.85	0.88	0.68	0.72	1.42			
0.60	1.79	0.84	0.88	0.67	0.71	1.56	0.85	0.88	0.68	0.72	2.23	0.85	0.88	0.68	0.71	1.43			
0.70	1.90	0.84	0.88	0.68	0.71	1.66	0.85	0.88	0.70	0.73	2.37	0.84	0.88	0.67	0.70	1.43			
0.80	2.01	0.84	0.88	0.68	0.71	1.77	0.86	0.88	0.71	0.75	2.53	0.83	0.88	0.65	0.68	1.43			
0.90	2.18	0.84	0.88	0.68	0.72	1.92	0.86	0.88	0.74	0.77	2.77	0.81	0.88	0.61	0.63	1.44			
1.00	2.95	0.61	2.95	0.54	0.59	2.55	0.84	2.55	0.75	0.78	3.45	0.76	3.22	0.52	0.54	1.35			

Figure A6.24 - Filtrasorb TL830 Camsizer morph measurements

	Percentile	Particle size				Particle size				Particle size				Aspect ratio			
		SPHT0	Symm0	b/l0	B/L_rec0	SPHT0	Symm0	b/l0	B/L_rec0	SPHT0	Symm0	b/l0	B/L_rec0	X _F max	X _F min		
AQUASORB K-6300	0.01	0.55	0.71	0.86	0.51	0.53	0.55	0.71	0.88	0.51	0.54	0.74	0.79	0.86	0.65	0.68	1.34
	0.02	0.60	0.68	0.85	0.48	0.51	0.58	0.70	0.87	0.50	0.53	0.82	0.79	0.85	0.65	0.67	1.41
	0.03	0.65	0.70	0.85	0.53	0.56	0.60	0.69	0.86	0.50	0.52	0.87	0.80	0.86	0.62	0.65	1.44
	0.04	0.69	0.71	0.86	0.55	0.57	0.63	0.71	0.86	0.53	0.56	0.92	0.79	0.87	0.62	0.64	1.47
	0.05	0.73	0.72	0.86	0.56	0.59	0.66	0.72	0.85	0.56	0.58	0.97	0.79	0.87	0.59	0.61	1.47
	0.06	0.76	0.73	0.85	0.58	0.61	0.68	0.72	0.86	0.55	0.57	1.00	0.78	0.86	0.60	0.63	1.47
	0.07	0.79	0.74	0.85	0.60	0.62	0.71	0.72	0.86	0.54	0.57	1.05	0.80	0.87	0.60	0.63	1.48
	0.08	0.83	0.76	0.86	0.59	0.61	0.73	0.71	0.86	0.54	0.57	1.09	0.78	0.86	0.60	0.63	1.49
	0.09	0.86	0.77	0.86	0.57	0.60	0.75	0.71	0.86	0.54	0.56	1.12	0.78	0.86	0.61	0.64	1.50
	0.10	0.89	0.76	0.86	0.56	0.59	0.77	0.72	0.86	0.55	0.58	1.15	0.78	0.86	0.63	0.66	1.50
	0.20	1.14	0.77	0.86	0.60	0.62	0.96	0.77	0.87	0.57	0.60	1.48	0.81	0.87	0.61	0.63	1.54
	0.30	1.35	0.81	0.87	0.61	0.64	1.14	0.78	0.87	0.61	0.64	1.73	0.81	0.87	0.62	0.65	1.53
	0.40	1.55	0.82	0.87	0.64	0.67	1.31	0.82	0.87	0.62	0.65	1.96	0.83	0.88	0.66	0.69	1.49
	0.50	1.72	0.83	0.87	0.65	0.69	1.46	0.83	0.88	0.63	0.66	2.16	0.84	0.88	0.67	0.70	1.48
	0.60	1.86	0.83	0.88	0.65	0.69	1.58	0.84	0.88	0.65	0.68	2.35	0.84	0.88	0.66	0.69	1.48
	0.70	2.01	0.84	0.88	0.65	0.68	1.70	0.84	0.88	0.66	0.69	2.56	0.83	0.88	0.64	0.67	1.51
	0.80	2.18	0.83	0.88	0.64	0.67	1.84	0.85	0.88	0.68	0.71	2.80	0.82	0.88	0.62	0.65	1.52
	0.90	2.40	0.84	0.89	0.65	0.68	2.07	0.86	0.88	0.71	0.75	3.10	0.82	0.88	0.60	0.63	1.50
1.00	3.60	0.69	3.60	0.54	0.58	3.25	0.98	0.96	0.91	0.93	3.75	0.78	0.87	0.56	0.59	1.15	

Figure A6.25 - Aquasorb K-6300 Camsizer morph measurements

	Percentile	Particle size				Particle size				Particle size				Aspect ratio			
		SPHT0	Symm0	b/l0	B/L_rec0	SPHT0	Symm0	b/l0	B/L_rec0	SPHT0	Symm0	b/l0	B/L_rec0	X _F max	X _F min		
RESORB HC	0.01	0.55	0.75	0.88	0.56	0.59	0.39	0.68	0.87	0.44	0.46	0.66	0.84	0.89	0.71	0.74	1.69
	0.02	0.59	0.77	0.88	0.58	0.61	0.44	0.72	0.88	0.48	0.50	0.72	0.83	0.89	0.70	0.73	1.63
	0.03	0.62	0.77	0.88	0.59	0.61	0.47	0.74	0.88	0.51	0.53	0.75	0.83	0.89	0.69	0.72	1.60
	0.04	0.64	0.77	0.88	0.59	0.61	0.50	0.75	0.88	0.52	0.54	0.78	0.84	0.89	0.70	0.73	1.56
	0.05	0.66	0.78	0.88	0.60	0.62	0.52	0.76	0.88	0.53	0.56	0.81	0.85	0.89	0.70	0.73	1.55
	0.06	0.68	0.79	0.88	0.61	0.64	0.54	0.76	0.89	0.54	0.57	0.83	0.85	0.89	0.69	0.72	1.54
	0.07	0.70	0.80	0.89	0.63	0.65	0.56	0.77	0.89	0.55	0.58	0.85	0.86	0.89	0.67	0.70	1.52
	0.08	0.71	0.80	0.89	0.63	0.66	0.57	0.77	0.89	0.56	0.59	0.87	0.86	0.89	0.67	0.70	1.51
	0.09	0.73	0.80	0.89	0.63	0.66	0.59	0.78	0.89	0.57	0.60	0.88	0.86	0.89	0.67	0.70	1.50
	0.10	0.74	0.80	0.89	0.63	0.66	0.60	0.78	0.89	0.58	0.61	0.90	0.86	0.89	0.67	0.70	1.50
	0.20	0.87	0.84	0.89	0.65	0.67	0.72	0.81	0.89	0.63	0.66	1.07	0.84	0.89	0.66	0.68	1.47
	0.30	1.00	0.84	0.89	0.65	0.67	0.84	0.83	0.89	0.65	0.67	1.22	0.84	0.89	0.65	0.68	1.45
	0.40	1.15	0.83	0.89	0.65	0.68	0.96	0.83	0.89	0.64	0.67	1.40	0.87	0.89	0.66	0.68	1.45
	0.50	1.30	0.86	0.89	0.66	0.68	1.09	0.84	0.89	0.65	0.68	1.58	0.87	0.89	0.67	0.69	1.45
	0.60	1.45	0.86	0.89	0.66	0.69	1.22	0.84	0.89	0.66	0.68	1.78	0.86	0.89	0.66	0.69	1.46
	0.70	1.61	0.86	0.89	0.66	0.69	1.36	0.86	0.89	0.66	0.69	2.00	0.86	0.89	0.65	0.68	1.47
	0.80	1.80	0.86	0.89	0.65	0.68	1.52	0.87	0.89	0.68	0.70	2.26	0.85	0.89	0.64	0.66	1.49
	0.90	2.07	0.85	0.89	0.65	0.68	1.75	0.88	0.89	0.70	0.73	2.64	0.83	0.89	0.62	0.64	1.50
1.00	3.35	0.84	3.35	0.67	0.71	3.00	0.90	0.91	0.80	0.85	3.50	0.79	0.88	0.55	0.58	1.17	

Figure A6.26 - Resorb HC Camsizer morph measurements

	Percentile	Particle size		Symm0		b/l0		B/L_rec0		Particle size		Symm0		b/l0		B/L_rec0		Aspect ratio Xf _{max} /X _{cmin}
		SPHT0	Symm0	b/l0	B/L_rec0	SPHT0	Symm0	b/l0	B/L_rec0	SPHT0	Symm0	b/l0	B/L_rec0					
NORIT GAC 830 SUPRA	0.01	0.61	0.65	0.84	0.47	0.50	0.49	0.63	0.85	0.40	0.43	0.76	0.85	0.90	0.74	0.78	1.57	
	0.02	0.66	0.73	0.85	0.57	0.60	0.51	0.65	0.85	0.43	0.45	0.82	0.84	0.88	0.72	0.76	1.60	
	0.03	0.69	0.74	0.86	0.58	0.61	0.54	0.66	0.85	0.44	0.47	0.86	0.85	0.87	0.69	0.72	1.60	
	0.04	0.71	0.74	0.86	0.58	0.61	0.56	0.68	0.86	0.46	0.49	0.89	0.84	0.87	0.69	0.72	1.60	
	0.05	0.73	0.75	0.86	0.59	0.62	0.57	0.69	0.86	0.48	0.51	0.92	0.83	0.87	0.68	0.72	1.60	
	0.06	0.75	0.75	0.86	0.60	0.63	0.59	0.71	0.86	0.51	0.54	0.94	0.83	0.87	0.68	0.72	1.59	
	0.07	0.76	0.75	0.86	0.60	0.63	0.60	0.72	0.86	0.53	0.55	0.96	0.83	0.87	0.68	0.71	1.59	
	0.08	0.77	0.75	0.86	0.60	0.63	0.62	0.73	0.86	0.53	0.56	0.98	0.82	0.87	0.67	0.71	1.58	
	0.09	0.79	0.75	0.86	0.60	0.63	0.63	0.73	0.86	0.54	0.57	1.00	0.82	0.87	0.67	0.71	1.58	
	0.10	0.80	0.76	0.86	0.60	0.63	0.64	0.74	0.86	0.55	0.58	1.01	0.82	0.87	0.67	0.70	1.57	
	0.20	0.91	0.78	0.86	0.61	0.65	0.75	0.75	0.86	0.60	0.64	1.15	0.80	0.86	0.65	0.68	1.54	
	0.30	1.01	0.79	0.86	0.62	0.66	0.84	0.78	0.86	0.62	0.66	1.28	0.80	0.86	0.63	0.66	1.52	
	0.40	1.11	0.78	0.86	0.62	0.66	0.93	0.79	0.86	0.64	0.68	1.42	0.81	0.86	0.63	0.66	1.52	
	0.50	1.24	0.78	0.86	0.63	0.67	1.04	0.79	0.86	0.65	0.69	1.59	0.80	0.86	0.62	0.65	1.52	
	0.60	1.38	0.80	0.86	0.63	0.67	1.18	0.79	0.86	0.66	0.70	1.78	0.79	0.86	0.62	0.66	1.51	
	0.70	1.57	0.80	0.86	0.64	0.68	1.33	0.81	0.86	0.66	0.70	2.01	0.79	0.86	0.62	0.66	1.51	
	0.80	1.80	0.80	0.86	0.65	0.69	1.54	0.81	0.86	0.67	0.71	2.31	0.79	0.86	0.63	0.66	1.50	
0.90	2.12	0.80	0.86	0.66	0.70	1.83	0.81	0.86	0.68	0.72	2.73	0.78	0.86	0.62	0.66	1.50		
1.00	3.60	0.72	3.60	0.49	0.52	3.05	0.75	0.82	0.77	0.80	3.79	0.72	0.85	0.53	0.56	1.24		

Figure A6.27 - GAC 830 Supra Camsizer morph measurements

Appendix A7 – Wetting hours of expansion experiments

SAMPLE NAME	EXPERIMENT NUMBER	DATE & TIME WETTED		DATE & TIME OF EXPANSION EXPERIMENT		DAYS WETTED	HOURS WETTED
Filtrisorb 300C	Pablo 001	26-Feb-19	4:56:00 PM	4-Mar-19	8:19:00 AM	5.64	135.38
Filtrisorb 300C	Pablo 002	26-Feb-19	4:56:00 PM	5-Mar-19	11:20:00 AM	6.77	162.40
Filtrisorb 300C	Pablo 003	26-Feb-19	4:56:00 PM	7-Mar-19	8:19:00 AM	8.64	207.38
Filtrisorb 300C	Pablo 004	26-Feb-19	4:56:00 PM	7-Mar-19	11:20:00 AM	8.77	210.40
Aquasorb KGA	Pablo 005	28-Feb-19	9:00:00 AM	8-Mar-19	10:00:00 AM	8.04	193.00
Aquasorb KGA	Pablo 006	28-Feb-19	9:00:00 AM	8-Mar-19	1:30:00 PM	8.19	196.50
Aquasorb KGA	Pablo 007	28-Feb-19	9:00:00 AM	14-Mar-19	8:19:00 AM	13.97	335.32
Aquasorb KGA	Pablo 008	28-Feb-19	9:00:00 AM	14-Mar-19	11:20:00 AM	14.10	338.33
Saratech	Pablo 009	28-Feb-19	1:26:00 PM	19-Mar-19	8:40:00 AM	18.80	451.23
Saratech	Pablo 010	28-Feb-19	1:26:00 PM	19-Mar-19	10:40:00 AM	18.88	453.23
Saratech	Pablo 011	28-Feb-19	1:26:00 PM	19-Mar-19	1:40:00 PM	19.01	456.23
Saratech	Pablo 012	28-Feb-19	1:26:00 PM	19-Mar-19	4:10:00 PM	19.11	458.73

Norit ROW o.8 S	Pablo 013	28-Feb-19	9:27:00 AM	21-Mar-19	8:40:00 AM	20.97	503.22
Norit ROW o.8 S	Pablo 014	28-Feb-19	9:27:00 AM	21-Mar-19	1:40:00 PM	21.18	508.22
Norit ROW o.8 S	Pablo 015	28-Feb-19	9:27:00 AM	21-Mar-19	4:10:00 PM	21.28	510.72
Norit RB4C	Pablo 016	28-Feb-19	9:45:00 AM	22-Mar-19	8:40:00 AM	21.95	526.92
Norit RB4C	Pablo 017	28-Feb-19	9:45:00 AM	22-Mar-19	1:40:00 PM	22.16	531.92
Norit RB4C	Pablo 018	28-Feb-19	9:45:00 AM	22-Mar-19	4:10:00 PM	22.27	534.42
Filtrisorb TL830	Pablo 019	28-Feb-19	10:05:00 AM	26-Mar-19	8:40:00 AM	25.94	622.58
Filtrisorb TL830	Pablo 020	28-Feb-19	10:05:00 AM	26-Mar-19	1:22:00 PM	26.14	627.28
Filtrisorb TL830	Pablo 021	28-Feb-19	10:05:00 AM	26-Mar-19	4:13:00 PM	26.26	630.13
Aquasorb K-6300	Pablo 022	28-Feb-19	10:25:00 AM	29-Mar-19	11:00:00 AM	29.02	696.58
Aquasorb K-6300	Pablo 023	28-Feb-19	10:25:00 AM	29-Mar-19	1:40:00 PM	29.14	699.25
Aquasorb K-6300	Pablo 024	28-Feb-19	10:25:00 AM	1-Apr-19	4:10:00 PM	32.24	773.75
Resorb HC	Pablo 025	28-Feb-19	10:58:00 AM	2-Apr-19	9:47:00 AM	32.95	790.82
Resorb HC	Pablo 026	28-Feb-19	10:58:00 AM	2-Apr-19	1:40:00 PM	33.11	794.70
Resorb HC	Pablo 027	28-Feb-19	10:58:00 AM	2-Apr-19	4:10:00 PM	33.22	797.20
Norit GAC 830S	Pablo 028	28-Feb-19	1:30:00 PM	4-Apr-19	8:40:00 AM	34.80	835.17
Norit GAC 830S	Pablo 029	28-Feb-19	1:30:00 PM	4-Apr-19	1:40:00 PM	35.01	840.17
Norit GAC 830S	Pablo 030	28-Feb-19	1:30:00 PM	4-Apr-19	4:10:00 PM	35.11	842.67

Appendix A8 – Orientation experiments observations

In this Appendix, more detailed observations on the orientation aspects of the RB4C rod-like GAC will be presented.

- **Flow from 172-196 [L/h]**

Only slight movement on the upper bed is observed due to low flow velocities, initial packed bed in the X-Z plane is approximately 0-35 degrees. Few outlier particles in the taken sample had angles from 35-50 degrees. The measured particle angles and observations are presented in Figure .

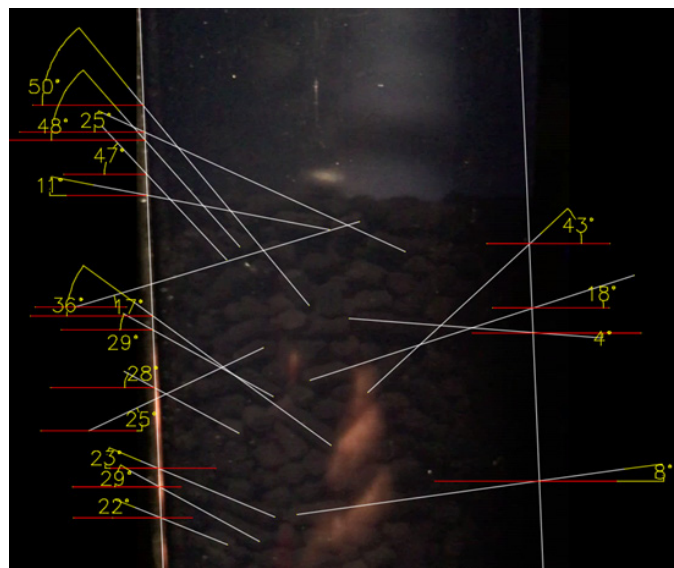


Figure A8.1 – Particle orientation angles at 172-196 [m/h]

- **Flow from 203-243 [m/h]**

Preferential flows were identified on middle of the X-Z plane of the upper bed. This causes particles to change their orientation from slightly inclined/horizontal (0-35 degrees or as initially packed) to higher angles (45-75 degrees). When these high angled particles find their way to the upper bed, there is enough space for them to change again their orientation to a stable horizontal position. When they are reoriented in a horizontal position, particles tend to push other particles on the sides of the bed making their orientation also change to a more inclined position. At these flow velocities, I observed higher velocity in the middle of the X-Z plane. Observations are presented in Figure .

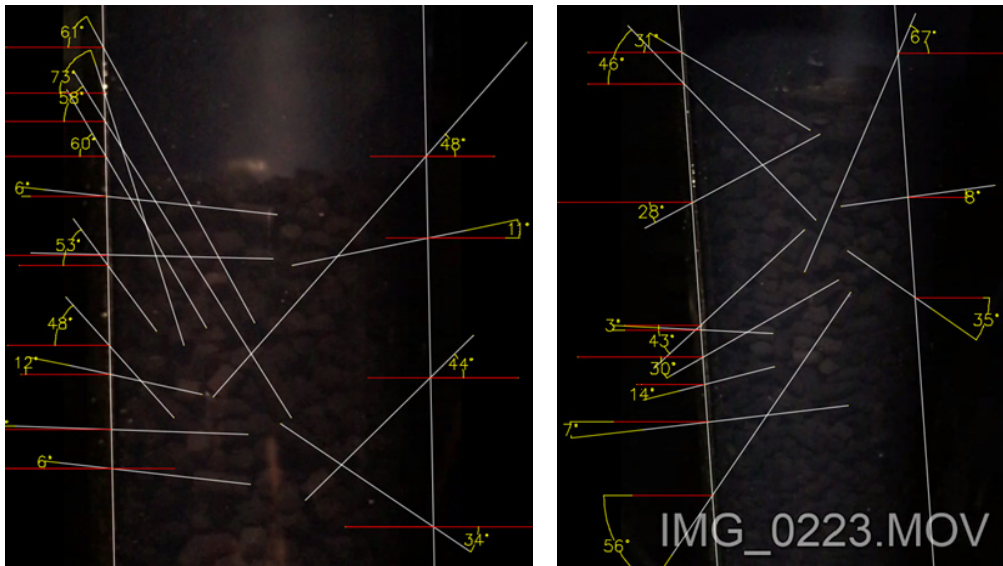


Figure A8.2– Particle orientation angles at 203-243 [m/h]

▪ Flow from 266-383 [L/h]

At this flow range, a preferential flow pattern was not identified. Changes in porosity in different parts of the bed create different flow paths and cause a variety of particle-to-particle interactions. Angles from 0-85 degrees were found, most particles are between 0-45 degrees and many reoriented particles were between 50-85 degrees. Overall, in the upper bed the angles of the particles were more inclined than in the lower part of the bed. The same single particle behavior applies as the rods go up in an inclined way and when enough space is available they tend to stay in a horizontal position. It is important to mention that the inclination of particles on lasts a few seconds. Observations are presented in Figure .

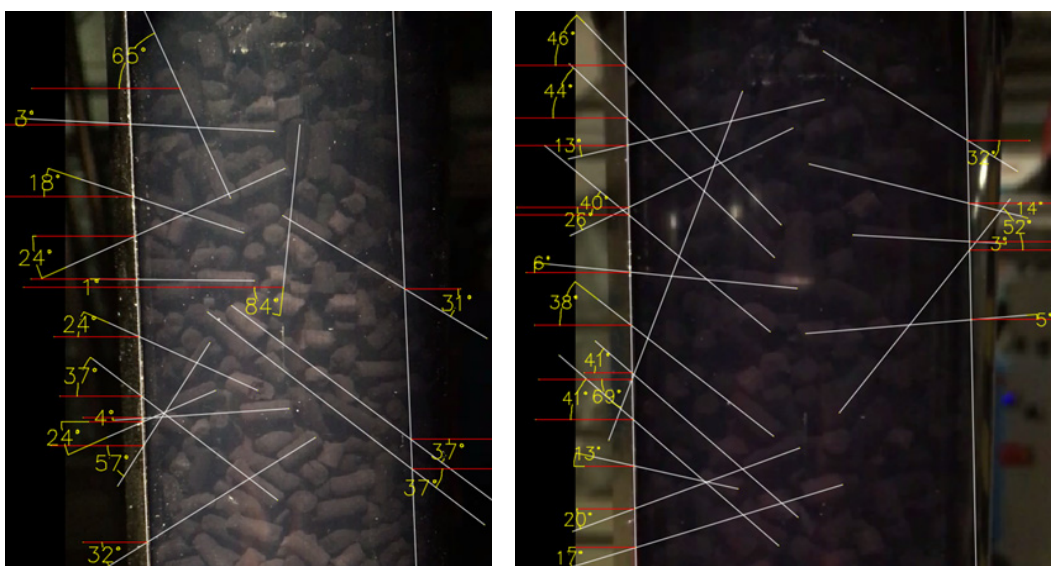


Figure A8.3– Particle orientation angles at 266-383 [m/h]

▪ **Flow 463-510 [L/h]**

At this regime, again no preferential flows were observed. The increase in porosity creates different flow paths that behave differently depending on the particle size. If a particle is able to fit through these channels, it will move up the bed; however, if the particle is not possible to fit through these created channels, particles tend to change their orientation due to particle-to-particle interaction. In general, angles ranging from 0-60 degrees were found. It is important to mention that starting from this regime, a lot of mixing is observed. Particle angles and other at this flow velocity are presented in Figure .

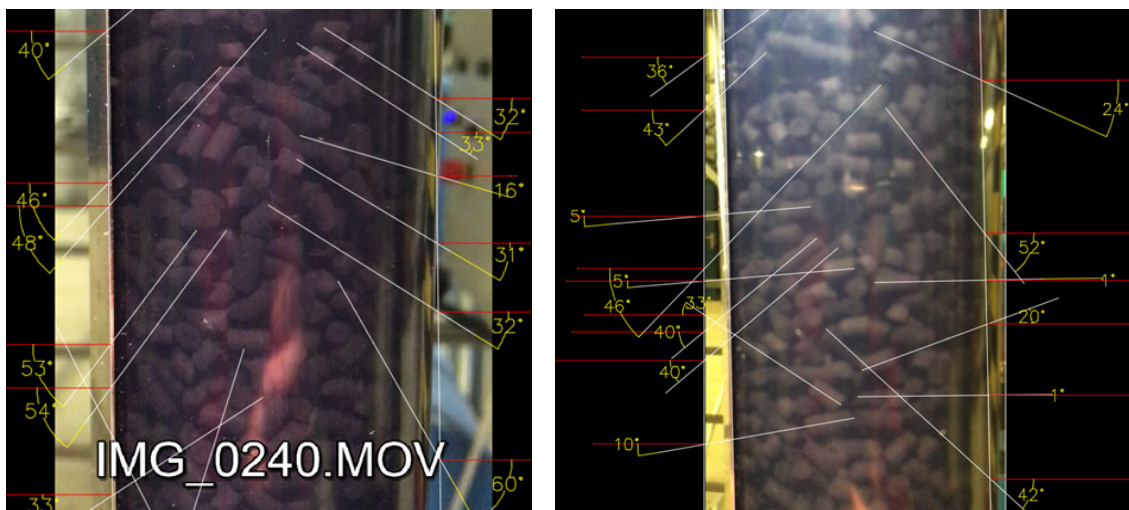


Figure A8.4 – Particle orientation angles at 463-510 [m/h]

▪ **Flow 560 [L/h]**

For this particular flow, particles on the upper bed have enough space available behave like a single particle (predominantly horizontal). Low aspect ratio of particles on the top bed fluidize easier than in the middle bed. Some preferential flows in the central part of the column are observed, but most particles have a horizontal position. Changes in porosity in in different parts of the bed cause high particle mixing. Most particles have angles between 0-35 degrees, but some inclined particles reached from 43-72 degrees. Particle angles are presented in Figure .



Figure A8.5- Particle orientation angles at 560 [m/h]

▪ **Flow 709 [L/h]**

Most particles in horizontal position due to higher bed porosity. Particles are more dilute and since there is enough space, particles tend to approximate to the single particle behavior equilibrium. At this flow velocity, it was observed that some particles tend to spin in the z-axis. Overall angles vary from 0-50 degrees, but predominantly under 30 degrees. Observations are presented in Figure .

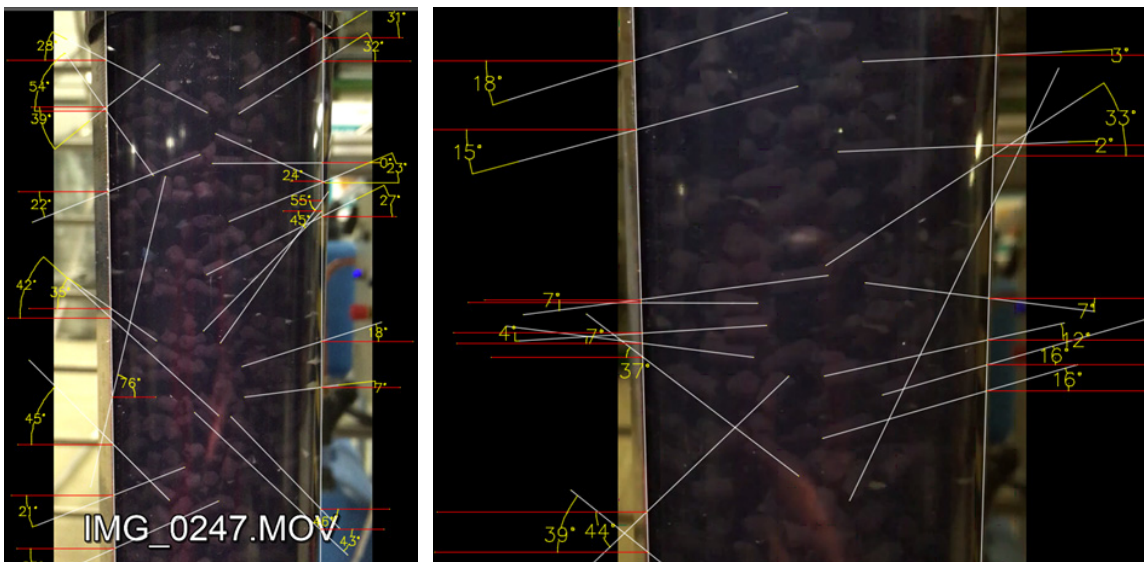


Figure A8.6 - Particle orientation angles at 709 [m/h]

▪ **Flow 733-843 [L/h]**

The increased porosity help particles be predominantly horizontal. Particle-to-particle interaction cause instantaneous changes in orientation of the particles, but they quickly recover to a predominant horizontal position. There is less influence of particle-to-particle interaction in the change of orientation due to the high porosity and overall available space in the bed. The typical angles found ranged from 0-35 degrees, the few inclined particles reached 45-65 degrees for the analyzed cases. Particle angles are presented in Figure .

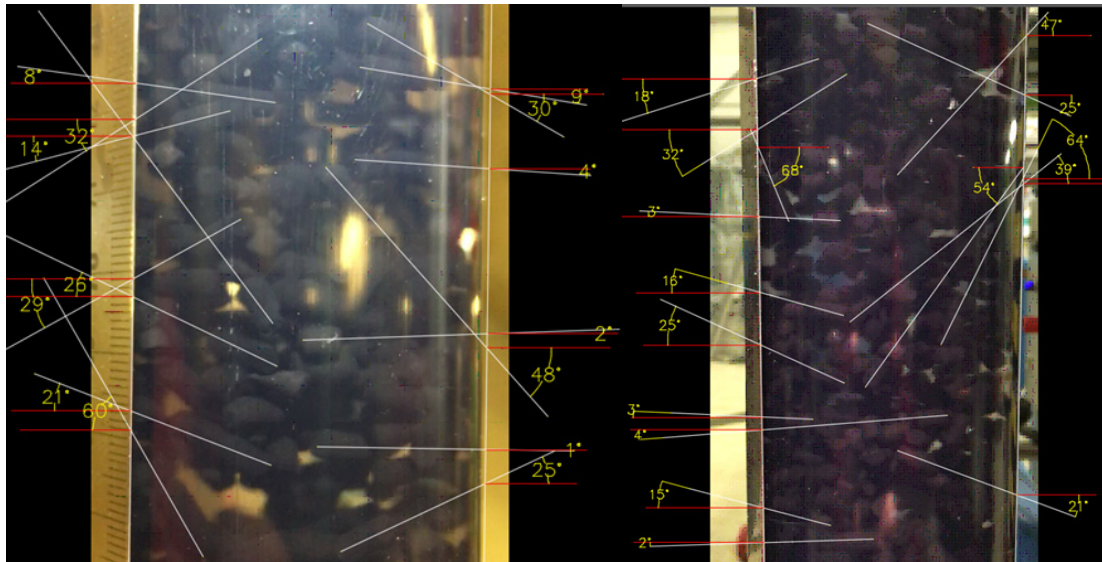


Figure A8.7 – Particle orientation angles at 733-843 [m/h]

- **Flow 873 [L/h]**

In this regime, particles have enough space to fluidize almost freely, which is why the orientation of particles is predominantly horizontal. Particles in the upper bed tend to be in equilibrium following a leaf-like sedimentation behavior. Slight particle-to-particle interaction causes surrounding particles to spin or briefly change their orientation and then stabilize rapidly in a horizontal position because of the available space. Observations are presented in Figure .

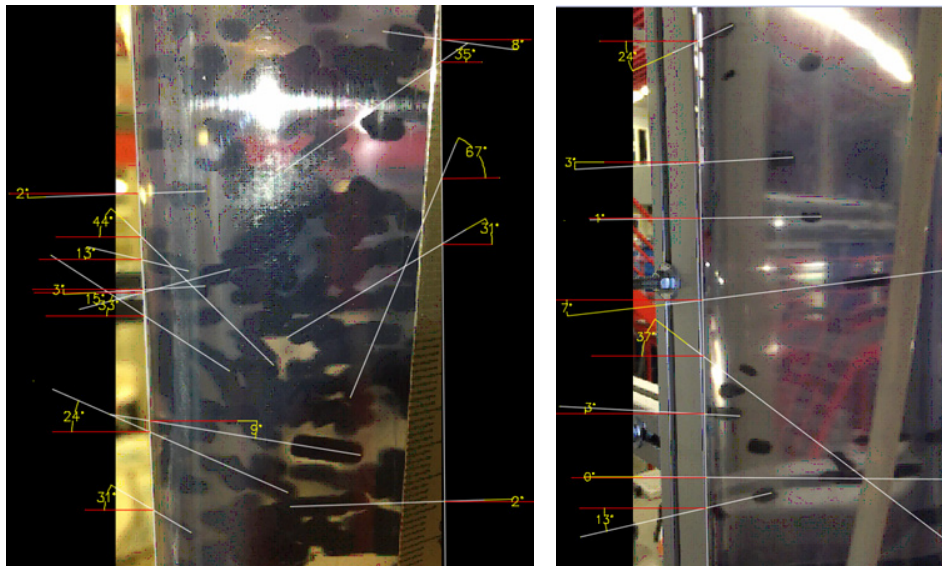


Figure A8.8– Particle orientation angles at 873 [m/h]

As a side experiment, the smaller rods (ROW o.8 supra) single particle fluidization was also tested. These smaller carbon rods follow approximately the same behavior as the RB₄C carbon. They tend to fluidize in an inclined position (57°) when sudden high flow velocities are induced. Observations are presented in Figure .

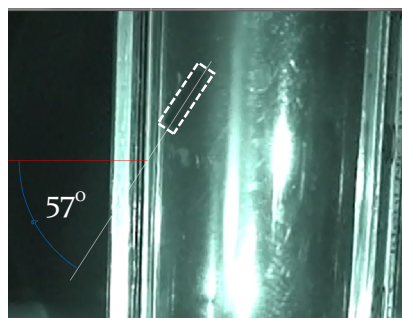


Figure A8.9 – ROW o.8 Supra fluidization [m/h]

It was observed that this carbon also tends to settle in a horizontal position following the minimum energy dissipation principle as seen in Figure . It is important to mention that it was much more difficult to get this carbon into equilibrium because of its sensitivity to flow velocity and tendency to attach to the internal walls of the tube.

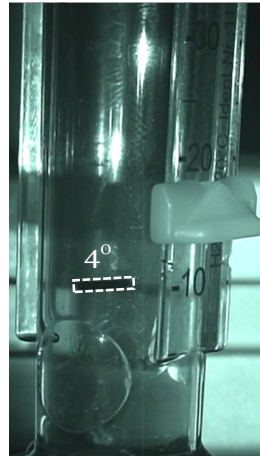


Figure A8.10 – ROW 0.8 Supra settling [m/h]

Appendix A9 – AquaGAC model

System definition

In order to clearly understand the model inputs, it is important first to define the system used for the current study. The system consists of a column with granular activated carbon (GAC) filled with water, however, one of the main properties of GAC is that it contains many internal pores, which are also filled with water. This changes the mass of the carbon and thus the density in fluidized conditions. The system is illustrated in Figures A9.1a, A9.1b and A9.1c, Figure A9.1a illustrates how the system looks to the naked eye, a GAC column with a bed of classified particles. If the inter-particle voids (porosity) would be eliminated from the GAC particles, the system would look something like Figure A9.1b. Even though not visible at first sight, the internal porosity of the GAC grains also contains a certain volume in the system, where the internal pores are filled with water and the closed pores are filled with air, this is illustrated in Figure A9.1c.

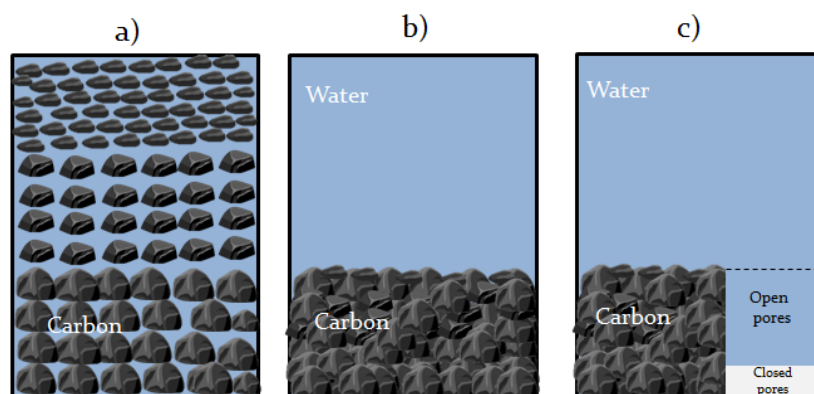


Figure A9.1 – System definition.

Volume definition

As briefly described in the section 3, it is of utmost importance to clearly define the volumes as many parameters are derived from them. Figure A9.2 illustrates the different volumes considered for the system used for the calculations and expression derivations.

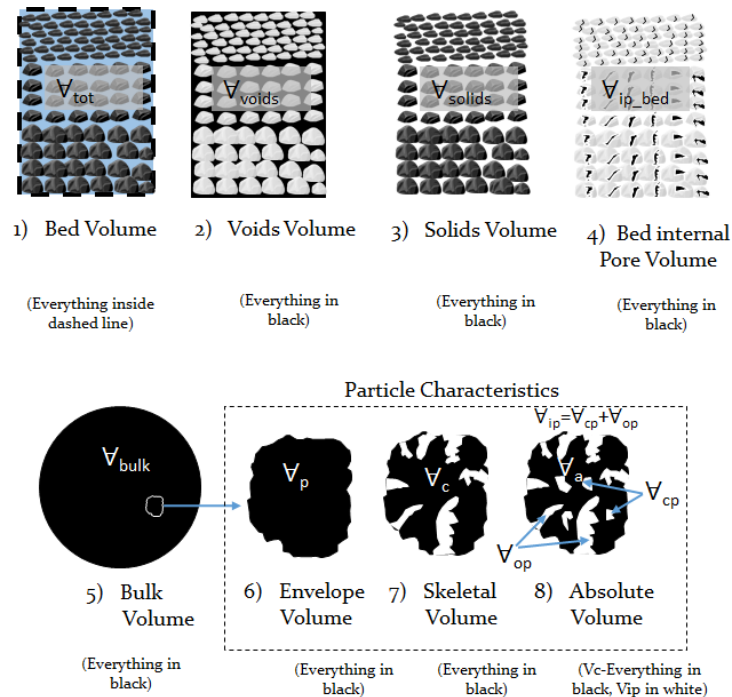


Figure A9.1 – Volume definition.

Nomenclature

Known:

m_c	Particle mass (solid and dry internal pores)	[kg]
V_{tot}	Total volume of bed or graduated cylindrical column	[m ³]
ρ_{bulk}	The bed or bulk density is the mass of adsorbent in a specific volume. This can simply be measured using a graduated cylindrical column	[kg/m ³]
ρ_c	Solid or skeleton density of carbon (measured mostly with closed pores)	[kg/m ³]
ρ_p	The dry envelope particle density or the mass of adsorbent per volume occupied by the particle (solid and internal dry pore volume)	[kg/m ³]
ρ_{wet}	Same as ρ_p although when internal pores are filled with water	[kg/m ³]
ρ_w	Density of ordinary water	[kg/m ³]
ρ_{air}	Density of ordinary air	[kg/m ³]
r_{cp}	Closed pore ratio (dry)	[%]

Unknown:

V_c	Pure or theoretical (rigid) carbon volume (no pores)	[m ³]
m_{op}	Open pore mass (wetted)	[kg]
V_{op}	Open pore volume (dry or wetted)	[m ³]
V_{cp}	Closed pore volume (dry)	[m ³]
V_{tp}	Volume of total pores (open and closed internal pores)	[m ³]
m_{cp}	Closed pore mass (dry air, can be ignored in general)	[kg]
V_{ext}	Volume occupied by or air or water (outside) between particles	[m ³]
V_p	Volume of porous particles (solid and internal pores)	[m ³]
ε_{ext}	External porosity, of activated carbon beds corresponds to the ratio of the volume of interparticle spaces to the total bed volume	[m ³ /m ³]
ε_i	Internal porosity is formed by the voids inside the particle	[m ³ /m ³]
m_{wet}	Total mass of wetted carbon particle	[kg]

Fluidisation:

ΔP_{max}	Maximum pressure difference over the particle bed	[Pa]
L_{mf}	Bed height at minimum fluidisation	[m]
ε_{mf}	Bed porosity at minimum fluidisation	[m ³ /m ³]

Calculations

▪ Mass balance

The wet mass of a sample of GAC particles is the sum of the mass of carbon skeleton, mass of the fluid in the open pores and the mass of air trapped in the closed pores, it can be calculated using equation A9.1.

$$m_{wet} = m_c + m_{op} + m_{cp} \quad (A9.1)$$

When the mass of air is ignored equation A9.1 then becomes:

$$m_{wet} = m_c + m_{op} \quad (A9.2)$$

▪ Volume balance

The envelope volume of the particles in the bed plus the external volume composes the total volume of the reactor bed (refer to equation A9.3). The carbon particles have an internal porosity consisting of open and closed pores, equation A9.3 then becomes equation A9.6.

$$V_{tot} = V_p + V_{ext} \quad (A9.3)$$

$$V_p = V_c + V_{op} + V_{cp} \quad (A9.4)$$

Or:

$$V_{ext} = V_{tot} - V_c - V_{op} - V_{cp} \quad (A9.5)$$

Or:

$$V_{tot} = V_c + V_{op} + V_{cp} + V_{ext} \quad (A9.6)$$

Ignoring the volume of closed pores, V_{cp} , equation A9.6 becomes A9.7.

$$V_{tot} = V_c + V_{ext} + V_{op} \quad (A9.7)$$

Rearranging equation A9.7, the open pore volume is:

$$V_{op} = V_p - V_c - V_{cp} \quad (A9.8)$$

Or:

$$V_{op} = V_{tot} - V_c - V_{ext} - V_{cp} \quad (A9.9)$$

▪ Bulk, wet and particle density

The bulk density can be determined in a straight forward manner as explained in section 4, using equation A9.10.

$$\rho_{bulk} = \frac{m_c}{V_{tot}} \quad (A9.10)$$

The wet density can be determined if both the wet mass and the envelope volume of the particles is known as shown in equation A9.11.

$$\rho_{wet} = \frac{m_{wet}}{V_p} \quad (A9.11)$$

$$\rho_{wet} = \frac{m_c + m_{op}}{V_p} \quad (A9.12)$$

So:

$$\rho_{wet} = \frac{m_c + m_{op}}{V_c + V_{op} + V_{cp}} \quad (A9.13)$$

The particle envelope density can be determined if both the dry mass and the envelope volume of the particles is known as shown in equation A9.14.

$$\rho_p = \frac{m_c}{V_p} \quad (A9.14)$$

By substituting equation A9.4 in equation A9.14 we obtain:

$$\rho_p = \frac{m_c}{V_c + V_{op} + V_{cp}} \quad (A9.15)$$

- External porosity

The external porosity can be determined with the ratio of the external volume and the total volume of the bed. The external porosity can be calculated using equation A9.16.

$$\varepsilon_{ext} = \frac{V_{ext}}{V_{tot}} \quad (A9.16)$$

And:

$$V_{tot} = V_p + V_{ext} \quad (A9.17)$$

Or:

$$V_{ext} = V_{tot} - V_p \quad (A9.18)$$

Combining equation A9.16 with A9.18, the external porosity can also be calculated in terms of the particle volume, as seen in equation A9.20.

$$\varepsilon_{ext} = \frac{V_{tot} - V_p}{V_{tot}} \quad (A9.19)$$

$$\varepsilon_{ext} = 1 - \frac{V_p}{V_{tot}} \quad (A9.20)$$

Substituting equation A9.14 in A9.20, we obtain equation A9.21.

$$\varepsilon_{ext} = 1 - \frac{m_c}{\rho_p V_{tot}} \quad (A9.21)$$

This can be rewritten to:

$$\varepsilon_{ext} = 1 - \frac{\rho_{bulk}}{\rho_p} \quad (A9.22)$$

- Open pore volume and wet particle mass

Combining wet (equation A9.12) and particle density (equation A9.14), it is possible to calculate the mass of the fluid inside the open pores, presented in equation A9.23.

$$m_{op} = m_c \left(\frac{\rho_{wet}}{\rho_p} - 1 \right) \quad (A9.23)$$

If the mass of the fluid inside the open pores is known, the wet particle mass can now be calculated with equation A9.2. The relationship between the wet and particle density is:

$$\rho_{wet} = \rho_p \left(1 + \frac{m_{op}}{m_c} \right) \quad (A9.24)$$

- Open pore volume ratio

The open pore volume (OPV) can be often found in literature or provided by manufacturers, it is measured in units of volume over units of mass:

$$OPV = \frac{V_{op}}{m_c} \quad (A9.25)$$

It is also possible to estimate the OPV from the experimental data using equation A9.12 and equations A9.14 to A9.A9.23. Parting from the fact that the open pores of GAC are filled with water, it is possible to calculate the OPV using the density of water.

$$\rho_w = \frac{m_{op}}{V_{op}} \quad (\text{A9.26})$$

Or:

$$V_{op} = \frac{m_{op}}{\rho_w} \quad (\text{A9.27})$$

Substituting equation A9.23 in equation A9.27 leads to:

$$V_{op} = \frac{m_c}{\rho_w} \left(\frac{\rho_{wet}}{\rho_p} - 1 \right) \quad (\text{A9.28})$$

Substituting equation A9.28 in A9.25, the OPV then becomes:

$$OPV = \frac{\left(\frac{\rho_{wet}}{\rho_p} - 1 \right)}{\rho_w} \quad (\text{A9.29})$$

Particle density can be checked using the measured wet and given OPV using the following equation:

$$\rho_p = \frac{\rho_{wet}}{\rho_w OPV + 1} \quad (\text{A9.30})$$

This same check can be performed for the wet density knowing both the particle density and the OPV with the following equation:

$$\rho_{wet} = \rho_p (\rho_w OPV + 1) \quad (\text{A9.31})$$

- Internal pore volume

The internal porosity can be estimated if the volume of open pores and the envelope volume of the particles is known:

$$\varepsilon_i = \frac{V_{op} + V_{cp}}{V_p} \quad (\text{A9.32})$$

Based on the wet and particle densities, the internal porosity can be calculated substituting equations A9.26 and A9.32 in equation A9.28 (volume of closed pores is for now ignored):

$$\varepsilon_i = \frac{\rho_{wet} - \rho_p}{\rho_w} \quad (A9.33)$$

A check of the wet density can be made using equation A9.34:

$$\rho_{wet} = \varepsilon_i \rho_w + \frac{\rho_{bulk}}{1 - \varepsilon_{ext}} \quad (A9.34)$$

A check for the bulk density can be made using equation A9.35:

$$\rho_{bulk} = (1 - \varepsilon_{ext})(\rho_{wet} - \varepsilon_i \rho_w) \quad (A9.35)$$

- Skeleton density

The skeleton density is defined as the mass of carbon over the skeletal volume of the sample, as presented in equation A9.36:

$$\rho_c = \frac{m_c}{V_c} \quad (A9.36)$$

Rearranging equation A9.36 to solve for the skeleton volume:

$$V_c = \frac{m_c}{\rho_c} \quad (A9.37)$$

Alternatively, by substituting equation A9.9 in equation A9.32, it is possible to calculate the internal porosity with the following expression:

$$\varepsilon_i = 1 - \frac{V_c}{V_p} - \frac{V_{cp}}{V_p} \quad (A9.38)$$

Substituting equations A9.14, and A9.36 in equation A9.38:

$$\varepsilon_i = 1 - \frac{\rho_p}{\rho_c} - \frac{\rho_p}{m_c} V_{cp} \quad (A9.39)$$

Accordingly, substituting equation A9.32 and A9.9 in equation A9.39:

$$\varepsilon_i = \frac{(1 - \varepsilon_{ext})V_{tot} - \frac{m_c}{\rho_c} - V_{cp}}{\frac{m_c}{\rho_p}} \quad (\text{A9.40})$$

With equations A9.14 and A9.36 both the skeleton and particle density can be checked using the following expressions:

$$\rho_c = \rho_p \frac{V_p}{V_c} \quad (\text{A9.41})$$

$$\rho_p = \rho_c \frac{V_c}{V_p} \quad (\text{A9.42})$$

Checking the skeleton density based on the particle density:

$$\rho_c = \frac{\rho_p m_c}{(1 - \varepsilon_i)m_c + \rho_p r_{cp} V_p} \quad (\text{A9.43})$$

- Closed pores

The assumed closed pore ratio is the closed pore volume divided by the particle volume:

$$r_{cp} = \frac{V_{cp}}{V_p} \quad (\text{A9.44})$$

- Correction factor for closed pores

Assuming that there is a certain closed pore volume, the volumes can be corrected using the following correction factor:

$$f_p = \frac{V_p}{\frac{V_{op} + V_c}{1 - r_{cp}}} \quad (\text{A9.45})$$

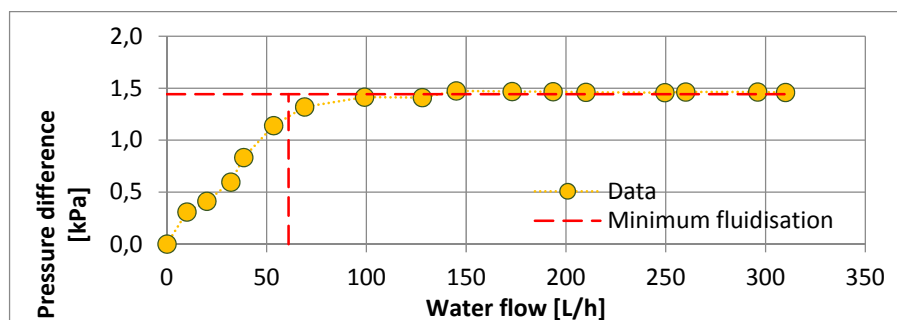
Appendix A10 – Expansion experiments data and results

Pressure difference

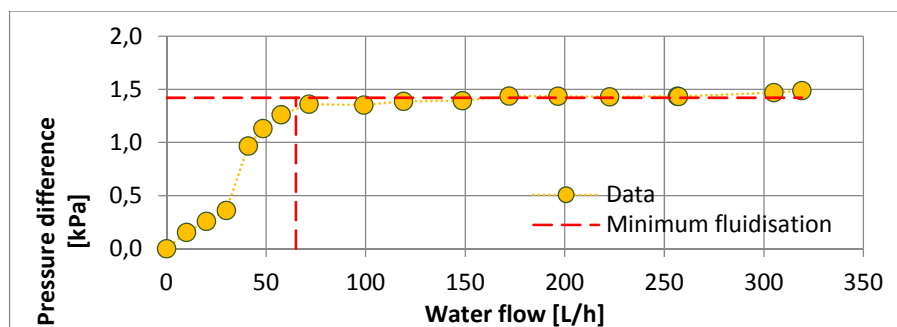
The following graphs will present the differential pressure measurements. As a guide, the following table illustrates which samples correspond with the experiment number.

Table 40 – Experiment number and sample name guide

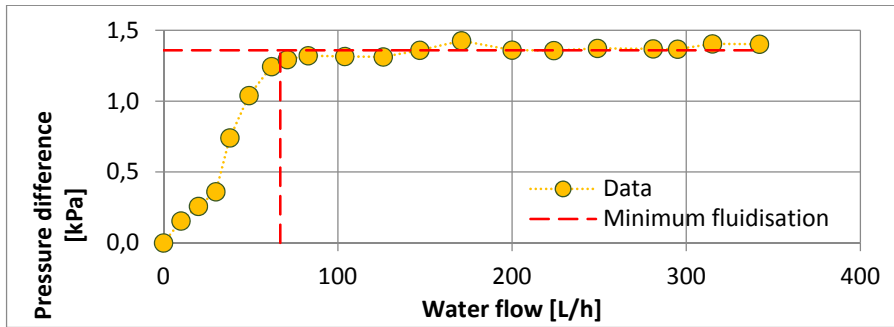
SAMPLE NAME	EXPERIMENT NUMBER
Filtrisorb 300 C	001-004
Aquasorb K-GA 830	005-008
Saratech Spherical	009-012
Norit ROW 0.8 Supra	013-015
Norit RB 4C	016-018
Filtrisorb TL830	019-021
Aquasorb K-6300	022-024
Resorb HC	025-027
Norit GAC 830 S	028-030



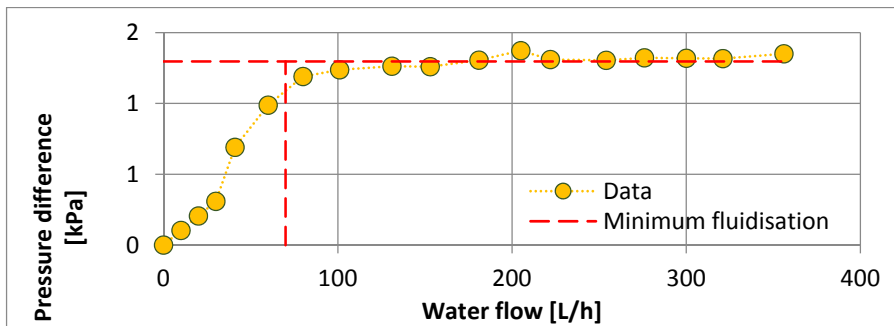
A10.1 – Differential pressure graph for experiment 001



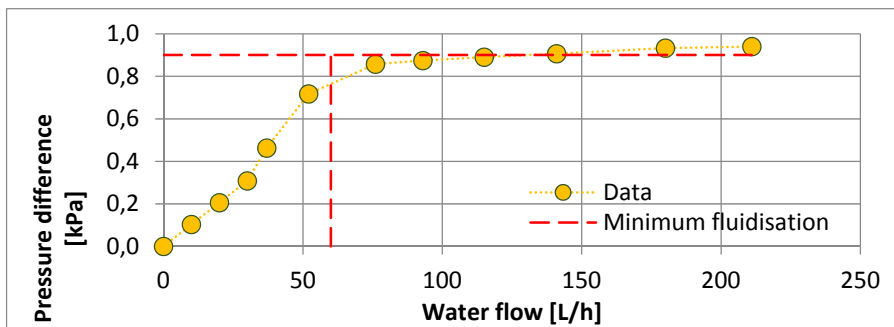
A10.2 – Differential pressure graph for experiment 002



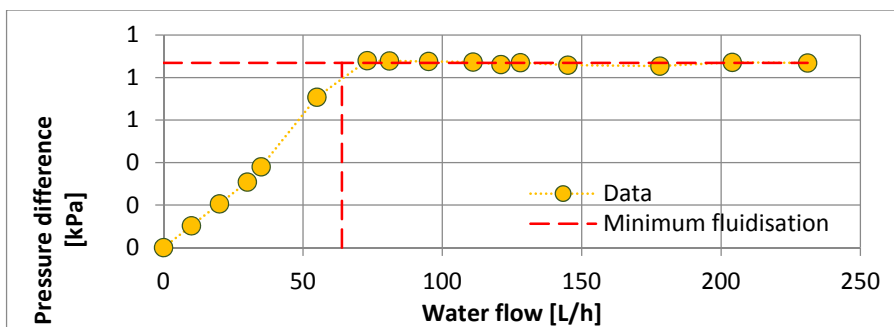
A10.3 - Differential pressure graph for experiment 003



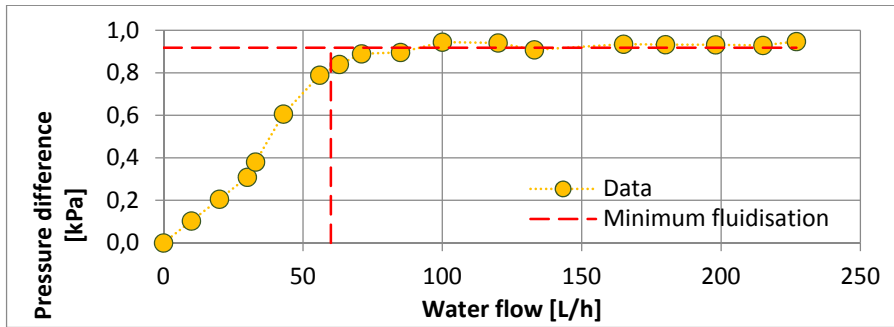
A10.4 - Differential pressure graph for experiment 004



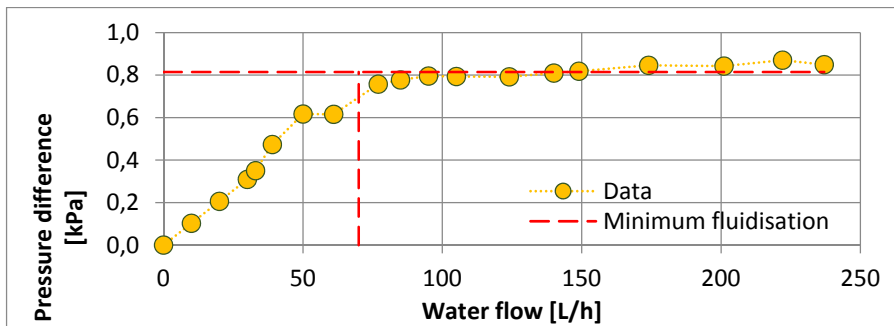
A10.5 - Differential pressure graph for experiment 005



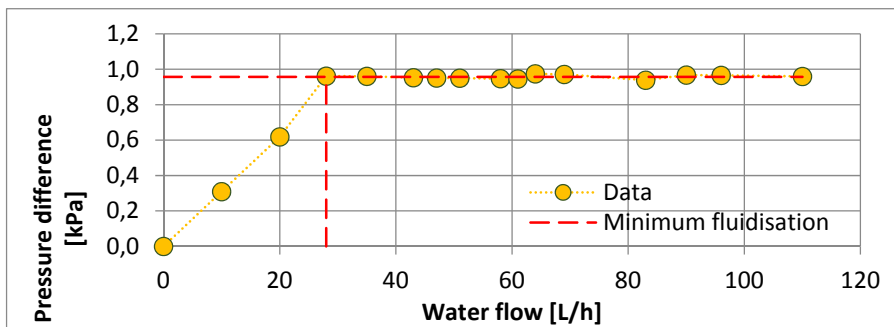
A10.6 - Differential pressure graph for experiment 006



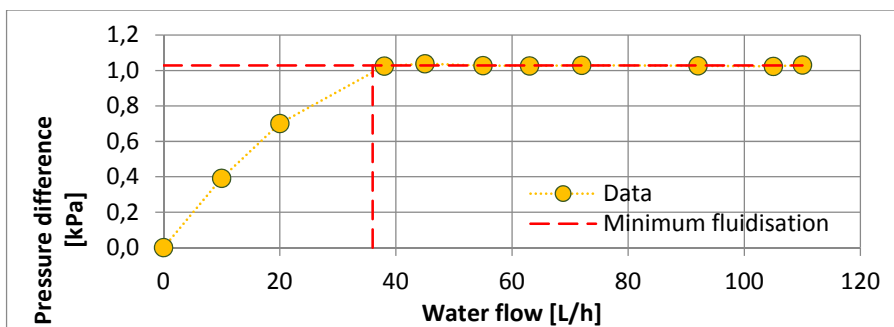
A10.7 - Differential pressure graph for experiment 007



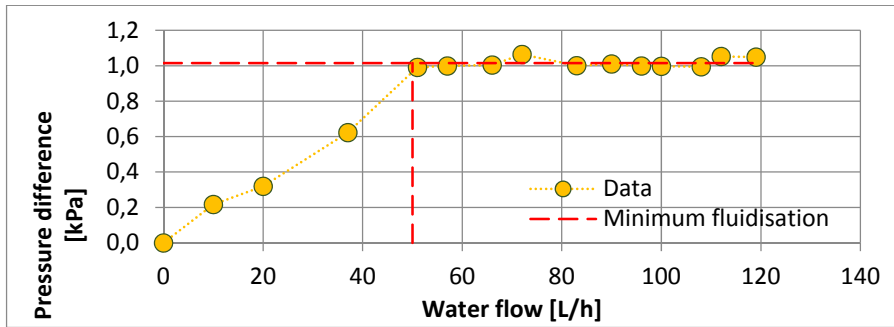
A10.8 - Differential pressure graph for experiment 008



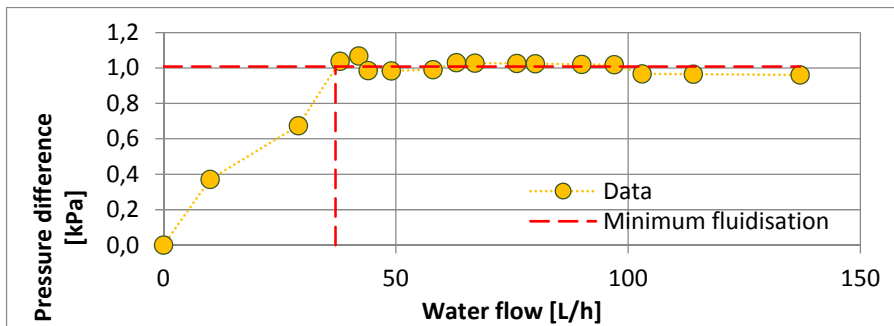
A10.9 - Differential pressure graph for experiment 009



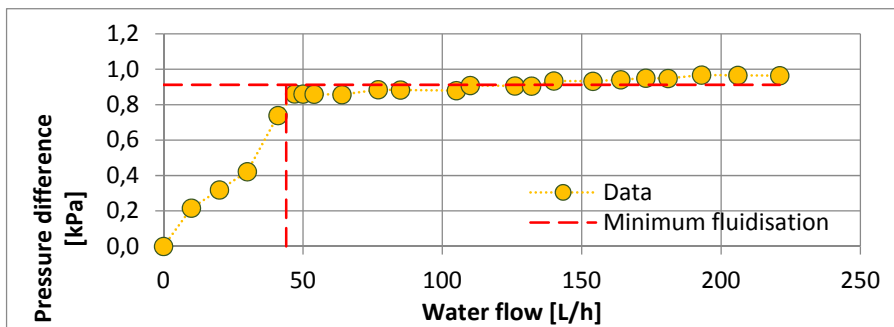
A10.10 - Differential pressure graph for experiment 010



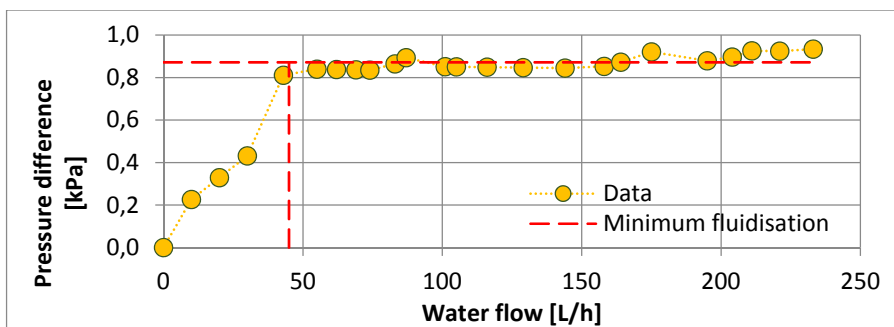
A10.11 - Differential pressure graph for experiment 011



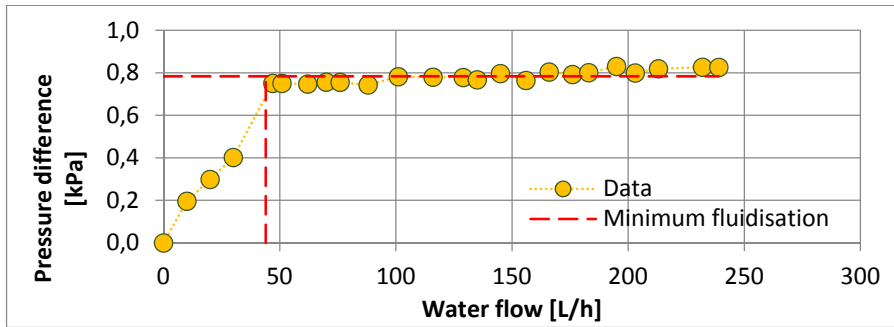
A10.12 - Differential pressure graph for experiment 012



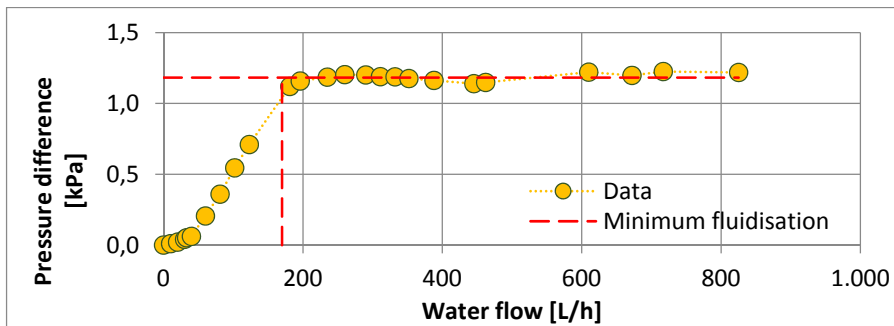
A10.13 - Differential pressure graph for experiment 013



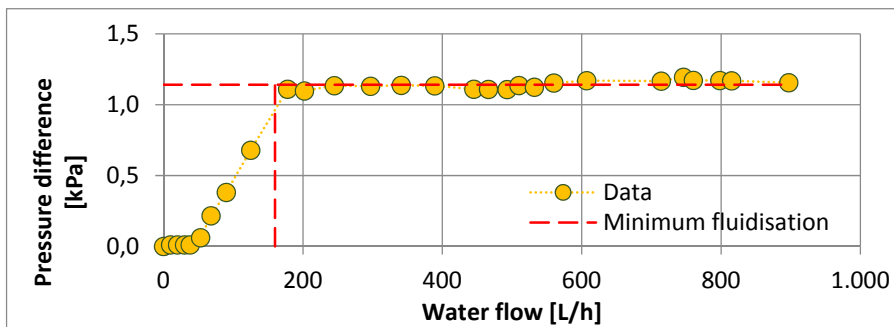
A10.14 - Differential pressure graph for experiment 014



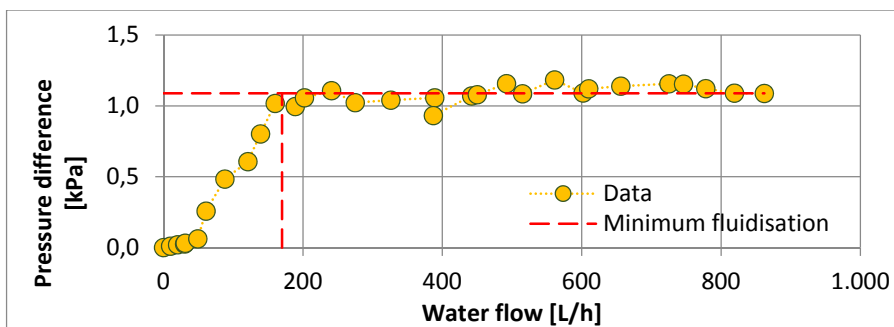
A10.15 - Differential pressure graph for experiment 015



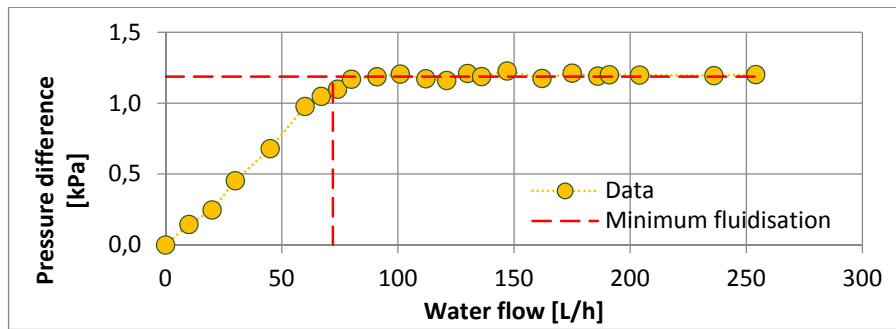
A10.16 - Differential pressure graph for experiment 016



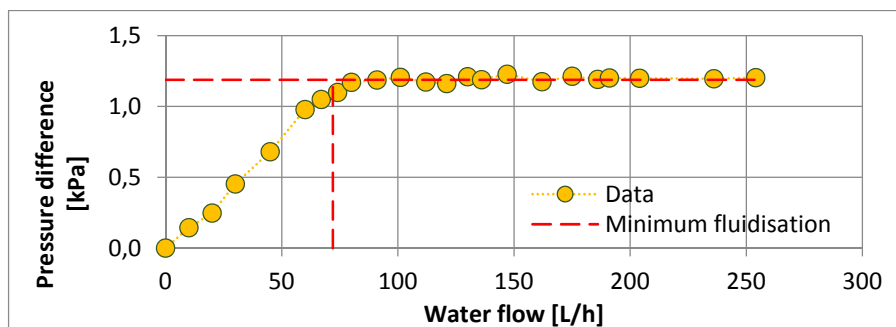
A10.17 - Differential pressure graph for experiment 017



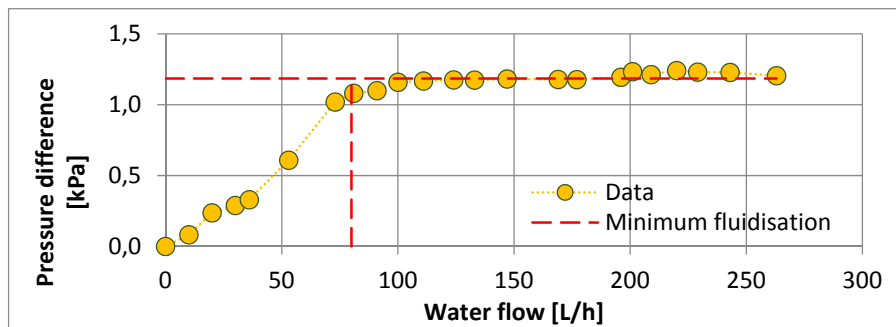
A10.18 - Differential pressure graph for experiment 018



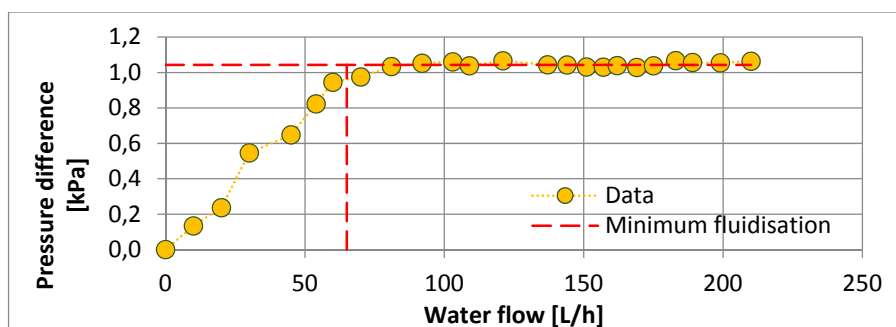
A10.19 - Differential pressure graph for experiment 019



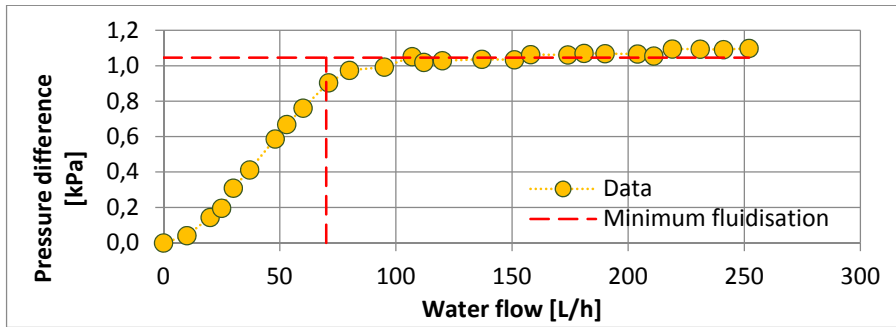
A10.20 - Differential pressure graph for experiment 020



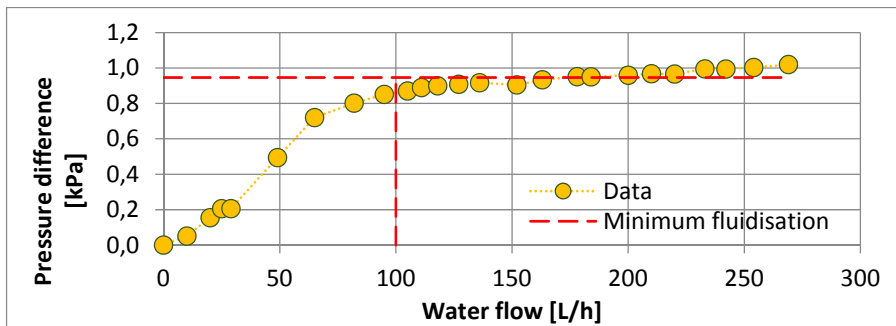
A10.21 - Differential pressure graph for experiment 021



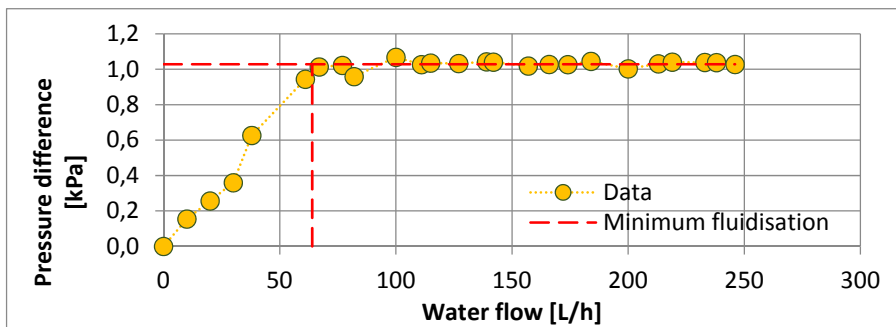
A10.22 - Differential pressure graph for experiment 022



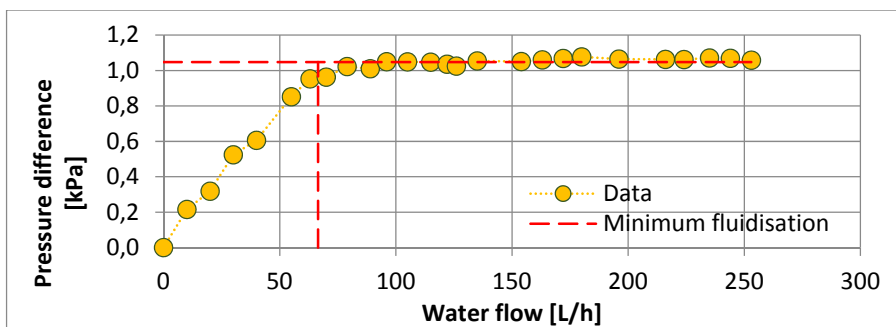
A10.23 - Differential pressure graph for experiment 023



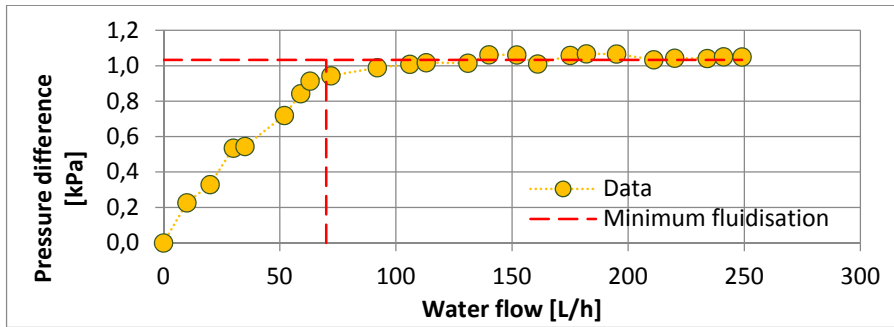
A10.24 - Differential pressure graph for experiment 024



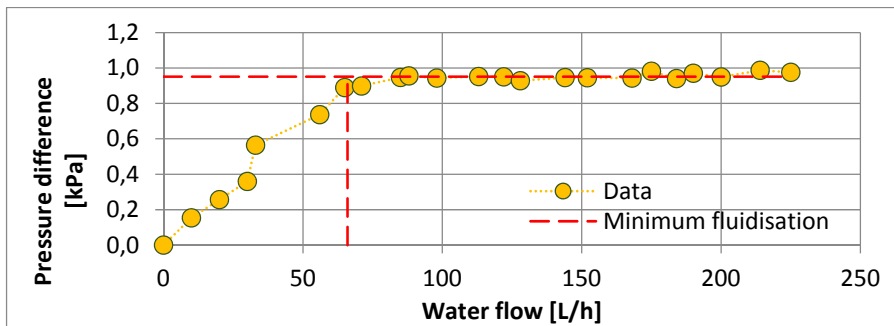
A10.25 - Differential pressure graph for experiment 025



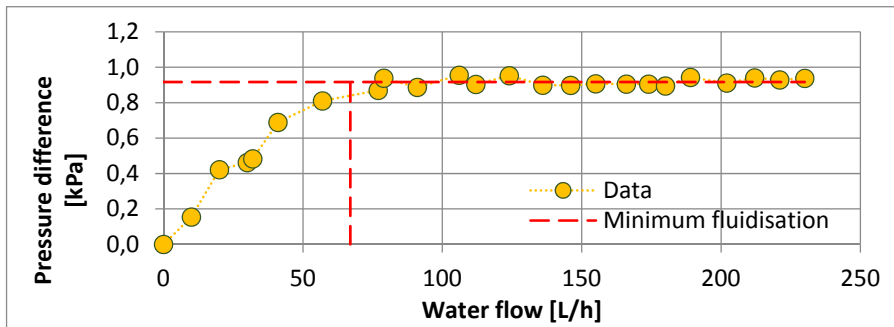
A10.26 - Differential pressure graph for experiment 026



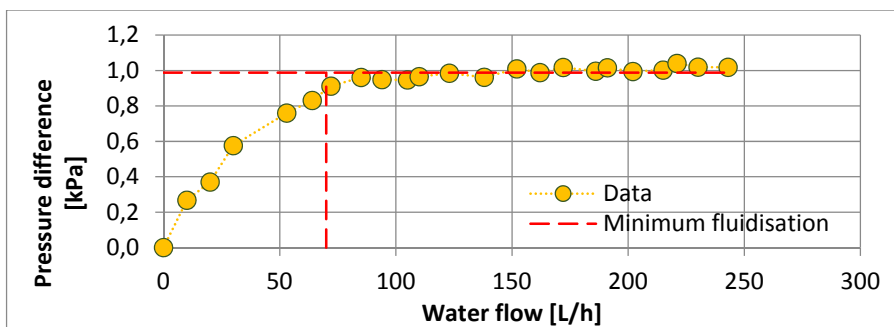
A10.27 - Differential pressure graph for experiment 027



A10.28 - Differential pressure graph for experiment 028



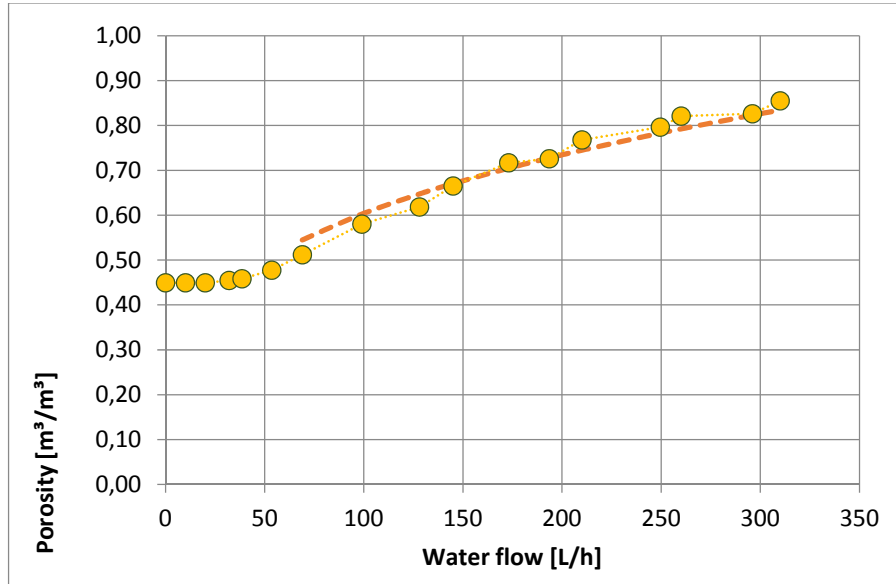
A10.29 - Differential pressure graph for experiment 029



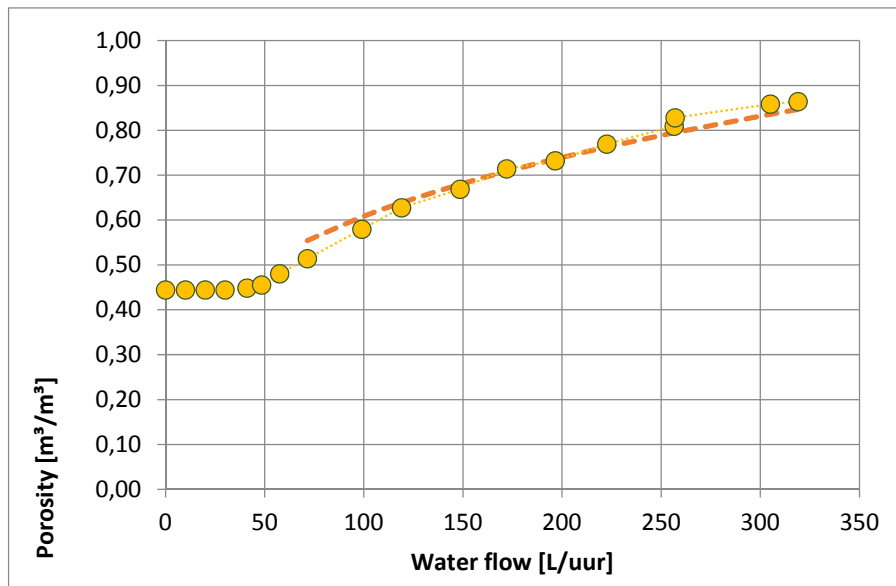
A10.30 - Differential pressure graph for experiment 030

Carman-Kozeny porosity prediction

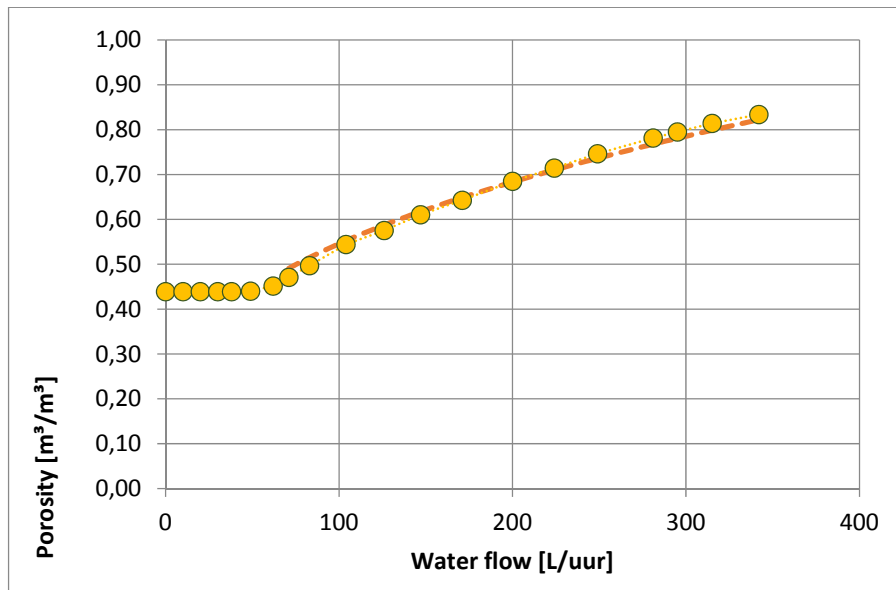
In the following graphs, the calculated porosity using the Carman-Kozeny model is presented. The input diameter is hydraulic diameter, also calculated using the Carman-Kozeny equation. The dashed line indicates the model prediction and the circles indicate the porosity using the measurements and the C-K hydraulic diameter.



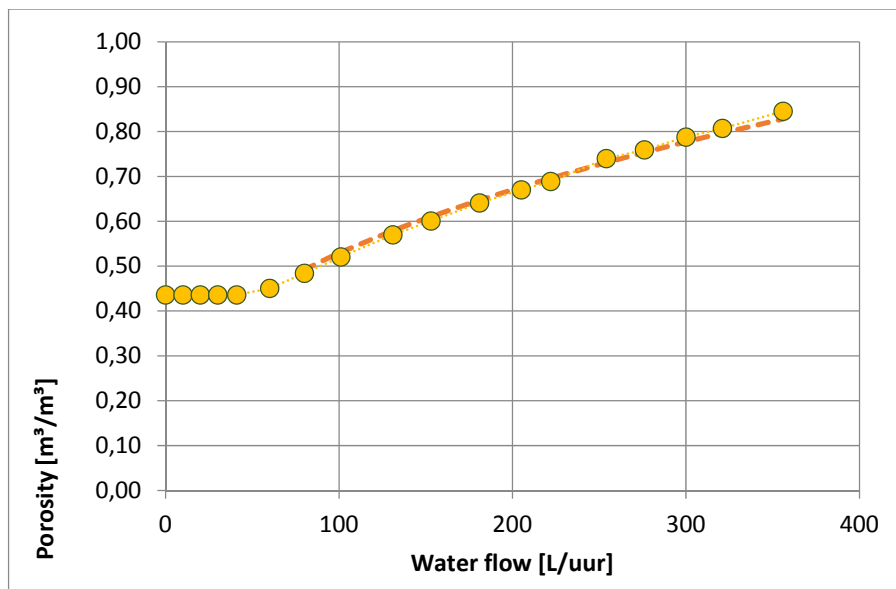
A10.31 – Carman-Kozeny predicted porosity for experiment 001



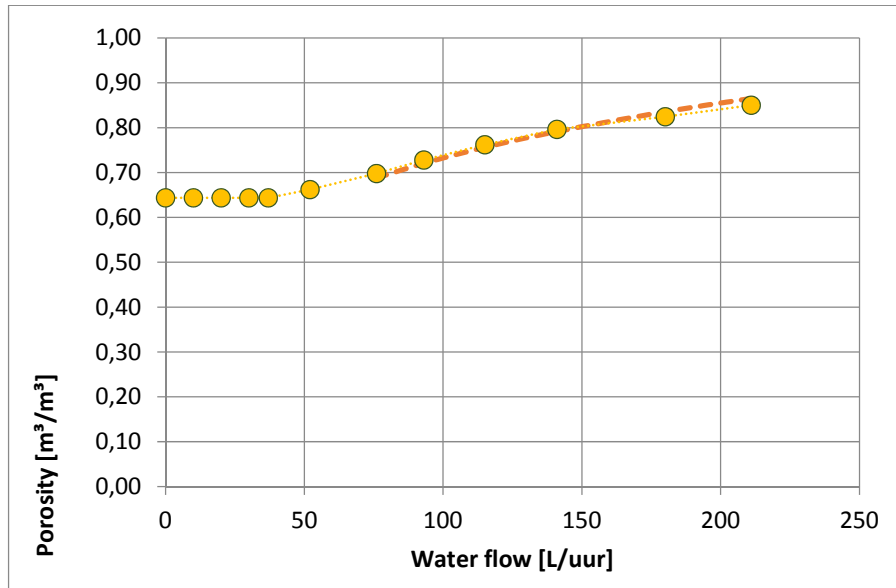
A10.32 – Carman-Kozeny predicted porosity for experiment 002



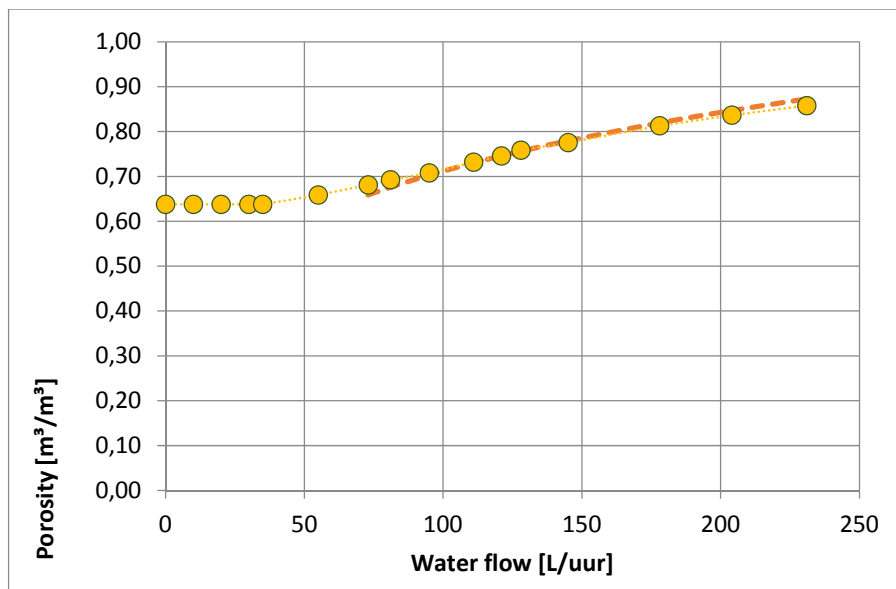
A10.33 – Carman-Kozeny predicted porosity for experiment 003



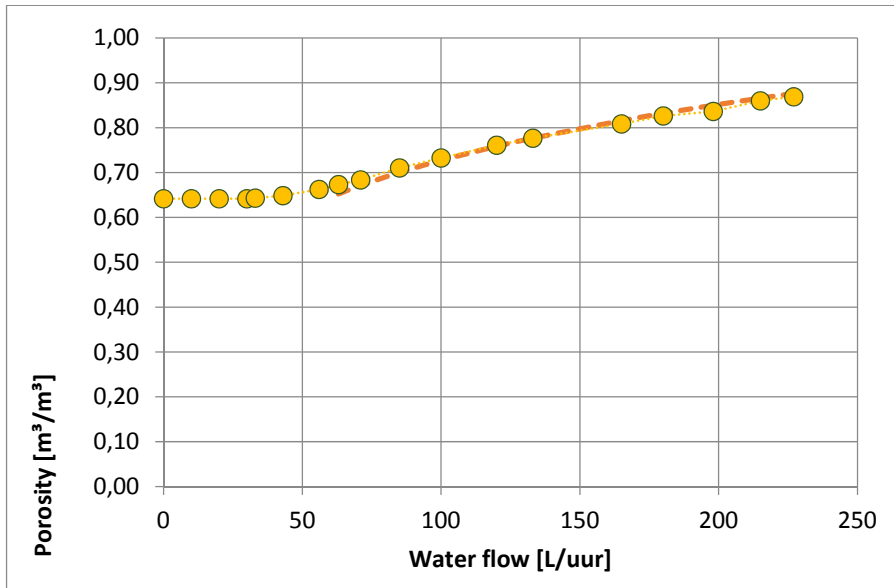
A10.34 – Carman-Kozeny predicted porosity for experiment 004



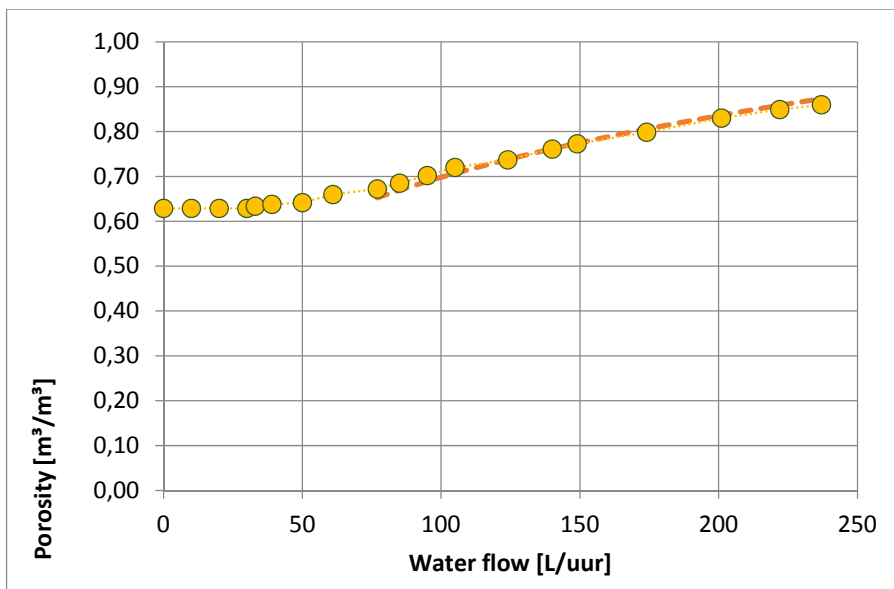
A10.35 – Carman-Kozeny predicted porosity for experiment 005



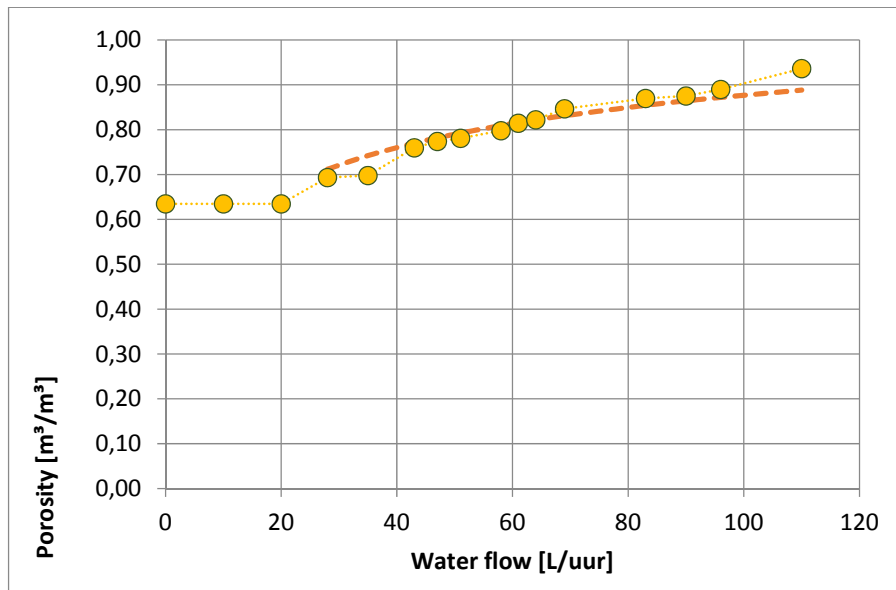
A10.36 – Carman-Kozeny predicted porosity for experiment 006



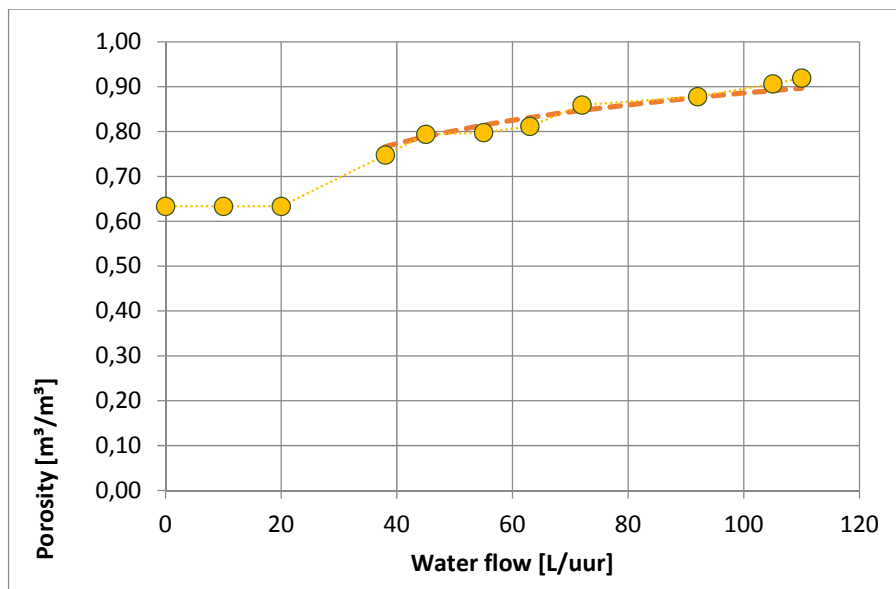
A10.37 – Carman-Kozeny predicted porosity for experiment 007



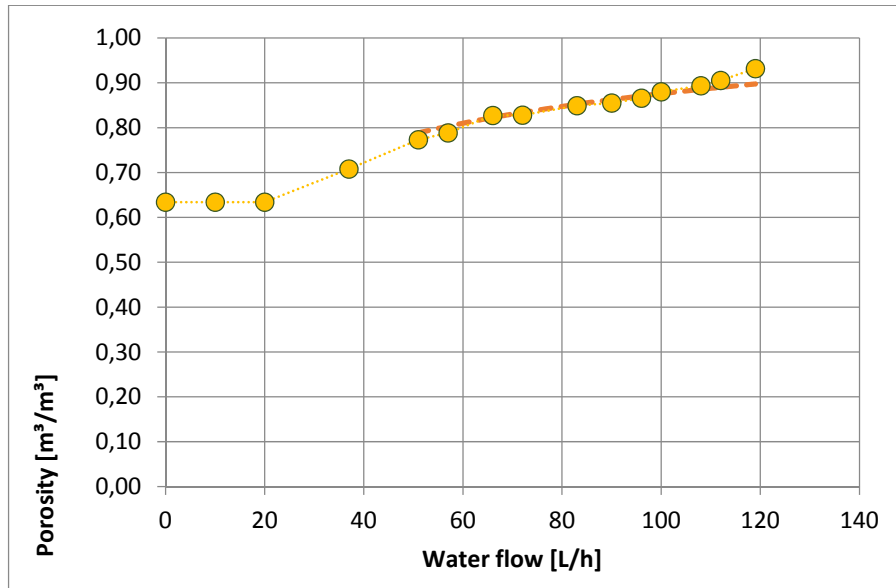
A10.38 – Carman-Kozeny predicted porosity for experiment 008



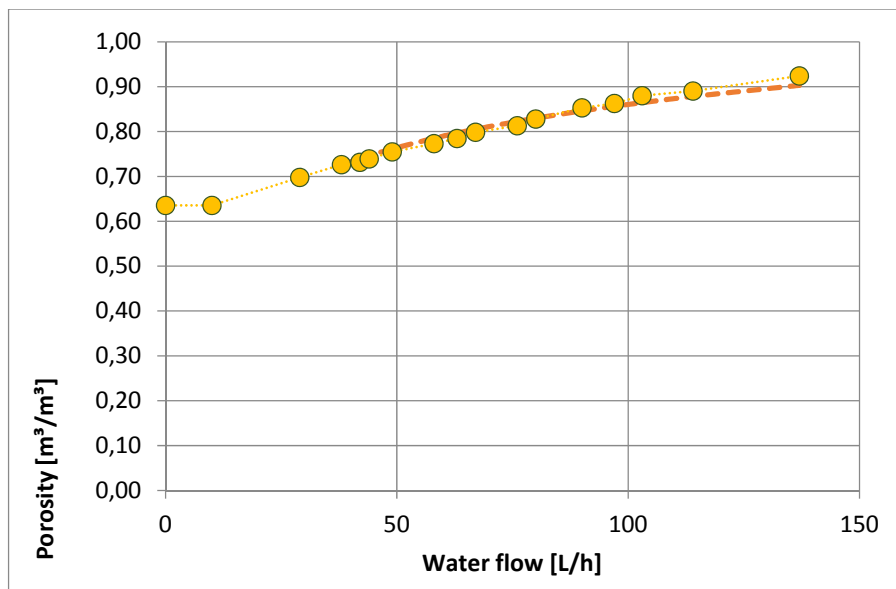
A10.39 – Carman-Kozeny predicted porosity for experiment 009



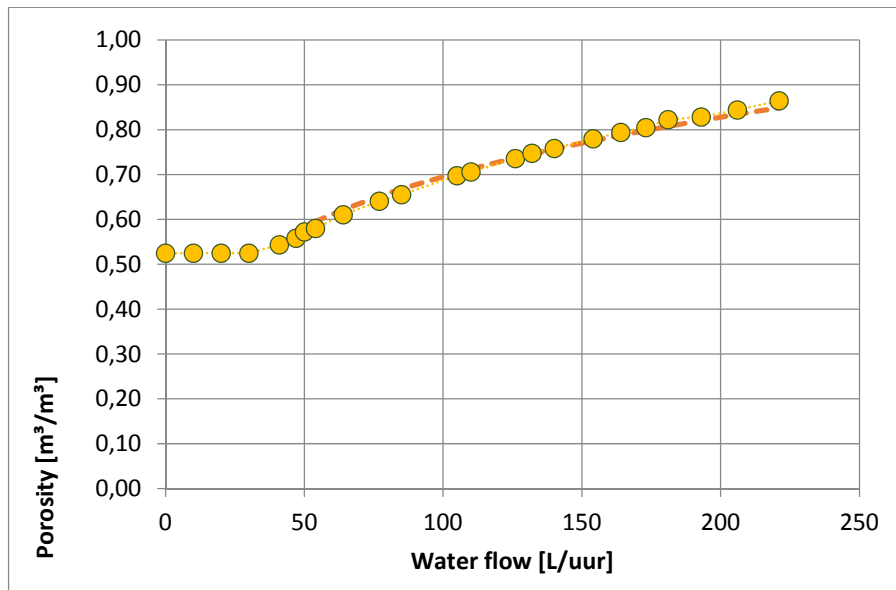
A10.40 – Carman-Kozeny predicted porosity for experiment 010



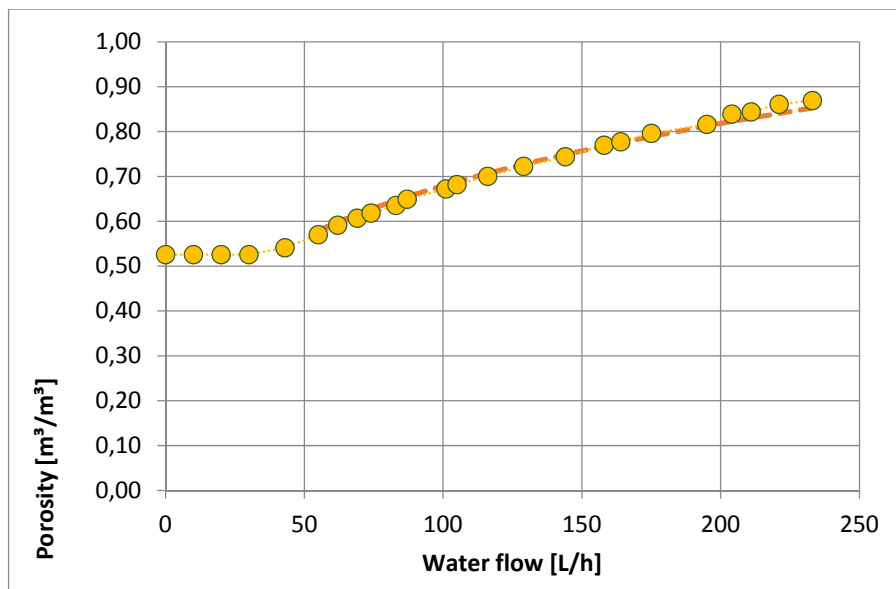
A10.41 – Carman-Kozeny predicted porosity for experiment 011



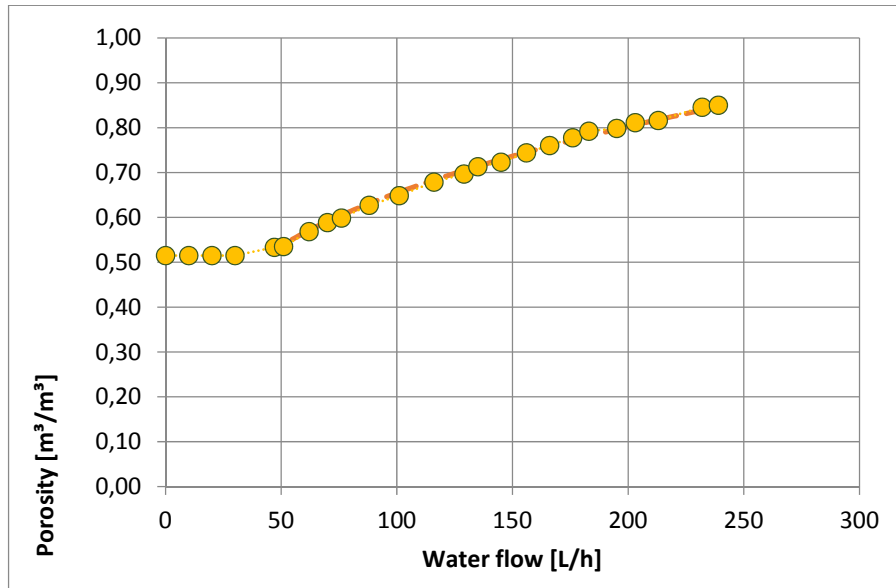
A10.42 – Carman-Kozeny predicted porosity for experiment 012



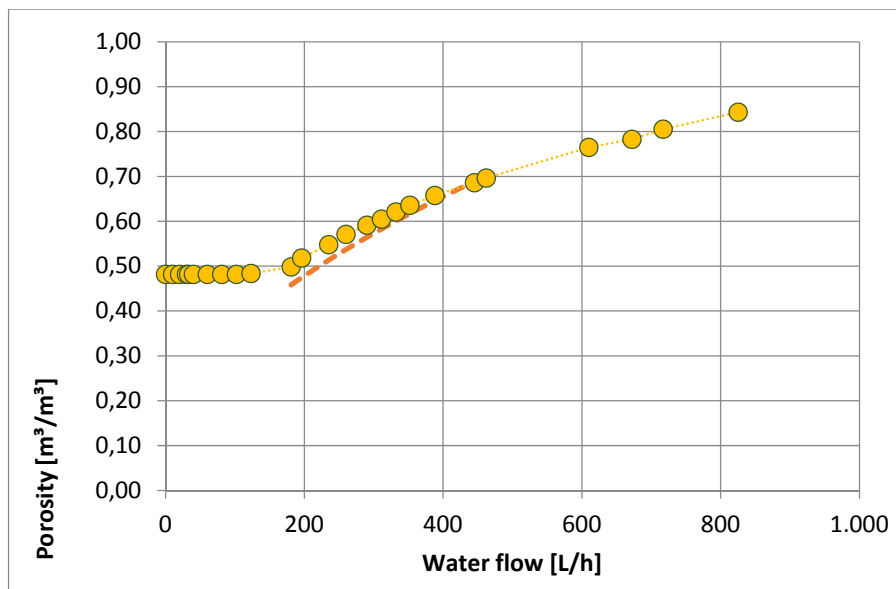
A10.43 - Carman-Kozeny predicted porosity for experiment 013

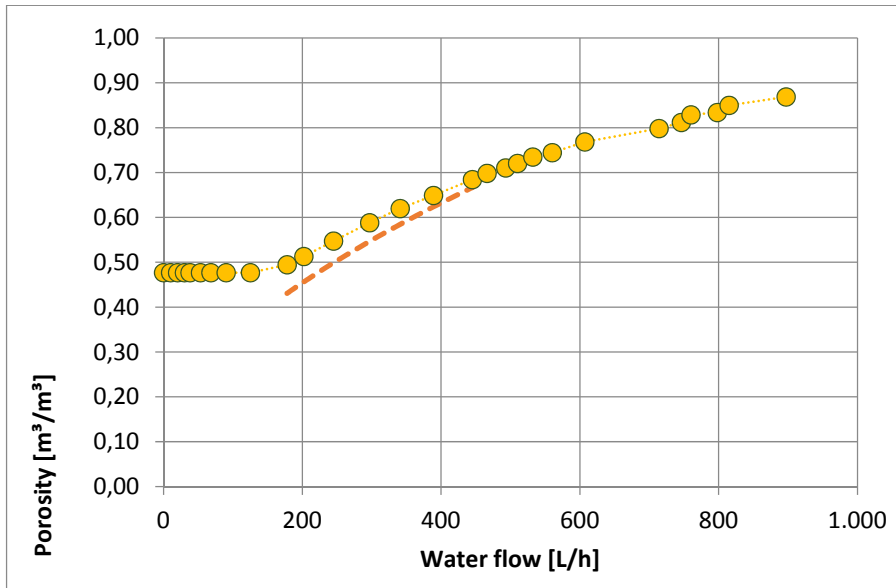


A10.44 - Carman-Kozeny predicted porosity for experiment 014

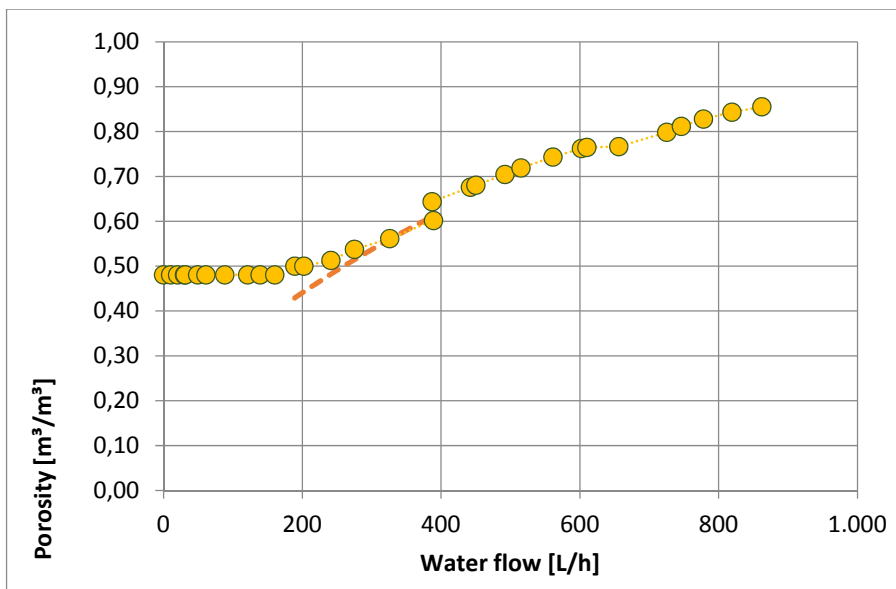


A10.45 – Carman-Kozeny predicted porosity for experiment 015

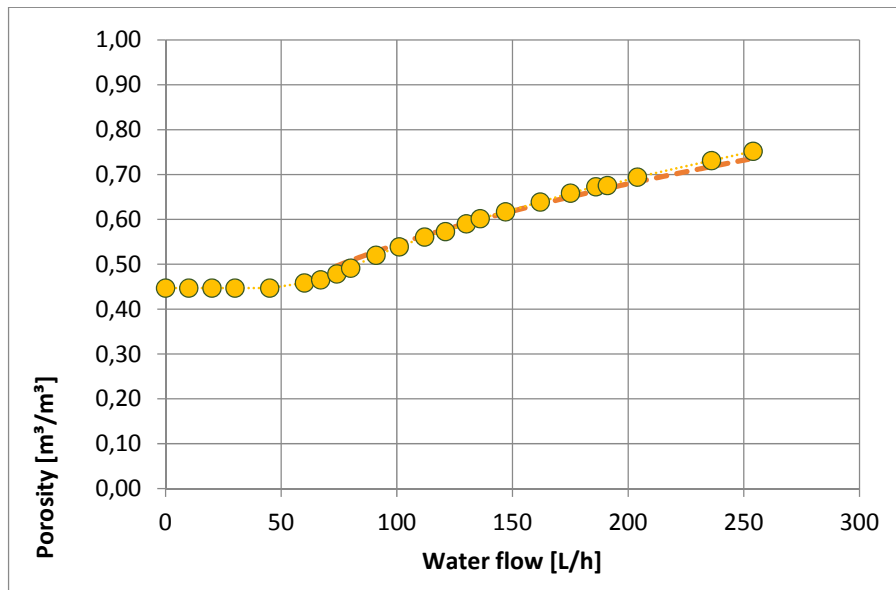




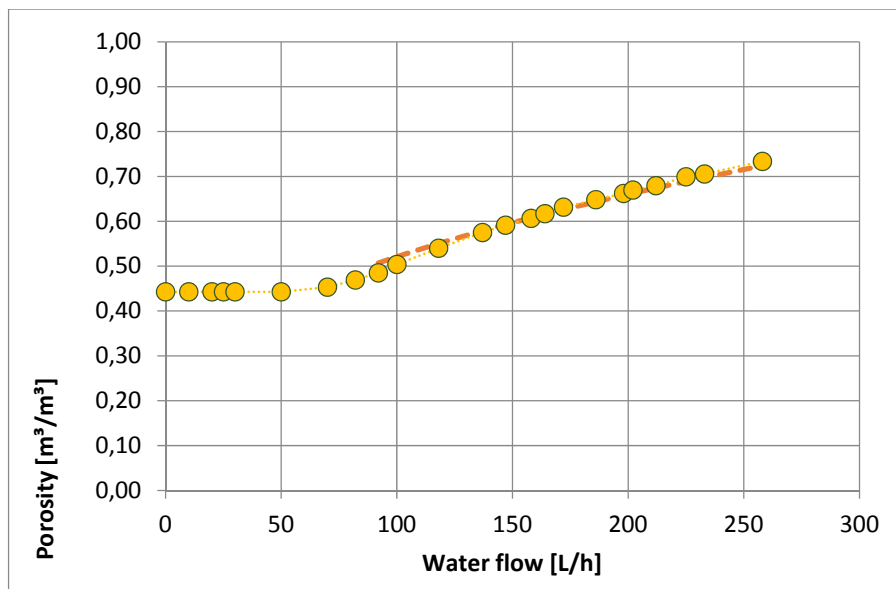
A10.47 – Carman-Kozeny predicted porosity for experiment 017



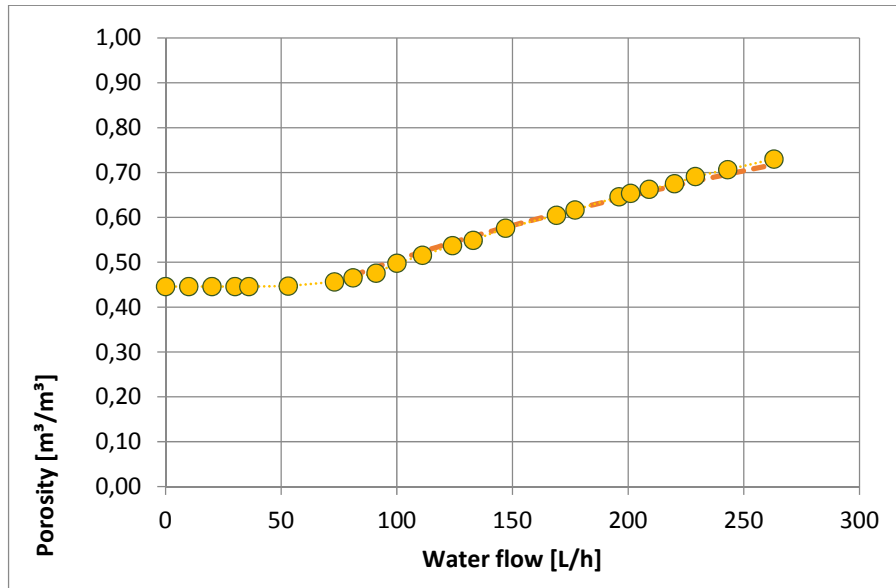
A10.48 – Carman-Kozeny predicted porosity for experiment 018



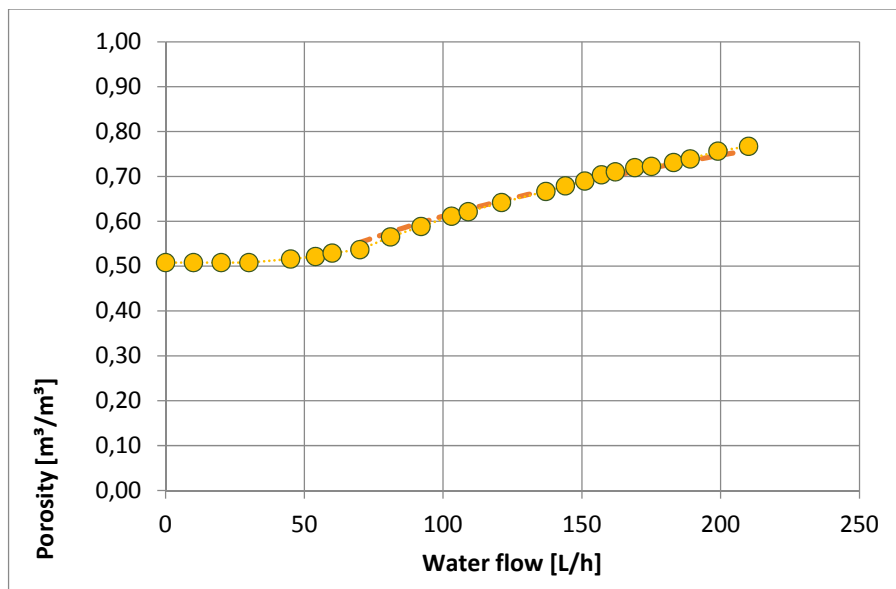
A10.49 – Carman-Kozeny predicted porosity for experiment 019



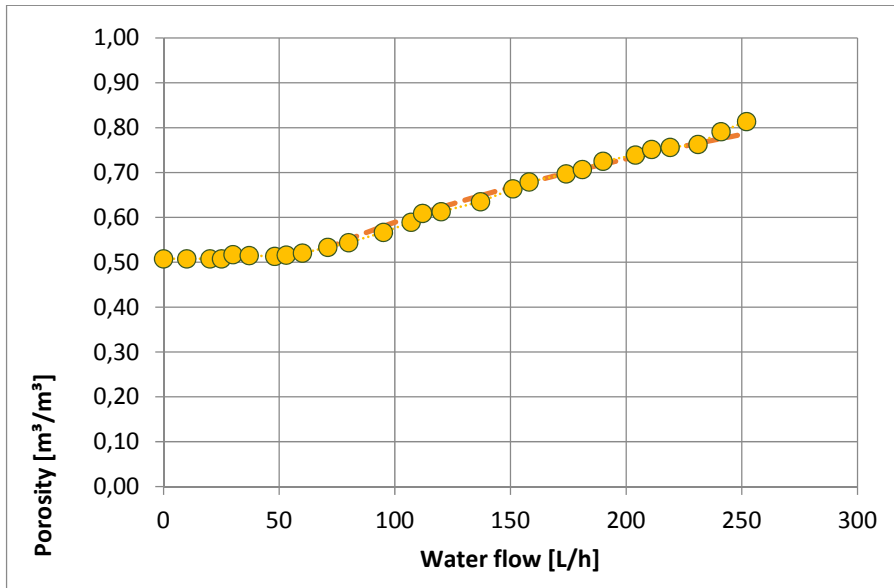
A10.50 – Carman-Kozeny predicted porosity for experiment 020



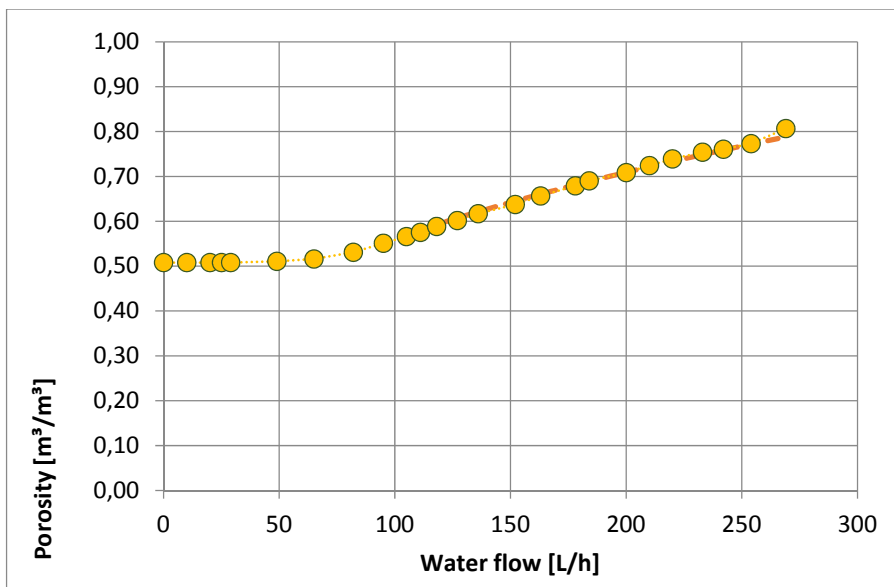
A10.51 – Carman-Kozeny predicted porosity for experiment 021



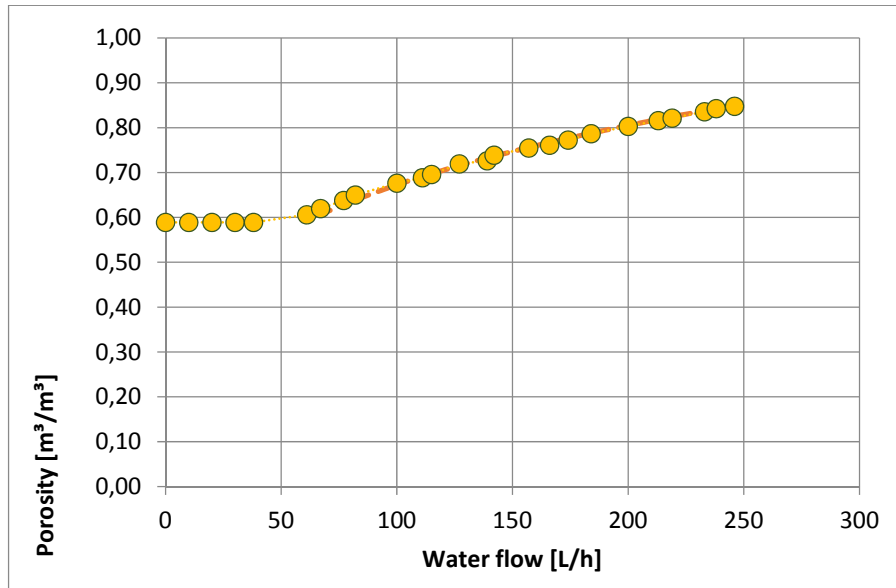
A10.52 – Carman-Kozeny predicted porosity for experiment 022



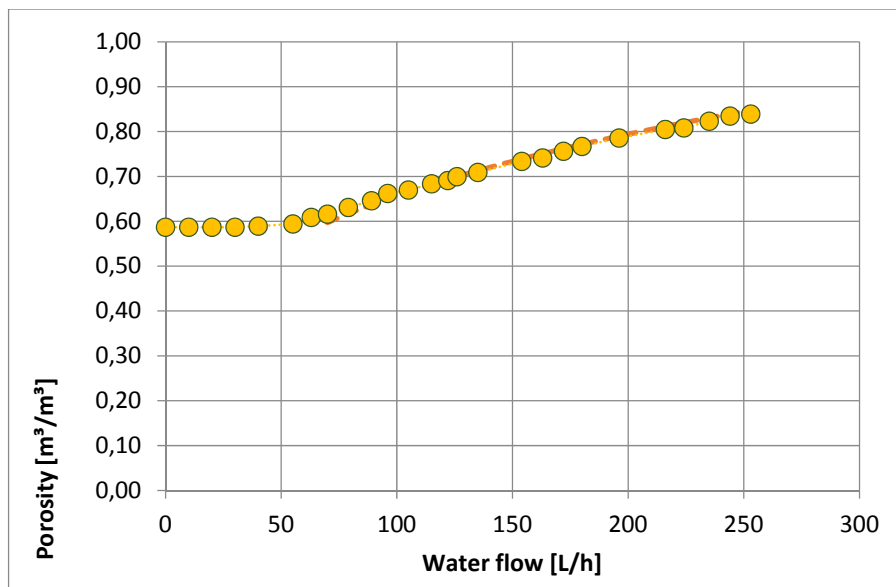
A10.53 - Carman-Kozeny predicted porosity for experiment 023



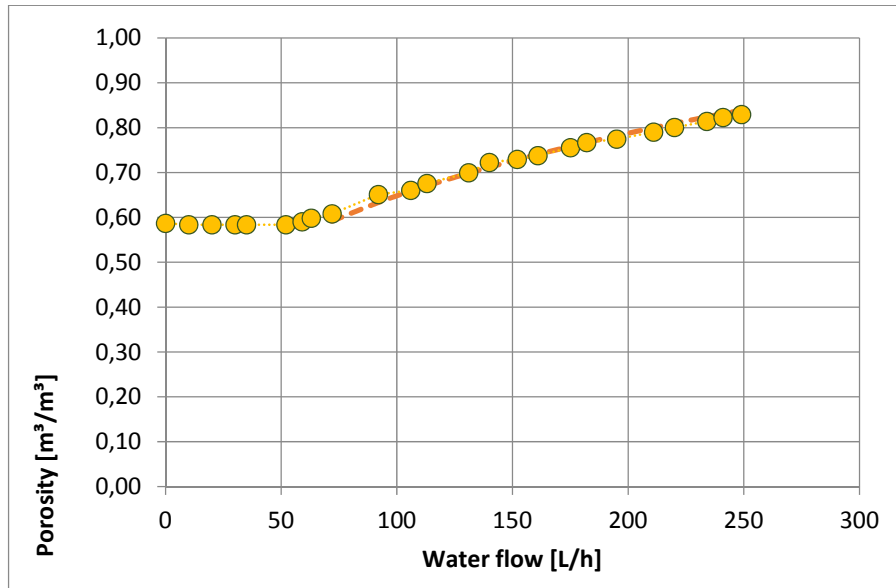
A10.54 - Carman-Kozeny predicted porosity for experiment 024



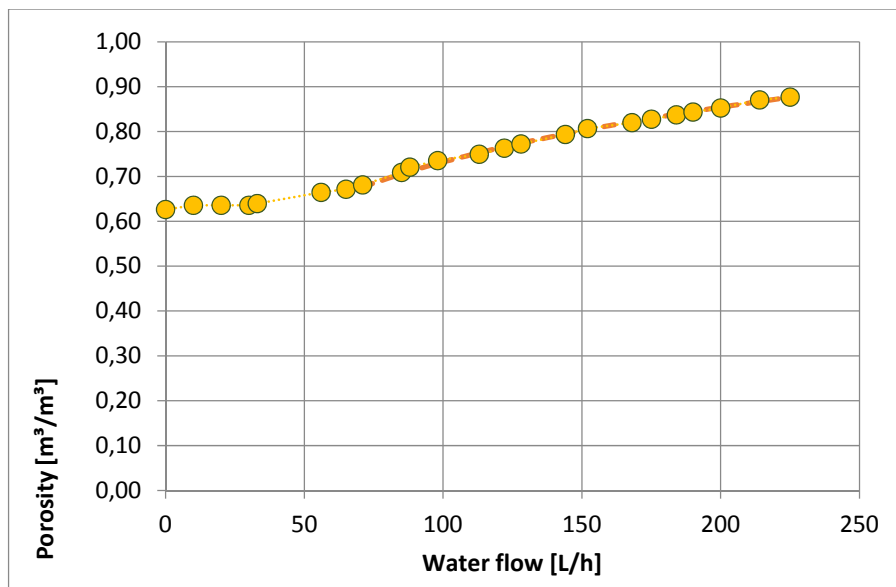
A10.55 – Carman-Kozeny predicted porosity for experiment 025



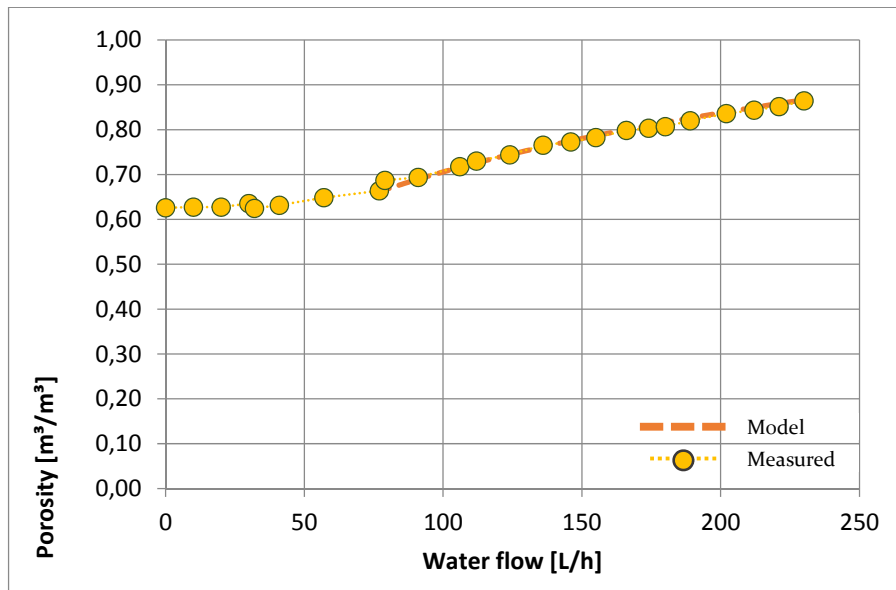
A10.56 – Carman-Kozeny predicted porosity for experiment 026



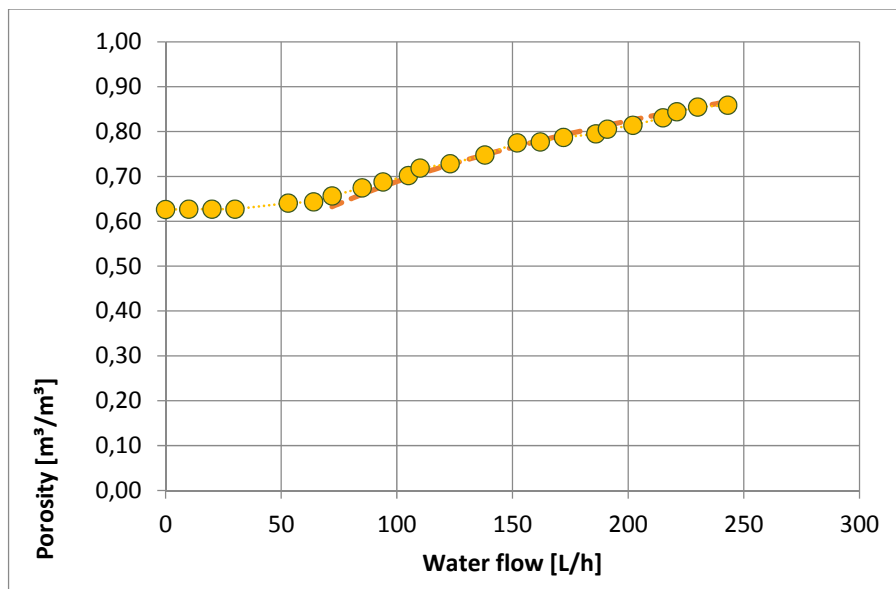
A10.57 – Carman-Kozeny predicted porosity for experiment 027



A10.58 – Carman-Kozeny predicted porosity for experiment 028



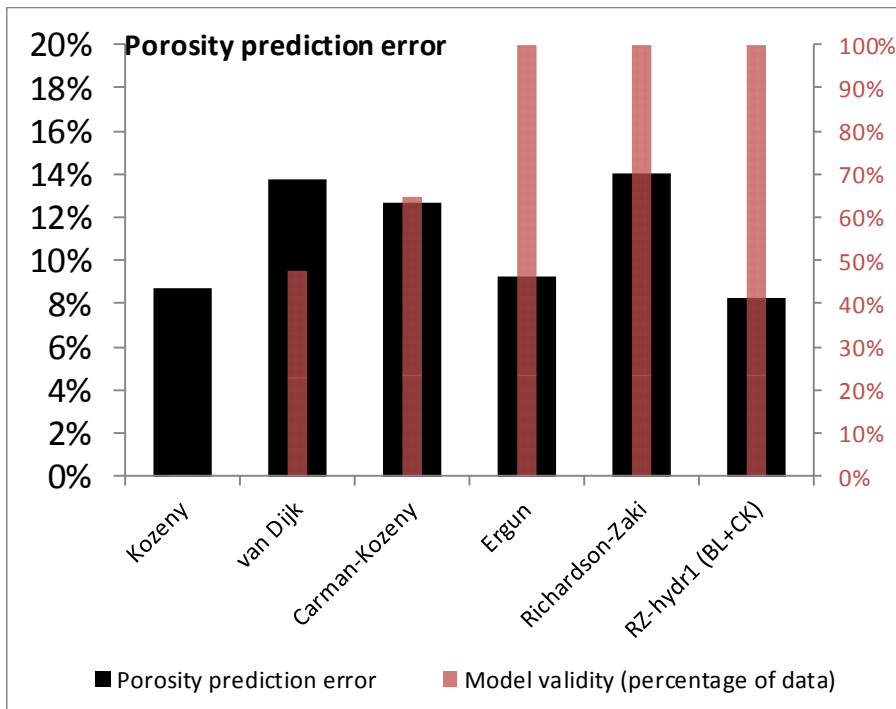
A10.59 – Carman-Kozeny predicted porosity for experiment 029



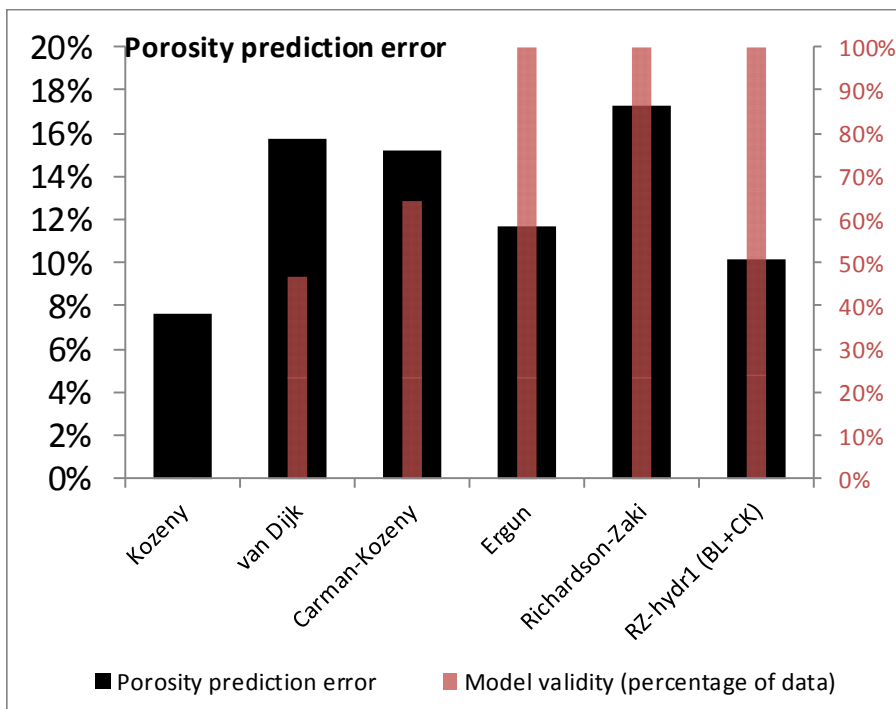
A10.60 – Carman-Kozeny predicted porosity for experiment 030

Porosity prediction error

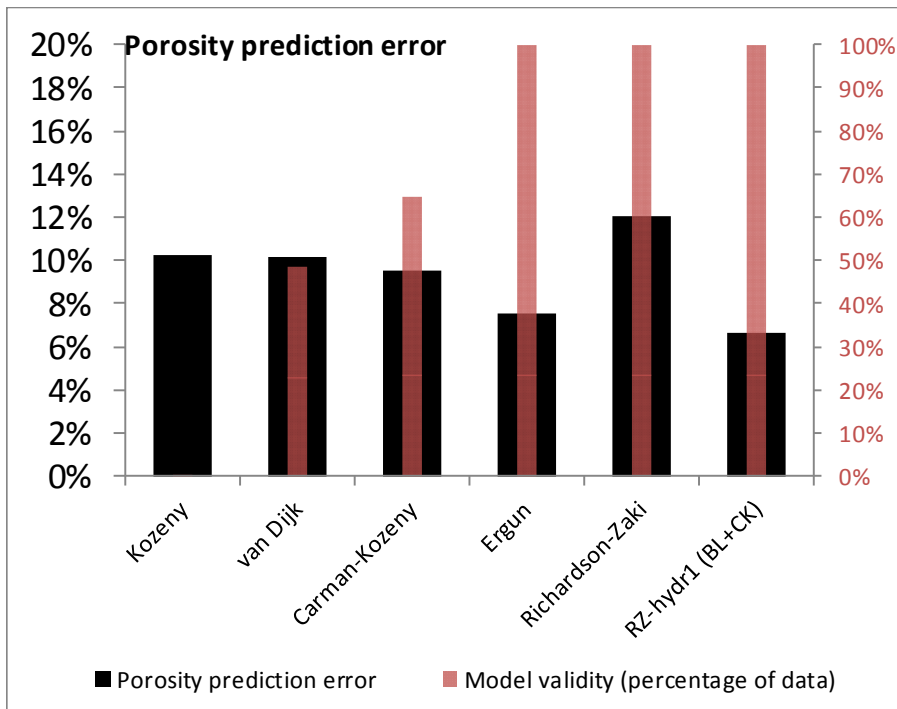
To further explore the influence of the particle size, the particle diameters obtained using the four different methods were evaluated by comparing it to the classical models. The results of the errors in the prediction of porosity of several classical models (including their validity depending on flow regime) are presented in the following figures.



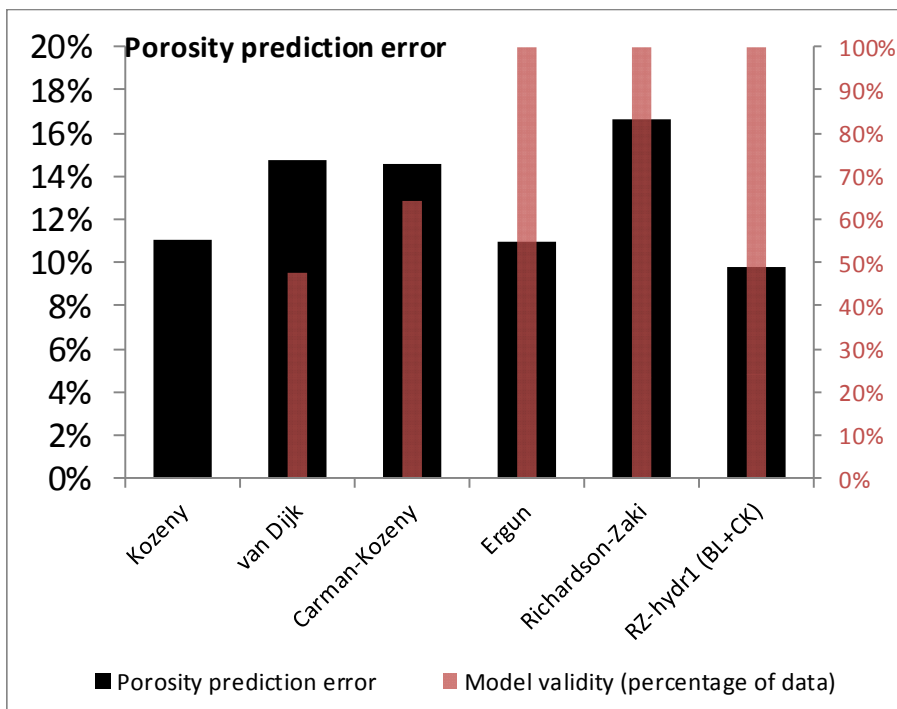
A10.61 – Porosity prediction error for Microscope d50



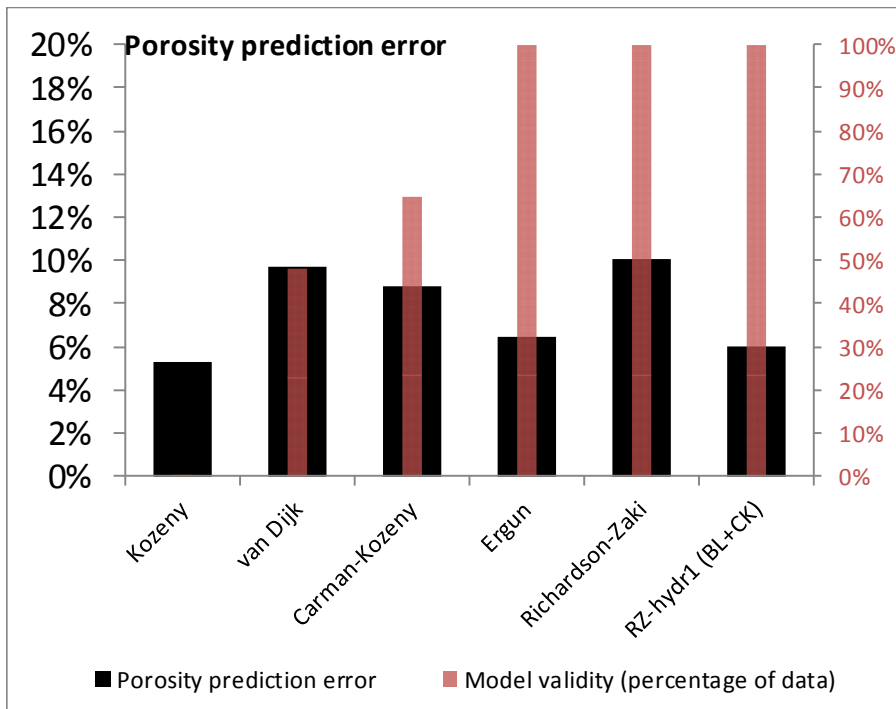
A10.62 – Porosity prediction error for ImageJ d50



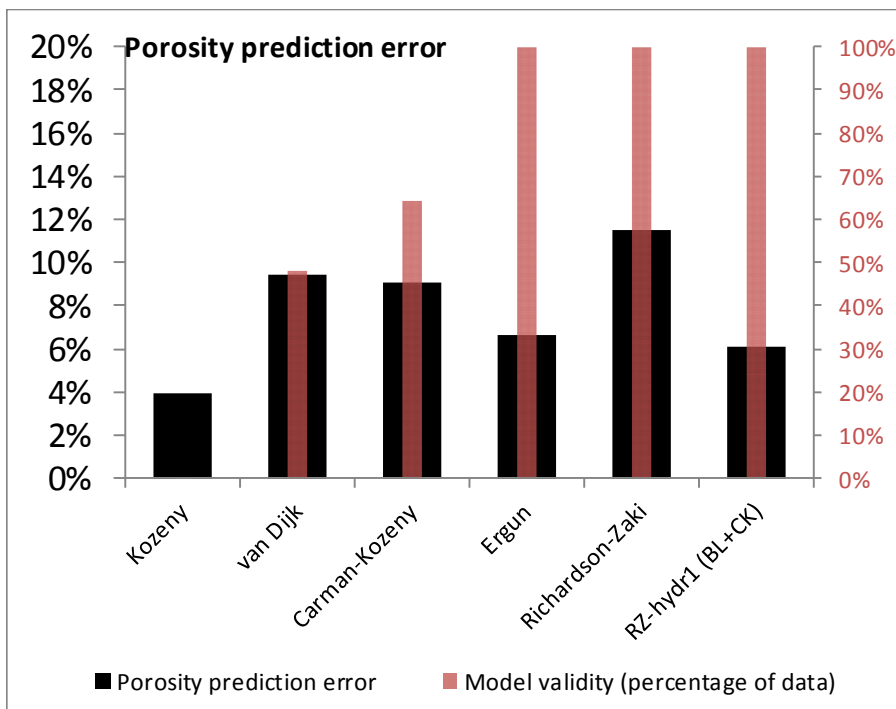
A10.63 – Porosity prediction error for Camsizer d50



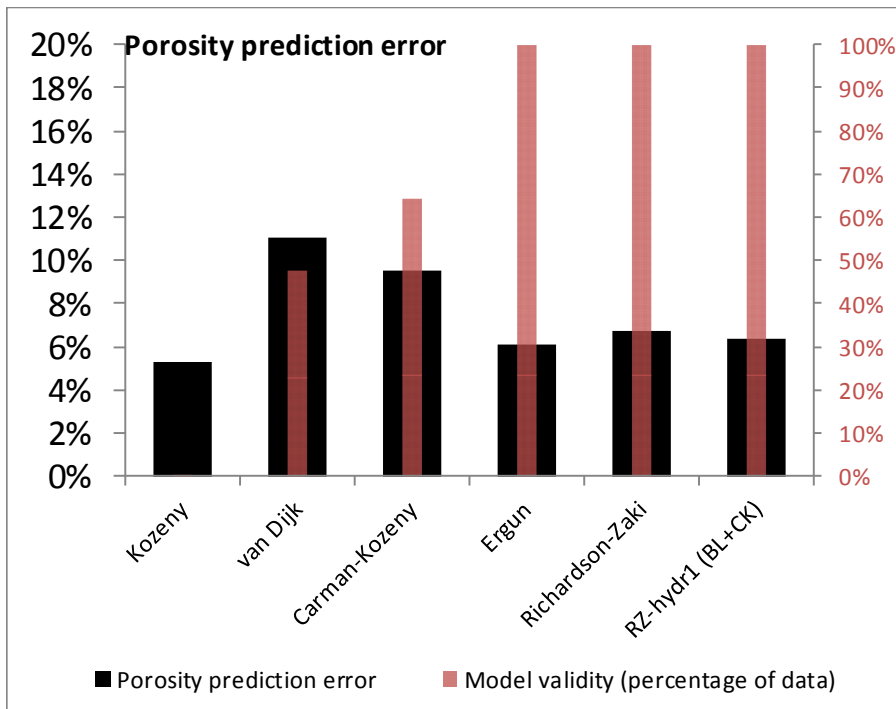
A10.64 – Porosity prediction error for sieve d50



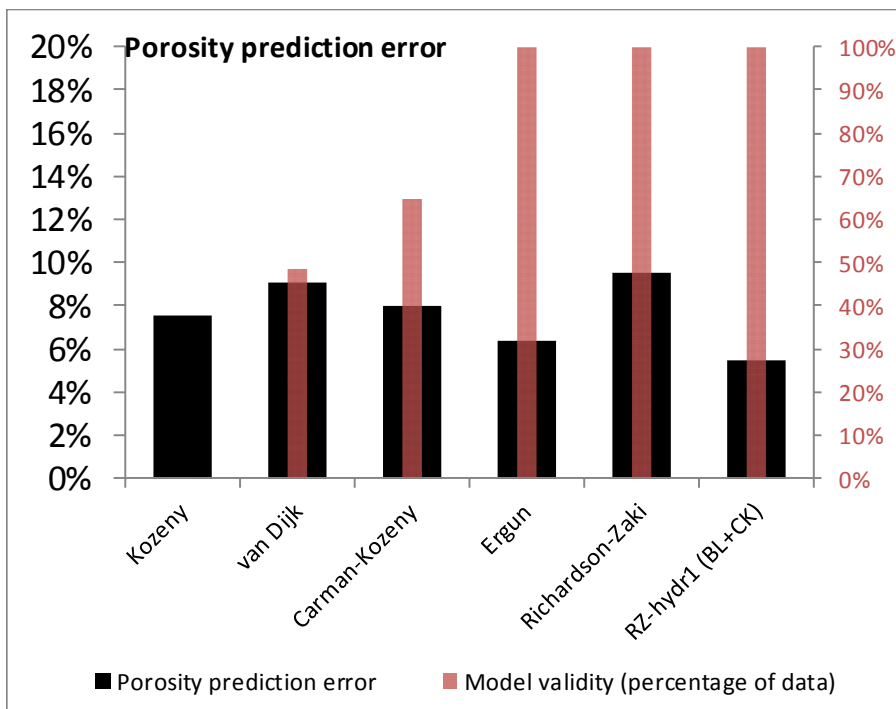
A10.65 – Porosity prediction error for microscope d10



A10.66 – Porosity prediction error for ImageJ d10



A10.67 – Porosity prediction error for Camsizer d10



A10.68 – Porosity prediction error for microscope d10

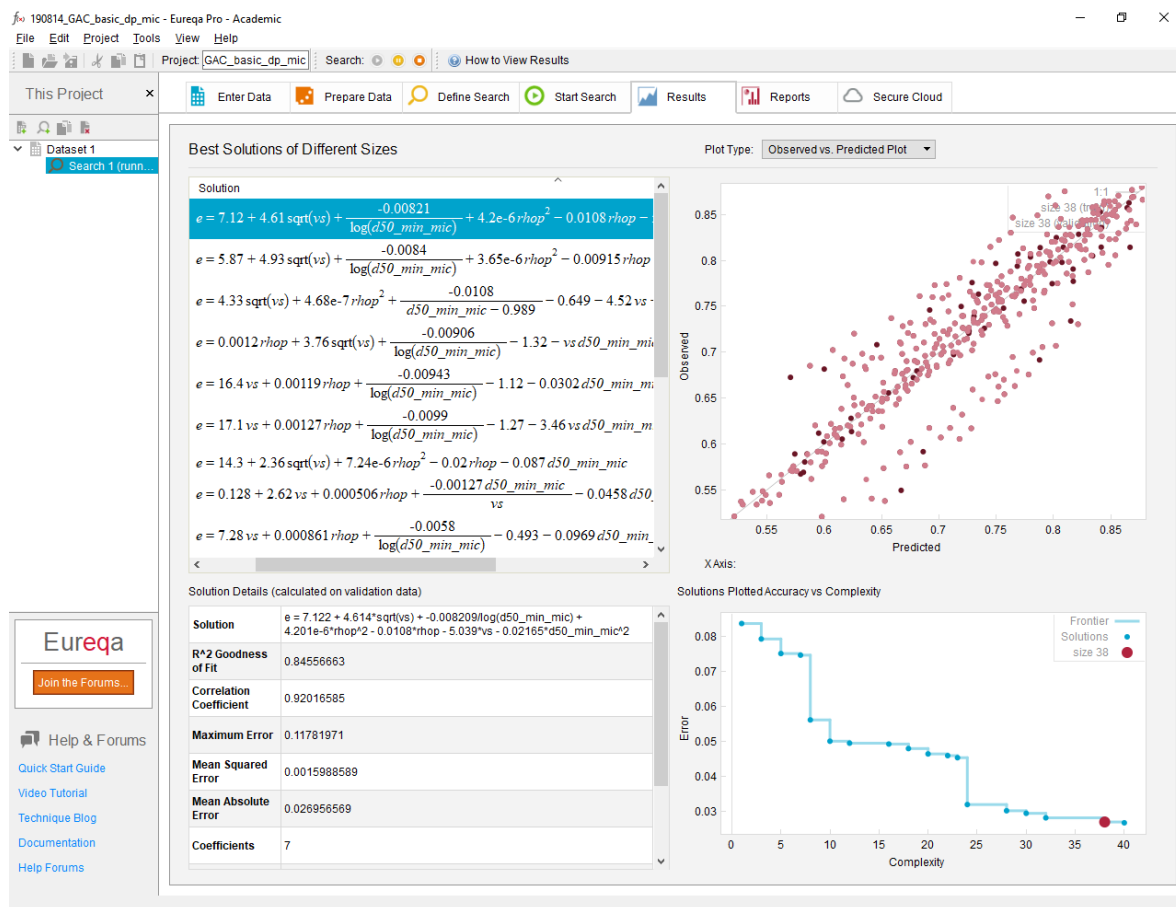
Appendix A11 – Symbolic regression outputs

In this section, the output of the symbolic regression simulations will be presented. In addition to the model outputs, both the obtained expression and correlation coefficient are presented. The nomenclature of the variable is presented at the end of this section.

- $\varepsilon = \varepsilon(v_s, v, \rho_{wet}, d_{50}) \rightarrow \text{DDM } 1$

$$e = 7.121596798718 + 4.61364191363207 * \text{sqrt}(vs) + -0.00820908789456294 / \log(d50_min_mic) + 4.20074183595287e-6 * \text{rhop}^2 - 0.0107971035071973 * \text{rhop} - 5.03907433157229 * vs - 0.021652804435104 * d50_min_mic^2$$

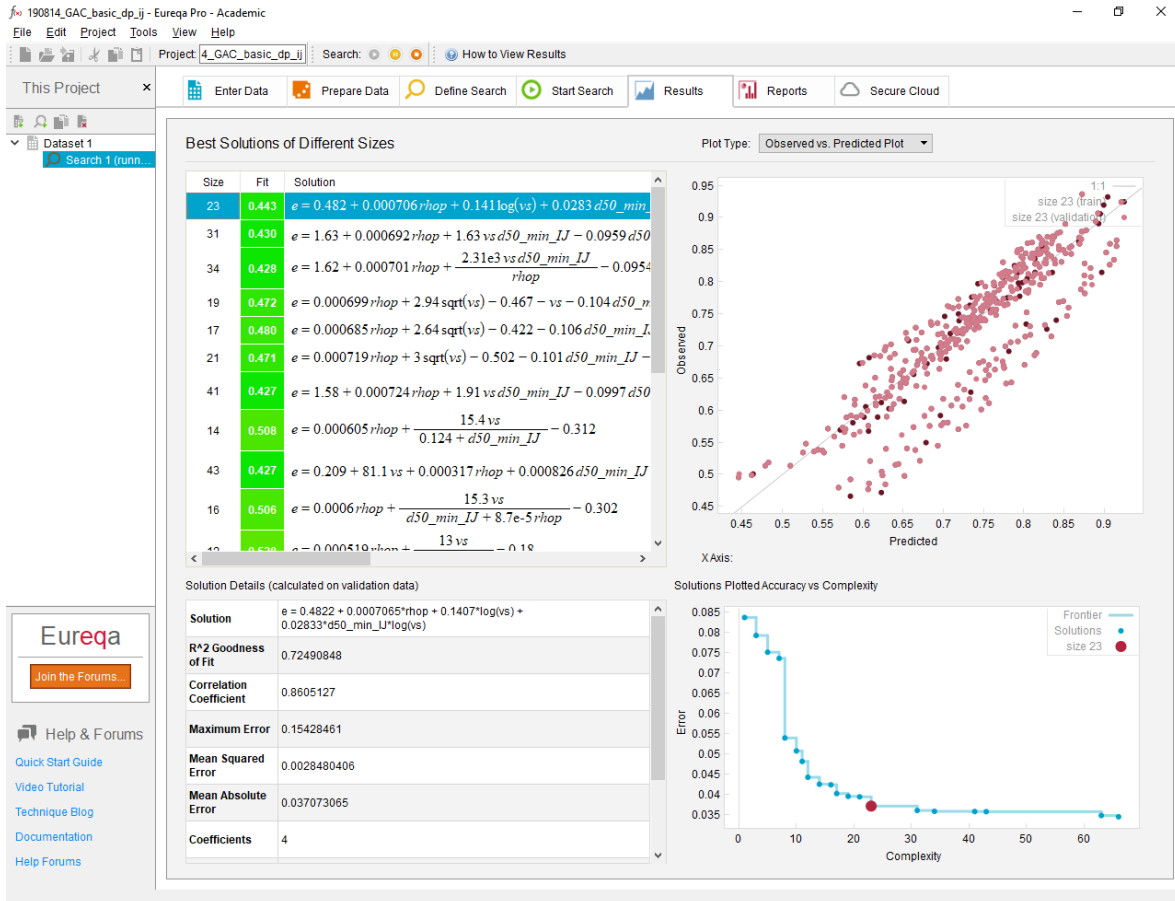
$$r^2 = 0.846$$



A11.1 – Symbolic regression outputs microscope measurements (DDM 1)

$$e = 0.482201951089131 + 0.000706499474930734 * \rho_{hop} + 0.140728073188326 * \log(vs) + 0.0283257474118857 * d_{50_min_IJ} * \log(vs)$$

$$R^2 = 0.725$$



A11.2 – Symbolic regression outputs ImageJ measurements (DDM 1)

$$e = 69434.3534040219 \cdot \mu + 0.000242534583414239 \cdot \rho_{hop} + 4.30656004610189 \cdot \sqrt{vs} + -0.000273197471052103 \cdot \log(vs) / \log(d50_min_cam) - 0.14179153135397 - 4.33188553138932 \cdot vs - 0.235776657461733 \cdot \log(d50_min_cam)$$

$R^2=0.937$

The screenshot shows the Eureka Pro software interface. The main window displays 'Best Solutions of Different Sizes' with a table of solutions. The top-right plot is an 'Observed vs. Predicted Plot' showing a strong positive correlation. The bottom-right plot is 'Solutions Plotted Accuracy vs Complexity', showing a sharp decrease in error as complexity increases, with a red dot indicating the selected solution at complexity 44.

Size	Fit	Solution
44	0.209	$e = 6.94e4 \mu + 0.000243 \rho_{hop} + 4.31 \sqrt{vs} + \frac{-0.0002731}{\log(d50_min_cam)}$
38	0.218	$e = 6.58e4 \mu + 0.000236 \rho_{hop} + 4.45 \sqrt{vs} + \frac{0.0010}{\log(d50_min_cam)}$
25	0.240	$e = 0.35 + 7.64e4 \mu + 1.94 vs + \frac{0.00209}{d50_min_cam - 1.01} + \frac{1}{a}$
23	0.260	$e = 0.363 + vs + 86485 \mu + \frac{0.002}{d50_min_cam - 1.01} + \frac{0.07}{d50}$
66	0.208	$e = 6.58e4 \mu + 0.000246 \rho_{hop} + 4.41 \sqrt{vs} + \frac{6.58e4}{d50_min_cam}$
21	0.285	$e = 0.416 + 1.81 vs + \frac{0.00203}{d50_min_cam - 1.01} + \frac{0.0985 + 10}{d50_min_cam}$
19	0.302	$e = 0.442 + vs + \frac{0.00189}{d50_min_cam - 1.01} + \frac{0.0763 + 12 vs}{d50_min_cam}$
17	0.345	$e = 0.447 + \frac{0.00195}{d50_min_cam - 1.01} + \frac{0.0708 + 13 vs}{d50_min_cam}$
15	0.445	$e = 0.803 + vs + \frac{0.0717}{d50_min_cam} + \frac{-0.00213 d50_min_cam}{d50_min_cam}$

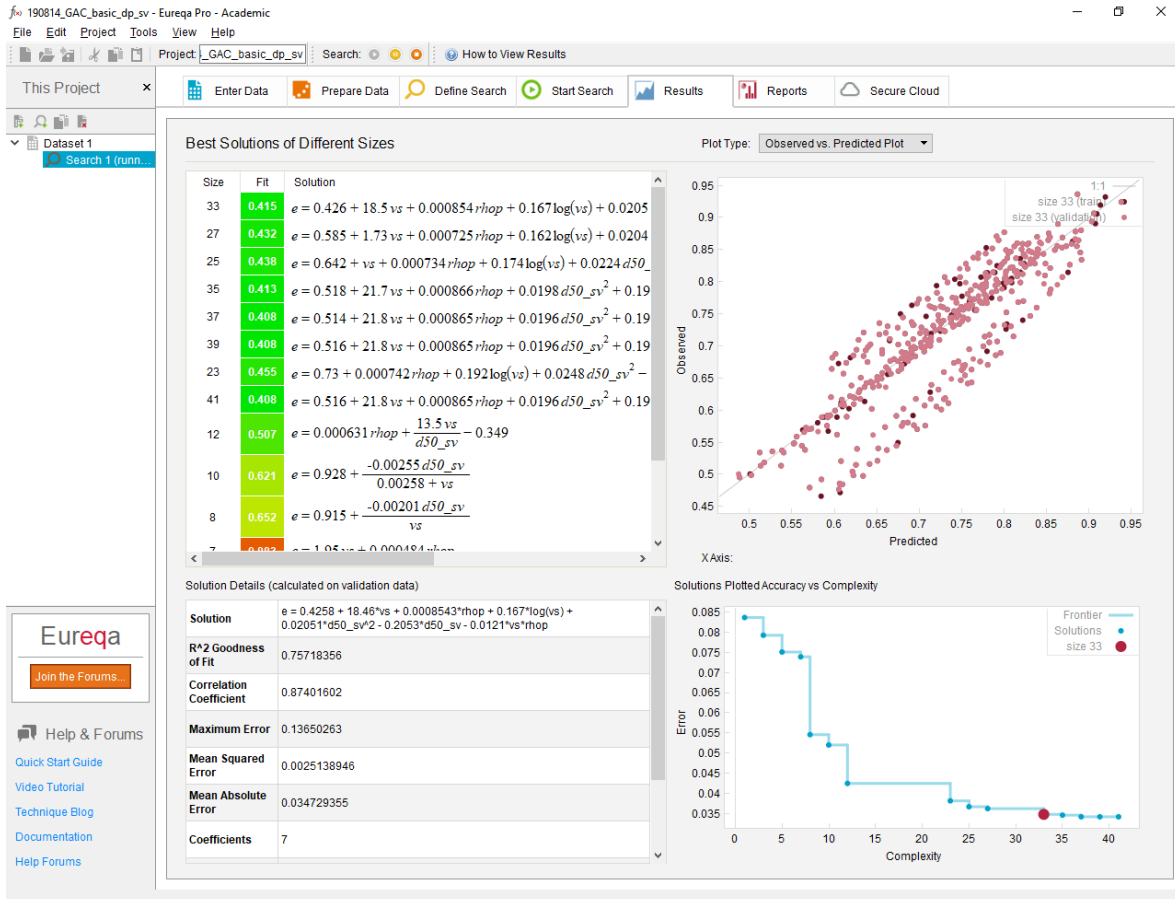
Solution Details (calculated on validation data)

Solution	$e = 6.943e4 \mu + 0.0002425 \rho_{hop} + 4.307 \sqrt{vs} + -0.0002732 \log(vs) / \log(d50_min_cam) - 0.1418 - 4.332 vs - 0.2358 \log(d50_min_cam)$
R² Goodness of Fit	0.93745218
Correlation Coefficient	0.96929787
Maximum Error	0.080292432
Mean Squared Error	0.00064756172
Mean Absolute Error	0.017448361
Coefficients	7

A11.3 – Symbolic regression outputs Camsizer measurements (DDM 1)

$$e = 0.425779787744361 + 18.4565244430857 * vs + 0.000854338717168793 * rhop + 0.167030500703928 * \log(vs) + 0.0205099039187543 * d50_sv^2 - 0.205256794561575 * d50_sv - 0.0121034835305304 * vs * rhop$$

$R^2=0.757$

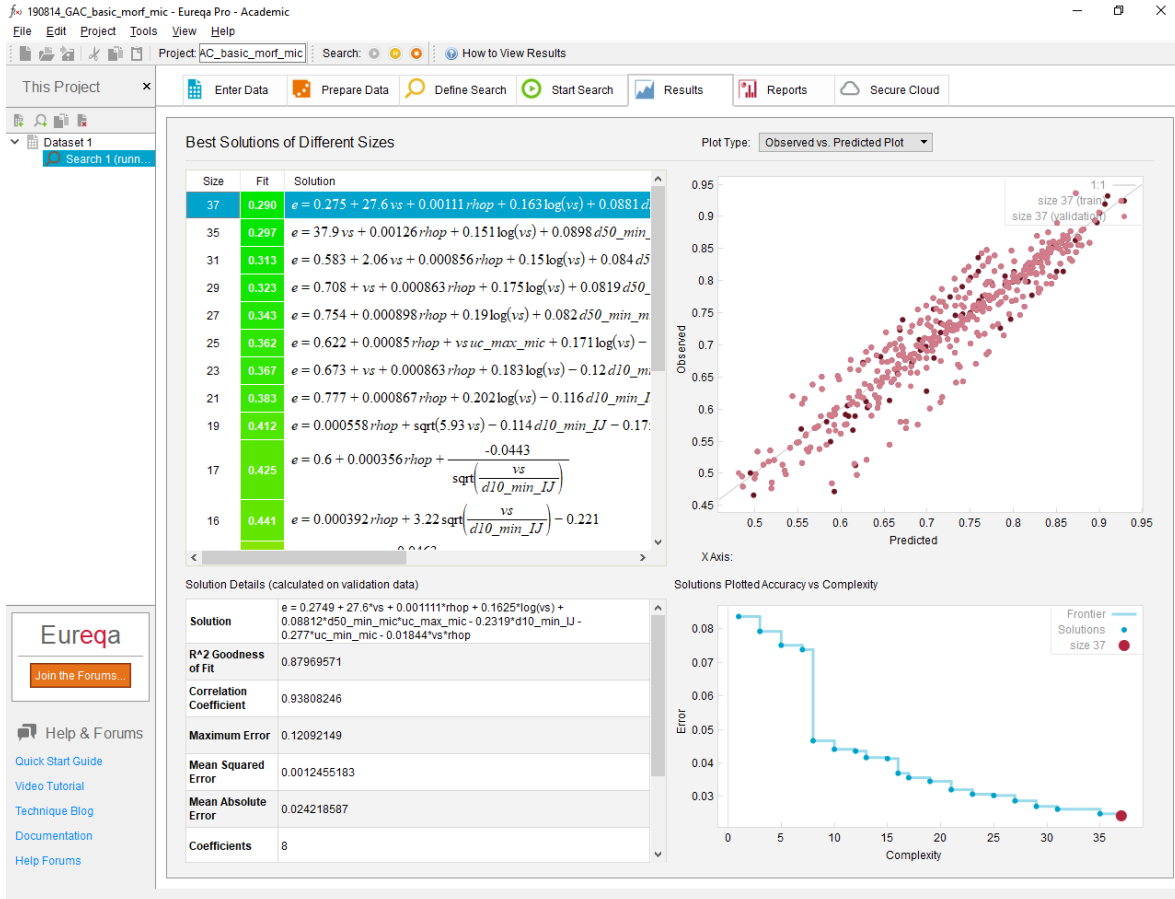


A11.4 – Symbolic regression outputs sieve measurements (DDM 1)

$$\varepsilon = \varepsilon(v_s, v, \rho_{wet}, d_{10,min}, d_{90,max}, d_{50,min}, d_{50,max}, uc_{min}, uc_{max}) \rightarrow \text{DDM 3}$$

$$e = 0.274886359592169 + 27.6006558961968 * vs + 0.001110165286692 * rhop + 0.162532514247876 * \log(vs) + 0.0881163487638454 * d50_min_mic * uc_max_mic - 0.231881761363333 * d10_min_IJ - 0.276994809306694 * uc_min_mic - 0.0184399074071506 * vs * rhop$$

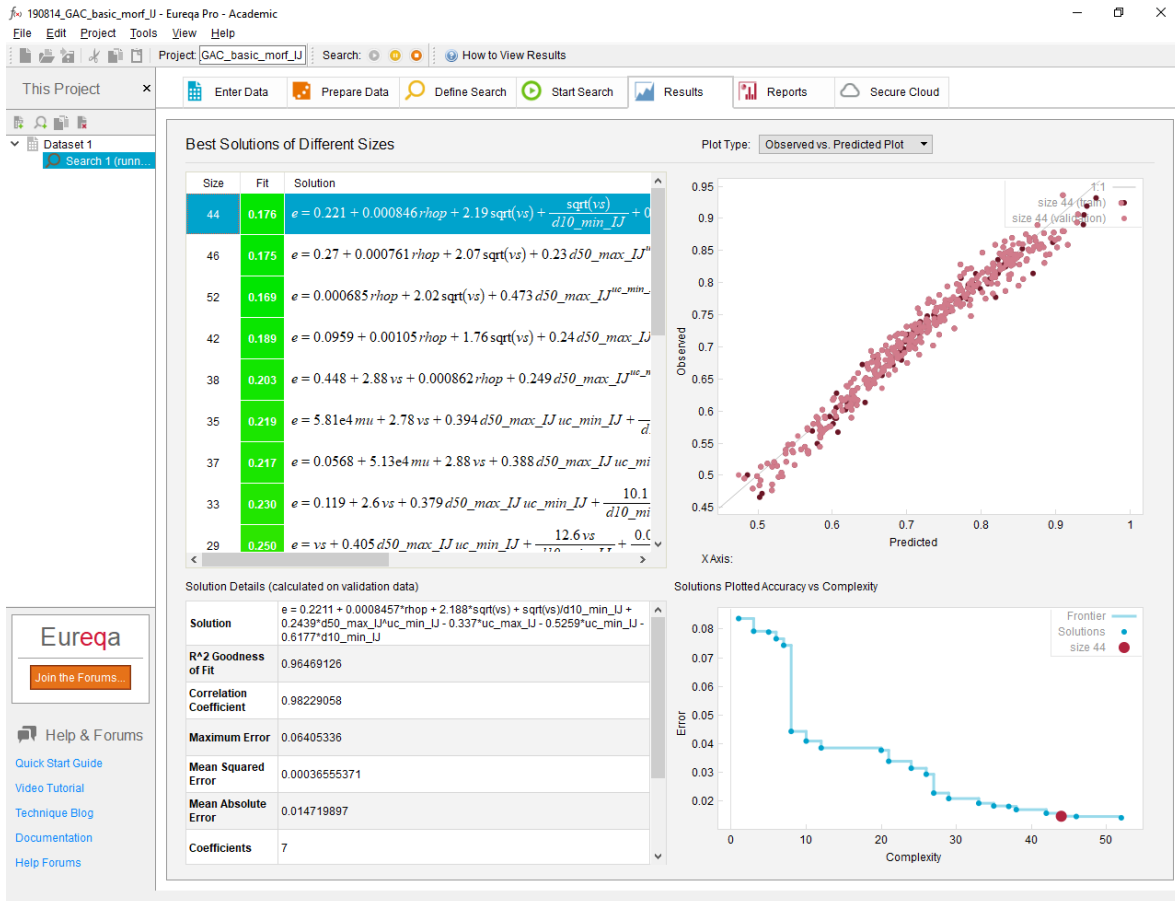
$r^2=0.880$



A11.5 – Symbolic regression outputs microscope measurements (DDM 3)

$$e = 0.221079084795635 + 0.000845700513222802 * \rho_{hop} + 2.18762175849013 * \sqrt{vs} + \sqrt{vs} / d_{10_min_IJ} + 0.243933943834515 * d_{50_max_IJ}^{uc_min_IJ} - 0.336952431082249 * uc_max_IJ - 0.525852535421596 * uc_min_IJ - 0.617722340115003 * d_{10_min_IJ}$$

$$r^2 = 0.964$$



A11.6 – Symbolic regression outputs ImageJ measurements (DDM 3)

$$e = 1.74458566237025 + d50_max_cam + 0.69492073179055*uc_min_cam + 0.143756153491319*\log(vs) + 2776054.10547709*vs*\mu - 0.292738073163989*d90_max_cam - 0.698553031776248*uc_max_cam - 1.21539618792599*d50_min_cam$$

$R^2=0.960$

The screenshot shows the Eureka software interface with the following components:

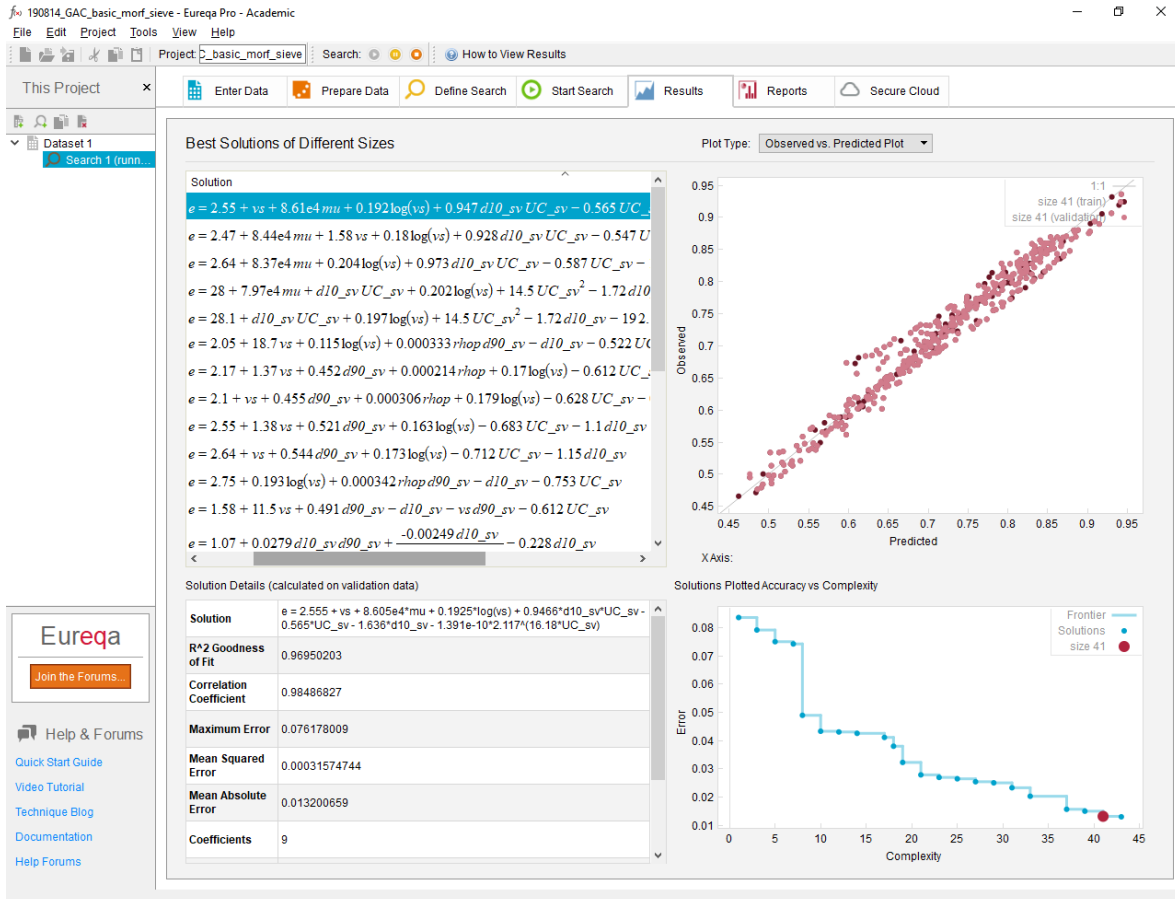
- Table of Best Solutions:**

Size	Fit	Solution
33	0.184	$e = 1.74 + d50_max_cam + 0.695 uc_min_cam + 0.144 \log(vs)$
35	0.183	$e = 1.77 + 1.04 d50_max_cam + 0.709 uc_min_cam + 0.151 \log(vs)$
41	0.181	$e = 1.75 + 1.13 d50_max_cam + 0.764 uc_min_cam + 0.151 \log(vs)$
31	0.199	$e = 2 + d50_max_cam + 8.07e4 \mu + 0.701 uc_min_cam + 0.151 \log(vs)$
27	0.242	$e = 2.07 + d50_max_cam + 0.69 uc_min_cam + 0.204 \log(vs)$
30	0.238	$e = 0.206 + 1.61 vs + 0.359 uc_min_cam + 0.318 d50_max_cam$
29	0.241	$e = 2.07 + 1.04 d50_max_cam + 0.708 uc_min_cam + 0.2051 \log(vs)$
26	0.263	$e = 0.329 + 0.363 uc_min_cam + 0.322 d50_max_cam + \dots$
23	0.398	$e = 0.917 + 8.9 vs + 0.779 d50_max_cam + 0.589 uc_min_cam$
25	0.394	$e = 0.933 + 9.81 vs + 0.807 d50_max_cam + 0.579 uc_min_cam$
21	0.465	$e = 0.975 + 7 vs + 0.346 uc_min_cam + 0.26 d50_max_cam - \dots$
20	0.485	$e = 0.471 + 12.9 vs + 4.08e-7 rhop^2 - 0.000903 rhc$
- Observed vs. Predicted Plot:** A scatter plot showing a strong positive linear correlation between predicted and observed values, with a regression line and a 1:1 reference line.
- Solutions Plotted Accuracy vs Complexity:** A step-down plot showing the error rate decreasing as the complexity of the model increases, with a frontier line and a specific solution (size 33) highlighted.
- Solution Details:**
 - Solution:** $e = 1.745 + d50_max_cam + 0.6949*uc_min_cam + 0.1438*\log(vs) + 2.776e6*vs*\mu - 0.2927*d90_max_cam - 0.6986*uc_max_cam - 1.215*d50_min_cam$
 - R² Goodness of Fit:** 0.9596463
 - Correlation Coefficient:** 0.97967003
 - Maximum Error:** 0.082670638
 - Mean Squared Error:** 0.00041778455
 - Mean Absolute Error:** 0.015376023
 - Coefficients:** 7

A11.7 – Symbolic regression outputs Camsizer measurements (DDM 3)

$$e = 1.74458566237025 + d50_max_cam + 0.69492073179055*uc_min_cam + 0.143756153491319*\log(vs) + 2776054.10547709*vs*\mu - 0.292738073163989*d90_max_cam - 0.698553031776248*uc_max_cam - 1.21539618792599*d50_min_cam$$

$R^2=0.960$

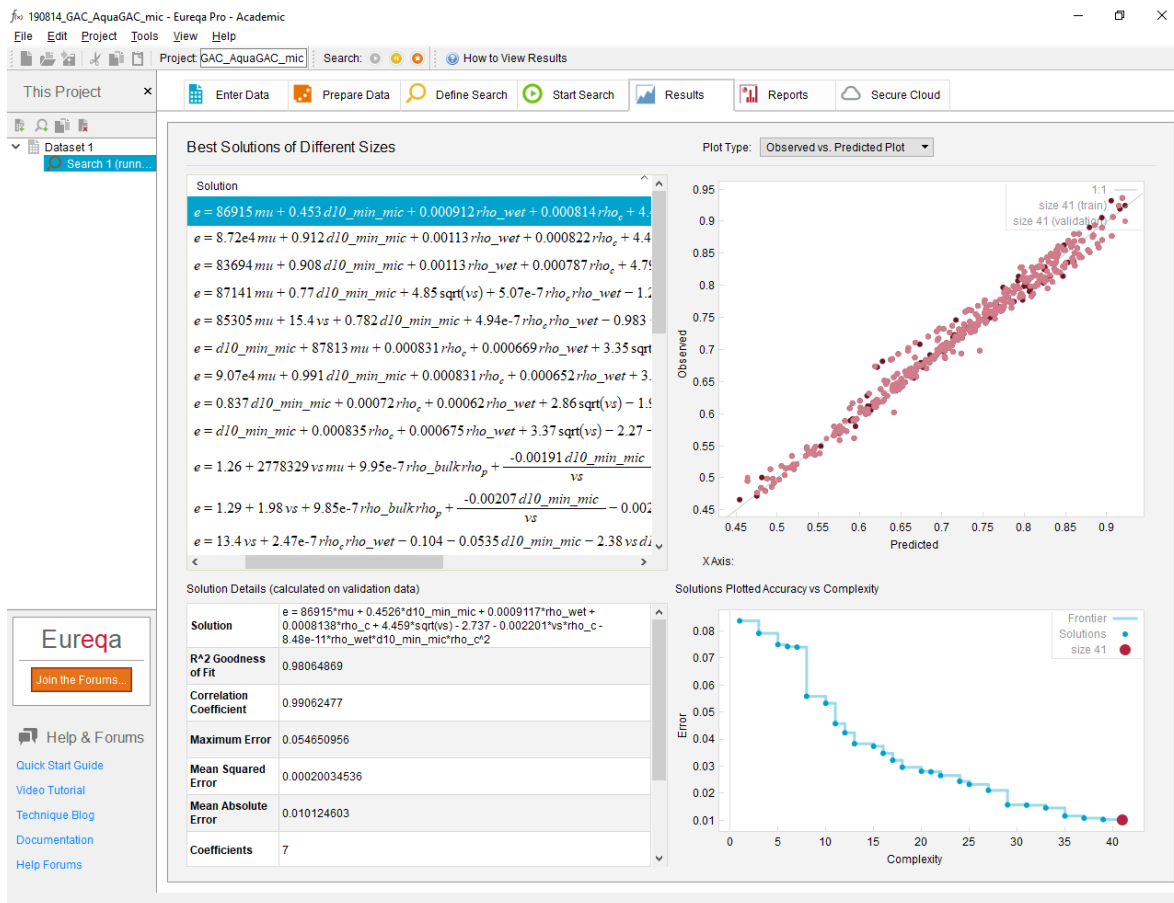


A11.8 – Symbolic regression outputs sieve measurements (DDM 3)

$$\varepsilon = \varepsilon(v_s, \rho_c, \rho_{bulk}, \rho_{wet}, \rho_p, d_{10,cam}, d_{90,cam}) \rightarrow \text{DDM 2}$$

$$e = 86915 \cdot \mu + 0.452569968510356 \cdot d_{10_min_mic} + 0.000911684675241894 \cdot \rho_{wet} + 0.000813756914750568 \cdot \rho_c + 4.45850207772022 \cdot \sqrt{v_s} - 2.73672397247582 - 0.00220092726214245 \cdot v_s \cdot \rho_c - 8.4795667962228e-11 \cdot \rho_{wet} \cdot d_{10_min_mic} \cdot \rho_c^2$$

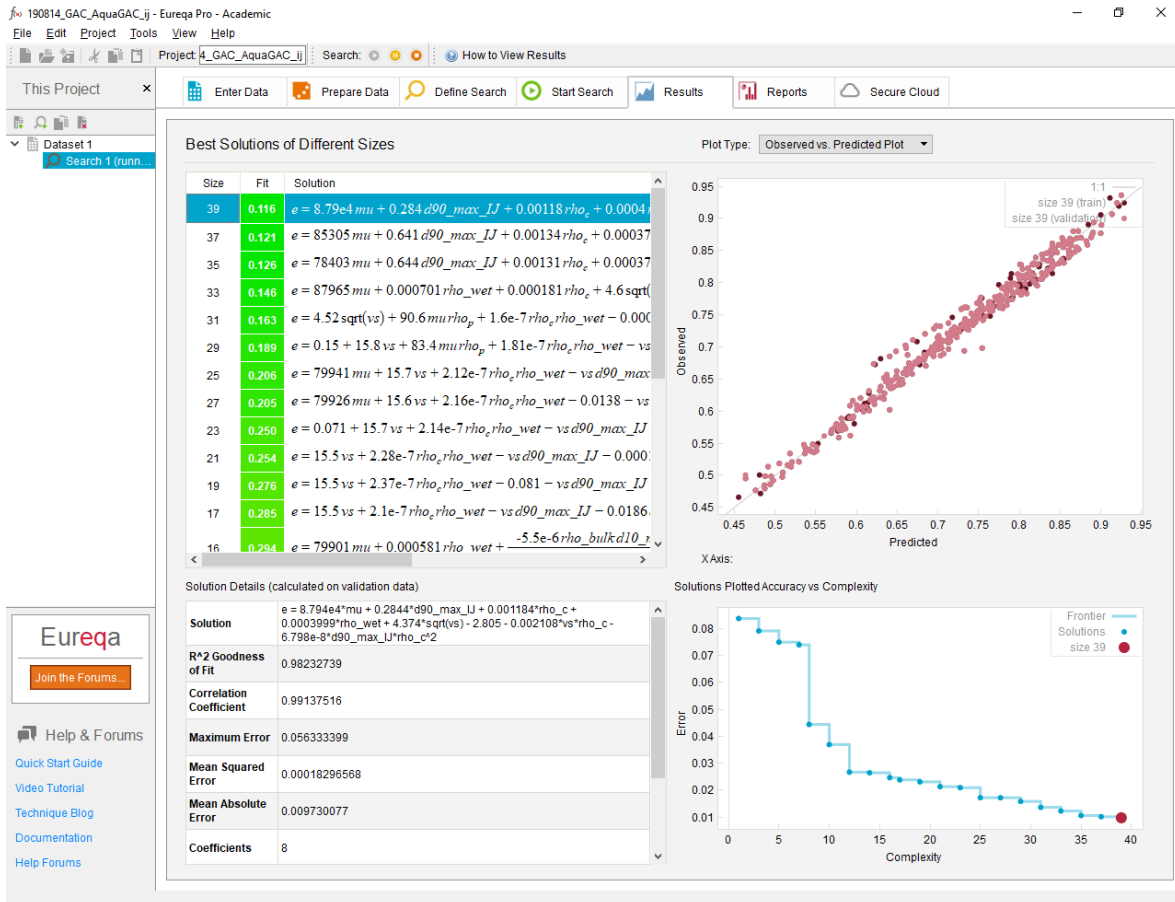
$$r^2 = 0.981$$



A11.9 – Symbolic regression outputs microscope measurements (DDM 2)

$$e = 87940.6520842292 * \mu + 0.284367094916555 * d90_max_IJ + 0.00118397838679878 * \rho_c + 0.000399859684451503 * \rho_wet + 4.37409509751969 * \sqrt{vs} - 2.80484098877486 - 0.00210750149564745 * vs * \rho_c - 6.79799030234076e-8 * d90_max_IJ * \rho_c^2$$

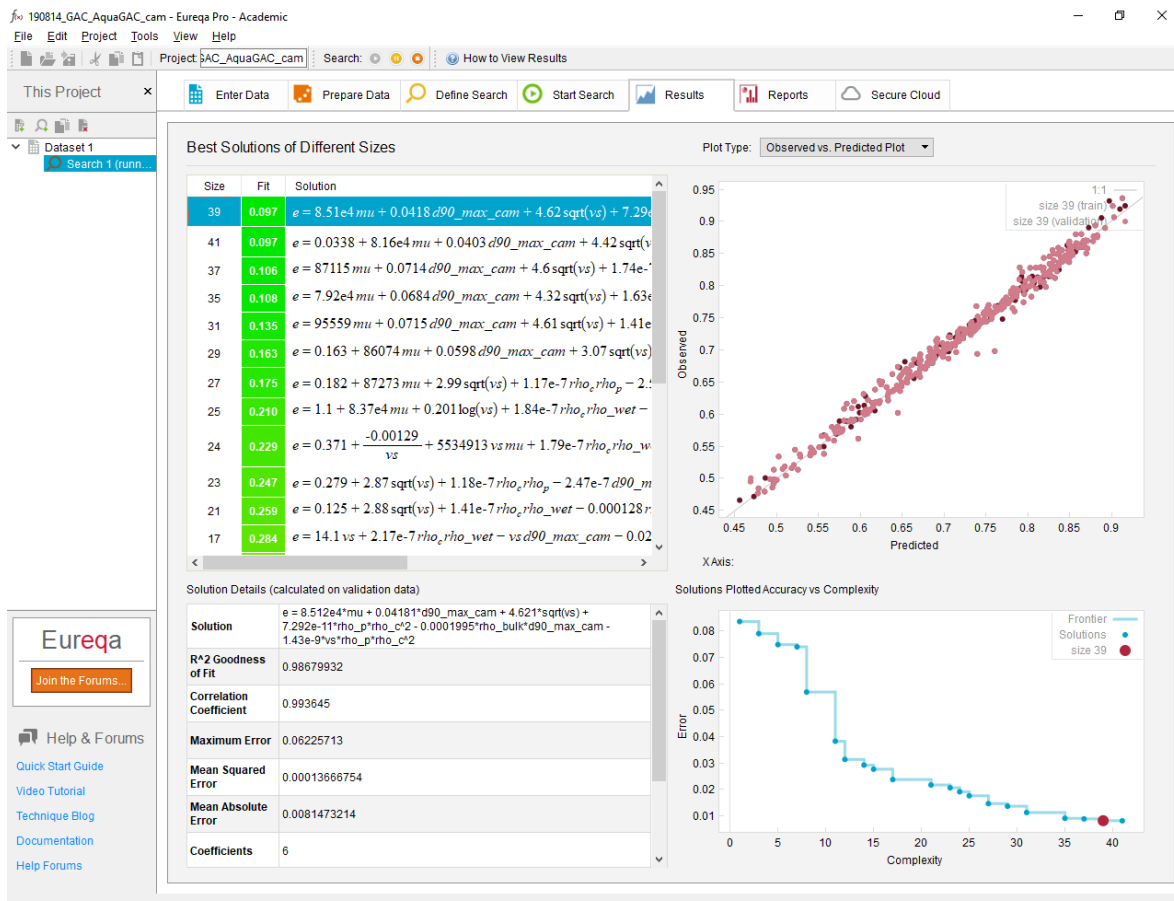
$$r^2 = 0.982$$



A11.10 – Symbolic regression outputs ImageJ measurements (DDM 2)

$$e = 85117.6107833098 \cdot \mu + 0.0418118097804086 \cdot d_{90_max_cam} + 4.62078395327982 \cdot \sqrt{vs} + 7.2923029456003e-11 \cdot \rho_p \cdot \rho_c^2 - 0.000199535868239078 \cdot \rho_{bulk} \cdot d_{90_max_cam} - 1.43037515333729e-9 \cdot vs \cdot \rho_p \cdot \rho_c^2$$

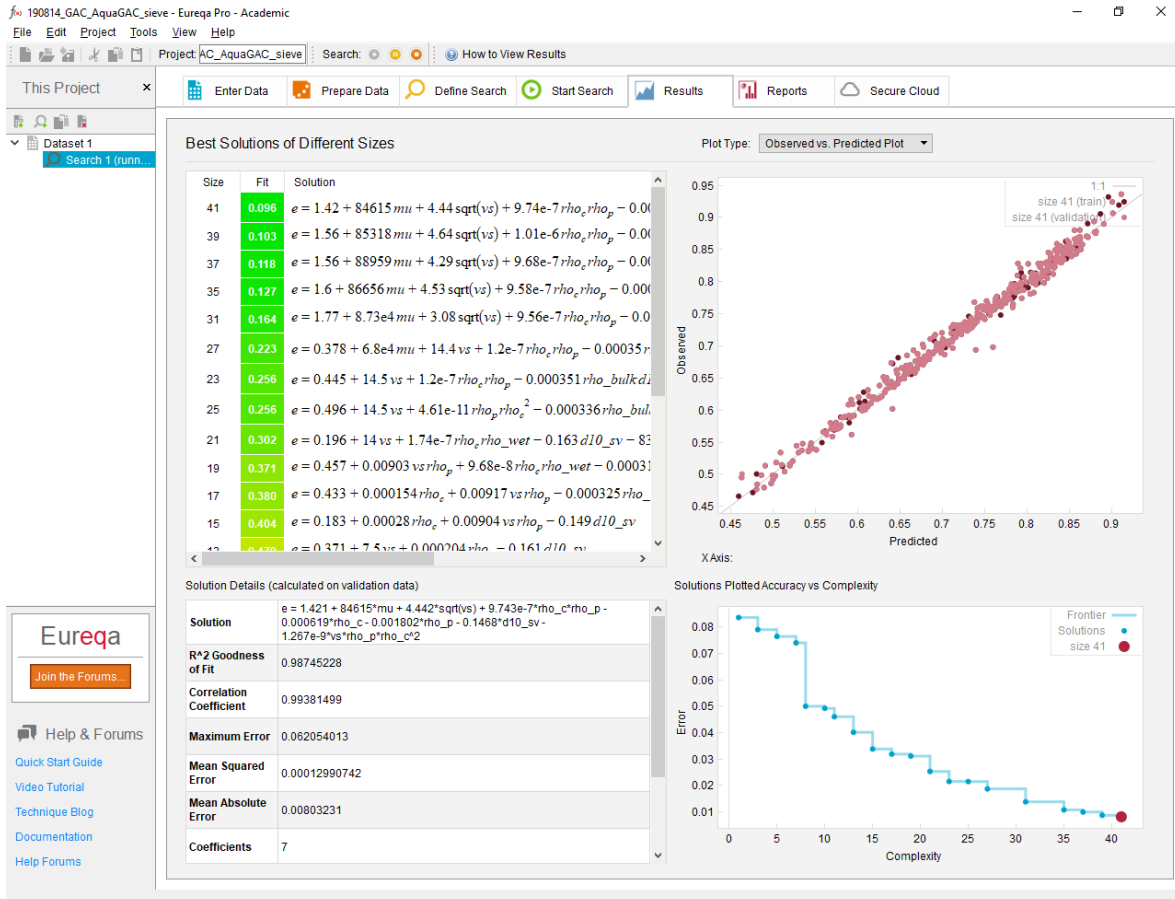
$$r^2 = 0.987$$



A11.11 – Symbolic regression outputs camsize measurements (DDM 2)

$$e = 1.42146588370743 + 84615 \cdot \mu + 4.44178716991241 \cdot \sqrt{vs} + 9.74287139587132e-7 \cdot \rho_c \cdot \rho_p - 0.000619027454135302 \cdot \rho_c - 0.00180247205502671 \cdot \rho_p - 0.146840981204452 \cdot d_{10_sv} - 1.26698525248786e-9 \cdot vs \cdot \rho_p \cdot \rho_c^2$$

$r^2 = 0.987$

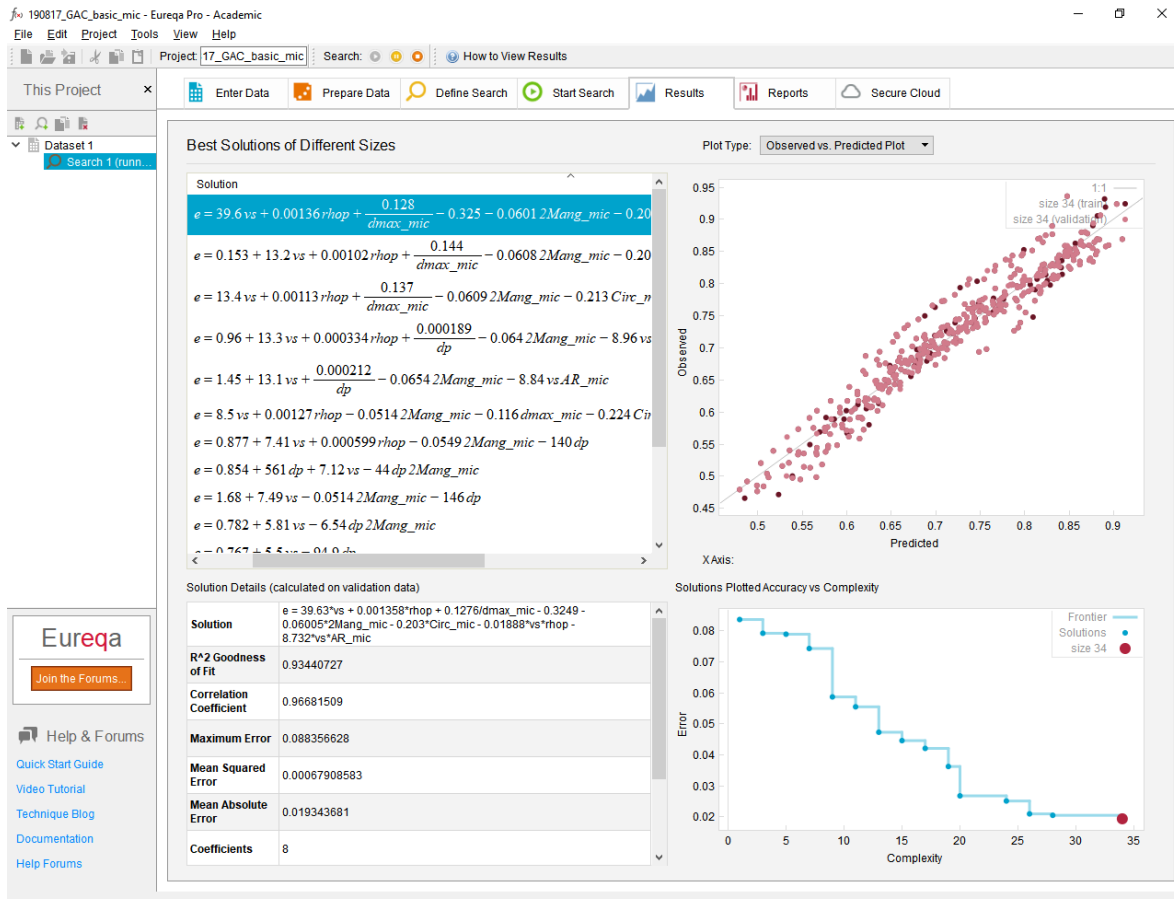


A11.12 – Symbolic regression outputs sieve measurements (DDM 2)

- $\varepsilon(v_s, v, \rho_{wet}, d_{max}, 2M_{ang}, AR, Circ) \rightarrow DDM_4$ (microscope)

$$e = 39.6301166232873 * v_s + 0.00135777764596453 * \rho_{hop} + 0.127555083189225 / d_{max_mic} - 0.324918233031637 - 0.0600510274368888 * 2M_{ang_mic} - 0.202951677174625 * Circ_mic - 0.0188847559407192 * v_s * \rho_{hop} - 8.73161077028406 * v_s * AR_mic$$

$$R^2 = 0.934$$

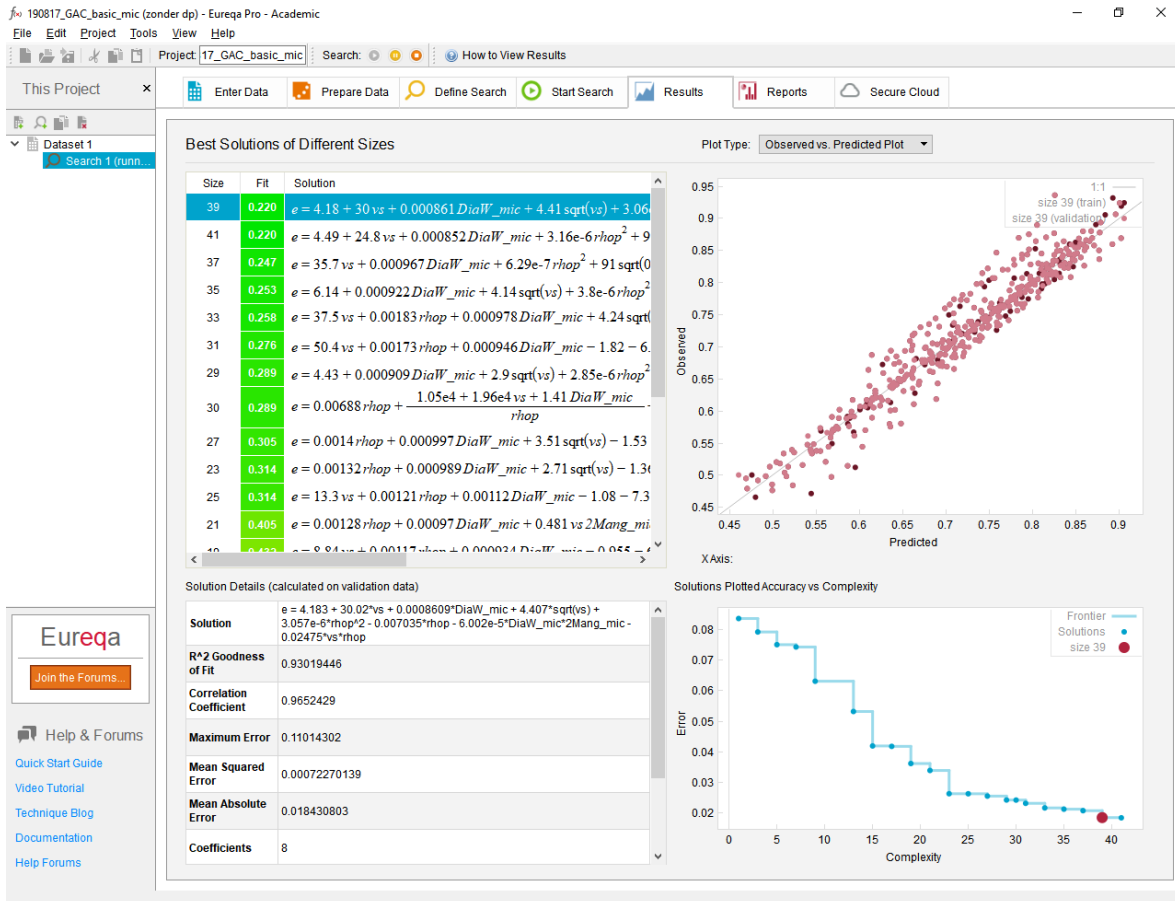


A11.13 – Symbolic regression outputs microscope measurements (DDM 4)

▪ $\epsilon(v_s, v, \rho_{wet}, 2M_{ang}, Dia_w) \rightarrow DDM_5$

$$e = 4.18337811351013 + 30.0233562232972 * v_s + 0.000860940323775956 * DiaW_mic + 4.40667095260425 * \text{sqrt}(v_s) + 3.05729177717648e-6 * \rho_{hop}^2 - 0.00703548197400454 * \rho_{hop} - 6.0024233358321e-5 * DiaW_mic * 2Mang_mic - 0.0247473759155606 * v_s * \rho_{hop}$$

$R^2 = 0.930$

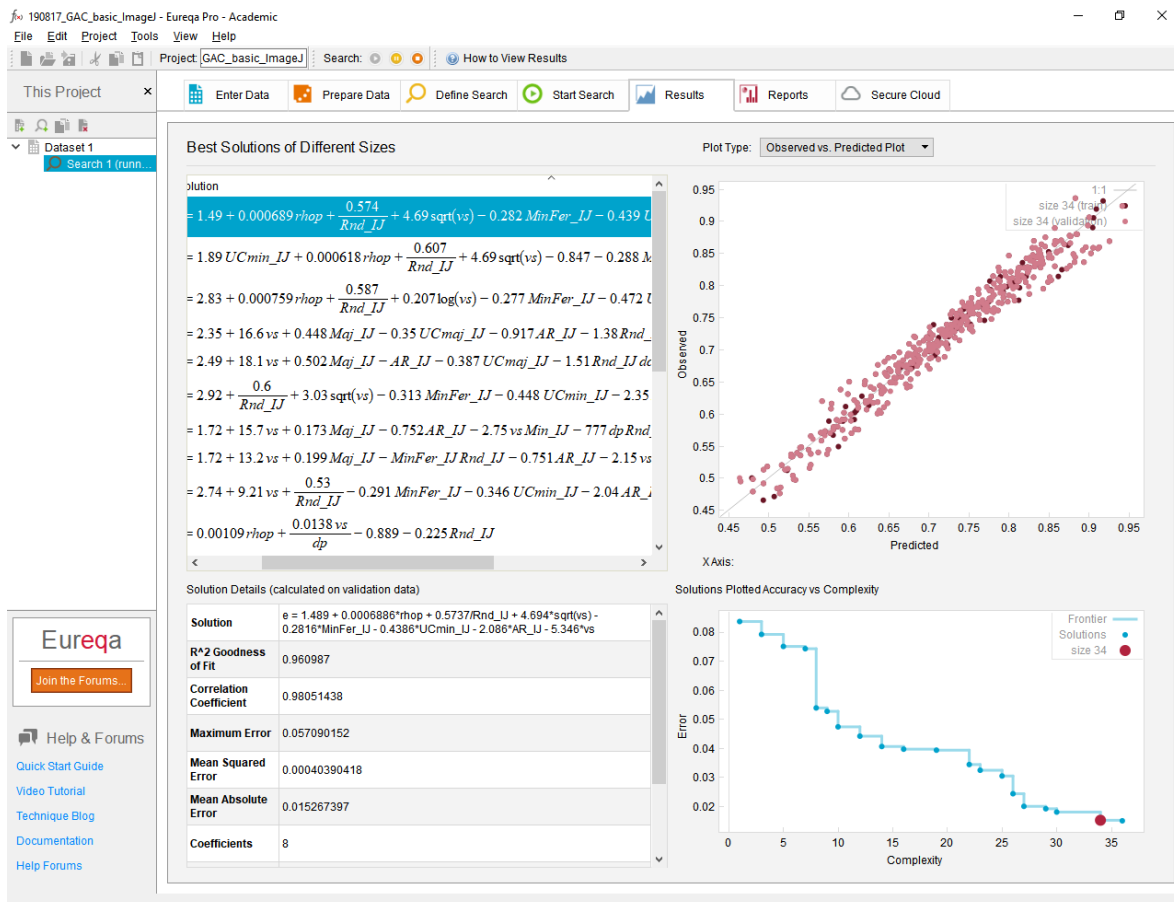


A11.14 – Symbolic regression outputs microscope measurements (DDM 5)

- $\epsilon(v_s, v, \rho_{wet}, rnd, Min_{Fer}, AR, UC_{min}) \rightarrow DDM 6 (ImageJ)$

$$e = 1.48887115705931 + 0.000688558717271011 * r_{hop} + 0.573714131947965 / Rnd_IJ + 4.69423888138102 * \sqrt{vs} - 0.281596748922725 * MinFer_IJ - 0.438577570752497 * UCmin_IJ - 2.0862202134662 * AR_IJ - 5.34569628117869 * vs$$

$r^2 = 0.960$

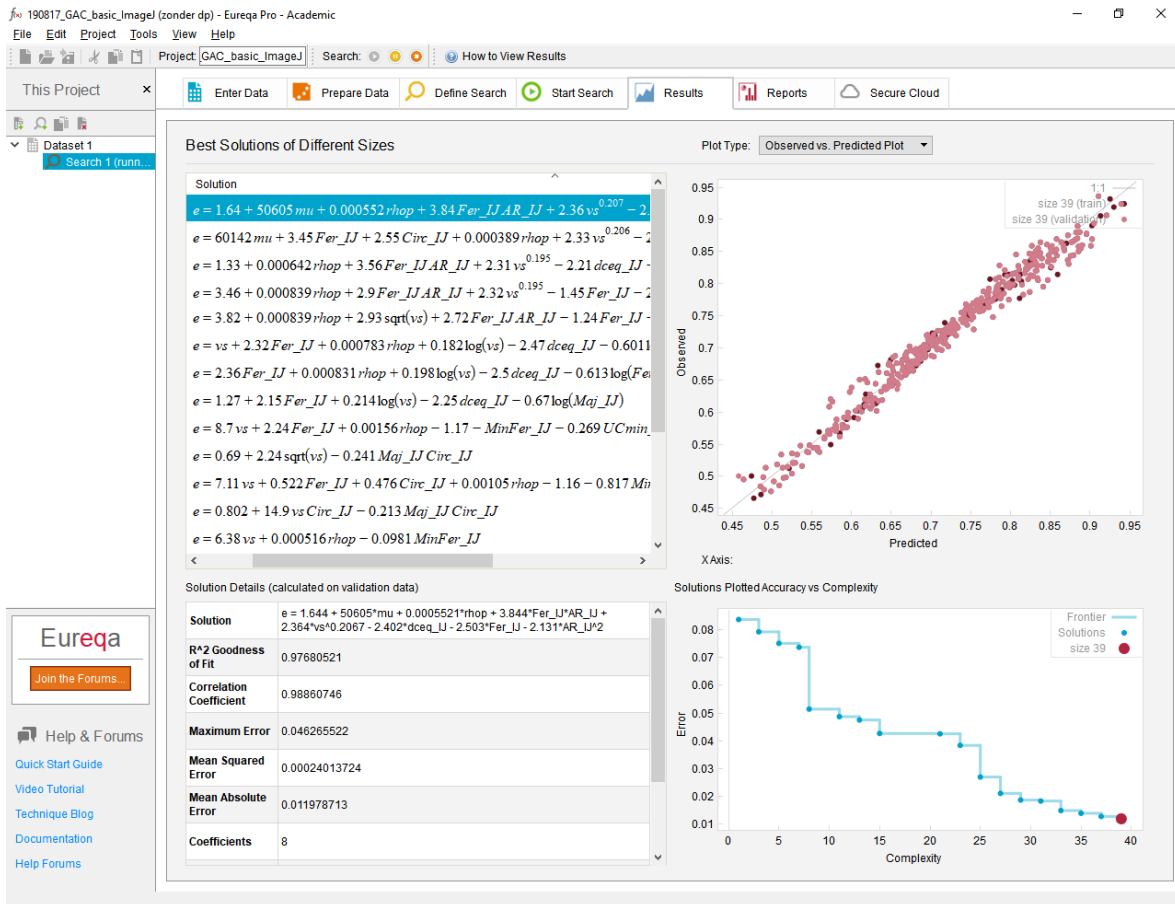


A11.15 – Symbolic regression outputs ImageJ measurements (DDM 6)

- $\epsilon(v_s, v, \rho_{wet}, rnd, Min_{Fer}, d_{ceg}, Fer, AR) \rightarrow DDM\ 7\ (Image)$

$$e = 1.64409984212064 + 50605 \cdot \mu + 0.000552110440975523 \cdot \rho_{hop} + 3.84438597848051 \cdot Fer_{IJ} \cdot AR_{IJ} + 2.36427864497289 \cdot vs^{0.206742782884534} - 2.40226017175752 \cdot d_{ceg_IJ} - 2.50331215487998 \cdot Fer_{IJ} - 2.13083014980831 \cdot AR_{IJ}^2$$

$R^2 = 0.977$

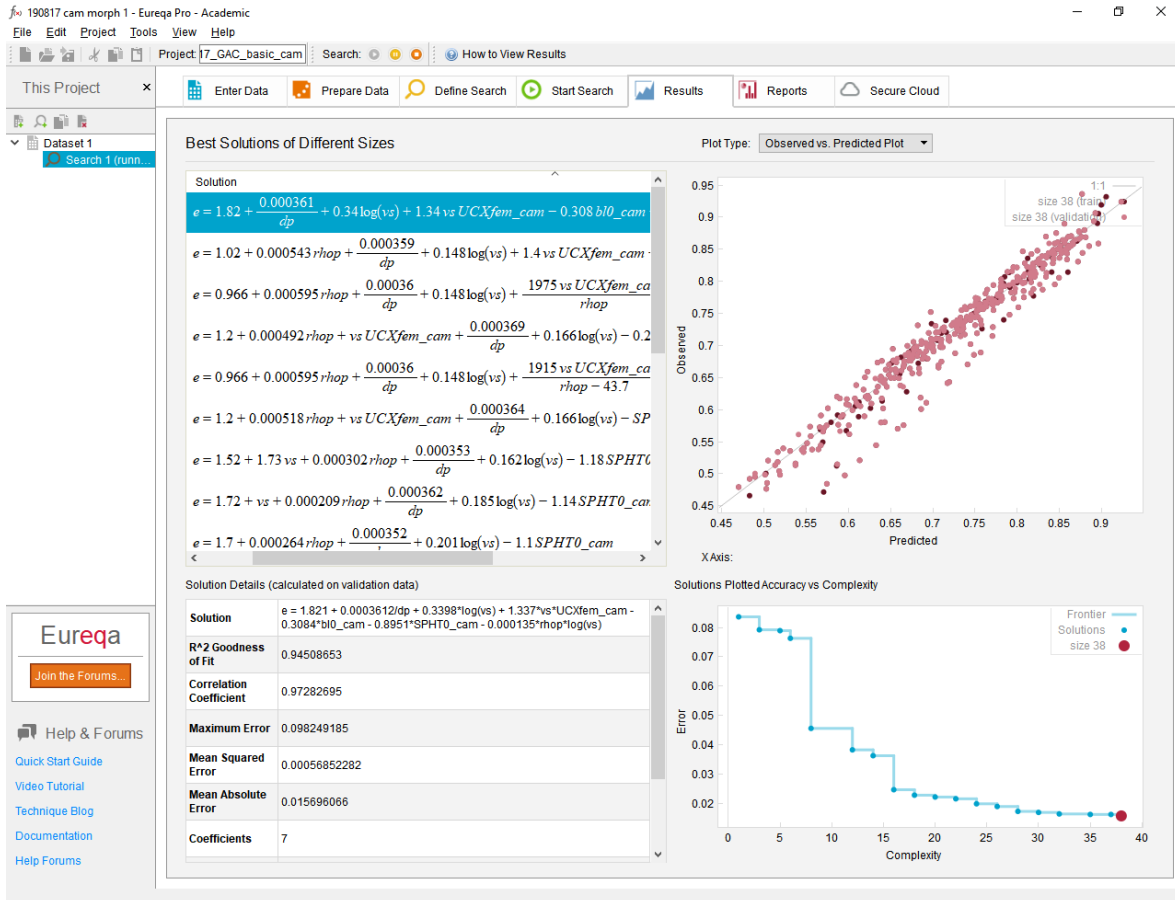


Att.16 – Symbolic regression outputs ImageJ measurements (DDM 7)

- $\epsilon(v_s, v, d_p, \rho_{wet}, bl_0, spht_0, UCx_0) \rightarrow DDM\ 8\ (Camsizer)$

$$e = 1.82060609195529 + 0.000361218091234448/dp + 0.339829024835084*\log(vs) + 1.33694491199222*vs*UCXfem_cam - 0.308439422420391*blo_cam - 0.89514500292175*SPHTo_cam - 0.000134976402395416*\rho_{hop}*\log(vs)$$

$R^2=0.945$

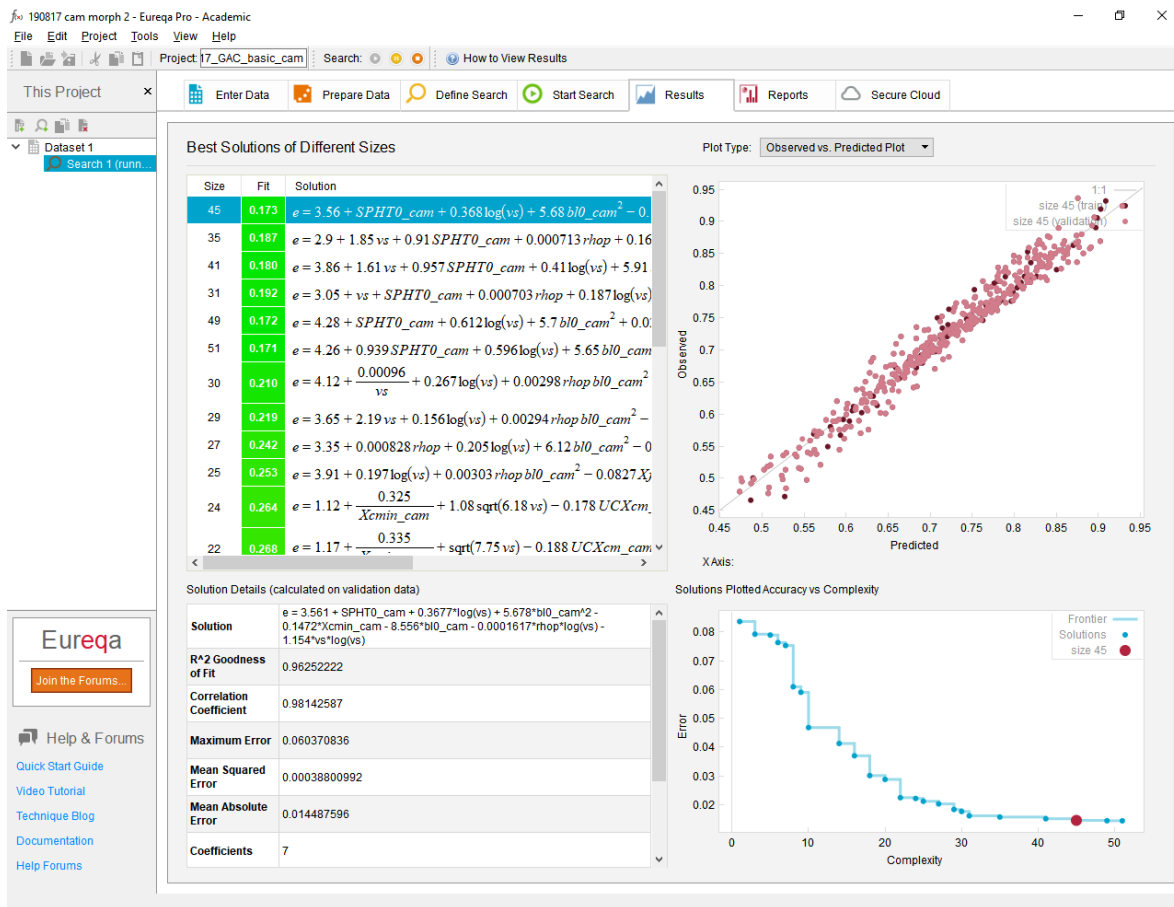


Am.17 – Symbolic regression outputs Camsizer measurements (DDM 8)

- $\epsilon(v_s, v, x_{c,min}, \rho_{wet}, bl_0, spht_0) \rightarrow DDM\ 9$ (Camsizer)

$$e = 3.56120803052656 + SPHT0_cam + 0.367713740895313 * \log(vs) + 5.67753231291994 * bl0_cam^2 - 0.147246125572455 * Xcmin_cam - 8.5555105568176 * bl0_cam - 0.000161708840465356 * \rho_{hop} * \log(vs) - 1.1541353093694 * vs * \log(vs)$$

$$r^2 = 0.963$$

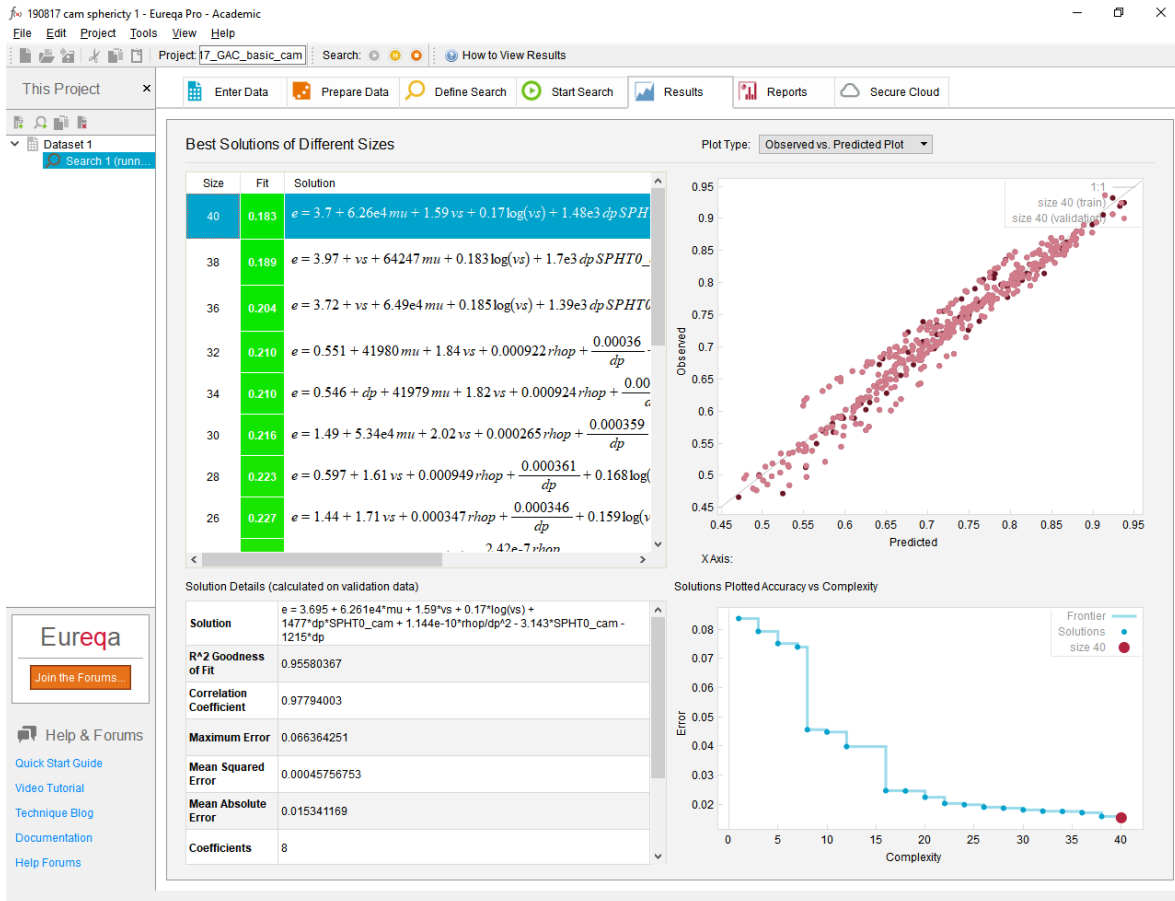


A11.18 – Symbolic regression outputs Camsizer measurements (DDM 9)

- $\epsilon(v_s, v, d_p, \rho_{wet}, spht_0) \rightarrow DDM\ 10$ (Camsizer)

$$e = 3.69546563079023 + 62608.0326295031 \cdot \mu + 1.59020331081951 \cdot v_s + 0.1699749236899 \cdot \log(v_s) + 1477.44217148437 \cdot dp \cdot SPHTO_cam + 1.14402022590614e-10 \cdot \rho_{hop}/dp^2 - 3.14311260496054 \cdot SPHTO_cam - 1215.4755135515 \cdot dp$$

$r^2=0.956$

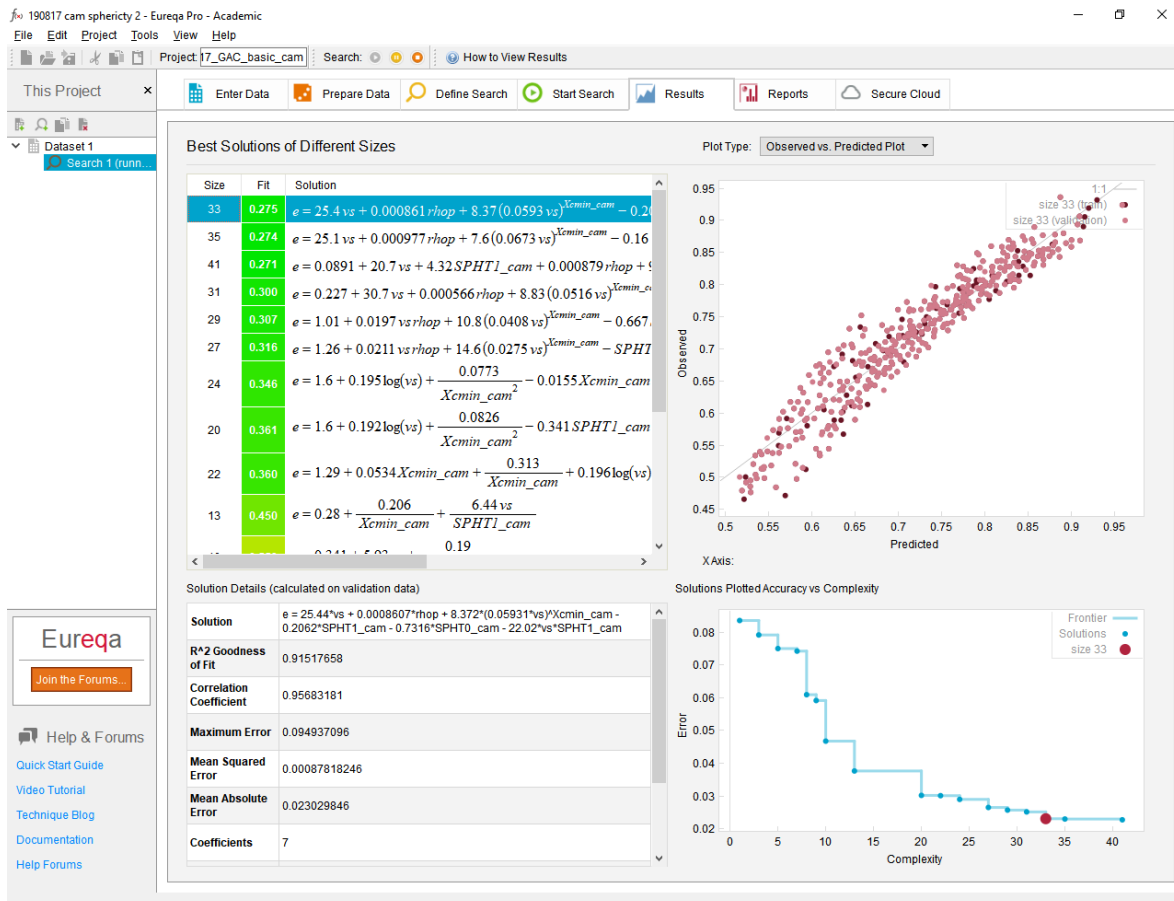


A11.19 – Symbolic regression outputs Camsizer measurements (DDM 10)

- $\mathcal{E}(v_s, v, x_{c,min}, \rho_{wet}, spht_0, spht_1) \rightarrow DDM_{11} (camsizer)$

$$e = 25.4431293690728 * vs + 0.000860743567032952 * rhop + 8.37238574466292 * (0.0593087913037627 * vs)^{Xcmin_cam} - 0.206220549961727 * SPHT1_cam - 0.731579874648063 * SPHT0_cam - 22.0187190114023 * vs * SPHT1_cam$$

$$r^2 = 0.915$$

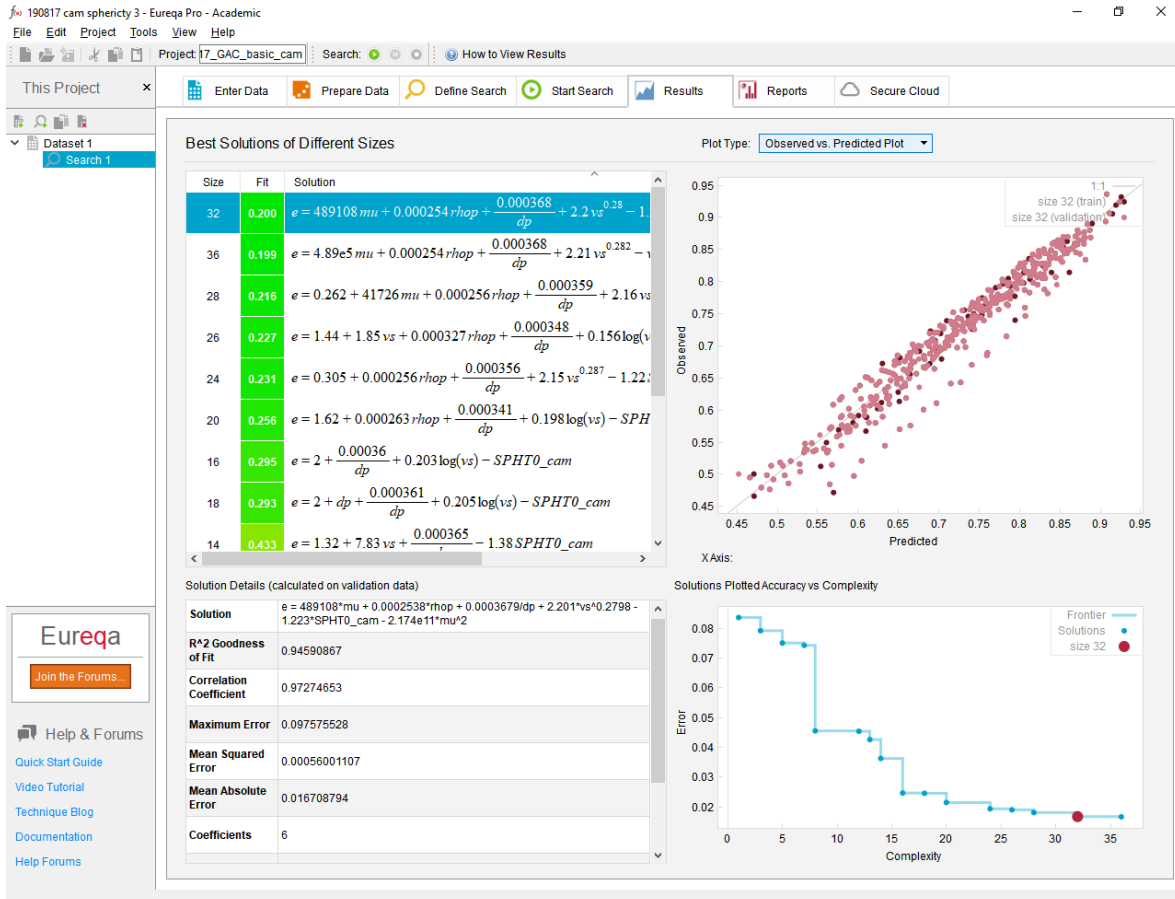


A11.20 – Symbolic regression outputs Camsizer measurements (DDM 11)

- $\epsilon(v_s, v, x_{c,min}, \rho_{wet}, spht_0) \rightarrow DDM 12 (camsizer)$

$$e = 489108 \cdot \mu + 0.000253819026495085 \cdot \rho_{hop} + 0.000367860847830381/dp + 2.20053178755678 \cdot v_s^{\wedge}0.279835188866413 - 1.22282222642243 \cdot SPHT0_cam - 217372641285.372 \cdot \mu^{\wedge}2$$

$$R^2 = 0.945$$

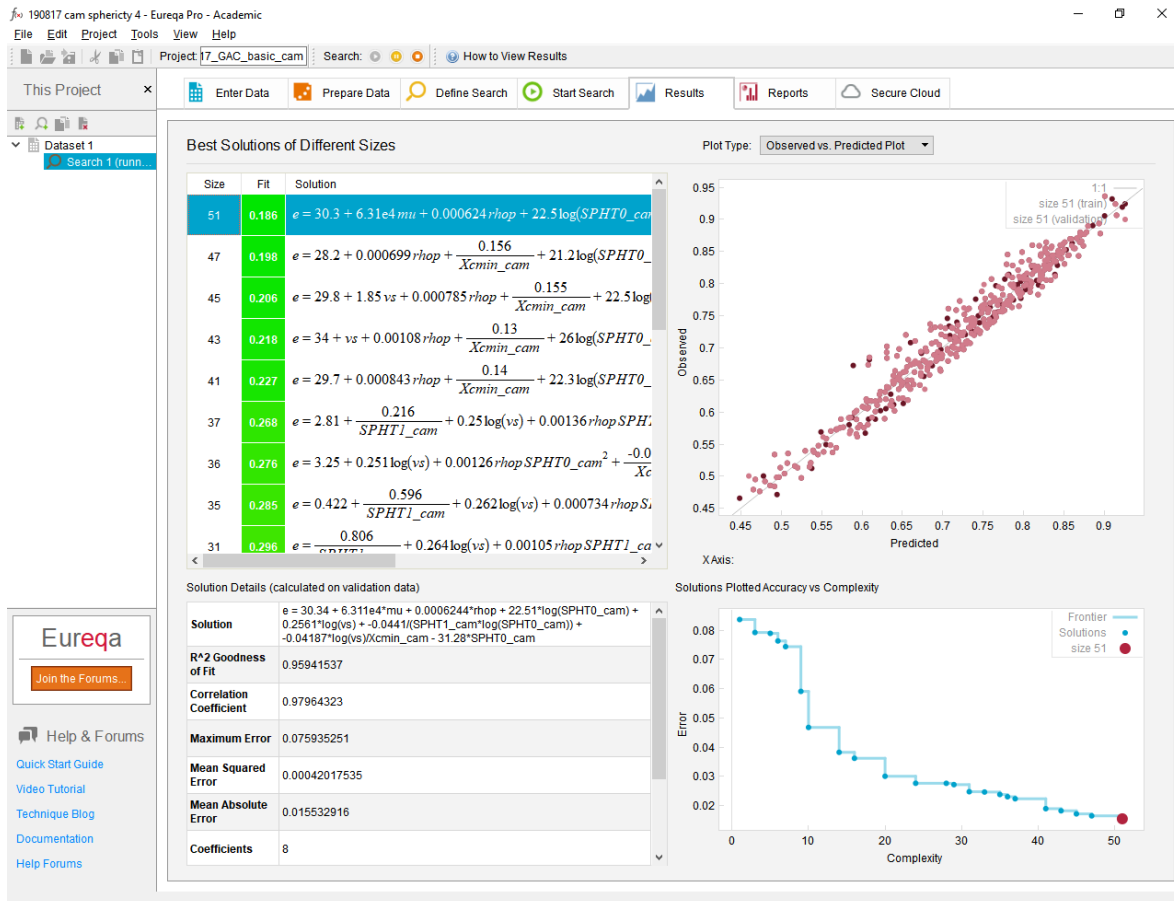


A11.21 – Symbolic regression outputs Camsizer measurements (DDM 12)

- $\epsilon(v_s, v, x_{c,min}, \rho_{wet}, sph, spht_0, spht_1) \rightarrow DDM_{13} (camsizer)$

$$e = 30.3356056993106 + 63113.7119965412 * \mu + 0.000624426918551764 * \rho_{hop} + 22.5136443287743 * \log(SPHTo_cam) + 0.25614049704322 * \log(vs) + - 0.0440999166017474 / (SPHT1_cam * \log(SPHTo_cam)) + - 0.0418680533524428 * \log(vs) / Xcmin_cam - 31.2810101439366 * SPHTo_cam$$

$$R^2 = 0.960$$

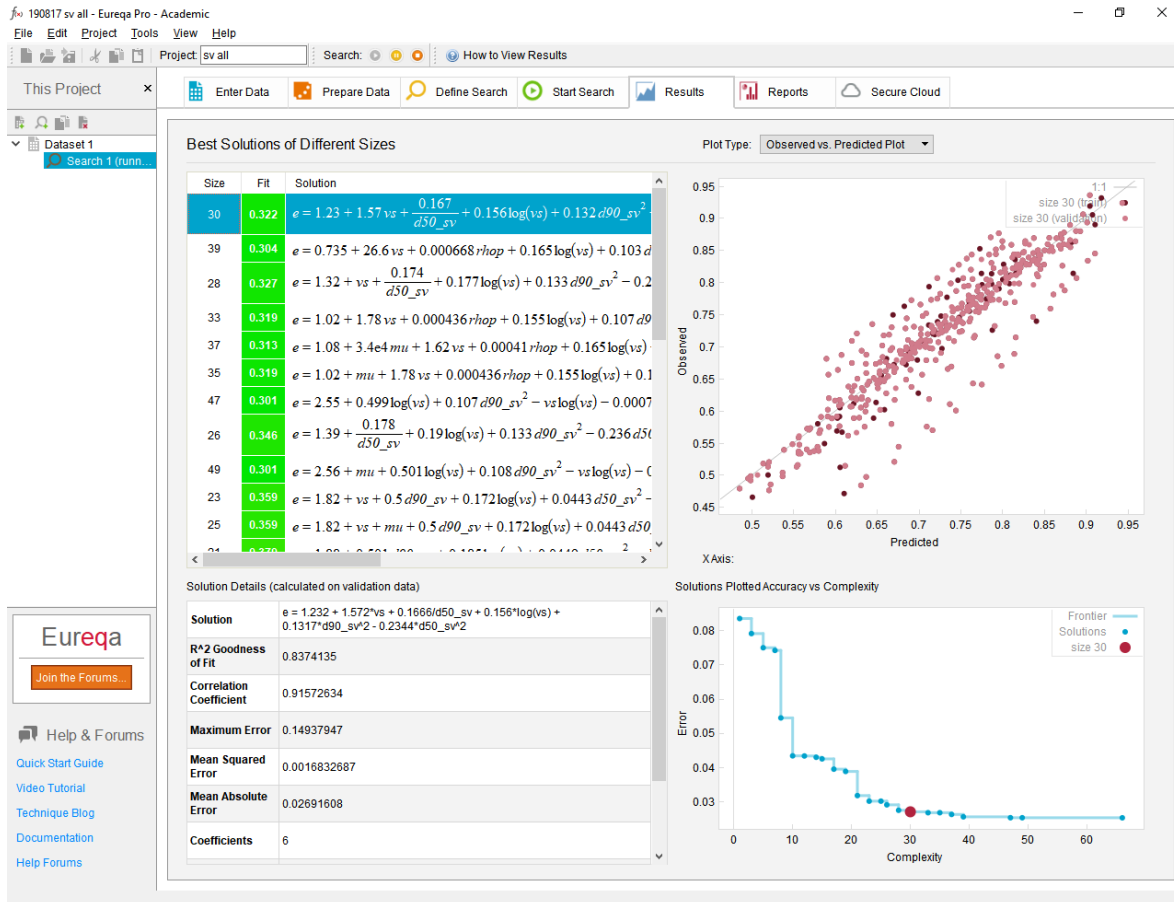


A11.22 – Symbolic regression outputs Camsizer measurements (DDM 13)

- $\epsilon(v_s, v, d_p, \rho_{wet}, d_{10}, d_{90}, d_{50}, UC) \rightarrow DDM 14$ (sieve)

$$e = 1.2323711210721 + 1.57239723147448 * vs + 0.166635312042398 / d50_sv + 0.155953014580797 * \log(vs) + 0.131738338199338 * d90_sv^2 - 0.234446603407859 * d50_sv^2$$

$$r^2 = 0.837$$



A11.23 – Symbolic regression outputs sieve measurements (DDM 14)

- $\mathcal{E}(v_s, v, d_p, \rho_{wet}, d_{10}, d_{90}, UC) \rightarrow \text{DDM 15 (sieve)}$

$$e = 2.78513848282785 + 83390.0741681267 \cdot \mu + 0.000798139930065826/vs + 0.268119836843535 \cdot \log(vs) + 1.35902464528884 \cdot d90_{sv} \cdot uc_{sv} - 0.504999265673363 \cdot uc_{sv} - 1.97317665351561 \cdot d90_{sv} - 0.00037171509874118 \cdot d90_{sv} \cdot \exp(4.16125779748895 \cdot uc_{sv})$$

$R^2=0.971$

The screenshot shows the Eureka Pro software interface. On the left, there is a sidebar with the Eureka logo and navigation links. The main area is divided into several panels:

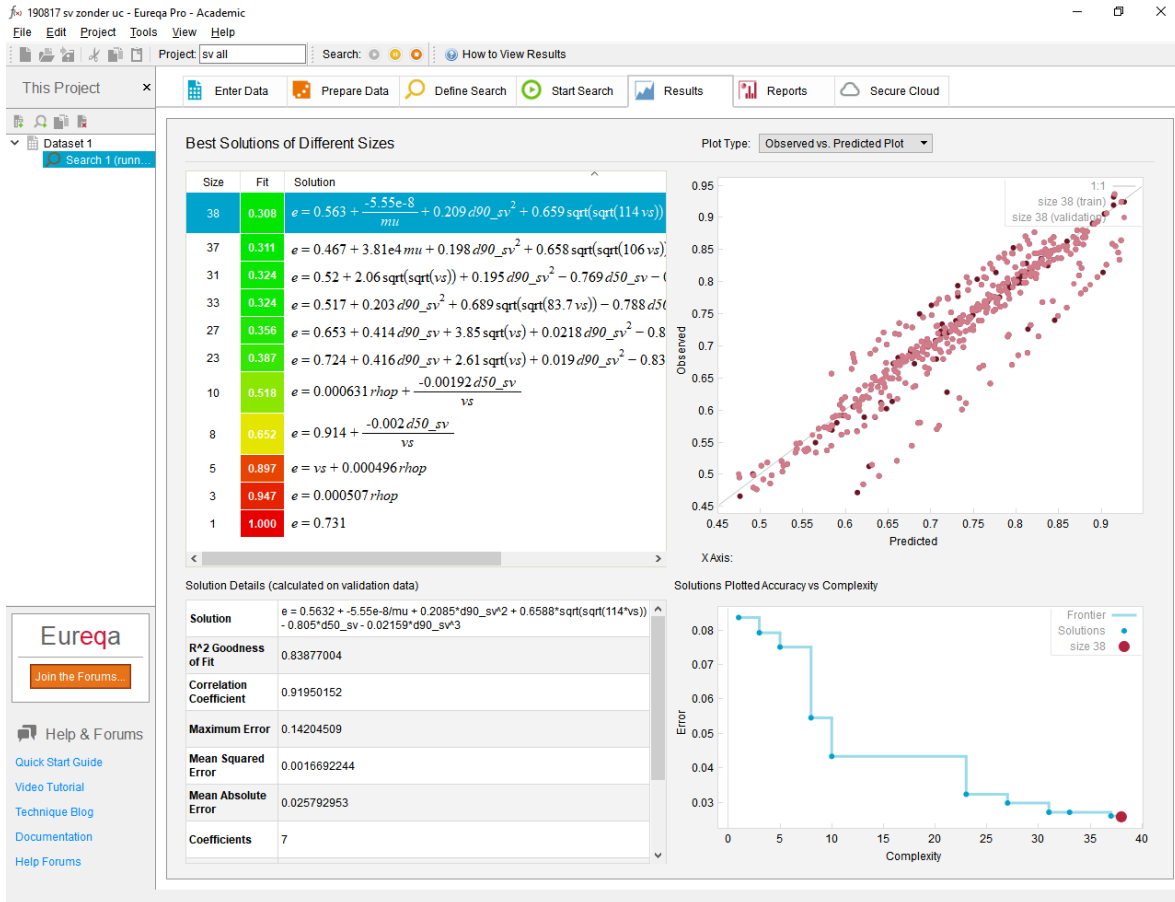
- Best Solutions of Different Sizes:** A table listing solutions with their size, fit, and mathematical equation. The top solution (Size 44) has a fit of 0.146 and is highlighted in blue.
- Solution Details (calculated on validation data):** A panel showing the full equation for the selected solution, along with statistical metrics: R² Goodness of Fit (0.97119188), Correlation Coefficient (0.98578136), Maximum Error (0.060241946), Mean Squared Error (0.00029825234), Mean Absolute Error (0.012208336), and Coefficients (9).
- Observed vs. Predicted Plot:** A scatter plot showing a strong positive linear correlation between predicted and observed values, with a diagonal line representing the identity function (y=x).
- Solutions Plotted Accuracy vs Complexity:** A step-down plot showing the error rate decreasing as the complexity of the solution increases. The frontier solution (Size 44) is marked with a red dot at complexity 44 and an error of approximately 0.012.

11.24 – Symbolic regression outputs sieve measurements (DDM 15)

- $\epsilon(v_s, v, d_p, \rho_{wet}, d_{10}, d_{90}, d_{50}) \rightarrow DDM\ 16\ (sieve)$

$$e = 0.563193355563503 + -5.55013136085066e-8/\mu + 0.208529767482366*d90_sv^2 + 0.658782021958192*\sqrt{\sqrt{(114.023596299073*vs)}} - 0.805006706680813*d50_sv - 0.0215885516357859*d90_sv^3$$

$$r^2=0.838$$



Att.25 – Symbolic regression outputs sieve measurements (DDM 16)

Symbolic Regression nomenclature

▪ Microscope

d_{max}	The maximum length between any two points that lie on the inner perimeter of the figure	[mm]
$Circ$	When the figure is a perfect circle, the maximum value is one. As it becomes long and thin, this value approaches zero	[mm]
AR	The area reation of the figure within the screen	[mm ²]
Per	The length of the perimeter of the figure. This is calculated as the length of the line that passes through the center of the pixels that make up the inner perimeter	[mm]
Dia_w	This is the distance between two parallel lines that sandwich the particle and are parallel to the line along the maximum diameter. It is calculated as the distance between the pixels that each of the two lines touches	[mm]
G_{2y}	This is the center of gravity secondary moment of the figure on the Y-axis. G is the center of gravity of the figure	[mm]
G_{pin}	The center of gravity product of inertia of the figure on the X and Y axes. G is the center of gravity of the figure	[mm]
$2M_{majX}$	This is the length of the figure's secondary moment major axis. Normalization is achieved by dividing by the area	[mm]
$2M_{ang}$	The figure's secondary moment major axis angle	[deg]

▪ ImageJ

Min_{Fer}	Minimum feret (calliper) diameter	[mm]
Fer	Feret diameter (maximum caliper) --> The longest distance between any two points along the selection boundary	[mm]
Maj	Primary axis of ellipse	[mm]
Min	Secondary axis of ellipse	[mm]
d_{ceg}	Circular equivalent diameter	[mm]
$Circ$	Circularity= $4\pi \cdot \text{area} / \text{perimeter}^2$	[mm]
UC_{min}	Uniformity coefficient of minimum diameter (ellipse)	[-]
UC_{maj}	Uniformity coefficient of maximum diameter (ellipse)	[-]
UC_{cir}	Uniformity coefficient of circular equivalent diameter	[-]

UC_{fer}	Uniformity coefficient of Feret diameter	[-]
AR	Aspect ratio= major axis/minor axis	[-]
Rnd	Roundness= $4 \cdot \text{area} / (\pi \cdot \text{major_axis}^2)$ =inverse of AR	[-]
<ul style="list-style-type: none"> ▪ Camsizer 		
$x_{c,min}$	Particle diameter determined from the smallest of all maximum chords of the particle projection. Also referred to as width of the particle projection. Suitable for comparison with sieve analysis. Minimum chord, this translates into the minimum diameter of the particle	[mm]
sph	Sphericity calculated from the perimeter P and area A of the particle projection. (Xarea)	[-]
$spht_0$	Sphericity calculated from the perimeter P and area A of the particle projection. (Xmin)	[-]
$spht_1$	Sphericity calculated from the perimeter P and area A of the particle projection. (Xfemin)	[-]
bl_0	Aspect (width-to-length) ratio of xc min and xFe max (Xarea)	[-]
bl_1	Aspect (width-to-length) ratio of xc min and xFe max (min)	[-]
bl_2	Aspect (width-to-length) ratio of xc min and xFe max (Xfemin)	[-]
UCx_{cm}	d60/d10 based on Xmin	[-]
$x_{f,max}$	Particle diameter determined from the longest of all measured Feret diameters of the particle projection referred to as length of the particle projection. Particularly suitable for measuring straight extrudates/fibres or rice grains (Xfemin)	[-]
UCx_{fe}	d60/d10 based on Xfemax	[-]